Axon Guidance by Molecular and Topographical Cues

by
Grace Nga Yin Li
M.Eng.Sc., University of New South Wales, 2004
B.S., University of California, Berkeley, 2002

Submitted in partial fulfillment of the
requirements for the degree of Doctor of Philosophy
in the Division of Biology and Medicine at Brown University

Providence, Rhode Island
May 2008

This dissertation by Grace N. Li is accepted in its present form by
the Division of Biology and Medicine as satisfying the dissertation requirement
for the degree of Doctor of Philosophy.

Date _____ _____

Diane Hoffman-Kim, Ph.D., Director

Recommended to the Graduate Council

Date _____ _____

Michael Lysaght, Ph.D., Reader

Date _____ _____

Jeffrey Morgan, Ph.D., Reader

Date _____ _____

Anubhav Tripathi, Ph.D., Reader

Date _____ _____

Ravi Bellamkonda, Ph.D., External Reader

Approved by the Graduate Council

Date _____ _____

Sheila Bonde, Dean of the Graduate School

Vita

Name: Grace Nga Yin Li

Date of birth: December 30, 1980

Place of Birth: Hong Kong

EDUCATION

- Ph.D. candidate, Biomedical Engineering, Expected graduation date: May 2008 Thesis title: Axon guidance by Multimolecular Cues, Brown University; Providence, Rhode Island
- M.Eng. Biomedical Engineering, December 2003 Thesis title: Biological performance of a novel synthetic furanone-based antimicrobial, University of New South Wales; Sydney, Australia
- B.S. Bioengineering, December 2002 University of California, Berkeley; Berkeley, California

EMPLOYMENT HISTORY

- Formulations Research Chemist I, ALZA Corporation, Intravenous Technology Development, Mountain View, California, 2001-2002

FELLOWSHIPS/AWARDS

- Kaplan Graduate Fellowship, Brain Science Program, Brown University, 2007
- University Fellowship, Brown University, 2004-2005
- International Academy of Medical and Biological Engineering Young Investigator prize– Highly commended, 8/2003

PUBLICATIONS

- Li GN and Hoffman-Kim D. Tissue engineered platforms of axon guidance. Tissue Engineering Part B: Reviews 14(1): 33-51, 2008.
- Li GN, Liu J, and Hoffman-Kim D. Multi-molecular gradients of permissive and inhibitory cues direct neurite outgrowth. Annals of Biomedical Engineering, 2008 Apr 5; [Epub ahead of print].
- Li GN and Hoffman-Kim D. Quantification of neurite outgrowth using a novel application of circular analysis. Submitted to J. Neurosci Meth, 2008.
- Li GN, Livi LL, Gourd CM, Deweerd ES, and Hoffman-Kim D. Genomic and morphological changes of neuroblastoma cells in response to three-dimensional matrices. Tissue Engineering 13: 1035-1047, 2007.
- Goldner JS, Bruder JM, Li GN, Gazzola D, and Hoffman-Kim D. Neurite bridging across micropatterned grooves. Biomaterials 27(3): 460-472, 2006.
- Baveja JK, Li GN, Nordon RE, Hume EB, Kumar N, Willcox MD and Poole-Warren LA. Biological performance of a novel synthetic furanone-based antimicrobial. Biomaterials 25(20):5013-21, 2004.

Abstracts

- Li GN, Cheng E and Hoffman-Kim D. Effects of RhoGTPases on Neurite Outgrowth on Multimolecular Gradients. Annual Meeting of the Biomedical Engineering Society, September 2007.

- Li GN, Deweerd E and Hoffman-Kim D. Neurite growth on gradients of inhibitory and permissive cues. Annual Meeting of the Biomedical Engineering Society, October 2006.

- Richardson J, Li GN and Hoffman-Kim D. Surface topography and adhesivity influence Schwann cell bridging. Annual Meeting of the Biomedical Engineering Society, October 2006.

- Deweerd ES, Li GN and Hoffman-Kim D. Promotion of neurite outgrowth on multimolecular gradients by modulating downstream Rho pathways. Annual Meeting of the Society for Biomaterials, April 2006.

- Gourd C, Deweerd E, Livi L, Li GN and Hoffman-Kim D. Genomic and morphological analysis of human neuroblastoma cell growth in three-dimensional matrices. Annual Meeting of the Society for Biomaterials, April 2006.

- Li GN, Liu J, Cheng E and Hoffman-Kim D. Neurite outgrowth on gradients of permissive and inhibitory cues. Annual Meeting of the Biomedical Engineering Society, October 2005.

- Li GN, Liu J and Hoffman-Kim D. Neurite outgrowth on multi-molecular gradients. Annual Meeting of the Society for Biomaterials, April 2005.

- Goldner J, Bruder J, Li GN, Gazzola D and Hoffman-Kim D. Neurite bridging across micropatterned grooves. Nanotech2004 Montreux, November 2004.

- Goldner JS, Bruder JM, Li GN, Gazzola D and Hoffman-Kim D. Effects of groove dimensions on neurite bridging across micropatterned grooves. Annual Meeting of the Biomedical Engineering Society, October 2004.

- Li GN, Baveja JK, Hume EB, Doran M, Nordon RE and Poole-Warren LA. Biological performance of a novel synthetic furanone-based antimicrobial. International Conference on Cellular Engineering, August 2003.

Manuscripts in progress

- Li GN, Deweerd E, Cheng E and Hoffman-Kim D. Promotion of neurite outgrowth on multi-molecular gradients by modulating Rho kinase. In preparation, 2008.

INVITED LECTURE

- University of Massachusetts, Dartmouth; Dartmouth, MA. Bioengineering and Biotechnology Conference. February, 2006.

PROFESSIONAL AFFILIATIONS

- Biomedical Engineering Society
- Society for Biomaterials

TEACHING EXPERIENCE

Teaching Assistant, Brown University, Providence, RI

- Techniques in Molecular and Cell Science, BI 2130, Fall 2005
- Organ Replacement, BI 1080, Spring 2006 and Spring 2007
- Exercise Physiology, BI 1160, Fall 2007 Graduate Student Advisor, 2004 – present.

VOLUNTEER EXPERIENCE

Rhode Island Department of Education, Math and Science Partnership at Harris Elementary School and Citizens Elementary School, Woonsocket, RI. 8/2007-present. Planning and implementation of after school science programs for elementary school students (Grades 3-5) with focus on experimentation for understanding of Rhode Island Grade Level Expectations.

Preface

The primary motivation for this work was to study the interactions between neurons and their local microenvironments that contain specific guidance cues such as micropatterned molecular cues or microgrooved topographies. The investigation of these cell-material interactions quantitatively measures the effects of specific parameters of guidance cues such as slope of concentration gradient and dimension of grooves on neurite outgrowth in a post-injury model. These applications have tremendous importance in adding to the knowledge base of the fields of neuroscience, pharmaceutical science and biotechnology.

The chapters in this thesis occur sequentially by their relevance to the research topic. The chapters are formatted in the style of sequential journal articles and each chapter 2 through 6 has the following sections: Introduction, Materials and Methods, Results, Discussion and References. Where applicable, an Appendix of supplemental data will be included. The first chapter will provide background information on the field of axon guidance with particular focus on the post injury environment and in vitro modeling of the nerve regenerative process in the spinal cord. I will discuss the challenges of axon guidance and growth after spinal cord injury and discuss the strategies that have been used to promote directed axonal growth in this environment as well as to study different classes of guidance cues. This chapter will focus on studies from the previous five years and concentrate on in vitro biomaterials platforms to study axon guidance.

There are three additional chapters each addressing a specific aim in the research project. The primary aim of Chapter 2 was to describe a novel application of circular statistical methods to quantify results from neurite outgrowth assays. Using both experimental data

from neurite outgrowth on micropatterned glass substrates and simulated data, I determined the suitability of a number of developed circular statistical tests on different types of neurite directional data. This study has been submitted to the Journal of Neuroscience Methods.

Chapter 3 describes the fabrication of adsorbed multimolecular gradients of laminin and chondroitin sulfate proteoglycans, and the evaluation of dorsal root ganglia neurite outgrowth patterns on those substrates. To address specific aim 1 to determine the optimal gradient parameters to maximize and direct neurite outgrowth, single cue, double cue opposing and double cue parallel gradients were assessed for their influence on cellular adhesion, neurite outgrowth and neurite direction. In particular, the roles of absolute concentration change versus relative concentration change as the mechanism of gradient sensing was investigated. This study has been published in the Annals of Biomedical Engineering in 2008.

Chapter 4 describes the optimization of specific gradient parameters, molecular concentration and slope, which were found to play a large role in promoting and directing neurite outgrowth from studies described in Chapter 3. Interactions between multimolecular gradients were observed and cellular reponses and neurite length appeared to vary non-linearly when gradient slope and direction were varied.

Chapter 5 investigates the role of the three-dimensional (3D) microenvironment of collagen I and Matrigel hydrogels on the genomic expression and morphology of neuroblastoma cells. To address specific aim 2, microarray analysis, quantitative reverse transcriptase polymerase chain reaction and microscopy studies were performed to evaluate cellular responses to their 3D microenvironment. Material properties such as elastic modulus and porosity were also evaluated. This study was published in Tissue Engineering in 2007.

Chapter 6 includes a summary of the results presented in Chapters 2 through 5, as well as possible future directions and recommendations of this work.

Appendix A is a review article published in Tissue Engineering in 2008 entitled "Tissue Engineered Platforms for Axon Guidance" which covers the microfabrication techniques and platforms developed for studying and directing neurite outgrowth in vitro.

Appendix B includes a smaller study on the influence of parallel gradients of different slope on neurite outgrowth, and the neuron and neurite response after the application of Rho kinase inhibitor Y27632. Dynamics of the neurite extension, retraction and turning processes are also investigated using timelapse microscopy over 24 hours.

Appendix C addresses specific aim 3, to determine the role of protein micropatterning on the phenomenon of cellular bridging over microgrooved substrates. Selective coating and micropatterns of laminin were applied using microcontact printing, adsorption and covalent attachment methods. Bridging by Schwann cells and dorsal root ganglia neurons were investigated, and cellular adhesion, motility and bridge formation dynamics were investigated.

Acknowledgements

I would first like to thank Diane Hoffman-Kim for allowing me to be part of her laboratory and her research program and being a wonderful mentor throughout my graduate school career both scientifically and in life. Over the course of the past four years, she taught me how to ask critical questions to both myself and others, how to think more creatively and from different perspectives at both scientific and managerial problems and how to trust myself and my judgments. I am also thankful for all the support and encouragement that she has given me in the everyday progress and setbacks that one meets along the way, and I am very thankful that she has been an advisor in every sense of the word.

I would also like to thank my thesis committee – Jeffrey Morgan, Michael Lysaght, Anubhav Tripathi and Ravi Bellamkonda– for their willingness to spend some of their time reading over my work and for all the valuable input they have given me.

Of course, thanks also go to the members of the Hoffman-Kim lab who have been working side by side with me over the course of the last four years: Elke Bremus-Koebberling, Jan Bruder, Celinda Kofron, Liane Livi, Elizabeth Deweerd, Jennifer Mitchel and Julie Richardson, who have served as sounding boards for my ideas both good and bad, and for looking over drafts of my writing, in varying degrees of quality and giving great input. Of particular mention are Celinda, who has allowed me to vent all the day-to-day frustrations in the lab, and Jan, who has cheerfully helped when and technical issues with computers or microscopes have arisen and taught me all the tricks to microscopy when I first arrived at Brown. I would especially like to thank Liane Livi and Elke Bremus-Koebberling, who gave

me sound advice when I needed it, and who encouraged and challenged me scientifically to be as rigorous and meticulous as they.

The undergraduate students who have worked directly with me have been of tremendous help: Jeffrey Liu, Elise Cheng, Julie Richardson, Matthew Finn, Jesse Thon, Jillian Harrison, Beverly See. Thank you, in particular for their conscientiousness and responsiveness to all aspects of experimental work and teamwork. I hope that they have gotten as much out of this research experience as I have.

I would also like to thank my past mentors Andrew Cheung, YP Zhang, Frances Wong, Laura Poole-Warren, Ross Odell and Robert Nordon. Without their guidance and advice over the last ten years, I would not be where I am now, or who I am now scientifically.

I am thankful to all my friends and family, particularly my parents Daniel and Loretta Li, my sister Joyce Li, and my roommate Heike Milhench. Without their support, I would not be here today, and I would be a lot more embarrassed to still be a student at this point in my life.

Lastly, I would like to thank my fiancé Michael Sherback for his continuous support and encouragement through all the big obstacles and the little ones, even all the way from Ithaca, New York. Without his help and perspective, I would not be able to accomplish all of these things that have made my life as wonderful and as crazy as it has been.

Contents

List of Tables

List of Figures

Chapter 1

Introduction

Summary

Neural tissue engineering for applications in nerve repair is expanding beyond the traditional focus of cells seeded in biological matrices. In vitro platforms incorporating multiple cues that are spatially and temporally distinct, allow a more specific and quantitative examination of cellular response to their environments, (reviewed in Li and Hoffman-Kim, 2008b). In this research project, *in vitro* platforms featuring different guidance cues have been used to investigate how neurons integrate complex guidance information to make growth decisions. These guidance cues included molecular chemotropic and topographical cues that can direct and promote neurite outgrowth. No single guidance cue studied thus far has been able to elicit directed and functional nerve regeneration, which underscores the complexity of the underlying mechanisms of axon guidance. Further research progress therefore calls for increasingly well-controlled fabrication of precise multicue environments to study how axon guidance occurs, with the goal of informing strategies to overcome nerve injury.

The current research project dealt specifically with the integration of molecular gradients and topographical cues to study how these cues work individually and in combinations to influence neurite growth. To this end, microfabrication techniques such as soft lithography and

micropatterning of proteins have been used to fabricate devices that allow us to have precise control of substrates for the culture and analysis of neurons and glia. Using these newer techniques that offer greater levels of precision, quantification and spatiotemporal control of cells' microenvironments, we apply these studies to determining key parameters for nerve regeneration. These microfabrication techniques included microfluidics, microcontact printing and three-dimensional (3D) cell culture, employed to investigate the effects of: (1) individual and combinatorial adsorbed molecular gradients to approximate the environment of the post-injury central nervous system, (2) the global effects of 3D extracellular microstructure on neuronal culture and (3) selective directional protein coatings on microgrooved topographies to direct neuronal adhesion and neurite extension along and across grooves. Such an approach included analysis of different cellular mechanisms and allowed us to approach the goals of neurite growth promotion and direction in a systematic and multifactorial manner.

Neurite outgrowth on multimolecular gradients

Biomolecular gradients have been shown to play roles in axon guidance both in the developing nervous system and after injury. Particularly, graded expression of substrate bound guidance cues play a critical role in guiding nerve growth. Elucidation of this phenomenon by which growth cones integrate multiple molecular gradients requires the ability to expose neurons to biomolecular gradients over the relevant microscale dimension in a quantifiable and controllable manner. By generating a microenvironment using soft lithography and microfluidic techniques, linear concentration gradients of inhibitory chondroitin sulfate proteoglycans (CSPG) and/or permissive laminin-1 (LN) were generated as single-cue gradients, parallel double-cue gradients, and opposing double-cue gradients with varying slopes. Gradient parameters of interest were molecular concentration, absolute versus relative concentration change over the width of a growth cone and gradient direction. Overall, dorsal root ganglia neurons extended neurites toward regions of lower CSPG and higher LN concentrations. Molecular concentration and gradient direction had the largest effects on cellular adhesion and directional neurite outgrowth. Both absolute and relative concentration affected neurite

outgrowth direction on single cue gradients (Li et al., 2008). Gradient parameters for double cue gradients were optimized to maximize cellular adhesion and neurite outgrowth. These results represent an important step towards understanding how neurite growth is guided by complex microenvironments containing multiple molecular cues.

Addition of molecules to modulate the inhibition of CSPG or the response of the neurons to CSPG removed the ability of the substrate to direct neurite growth. Addition of chondroitinase ABC to enzymatically cleave chondroitin sulfate sugar chains appeared to be more inhibitory for cellular adhesion, with no change in neurite length, when compared to the untreated control. Addition of Y27632, a pharmacological inhibitor against Rho kinase, a molecule hypothesized to be in the signaling pathway for CSPG, did not yield a significant difference in cellular adhesion to the substrate but significantly increased neurite length.

Quantitative analysis of neurite outgrowth patterns using circular statistical methods

Neurite outgrowth direction was analyzed using circular statistical methods. Circular statistics is a subdiscipline of statistics that deals with directional data, such as angles, axes or rotations, as unit vectors. Angular data, such as neurite outgrowth angles are much better described and visualized using circular methods such as vector components and circular histograms which reflect the actual geometry of the experimental data. Many types of circular statistical methods have been developed. Analysis of different types of experimental neurite directional data and hypothesis testing using circular methods allowed us to determine the suitability of a number of developed circular statistical tests and develop a better tool for evaluating neurite outgrowth *in vitro*. One-sample uniformity tests were performed to describe the distribution of data, in this case the pattern of neurite outgrowth on substrates presenting protein gradients. Multisample tests were performed to compare different distributions of neurite outgrowth on different types of substrates. Appropriate statistical tests are data dependent, as theoretical statistical models have underlying assumptions that the

data need to comply with. A summary of circular statistical tests and their corresponding assumptions are used in different experimental and simulated examples and described in (Li and Hoffman-Kim, 2008a).

Neurite outgrowth in three-dimensional matrices

Interactions of neurons with the three-dimensional (3D) architecture of biological hydrogel matrices were studied in the context of genomic profiles, cellular morphology and material properties of the matrices. The influence of 3D culture on cells has been well studied, but matrices studied commonly incorporate multiple components that are known to affect cell growth. In this project, the specific differences in gene expression and morphology of neurons cultured in 2D versus 3D were investigated. Material properties are known to have direct effects on cell culture, and matrices were characterized with the description of mechanical properties and microstructural properties. SH-SY5Y neuroblastoma cells responded to geometry by differentially regulating cell spreading and genes associated with actin in similar patterns for both collagen I and Matrigel. We observed that neurite outgrowth and the expression of the gene encoding for neurofilament varied with the type of material, where fibrillar structure and high stiffness increased neurite outgrowth (Li et al., 2007). These results suggest complex cell–material interactions in 3D, in which the dimension of the culture material influences gene expression and cell spreading and the structural and mechanical properties of the culture material influence gene expression and neurite outgrowth.

Schwann cell growth on selectively coated microgrooved topographies

Topography has been shown to guide axon growth through contact guidance mechanisms. Interactions of cells with a microenvironment that presents both protein tracks and microgrooves allow us to present two directional guidance cues that act via different mechanisms, to investigate the synergy or hierarchy of these classes of guidance cues. Permissive

LN or inhibitory CSPG stripes were adsorbed onto grooved substrates via microcontact printing. Selected surfaces were coated: plateaus, walls and grooves or the total substrate surface. Patterns of adsorbed proteins were further presented either aligned or orthogonal to the underlying groove direction. Schwann cell "bridging" morphology was studied, where cellular processes supported a cell across a microgroove (groove-plateau-depth dimension: 50-70-50µm) with no underlying support (Goldner et al., 2006). Selective coatings of substrates yielded Schwann cell bridges of different morphologies. Substrates with total or plateau coatings supported predominantly bridges on the plateau level, while groove-coated substrates supported bridges that anchored on groove walls. Schwann cell motility and dynamics during the bridging process were studied using timelapse microscopy and cell soma were tracked through focal planes along the z-axis. Schwann cells showed a large variation in motility and trajectory during the bridging process. These results suggest that both molecular and topographical cues can direct Schwann cell adhesion and process formation, may act in a synergistic manner to guide cellular responses, and that the interactions between the Schwann cells and their microenvironment are complex and dynamic.

Conclusions and summary of major findings

The results in this thesis suggest that spatial patterning of molecular guidance cues and physical cues such as topography and microstructure can play a large role in promoting neuronal adhesion and neurite growth in a directed manner to overcome inhibition at the glial scar. Circular statistical methods have also been applied in the neuroscience field to better describe and quantify neurite behavior *in vitro*.

The major findings in this project are: concentration gradients of LN and CSPG, two molecules found in the glial scar, are able to elicit directional neurite growth towards the areas of higher LN and lower CSPG concentration, in single cue gradients as well as double cue opposing gradients. This effect was not seen on uniformly coated LN substrates or double cue parallel gradients. Gradient parameters of molecular concentration and gradient direction have large effects on cellular adhesion and neurite outgrowth.

Topography and architecture affected neuronal gene expression and morphology, which differed in 2D versus 3D cultures, and in different biomatrices. Of the 1766 genes that were differentially regulated due to differences in geometry, gene expression of ornithine decarboxylase, midkine, important for metabolism and signaling respectively were up-regulated while gene expression for talin 1, filaminin A, actinin1 α1, fibronectin 1, collagen type III α1, important for cytoskeleton and extracellular matrix were down-regulated. Collagen I and Matrigel had different physical properties such as elasticity, microstructure and porosity, which induced changes in neurite outgrowth potential. Microgrooved topography and molecular cues were observed to affect Schwann cell cultures. Laminin is well known to be highly permissive for Schwann cell alignment and growth, and appeared to be necessary for anchorage of processes on plateau surfaces for the formation of bridges.

Taken together, these results suggest that specific presentation of guidance cues can elicit specific neuronal and glial responses. Interactions between neurons and their microenvironments are complex, but using *in vitro* platforms that can present controlled spatial cues and quantitative analysis of the resulting biological response can provide detailed information on how guidance cues act.

References

Goldner JS, Bruder JM, Li G, Gazzola D, Hoffman-Kim D. Neurite bridging across micropatterned grooves. Biomaterials, 2006; 27: 460-72.

Li G, Liu J, Hoffman-Kim D. Multi-Molecular Gradients of Permissive and Inhibitory Cues Direct Neurite Outgrowth. Annals of Biomedical Engineering, 2008; in press.

Li GN, Hoffman-Kim D. Evaluation of neurite outgrowth using a novel application of circular analysis. Journal of Neuroscience Methods, 2008a; submitted.

Li GN, Hoffman-Kim D. Tissue-Engineered Platforms of Axon Guidance. Tissue Engineering Part B: Reviews, 2008b; 14: 33-51.

Li GN, Livi LL, Gourd CM, Deweerd ES, Hoffman-Kim D. Genomic and morphological changes of neuroblastoma cells in response to three-dimensional matrices. Tissue Eng, 2007; 13: 1035-47.

Specific Aims

Neurons in development and post injury are in a complex environment with a myriad of cues which taken together, is usually portrayed as a global "permissive" or "inhibitory" environment. Describing the net overall state of the cellular environment ignores much of the detail and simplifies much of the complexity that is present at the local level. Our long term goal is to elucidate the cellular and molecular mechanisms that underlie axon guidance decisions, and to then use this knowledge to build systems that can direct and promote appropriate axonal growth. Our working hypothesis is that neurons can sense multiple cues in a complex environment and respond by integrating their competing, synergistic or balancing effects. To test this hypothesis I propose the following specific aims:

Aim 1. Determine the optimal gradient parameters for maximal and directional neurite growth on multimolecular gradients over 24 hours.

The presentation of molecular cues *in vivo* is highly complex. In development and in the post injury environment of the central nervous system, combinations of both permissive and inhibitory cues are presented to a growth cone in its immediate microenvironment, either simultaneously, with distinct borders or in a gradient. Hence it is important to understand how these cues are integrated by the growth cone. Important factors to investigate are: absolute and relative concentration changes, relative gradient directions, and gradient shape. By varying the slope (slope) and relative direction of permissive (laminin) and inhibitory (chondroitin sulfate proteoglycans) protein gradients, we can a) determine the effects of

the protein gradients individually and in combination, b) precisely control the absolute and relative concentration change and c) control the relative directions of the gradients, to quantify the effects of these gradient parameters on differential neuron adhesion and directional neurite outgrowth using circular statistical methods.

Aim 2. Determine the role of geometry and microstructure of three-dimensional microenvironments on changes in genomic profiles and morphologies of neuroblastoma cultures.

Three-dimensional (3D) cell culture has been shown to have differential effects on a wide range of cell functions including proliferation, migration, metabolism and growth. It is important to characterize the changes that occur within the cell and understand how physical cues such as topography and architecture may influence these changes. By investigating changes in global gene expression profiles and morphologies of neurons using DNA microarray technology and microscopy techniques, we aim to correlate neuronal growth patterns with physical parameters of their 3D microenvironment.

Aim 3. Determine the role of protein micropattterns and cell type on the formation of cellular bridges .

The phenomenon of cellular bridging, an event where a process extends from one plateau to another on a grooved substrate with no underlying support (1), allows us to study a specific influence of contact guidance and tension generation. Using microfabrication techniques, we will fabricate platforms that will incorporate topographical cues with varied micropatterns of substrate bound molecular cues which will allow testing of the role of anchorage in the formation of cellular bridges. We hypothesize that sharp laminin coated surfaces on distal plateaus are necessary for tension generation required for bridging. Using timelapse microscopy to study dorsal root ganglia and Schwann cell motility under different phases of

bridge formation, we can characterize stereotypic Schwann cell trajectories and model the forces required for bridging with inputs taken from experimental data.

Relevance

Traumatic injury to the spinal cord often results in irreversible loss of function because nerves of the central nervous system (CNS) do not regenerate spontaneously. Describing the net overall state of the cellular environment ignores much of the detail and simplifies much of the complexity that is present at the local level. Experimental research using traditional biological techniques has provided valuable information regarding the neuronal response to individual guidance cues. However, the local environment that growing nerves face is inherently complex and contains a rich mixture of cues whose collective influence on growing nerves is not completely understood. Tissue engineering techniques have been employed by biomedical engineers and neuroscientists to model the complex *in vivo* environment of the nervous system as a means to isolate and study the specific interactions of these cues with the neurons on which they act. Our long term goal is to elucidate the cellular and molecular mechanisms that underlie axon guidance decisions, and to then use this knowledge to build systems that can direct and promote appropriate axonal growth. Our working hypothesis is that neurons can sense multiple cues in a complex environment and respond by integrating their competing, synergistic or balancing effects.

1.1 Background and significance

Historically, tissue engineering strategies have been used in efforts to develop therapies for peripheral nerve and spinal cord injury, combining biomaterials, cell therapy, and drug delivery approaches (Chalfoun et al., 2006; Fry, 2001; Lavik and Langer, 2004; Schmidt and Leach, 2003; Zhang et al., 2005a). Strategies for nervous system repair include preventing cell death by delivering anti-inflammatory agents and neuroprotective agents, and also promoting axonal growth to appropriate targets. Both the intrinsic growth capacity of cells

and the extracellular environment contribute to the ability for axon regeneration. Manipulating the cells' local microenvironment has been a particular focus of much research, from nerve grafts to engineered constructs. Regenerative repair in the peripheral nervous system (PNS) is thought to be possible due to the presence of growth-promoting cues provided by supportive glia (i.e., Schwann cells; SCs), macrophages and monocytes. More serious injuries to the PNS require surgical intervention, most commonly autologous nerve grafts (reviewed in (Fawcett and Keynes, 1990; Meek and Coert, 2002). Regenerative capacity of the central nervous system (CNS) is much reduced due to the inhibitory post-injury environment comprised of degenerating myelin and the glial scar, formed by hypertrophic reactive astrocytes. Similar transplantation strategies for CNS injuries using embryonic spinal cord (McDonald et al., 1999) or peripheral nerve tissue have met with limited success (reviewed in (Lakatos and Franklin, 2002)). The conventional paradigm of tissue engineering in which cells and scaffold materials are combined to replace or regenerate diseased or injured tissue, initially seemed particularly applicable to the problems of nerve injury. However, successful nerve regeneration with complex, precise connections has been found to require more than the substitution of engineered tissue for injured tissue. A consensus has emerged that it will ultimately require the coordinated presentation of multiple permissive signals, to be incorporated into tissue engineered biomaterial platforms designed to promote regrowth.

1.2 Challenges to spinal cord repair

Nerves fail to regenerate after spinal cord injury and current medical technology is unable to effectively manipulate the process of nerve regeneration. This research seeks to contribute to this process by quantifying how guidance cues both individually and in combination promote axon growth in an inhibitory environment. Spinal cord injury affects 250,000 Americans with 11,000 new injuries occurring each year. To date, there is still a critical gap in the knowledge base that informs strategies to provide growth-promoting cues to injured neurons.

When a nerve is injured, a major cause of the failure of axon regeneration in the CNS is the inhibitory nature of the glial environment. Damage to CNS axons will always produce

a glial scar, where reactive astrocytes hyperproliferate, oligodendrocytes are injured and myelin degenerates to form a mechanical and chemical barrier to axon regrowth. The area over which axon regeneration must occur to regain function, falls inevitably over a developing or established glial scar.

Hence understanding the mechanisms underlying axon guidance by multiple cues is a critical aspect of nerve regeneration, and one that can best be addressed using tissue engineering approaches. Evans (Gregory, 2001) has reviewed the strategies for traditional tissue-engineered constructs for nerve repair by component: scaffolds, support cells, growth factors and extracellular matrix. Scaffolds are biomaterials-based and can be biological or synthetic (Flaim et al., 2005). Support cells include glial cells of both the central and peripheral nervous system, neural progenitor cells (NPCs) and cells genetically modified to secrete growth promoting molecules (Chen et al., 2005; Keilhoff et al., 2006; Thompson and Buettner, 2006). Growth factors can improve neuronal viability and increase neurite initiation and outgrowth. Extracellular matrix can increase cellular adhesion, migration and neurite initiation and extension. Incorporation of these permissive molecules is one way of promoting axogenesis and neurite growth.

1.3 Cues from developmental neurobiology

Axon guidance has been a topic of study in neuroscience for many decades, both in developmental neurobiology and in nerve regeneration, and many cues have been identified that influence axon pathfinding. A number of these guidance cues are soluble factors such as ephrins, netrins and semaphorins (Chilton, 2006; David and Lacroix, 2003; Mueller, 1999; Raivich and Makwana, 2007; Serini and Bussolino, 2004). Studies have identified different mechanisms of action that include axon guidance such as permissive, inhibitory, outgrowth promoting, outgrowth suppressing, chemoattractive and chemorepulsive activities (Figure 1.1 (Baier and Bonhoeffer, 1994)). Further, some molecules such as netrin-1 and Sema3A have bifunctional roles that can repel some growth cones while simultaneously attracting others which adds to the flexibility of axon guidance produced in the developing nervous system

(Colamarino and Tessier-Lavigne, 1995; Polleux et al., 2000). Other categories of guidance cues include bound factors that guide through neuron-matrix interactions (Daniel M. Suter, 2000; Derek N. Adams, 2005; Dertinger et al., 2002b; McFarlane, 2003), topographical cues that influence nerve growth by contact guidance (Cai et al., 2005; Dowell-Mesfin et al., 2004; Goldner et al., 2006; Mahoney et al., 2005; Manwaring et al., 2004; Walsh et al., 2005) and electrical cues that affect the rate and direction of nerve growth (McCaig et al., 2002; Patel and Poo, 1982; Schmidt et al., 1997).

From the developing nervous system, guidance mechanisms have been observed from the process of the formation of topographic maps that provide a means for neurons to reach their target region and distribute in an orderly, stereotypical arrangement within these regions. By studying the factors that give rise to such precise and ordered connections that require the recognition of particular subsets of target regions, one can gain insight on how to reproduce such precision in a post-injury environment. To reach their targets, axons can be influenced by far-reaching, diffusible chemotropic molecules (Goodhill, 1997), reviewed in (Goodman, 1996). Further mechanisms exist to guide axons within the target may include target-derived growth factors with much shorter range guidance that may induce axonal branching (Bastmeyer and O'Leary, 1996). Several mechanisms have also been proposed that allow for recognition of specific targets, including type specificity, positional specificity or chemospecificity. Chemospecificity has been of particular interest and has been widely studied, as surgical techniques to move target areas have shown that axons continue to project to their preferred target regions. On example is the retinotectal system, where retinal axons have been observed to recognize different parts of the tectum, independent of the path to the tectum or if the location of the tectum has moved (Fujisawa, 1981; Hope et al., 1976). These observations have suggested underlying molecular mechanisms that include the use of molecular gradients to build this topographical mapping phenomenon.

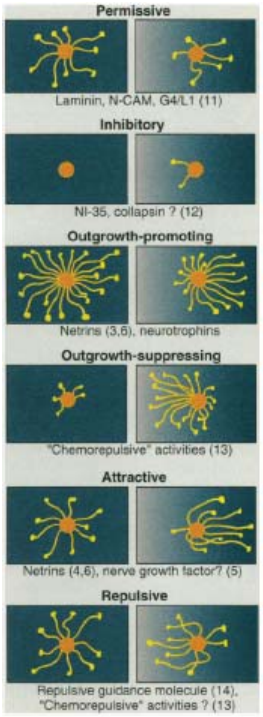

Figure 1.1: Mechanisms of action of molecular guidance cues. (Baier and Bonhoeffer, 1994)

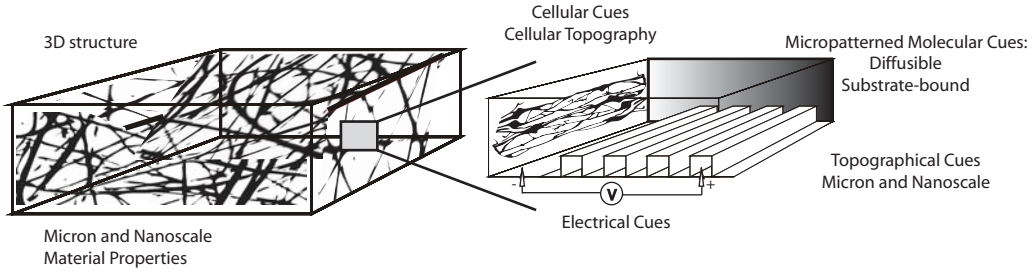

Figure 1.2: Tissue engineered platforms of axon guidance.

1.4 In vitro biomaterials platforms to study effects of guidance cues

Tissue engineering approaches can be used to create more *in vivo*-like platforms for studies of axon guidance, because they allow the generation of precisely controlled microenvironments that mimic specific features of the local *in vivo* environment. These platforms can incorporate three dimensions, cocultures of different cell types and defined presentation of molecules, in order to study key neuronal functions. One particular advantage of tissue engineered platforms of neural microenvironments is that they can present several types of cues in a synergistic or a competitive manner to elucidate their relative importance (Figure 1.2).

For the past few decades, micropatterned substrates have been used as tools to study and direct neurite outgrowth. Initially, molecular cues were patterned using simple techniques that allowed the investigation of guidance effects, but lacked reproducibility and precision on the cellular level, at the physiologically relevant micron scale. With the implementation of microlithography adapted from the microelectronics industry (Connolly, 1994; Folch and Toner, 2000a), patterned features of proteins and topographies could produce polymer

substrates for cell culture using techniques such as soft lithography and rapid prototyping (reviewed by (Li et al., 2003). More recently, laser ablation has been used to fabricate polymer substrates with diverse geometries. High energy laser pulses can be used to remove material in specific geometries to create microstructures on a surface with the size range <15um, which then serve as substrates for cell culture (reviewed by (Folch and Toner, 2000b).

Microfluidic channels are another method of producing substrates with requisite micropatterns to study axon guidance and neurite growth. These channels allow for fabrication of concentration gradients by diffusive mixing under laminar flow conditions. Laminar flow is generated in microchannels on the order of 50um at low flow rates controlled by a syringe pump. This is due to the low Reynolds number achieved by the slow flow and the small dimensions. The Reynolds number is the ratio of inertial forces to the viscous forces acting on a small unit of fluid, calculated by: $Re = \frac{\rho U^2 V}{\mu U S} = \frac{\rho U L}{\mu}$ where μ =viscosity =$0.01\frac{g}{cm*s}$, ρ = density = $1\frac{g}{cm^3}$, U = average flow rate = 1 $\frac{cm}{s}$, L = characteristic linear dimension = $\frac{V}{S}$, V =volume, S =surface area of walls.

For the devices in this study, flow rate is held at 1cm/s, such that Re<1. The surfaces of constant flow speed are smooth and random fluctuations of flow in time are absent so that when multiple streams of different proteins are present, adjacent streams remain chemically distinct except for diffusive mixing at their interface (Whitesides, Jun2001,). Due to this feature, soluble gradients can be formed simply by serial dilution of adjacent streams (Dertinger et al., 2002a; Dertinger et al., 2001; Jeon et al., 2002; Lin et al., 2004). Grooved microchannels have been studied for inducing turbulent or chaotic flow, particularly herringboned grooves that have rotated oblique angles (Stroock et al., 2002a; Stroock et al., 2002b). However, simulations varying groove aspect ratio (α), using computation fluid dynamics programs have shown that at low groove aspect ratios (α=0.05), there is no significant irregularity in flow, showing no evidence for chaotic mixing, and at higher groove aspect ratio (α=0.3), there was a more jumbled flow pattern but did not indicate chaotic mixing (Wang et al., 2003).

1.5 Molecular cues

The presentation of molecular cues *in vivo* is highly complex. In development and in the post injury environment of the CNS, combinations of both permissive and inhibitory cues are presented to a growth cone in its immediate microenvironment, either simultaneously, with distinct borders or in a gradient. The complexity of the local post-injury CNS environment has motivated the development of *in vitro* models of the glial scar, which have largely focused on patterning the chemical cues present, particularly permissive laminins (LN) and inhibitory chondroitin sulfate proteoglycans (CSPGs (Le Beau et al., 1995; Tom et al., 2004)). The use of anisotropy in presenting chemical cues either through gradients or stripes to provide directional bias has been largely successful *in vitro*. Recent advances in microfabrication techniques in microfluidics and microcontact printing have increased our capacity to present directional information on a biologically relevant scale. Optimal dimensions of features range from tens to hundreds of microns (Dertinger et al., 2002b; Song et al., 2006; Yeung et al., 2001), and can be used in combination with other types of guidance cues for synergy in a more complex microenvironment.

1.5.1 Adhesion molecules and Extracellular matrix

Micropatterns of molecular cues are used to direct neuronal growth and cell adhesion (Cornish et al., 2002; Offenhausser et al., 2007; Oliva et al., 2003). Neurons from rat brain stem and cortices preferentially adhere to regions coated with permissive guidance cues such as LN and neurite outgrowth follows the micropatterned tracks (Vogt et al., 2005; Yeung et al., 2001). Cellular adhesion and neurite extension onto underlying line or grid patterned microcontact printed substrates have been observed in both dissociated neurons (Vogt et al., 2005) and brain slices (Yeung et al., 2001). Optimal dimensions of nodes for neuronal adhesion for cells were found to be in the range of 14-20µm (Yeung et al., 2001). DRG neurite attachment was found to be dependent on FN stripe width, with a minimum width of ˜30µm required for cell attachment and neurite extension (Zhang et al., 2005b). In order to direct neurite growth to specific patterns of

the substrate, several micropatterning techniques have been used, including "inking" elastomeric stamps and using adsorption to transfer patterns (Yang et al., 2005b), covalent binding of "inked" elastomeric stamps using 1-ethyl-3-(3-dimethylaminopropyl) carbodiimide/N-hydroxysuccinimide (EDC/NHS) chemistry, photoimmobilization of molecules using polyallylamine conjugation to N-4-(azidobenzoyloxy)succinimide) (PAA-azido chemistry) (Gomez et al., 2007a; Gomez and Schmidt, 2007; Luo and Shoichet, 2004) and other methods of protein immobilization using commercially available heterobifunctional crosslinkers (Zhang et al., 2005b). Song et al. used photolithography and EDC/NHS chemistry to micropattern poly-L-lysine (pLL) and/or LN on regions of conductive polypyrrole (pPy). Hippocampal neurons adhered and extended neurites only on the pattern of pLL or LN, demonstrating a method for fabricating micropatterns of molecular guidance cues in combination with conductive polymers. More recently, neurite outgrowth assays have also focused on peptides that correspond to locations of cell binding sites on permissive extracellular molecules such as LN or fibronectin (FN). These key peptides include: Arg-Gly-Asp (RGD) (Tashiro et al., 1991), Ile-Lys-Val-Ala-Val (IKVAV) (Tashiro et al., 1989) and Tyr-Ile-Gly-Ser-Arg (YIGSR) (Graf et al., 1987; Massia et al., 1993) which have been shown to mediate cell attachment, spreading, migration and neurite outgrowth; they have been incorporated into assays evaluating the effect of molecular cues on axon guidance, the results of which will be described in a later section. Micropatterned cues allow highly controlled directional guidance of neuronal adhesion and axonal growth.

Incorporation of extracellular matrix molecules in a 3D matrix has also been investigated (Cao and Shoichet, 2002; Dodla and Bellamkonda, 2006; Yu and Bellamkonda, 2001). Neuroblastoma cells showed increased cell adhesion on alginate gels that were coated with LN or covalently linked to YIGSR peptide, and showed increased neurite number and length on YIGSR peptide linked gels in a ligand density dependent manner (Dhoot et al., 2004). Luo and Shoichet (Luo and Shoichet, 2004) have demonstrated that DRG neurites will grow preferentially in channels modified to present GRGDS peptide in a 3D agarose gel. Dodla and Bellamkonda (Dodla and Bellamkonda, 2006) have shown that concentration gradients of photo-immobilized LN-1 in 3D agarose gels can direct DRG neurite growth in the direc-

tion of higher LN-1 concentration. Further, gels presenting concentration gradients of LN-1 promote faster neurite extension than gels presenting isotropic LN-1 concentrations, which implies that patterning of chemical cues may be a separate parameter to be optimized within the complexity of the 3D environment. Embryonic cortical neurons have been challenged with choices between competing growth options of poly-D-lysine (PDL), 3D Matrigel and microtopography. When presented with 2D PDL adsorbed surfaces and intermediate layer of 3D-gelled Matrigel, neurons appeared to prefer PDL-coated 2D surfaces. When presented with 2D PDL adsorbed surfaces, 3D Matrigel and grooved topography (3.5-15µm), neurites preferred to extend into the 3D gel layer of Matrigel rather than along PDL surfaces (walls and grooves) of the topographical substrates, differing from the result of neurite turning into grooves in the absence of Matrigel. Growth cones therefore make growth decisions that balance permissiveness and obstacles in topography and 3D architecture, resulting in directional growth to minimize turning while remaining on the most permissive substrate available (Li and Folch, 2005).

1.5.2 Molecular concentration gradients

Axon guidance by concentration gradients of soluble guidance cues has been studied extensively *in vitro*. Trophic factors such as nerve growth factor (NGF), brain derived neurotrophic factor (BDNF), insulin-like growth factor (IGF-1, IGF-2) and fibroblast growth factor (FGF) have been found to elicit turning of growth cones toward the molecule of interest (Boyd and Gordon, 2003; Jones et al., 2003; Kato and Lindsay, 1994). Gene therapy experiments using lentiviral vectors expressing NT-3 (Taylor et al., 2006) have shown that increased growth through and beyond the inhibitory glial scar region is achievable, but longer distance growth was not obtainable with the trophic stimulus alone, as the presence of a continuing growth factor gradient beyond the lesion did not stimulate growth into those areas.

Studies of molecular cues have found that chemotropic and extracellular matrix (ECM) guidance cues attract or repel growth cones over a large distance range (Dickson, 2002; Rosoff et

al., 2005; Rosoff et al., 2004a; Tessier-Lavigne and Goodman, 1996). Micropatterned molecular cues have also been studied, particularly protein gradients to orient and direct neurite growth. Nerve growth factor (NGF) is a chemoattractive diffusible factor that is presented in a gradient as a function of distance from the source and is able to elicit directed neurite outgrowth and growth cone turning *in vitro* (Cao and Shoichet, 2001). Graded expression of matrix molecules have been found *in vivo* in development such as the Eph/Ephrin system in the developing retinotectal system and proteoglycans in the post injury glial scar environment where CSPG and keratin sulfate proteoglycans (KSPG) are increasingly expressed approaching the lesion site (reviewed by (Silver and Miller, 2004)). The mechanism of axonal response to protein gradients is not well understood. LN has been suggested to guide neurites in a manner similar to chemotaxis, where the growth cone machinery measures local differences in LN concentration and directs growth toward the direction of higher levels (Devreotes and Zigmond, 1988; Kindt and Lander, 1995). Experimental work has suggested that axons could be guided by a wide range of parameters including the absolute molecular concentration, the sign, direction, and slope of the gradient (Baier and Bonhoeffer, 1992; Britland and McCaig, 1996; Isbister et al., 2003; Rosentreter et al., 1998; Song et al., 1998).

Cells are affected by their local environment and respond to chemical and mechanical stimuli in adhesion and migration processes. In the specialized case of axon guidance, the ability of a growth cone to respond to such guidance cues using these underlying mechanisms has been studied extensively for soluble and matrix bound factors. Sperry proposed the chemoattraction model as the mechanism of long range axon guidance during development (Sperry, 1963); Carter proposed a theoretical model for haptotaxis and cell motility (Carter, 1967), and contact guidance was proposed to be the mechanism for aligning axons to collagen fibrils (Ebendal, 1976). Mathematical models of axon guidance have been proposed that simulate the simple case of any attractive or repulsive cue presented to a growth cone (Buettner, 1994; Maskery et al., 2004). These models are generally phenomenological, and contain a deterministic domain and a stochastic domain, where the deterministic domain refers to the cellular response to external cues, and the stochastic regime reflects the randomness observed in growth cone "sampling" seen using timelapse microscopy, and the inherent instability of

microtubules (reviewed by Maskery and Shinbrot, 2005).

Mathematical models suggest that fractional concentrations of soluble gradients must be >2% to be sensed by the growth cone, whereas fractional concentrations of substrate bound gradients must be >10%, predicting that growth cones are more sensitive to soluble gradients. The maximum guidance range of gradients have been calculated to be 1mm for soluble gradients and 1cm for substrate bound gradients for either the absolute concentration change case or the fractional concentration change case (Goodhill, 1998; Goodhill and Baier, 1998; Goodhill et al., 2004; Goodhill and Urbach, 1999; Goodhill and Baier, 1998). In order to generate gradients *in vitro* with the enough precision to change the concentration <10% over the width of a growth cone (10-20μm), microfluidic techniques have been highly useful, and reviewed in Keenan and Folch (Keenan and Folch, 2008), with the perspecitve of how the technology of making concentration gradients over the microscale has developed.

Bellamkonda (Bellamkonda, 2006) has discussed the concept of anisotropy in structural and molecular contexts of scaffold design, where anisotropy may facilitate faster and more robust regeneration by exploiting the sensitivity of the growth cone to elicit directional growth. For molecular cues, anisotropy translates to concentration gradients across the dimensions of a growth cone. Concentration gradients of soluble neurotrophic factors have been widely studied as they can be easily generated through diffusion (Rosoff et al., 2004b), and they have been shown to contribute to the process of chemotaxis. Concentration gradients of substrate bound molecules have also been generated using techniques such as micropatterning(Cornish et al., 2002), microfluidics, and self-assembly of monolayers to covalently bind peptides (Derek N. Adams, 2005; Dertinger et al., 2002b). von Philipsborn et al. (von Philipsborn et al., 2006) showed guidance of retinal ganglia growth cones by discontinuous ephrinA5 gradients generated by microcontact printing. Neurite stop decisions depended on gradient slope as well as the concentration of ephrinA5 present locally, where a decreasing slope and lower ephrinA5 concentrations allowed further growth onto the gradient area. Adams et al. (Derek N. Adams, 2005) demonstrated guidance of dorsal root ganglia (DRG) explants by an increasing concentration gradient generated by photo-immobilization of the IKVAV peptide. On these substrates, growth cones were able to turn up a gradient with a 10-25%

fractional difference in IKVAV concentration over 30µm. Li et al. (Li et al., 2007a) have shown changes in neuronal response over a larger range of fractional concentration difference; a 4% fractional difference in LN concentration over 25µm resulted in fewer DRG neurites oriented toward higher LN concentration, whereas a 100% fractional concentration change over 25µm resulted in more neurites oriented toward the higher LN concentration. Multi-molecular opposing gradients fabricated to present high concentrations of LN intermixed with low concentrations of CSPG were able to direct DRG neurite orientation in a similar manner as single-cue LN gradients, guiding neurite outgrowth in the direction of higher LN and lower CSPG concentrations.

1.6 Topographical cues

Topographical cues influence nerve growth and regeneration by contact guidance, and can be combined with adhesion molecules that also play a role in contact guidance. Neurons have the capacity to respond to topographical features in their microenvironments, and they have been shown to adhere, migrate, and orient their axons to navigate surface features such as grooves in substrates in both the micro- and nanoscales. Using microfabrication techniques such as photolithography and soft lithography, topographic guidance of neurite outgrowth has been explored *in vitro* with culture substrates that contain well-defined micropatterned features.

1.6.1 Microgrooved topographies and cellular morphologies

Repeating rectangular microgrooves have been extensively studied to direct neurite growth and alignment along a particular axis. Mahoney et al. (Mahoney et al., 2005) studied the effects of microchannels of 20-60 µm width and 11 µm depth on PC12 cell cultures. Neurites were directed along the axis of the grooves, with microchannels of 20-30µm most effective at neurite direction. Polypropylene filaments have been found to direct DRG neurites and SCs from DRG explants along the long axis of the filaments tested with an optimal filament

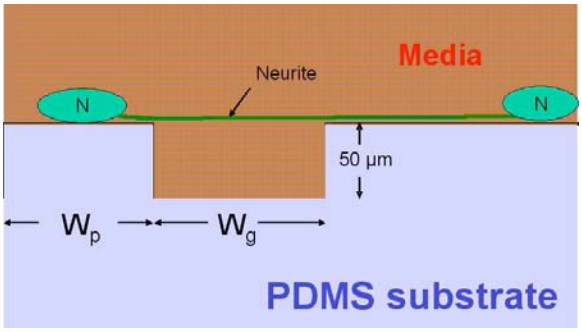

Figure 1.3: Schematic of cellular bridge where the cellular processes span across grooves with no underlying support.
Illustration by Jan Bruder.

diameter of 5µm. The addition of FN and LN coatings on the filaments increased the maximal neurite lengths as compared to uncoated controls, and interestingly, resulted in neurite outgrowth that preceded migrating SCs (Wen and Tresco, 2006).

Topographical cues have also generated unexpected neurite morphologies. Goldner et al. (Goldner et al., 2006) have observed the phenomenon of neurite "bridging" where a subset of DRG neurites can span grooves coated with LN varying from 30-200µm width and 50µm depth with no underlying support (Figure 1.3). Several cell types including hippocampal neurons, rat B104 neuroblastoma cell and SCs were all shown to exhibit the bridging morphology. Neurites were observed to climb up the groove walls to generate such bridges, suggesting complex cell dynamics in response to micro-topography.

Nanotopography to promote cell growth has been a subject of interest for many biological applications and for axon guidance in particular. Nanotopography has been presented to cells *in vitro* via nanoscale etches into silicon wafers (Fan et al., 2002a; Fan et al., 2002b), nanofibers on the surfaces of scaffolds (Ahmed et al., 2006; Yang et al., 2005a) and carbon nanotubes (CNT) on flat surfaces (Lovat et al., 2005; Nguyen-Vu et al., 2006; Waid et al., 2004; Wang et al., 2006). Methods of fabrication have been reviewed in Norman and Desai(Norman and Desai, 2006), including a list of ordered versus unordered nanotopographies that can be generated using methods such as chemical etching with hydrofluoric acid to generate unordered nanoscale grooves, and more controllable electrospinning with well-studied polymeric materials such as PLA and PLGA which may be aligned or unaligned.

Neuronal adhesion and viability on nanotopography have been most widely studied, and results vary depending on the type of nanoscale substrate presented. Chemical etching of silicon wafers found an optimal surface nano-roughness of 20-50nm to be the most permissive for attachment of primary neurons isolated from the substantia nigra (Fan et al., 2002a). Electrospun polyamide nanofibers with a median diameter of 180nm supported neuronal growth and covalently linked tenascin-C-derived peptides increased the neurite outgrowth of a number of CNS primary neurons including cerebellar granule, cerebral cortical, hippocampal, motor and DRG neurons, indicating that nanotopography may act synergistically with molecular cues to promote neurite growth (Ahmed et al., 2006). Nanofibrillar meshes presenting IKVAV peptides have also been fabricated using self assembly of amphiphilic peptides around cells in culture medium. These IKVAV linked nanofibers differentiated NPCs more rapidly than the addition of soluble IKVAV peptide or LN (Silva et al., 2004). Cellular responses to substrates presenting carbon nanotubes have been evaluated; hippocampal cells have been stimulated using CNT microelectrodes (Wang et al., 2006), PC12 neurite formation has been supported by 2% CNT containing polycarbonate urethane (Waid et al., 2004), and astrocytes have been shown to have decreased adhesion on CNT/polycarbonate urethane substrates and decreased alkaline phosphatase production on low surface energy nanophase fibers (McKenzie et al., 2004). Using nanoscale fabrication methods, it will be exciting to generate biomaterials platforms that study combinations of nanoscale guidance cues with other important cues such as electrical stimulation and molecular cues.

Neurons have the capacity to respond to topographical features in their microenvironments, and grooves have been a widely studied geometry. The progression of guidance cues from micro- to nanoscale resolution has shown that the guidance range encompasses both length scales and can affect cell functions from cell differentiation of NPCs to neurite morphology such as orientation, direction and length.

1.6.2 Dynamics of cell motility and process formation

A simple model (Equations 1.1 and 1.2) is adapted from the Langevin equation for Brownion motion describing fibroblast motility (Dunn and Brown, 1987) from (Buettner, 1994). This model was used to simulate a sharp border between a permissive and nonpermissive substrate, LN and albumin. So the assumption that the receptor-mediated interaction between the growth cone and the substrate requires a critical number of receptors bound to the permissive cue. Using these parameters, the model predicted that filopodial initiation follows a Poisson distribution, length follows an exponential probability density function and the rates of extension and retraction follow a linear relationship. Filopodia length and angle can be predicted by predicting x and y coordinates at time t (Equation 1.3 and predicting the filopodia initiation angle from x and y coordinates over time (Equation 1.4).

(Buettner, 1994)

$$\frac{dv}{dt} = -\beta v + n(t) \tag{1.1}$$

$$\beta = \frac{1}{\tau}; \alpha = \frac{2s^2}{\tau} \tag{1.2}$$

$$x_t = x_o + L\cos\theta, y_t = y_0 + L\sin\theta \tag{1.3}$$

$$x_0 = x_c + r_g(\theta)\cos\theta, y_0 = y_c + r_g(\theta)\sin\theta \tag{1.4}$$

where β = deterministic regime, determined experimentally from directional persistence time τ or root-mean-square speed s of filopodial movement,

and $n(t)$ =stochastic regime, which can be obtain from random Gaussian distribution.

1.7 Key signaling molecules involved in cell motility and process formation

Guidance cues exert differential effects through specific ligand-receptor complexes and various adaptors and mediators that converge on similar cytoskeletal proteins to modulate response. Rho family of GTPases are involved in actin assembly, particularly Cdc42, Rac and Rho. DRG neurons grown on patterned chemical substrates and topographical substrates both separately and in combination can be used to determine the precise roles of the Rho GTPases in transducing chemical and topographical cues into cytoskeletal reorganization. Cdc42 has been found to be involved in gradient sensing, Rac has been hypothesized to play a role in stabilization of actin filaments.

Cytoskeletal reorganization via RhoGTPases plays a role in neurite growth by regulating cell polarity and cell motility. Any external cue that results in a change in neurite behavior e.g. turning, extension or retraction, requires changes in the cytoskeleton. Recently, the family of Rho GTPases, molecular switches that regulate signal transduction pathways linking plasma membrane receptors to filamentous actin, have been shown to be highly involved in growth cone guidance and pathfinding, particularly in inhibitory environments like the glial scar and CSPG substrates (reviewed in Dergham et al., 2002; Etienne-Manneville and Hall, 2002; Luo, 2000). The Rho signaling pathway mediates neurite growth inhibition by a number of repulsive guidance cues, such as CSPGs and myelin (Dergham et al., 2002; Jain et al., 2004; Lehmann et al., 1999), plays a role in glial scar inhibition, and inhibition or inactivation of Rho is sufficient to stimulate axon regeneration in inhibitory environments (Dergham et al., 2002; Madura et al., 2004). Activation of Rac or Cdc42 promotes neurite formation and extension, while Rho activation induces growth cone collapse and neurite retraction through the assembly of contractile actin and myosin filaments (Govek et al., 2005; Hall, 1998). Cdc42 has been of particular interest as it promotes the formation of filopodia and plays a role in cell polarity in yeast, Saccharomyces cerevisiae, in addition to its role in promoting neurite outgrowth. Giniger has hypothesized a model for the roles of Rho family GTPases to each other. In Swiss 3T3 fibroblasts microinjection of active Rac or

Cdc42 leads to immediate changes in lamellipodia and filopodia respectively, and a delayed Rho-dependent change in stress fibers occurs. Rho GTPases may be a convergence point between multiple signal transduction pathways, as inhibition of these molecules have been found to cause a variety of effects (Giniger, 2002).

1.8 Combination of guidance cues on *in vitro* platforms to study interactions between cues

Growth cones are capable of integrating multiple cues simultaneously to make a net guidance decision. Recent studies have addressed the question of how growth cones interpret two or more guidance cues simultaneously. Guidance cues are highly conserved yet have diverse effects on cellular behavior. This suggests that the growth cone's capacity to integrate numerous recognition pathways as it grows allows it to respond to the intricate cues present in the CNS. Besides ligand diversity and response to single gradients, guidance integration can occur to allow combinations of receptors and ligands to yield differential effects (reviewed by (Yu and Bargmann, 2001)). Drosophila motoneuron growth cones can integrate semaphorin II and netrins (Winberg et al., 1998), and Xenopus spinal neurons show reversed growth cone turning when netrin-1 is applied singly or with Slit (Stein and Tessier-Lavigne, 2001), showing multiple instances when growth cones must integrate contrasting information to make a guidance decision. The hypothesized mechanism of this integration is that a summation of the cues occurs at the growth cone but the signal convergence point is unknown, whether it is at the level of the ligand-receptor complex or further downstream (Rose and Chiba, 1999). Growth cones can also integrate multiple types of guidance cues; Xenopus spinal cord neurons have been found to integrate both electrical and adhesive cues, where for most of the neurons, the galvanotropic cue was insufficient to reorient the alignment from LN tracks, but a subset of neurons responded to the electrical cue even in the presence of opposing LN guidance (Britland and McCaig, 1996). DRG neurons have been found to integrate adhesive cues and topographical cues, where alignment to grooves could be promoted with parallel LN tracks, and alignment could be pushed to the orthogonal direction from

grooves when orthogonal LN tracks were presented. This suggests that a hierarchy exists where adhesive cues are more influential than topographical or electrical cues, but that the growth cone can integrate directional information.

Combinations of defined topographical and molecular cues revealed synergies between cues. Gomez et al. (Gomez et al., 2007b) studied the combined effects of NGF and microtopography of microchannels on axon initiation/polarization and axon elongation of hippocampal neurons. When presented with microchannel substrates of 1-2µm widths and 400-800µm depths containing immobilized NGF on the surface, hippocampal neurons responded to the combination of molecular and topographical stimulation with the longest neurites. The observations that topography had a stronger effect on polarization but no effect on elongation suggested that both cues are required for maximal neurite growth (Gomez et al., 2007b; Gomez and Schmidt, 2007). Foley et al. (Foley et al., 2005) observed that neuritogenesis of PC12 cells cultured with sub-optimal concentrations of NGF in media, was modulated by topographic feature size where neuritogenesis was increased when cells were cultured on ridges of 70 and 250nm as compared to wider ridges (400-1900nm) and flat surfaces. Synergy between topography and adsorbed extracellular matrix molecules of LN also promoted neurite alignment and outgrowth onto microgrooves (Miller et al., 2002). DRGs cultured on substrates with groove depths of greater than 3 µm and groove widths of 10 µm in combination with 200µg/mL of LN showed maximal neurite outgrowth and alignment of up to 95%. Zhang et al. (Zhang et al., 2006) developed a hybrid template that combines topographical and molecular cues with channels of 5µm depth and 20-40µm width connecting to nodes of 50-100µm widths and pLL to achieve geometric control over neurite connections for the application of microelectronic circuits. Hippocampal neurites extended on pLL tracks and avoided regions where no pLL was present. Studies such as these facilitate the investigation of hierarchies and synergies between cues.

1.9 Three-dimensional environment and axon guidance

Comparisons of cellular growth in standard 2-dimensional (2D) monolayer cultures and 3-dimensional (3D) matrix cultures that more closely resemble *in vivo* environments have shown clear phenotypic differences. For example, previous studies have revealed differences in cell surface area, stress fiber distribution, cell migration, focal adhesions, neurite and growth cone dimensions, and protein and gene expression. Tissue engineering approaches have allowed the development of assay formats that include the third dimension as a controllable and defined parameter, and are used to elucidate cell-material interactions between neurons and their extracellular matrix. Three-dimensional matrices that have been explored include biologically based matrices such as alginate (Dhoot et al., 2004; Mosahebi et al., 2001; Novikova et al., 2006), collagen I (Cullen et al., 2007; Li et al., 2007b; Ma et al., 2004; O'Connor et al., 2001; O'Connor et al., 2000; Phillips et al., 2005; Willits and Skornia, 2004), Matrigel™ (Matrigel)(Li et al., 2007b; Novikova et al., 2006) and fibrin (Ju et al., 2007; Régis Pittier, 2005), as well as synthetic polymer based scaffolds such as poly lactide (PLA)(Bini et al., 2004; Ngo et al., 2003), poly lactide-co-glycolide (PLGA) and agarose (Dodla and Bellamkonda, 2006). Studies have characterized 3D matrices with regard to their chemical and mechanical properties and their ability to support neuronal growth. Collagen gels have been used successfully to differentiate neural stem cells (Ma et al., 2004) and NPCs (O'Connor et al., 2000) with FGF in the culture medium, and functional synapses have formed in the cultures (Ma et al., 2004). Addition of Matrigel to rat sympathetic neurons plated on pLL substrates has been shown to induce rapid axogenesis with corresponding changes in microtubule organization. Another aspect of differential regulation of neuronal cell culture in 3D can be reflected in the global gene expression of neurons. Li et al. (Li et al., 2007b) showed using microarray analysis that differentially regulated genes between 2D and 3D culture of SH-SY5Y neuroblastoma cells included those involved in cytoskeletal reorganization, extracellular matrix, metabolism and signaling. Gene expression trends were maintained over cultures in different matrices (collagen and Matrigel) but morphological differences in 2D and 3D cultures such as cell spreading and neurite growth appeared to be material-specific. The stiffer 3D matrix of collagen supported longer neurites than 2D collagen, whereas in

the softer Matrigel, neurons in 3D extended shorter neurites than neurons in 2D.

Physical and mechanical cues such as stiffness have been known to impact a multitude of cell functions such as adhesion, proliferation, migration, differentiation and morphology. Durotaxis has been observed in many cell types, including neurons (Georges and Janmey, 2005). Neurite extension both during development and after an injury requires mechanical interactions between growth cone and substrate. Parameters that have been shown to influence DRG neurite extension include: substrate mechanical properties (Balgude et al., 2001), ligand concentration (Schense and Hubbell, 2000) and geometry. Mechanical effects appear to be highly dependent on cell type and the range of moduli presented. Leach et al. (Leach et al., 2007) tested the NGF-dependent response of PC-12 cells on polyacrylamide substrates with varying stiffness, and by controlling the amount of FN present, kept the adhesive ligand concentration constant over the samples tested. The range of substrate stiffness tested (7-19kPa) spanned the physiological range as well as "very soft" and "very stiff" substrates. A threshold response was observed where the softest substrates supported fewer and shorter neurites, but above a threshold of ~100 Pa, longer and more branched neurites were observed regardless of increasing shear modulus of the substrate. Willits and Skornia (Willits and Skornia, 2004) studied the effects of mechanical stiffness on chick DRG neurons. By varying the concentration of collagen used to gel the matrix, varying stiffnesses (2.2-17Pa) were generated. After four days in culture, softer matrices resulted in longer neurite lengths. In this experimental setup, it is interesting to note that an increase in interfiber diameter corresponds with the decrease in mechanical stiffness and collagen concentration, a geometric constraint which may contribute to the observed cellular response. Analysis and modeling suggested complex non-linear cell-material interactions.

Mechanical stiffness has been found to influence other cell types, including astrocytes (Georges et al., 2006). On soft gels of polyacrylamide with a shear modulus of 200Pa, suppression of astrocyte growth has been observed in both monoculture and coculture experiments, with low attachment and spreading and disorganized F-actin. This behavior is in contrast with the growth of cortical neurons on the same soft substrates tested, where coculture experiments show a significantly higher proportion of cortical neurons versus astrocytes on the soft

over the hard (9kPa shear modulus) substrates (Georges et al., 2006). These studies point toward the development of materials tailored to support specific cell populations within the nervous system.

Combining 3D environments with molecular guidance cues for neurite outgrowth to study the effects of cues in a more *in vivo*-like environment is a logical extension of neuronal assay formats in 3D. Neurotrophic factors can be incorporated into 3D cultures by the addition of growth factors to culture medium(Deister and Schmidt, 2006), or in a more controlled manner by covalent linkages between the growth factor and the matrix (Cao and Shoichet, 2002; Kapur and Shoichet, 2003, 2004; Luo and Shoichet, 2004). Steepness of NGF gradients was found to attract DRG (Rosoff et al., 2004b) and PC12 (Kapur and Shoichet, 2004) neurite growth up the concentration gradient on collagen gels (Rosoff et al., 2004b) and poly(2-hydroxyethylmethacrylate)(Kapur and Shoichet, 2004) respectively. Cao and Shoichet (Cao and Shoichet, 2003) observed a synergistic effect on DRG outgrowth with NGF and NT-3 presented in 3D agarose. When NT-3 was applied individually, there was no directional growth. When the two growth factors were applied together, the guidance range of neurites towards higher concentrations of NGF and NT-3 exceeded the guidance range of an NGF gradient alone. Deister and Schmidt (Deister and Schmidt, 2006) adapted a DRG explant assay in a shallow collagen gel to study the combinations of neurotrophic factors in culture. After adding NGF, glial derived neurotrophic factor (GDNF) and ciliary neurotrophic factor (CNTF) individually and in combination, total neurite outgrowth and length were evaluated. The combination of three factors increased both neurite outgrowth and length over cultures containing individual factors at the optimal concentration, implying that interactions between neurotrophic factors can increase neuronal responsiveness in 3D.

1.10 Closing remarks

The progression of tissue engineering platforms from 2D to 3D has been widely noted. The capacity to integrate guidance cues of interest in a specific and controlled manner has enabled

researchers to add a layer of complexity to *in vitro* systems for axon guidance to more closely mimic the local *in vivo* environment while maintaining the ability for quantitative analysis.

Successful nerve growth requires the coordinated presentation of multiple cues, many of which have been incorporated individually into biomaterial platforms designed to promote regrowth. Quantitative data relating neurite extension to temporal and spatial combinations of molecular, cellular and geometric cues are not yet available. Consequently, current approaches to nerve regeneration lack design parameters to develop nerve guidance therapies. The experiments described in this proposal will allow us to determine these design parameters by 1) identifying and quantifying the threshold level of these cues that are necessary to elicit a response, 2) presenting molecules and unique geometries in combination *in vitro* to test if these combinations act synergistically or in hierarchy to enhance neurite outgrowth and 3) determining if the cytoskeletal pathways by which molecular cues and topographical cues are transduced work synergistically or competitively, by adding pharmacological inhibitors to disrupt or stabilize key cytoskeletal proteins. Each stage of our experiments will provide key data for a more complete and integrated understanding of the mechanisms underlying nerve injury and regeneration and look towards new strategies of overcoming the glial scar to gain functional recovery after spinal cord injury.

1.11 References

Ahmed I, Liu HY, Mamiya PC, Ponery AS, Babu AN, Weik T, Schindler M, Meiners S. Three-dimensional nanofibrillar surfaces covalently modified with tenascin-C-derived peptides enhance neuronal growth \emph{in vitro}. J Biomed Mater Res A, 2006; 76: 851-60.

Baier H, Bonhoeffer F. Attractive axon guidance molecules. Science, 1994; 265: 1541-2. Baier H, Bonhoeffer F. Axon guidance by gradients of a target-derived component. Science, 1992; 255: 472-5.

Balgude AP, Yu X, Szymanski A, Bellamkonda RV. Agarose gel stiffness determines rate of DRG neurite extension in 3D cultures. Biomaterials, 2001; 22: 1077-84.

Bastmeyer M, O'Leary DD. Dynamics of target recognition by interstitial axon branching along developing cortical axons. J Neurosci, 1996; 16: 1450-9.

Bellamkonda RV. Peripheral nerve regeneration: an opinion on channels, scaffolds and anisotropy. Biomaterials, 2006; 27: 3515-8.

Bini TB, Gao S, Xu X, Wang S, Ramakrishna S, Leong KW. Peripheral nerve regeneration by microbraided poly(L-lactide-<I>co</I>-glycolide) biodegradable polymer fibers. Journal of Biomedical Materials Research Part A, 2004; 68A: 286-95.

Boyd JG, Gordon T. Neurotrophic factors and their receptors in axonal regeneration and functional recovery after peripheral nerve injury. Mol Neurobiol, 2003; 27: 277-324.

Britland S, McCaig C. Embryonic Xenopus neurites integrate and respond to simultaneous electrical and adhesive guidance cues. Exp Cell Res, 1996; 226: 31-8.

Britland S, Perridge C, Denyer M, Morgan H, Curtis A, Wilkinson C. Morphogenetic guidance cues can interact synergistically and hierarchically in steering nerve cell growth. Experimental Biology Online, 1997; 1: 1.

Buettner HM. Nerve growth dynamics. Quantitative models for nerve development and regeneration. Ann N Y Acad Sci, 1994; 745: 210-21.

Cai J, Peng X, Nelson KD, Eberhart R, Smith GM. Permeable guidance channels containing microfilament scaffolds enhance axon growth and maturation. J Biomed Mater Res A, 2005; 75: 374-86.

Cao X, Shoichet MS. Defining the concentration gradient of nerve growth factor for guided neurite outgrowth. Neuroscience, 2001; 103: 831-40.

Cao X, Shoichet MS. Investigating the synergistic effect of combined neurotrophic factor concentration gradients to guide axonal growth. Neuroscience, 2003; 122: 381-9.

Cao X, Shoichet MS. Photoimmobilization of biomolecules within a 3-dimensional hydrogel matrix. J Biomater Sci Polym Ed, 2002; 13: 623-36.

Carter SB. Haptotaxis and the mechanism of cell motility. Nature, 1967; 213: 256-60.

Chalfoun CT, Wirth GA, Evans GR. Tissue engineered nerve constructs: where do we stand? J Cell Mol Med, 2006; 10: 309-17.

Chen YY, McDonald D, Cheng C, Magnowski B, Durand J, Zochodne DW. Axon and Schwann cell partnership during nerve regrowth. J Neuropathol Exp Neurol, 2005; 64: 613-22.

Chilton JK. Molecular mechanisms of axon guidance. Developmental Biology, 2006; 292: 13.

Colamarino SA, Tessier-Lavigne M. The axonal chemoattractant netrin-1 is also a chemorepellent for trochlear motor axons. Cell, 1995; 81: 621-9.

Connolly P. Bioelectronic interfacing: micro- and nanofabrication techniques for generating predetermined molecular arrays. Trends Biotechnol, 1994; 12: 123-7.

Cornish T, Branch DW, Wheeler BC, Campanelli JT. Microcontact Printing: A Versatile Technique for the Study of Synaptogenic Molecules. Molecular and Cellular Neuroscience, 2002; 20: 140.

Cullen D, Lessing M, LaPlaca M. Collagen-Dependent Neurite Outgrowth and Response to Dynamic Deformation in Three-Dimensional Neuronal Cultures. Annals of Biomedical Engineering, 2007; 35: 835.

Suter D, Forster P. Substrate-cytoskeletal coupling as a mechanism for the regulation of growth cone motility and guidance. Journal of Neurobiology, 2000; 44: 97-113.

David S, Lacroix S. Molecular approaches to spinal cord reapir. Annual Review of Neuroscience, 2003; 26: 411-40.

Deister C, Schmidt CE. Optimizing neurotrophic factor combinations for neurite outgrowth. J Neural Eng, 2006; 3: 172-9.

Adams DN, Kao EY, Hypolite CL, Distefano MD, Hu WS, Letourneau PC.Growth cones turn and migrate up an immobilized gradient of the laminin IKVAV peptide. Journal of Neurobiology, 2005; 62: 134-47.

Dergham P, Ellezam B, Essagian C, Avedissian H, Lubell WD, McKerracher L. Rho signaling pathway targeted to promote spinal cord repair. J Neurosci, 2002; 22: 6570-7.

Dertinger SKW, Chiu DT, Jeon NL, Whitesides GM. Generation of Gradients Having Complex Shapes Using Microfluidic Networks. Anal. Chem., 2001; 73: 1240-6.

Dertinger SKW, Jiang X, Li Z, Murthy VN, Whitesides GM. Gradients of substrate-bound laminin orient axonal specification of neurons. PNAS, 2002b; 99: 12542-7.

Devreotes PN, Zigmond SH. Chemotaxis in eukaryotic cells: a focus on leukocytes and Dictyostelium. Annu Rev Cell Biol, 1988; 4: 649-86.

Dhoot NO, Tobias CA, Fischer I, Wheatley MA. Peptide-modified alginate surfaces as a growth permissive substrate for neurite outgrowth. Journal of Biomedical Materials Research Part A, 2004; 71A: 191-200.

Dickson BJ. Molecular mechanisms of axon guidance. Science, 2002; 298: 1959-64.

Dodla MC, Bellamkonda RV. Anisotropic scaffolds facilitate enhanced neurite extension *in vitro*. J Biomed Mater Res A, 2006; 78: 213-21.

Dowell-Mesfin NM, Abdul-Karim MA, Turner AMP, Schanz S, Craighead HG, Roysam B, Turner JN, Shain W. Topographically modified surfaces affect orientation and growth of hippocampal neurons. Journal of Neural Engineering, 2004; 1: 78.

Dunn GA, Brown AF. A unified approach to analysing cell motility. J Cell Sci Suppl, 1987; 8: 81-102.

Ebendal T. The relative roles of contact inhibition and contact guidance in orientation of axons extending on aligned collagen fibrils *in vitro*. Exp Cell Res, 1976; 98: 159-69.

Etienne-Manneville S, Hall A. Rho GTPases in cell biology. Nature, 2002; 420: 629.

Fan YW, Cui FZ, Chen LN, Zhai Y, Xu QY, Lee IS. Adhesion of neural cells on silicon wafer with nano-topographic surface. Applied Surface Science, 2002a; 187: 313.

Fan YW, Cui FZ, Hou SP, Xu QY, Chen LN, Lee IS. Culture of neural cells on silicon wafers with nano-scale surface topograph. Journal of Neuroscience Methods, 2002b; 120: 17.

Fawcett JW, Keynes RJ. Peripheral Nerve Regeneration. Annu. Rev. Neurosci, 1990; 13: 4350. Flaim CJ, Chien S, Bhatia SN. An extracellular matrix microarray for probing cellular differentiation. Nat Meth, 2005; 2: 119.

Folch A, Toner M. Microengineering of cellular interactions. Annu Rev Biomed Eng, 2000a; 2: 227-56.

Foley JD, Grunwald EW, Nealey PF, Murphy CJ. Cooperative modulation of neuritogenesis by PC12 cells by topography and nerve growth factor. Biomaterials, 2005; 26: 3639.

Fry EJ. Central Nervous System Regeneration: Mission Impossible? Clinical and Experimental Pharmacology and Physiology, 2001; 28: 253-8.

Fujisawa H. Retinotopic analysis of fiber pathways in the regenerating retinotectal system of the adult newt cynops Pyrrhogaster. Brain Res, 1981; 206: 27-37.

Georges PC, Janmey PA. Cell type-specific response to growth on soft materials. J Appl Physiol, 2005; 98: 1547-53.

Georges PC, Miller WJ, Meaney DF, Sawyer ES, Janmey PA. Matrices with Compliance Comparable to that of Brain Tissue Select Neuronal over Glial Growth in Mixed Cortical Cultures. Biophys. J., 2006; 90: 3012-8.

Giniger E. How do Rho family GTPases direct axon growth and guidance? A proposal relating signaling pathways to growth cone mechanics. Differentiation, 2002; 70: 385-96.

Goldner JS, Bruder JM, Li G, Gazzola D, Hoffman-Kim D. Neurite bridging across micropatterned grooves. Biomaterials, 2006; 27: 460-72.

Gomez N, Chen S, Schmidt CE. Polarization of hippocampal neurons with competitive surface stimuli: contact guidance cues are preferred over chemical ligands. Journal of The Royal Society Interface, 2007a; 4: 223.

Gomez N, Lu Y, Chen S, Schmidt CE. Immobilized nerve growth factor and microtopography have distinct effects on polarization versus axon elongation in hippocampal cells in culture. Biomaterials, 2007b; 28: 271.

Gomez N, Schmidt CE. Nerve growth factor-immobilized polypyrrole: bioactive electrically conducting polymer for enhanced neurite extension. J Biomed Mater Res A, 2007; 81: 135-49.

Goodhill GJ. Diffusion in axon guidance. Eur J Neurosci, 1997; 9: 1414-21.

Goodhill GJ. Mathematical guidance for axons. Trends in Neurosciences, 1998; 21: 226.

Goodhill GJ, Baier H. Axon guidance: stretching gradients to the limit. Neural Comput, 1998; 10: 521-7.

Goodhill GJ, Gu M, Urbach JS. Predicting Axonal Response to Molecular Gradients with a Computational Model of Filopodial Dynamics. Neural Comp., 2004; 16: 2221-43.

Goodhill GJ, Urbach JS. Theoretical analysis of gradient detection by growth cones. J Neurobiol, 1999; 41: 230-41.

Goodman CS. Mechanisms and Molecules that Control Growth Cone Guidance. Annual Review of Neuroscience, 1996; 19: 341-77.

Govek EE, Newey SE, Van Aelst L. The role of the Rho GTPases in neuronal development. Genes Dev, 2005; 19: 1-49.

Graf J, Ogle RC, Robey FA, Sasaki M, Martin GR, Yamada Y, Kleinman HK. A pentapeptide from the laminin B1 chain mediates cell adhesion and binds to 67000 laminin receptor. Biochemistry, 1987; 26: 6896-900.

Evans GRD. Peripheral nerve injury: A review and approach to tissue engineered constructs. The Anatomical Record, 2001; 263: 396-404.

Hall A. Rho GTPases and the actin cytoskeleton. Science, 1998; 279: 509-14.

Hope RA, Hammond BJ, Gaze RM. The arrow model: retinotectal specificity and map formation in the goldfish visual system. Proc R Soc Lond B Biol Sci, 1976; 194: 447-66.

Isbister CM, Mackenzie PJ, To KC, O'Connor TP. Gradient slope influences the pathfinding decisions of neuronal growth cones *in vivo*. J Neurosci, 2003; 23: 193-202.

Jain A, Brady-Kalnay SM, Bellamkonda RV. Modulation of Rho GTPase activity alleviates chondroitin sulfate proteoglycan-dependent inhibition of neurite extension. J Neurosci Res, 2004; 77: 299-307.

Jones DM, Tucker BA, Rahimtula M, Mearow KM. The synergistic effects of NGF and IGF-1 on neurite growth in adult sensory neurons: convergence on the PI 3-kinase signaling pathway. Journal of Neurochemistry, 2003; 86: 1116-28.

Ju YE, Janmey PA, McCormick ME, Sawyer ES, Flanagan LA. Enhanced neurite growth from mammalian neurons in three-dimensional salmon fibrin gels. Biomaterials, 2007; 28: 2097-108.

Kapur TA, Shoichet MS. Chemically-bound nerve growth factor for neural tissue engineering applications. J Biomater Sci Polym Ed, 2003; 14: 383-94.

Kapur TA, Shoichet MS. Immobilized concentration gradients of nerve growth factor guide neurite outgrowth. J Biomed Mater Res A, 2004; 68: 235-43.

Kato AC, Lindsay RM. Overlapping and Additive Effects of Neurotrophins and CNTF on Cultured Human Spinal Cord Neurons. Experimental Neurology, 1994; 130: 196.

Keilhoff G, Goihl A, Stang F, Wolf G, Fansa H. Peripheral nerve tissue engineering: autologous Schwann cells vs. transdifferentiated mesenchymal stem cells. Tissue Eng, 2006; 12: 1451-65.

Kindt RM, Lander AD. Pertussis toxin specifically inhibits growth cone guidance by a mechanism independent of direct G protein inactivation. Neuron, 1995; 15: 79-88.

Lakatos A, Franklin RJM. Transplant mediated repair of the central nervous system: an imminent solution? Current Opinion in Neurology December, 2002; 15: 701-5.

Lavik E, Langer R. Tissue engineering: current state and perspectives. Appl Microbiol Biotechnol, 2004; 65: 1-8.

Le Beau JM, Liuzzi FJ, Depto AS, Vinik AI. Up-regulation of laminin B2 gene expression in dorsal root ganglion neurons and nonneuronal cells during sciatic nerve regeneration. Exp Neurol, 1995; 134: 150-5.

Leach JB, Brown XQ, Jacot JG, DiMilla PA, Wong JY. Neurite outgrowth and branching of PC12 cells on very soft substrates sharply decreases below a threshold of substrate rigidity. Journal of Neural Engineering, 2007; 4: 26.

Lehmann M, Fournier A, Selles-Navarro I, Dergham P, Sebok A, Leclerc N, Tigyi G, McKerracher L. Inactivation of Rho signaling pathway promotes CNS axon regeneration. J Neurosci, 1999; 19: 7537-47.

Li G, Liu J, Hoffman-Kim D. Multi-Molecular Gradients of Permissive and Inhibitory Cues Direct Neurite Outgrowth. Annals of Biomedical Engineering, 2008, epublished ahead of print.

Li GN, Livi LL, Gourd CM, Deweerd ES, Hoffman-Kim D. Genomic and morphological changes of neuroblastoma cells in response to three-dimensional matrices. Tissue Eng, 2007; 13: 1035-47.

Li Jeon N, Baskaran H, Dertinger SK, Whitesides GM, Van de Water L, Toner M. Neutrophil chemotaxis in linear and complex gradients of interleukin-8 formed in a microfabricated device. Nat Biotechnol, 2002; 20: 826-30.

Li N, Folch A. Integration of topographical and biochemical cues by axons during growth on microfabricated 3-D substrates. Exp Cell Res, 2005; 311: 307-16.

Li N, Tourovskaia A, Folch A. Biology on a chip: microfabrication for studying the behavior of cultured cells. Crit Rev Biomed Eng, 2003; 31: 423-88.

Lin F, Saadi W, Rhee SW, Wang SJ, Mittal S, Jeon NL. Generation of dynamic temporal and spatial concentration gradients using microfluidic devices. Lab Chip, 2004; 4: 164-7.

Lovat V, Pantarotto D, Lagostena L, Cacciari B, Grandolfo M, Righi M, Spalluto G, Prato M, Ballerini L. Carbon Nanotube Substrates Boost Neuronal Electrical Signaling. Nano Lett., 2005; 5: 1107-10.

Luo L. Rho GTPases in neuronal morphogenesis. Nat Rev Neurosci, 2000; 1: 173-80.

Luo Y, Shoichet MS. A photolabile hydrogel for guided three-dimensional cell growth and migration. Nat Mater, 2004; 3: 249.

Ma W, Fitzgerald W, Liu QY, O'Shaughnessy TJ, Maric D, Lin HJ, Alkon DL, Barker JL. CNS stem and progenitor cell differentiation into functional neuronal circuits in three-dimensional collagen gels. Experimental Neurology, 2004; 190: 276.

Madura T, Yamashita T, Kubo T, Fujitani M, Hosokawa K, Tohyama M. Activation of Rho in the injured axons following spinal cord injury. EMBO Rep, 2004; 5: 412-7.

Mahoney MJ, Chen RR, Tan J, Saltzman WM. The influence of microchannels on neurite growth and architecture. Biomaterials, 2005; 26: 771-8.

Manwaring ME, Walsh JF, Tresco PA. Contact guidance induced organization of extracellular matrix. Biomaterials, 2004; 25: 3631-8.

Maskery S, Shinbrot T. Deterministic and stochastic elements of axonal guidance. Annu Rev Biomed Eng, 2005; 7: 187-221.

Maskery SM, Buettner HM, Shinbrot T. Growth cone pathfinding: a competition between deterministic and stochastic events. BMC Neurosci, 2004; 5: 22.

Massia SP, Rao SS, Hubbell JA. Covalently immobilized laminin peptide Tyr-Ile-Gly-Ser-Arg (YIGSR) supports cell spreading and co-localization of the 67-kilodalton laminin receptor with alpha-actinin and vinculin. J. Biol. Chem., 1993; 268: 8053-9.

McCaig CD, Rajnicek AM, Song B, Zhao M. Has electrical growth cone guidance found its potential? Trends Neurosci, 2002; 25: 354-9.

McDonald JW, Liu X-Z, Qu Y, Liu S, Mickey SK, Turetsky D, Gottlieb DI, Choi DW. Transplanted embryonic stem cells survive, differentiate and promote recovery in injured rat spinal cord. Nat Med, 1999; 5: 1410.

McFarlane S. Metalloproteases: Carving Out a Role in Axon Guidance. Neuron, 2003; 37: 559.

McKenzie JL, Waid MC, Shi R, Webster TJ. Decreased functions of astrocytes on carbon nanofiber materials. Biomaterials, 2004; 25: 1309.

Meek MF, Coert JH. Clinical Use of Nerve Conduits in Peripheral-Nerve Repair: Review of the Literature. J reconstr Microsurg, 2002; 18: 097-110.

Miller C, Jeftinija S, Mallapragada S. Synergistic effects of physical and chemical guidance cues on neurite alignment and outgrowth on biodegradable polymer substrates. Tissue Eng, 2002; 8: 367-78.

Mosahebi A, Simon M, Wiberg M, Terenghi G. A Novel Use of Alginate Hydrogel as Schwann Cell Matrix. Tissue Engineering, 2001; 7: 525-34.

Mueller BK. Growth Cone Guidance: First Steps Towards a Deeper Understanding. Annual Review of Neuroscience, 1999; 22: 351-88.

Ngo TTB, Waggoner PJ, Romero AA, Nelson KD, Eberhart RC, Smith GM. Poly(L-Lactide) microfilaments enhance peripheral nerve regeneration across extended nerve lesions. Journal of Neuroscience Research, 2003; 72: 227-38.

Nguyen-Vu TD, Chen H, Cassell AM, Andrews R, Meyyappan M, Li J. Vertically aligned carbon nanofiber arrays: an advance toward electrical-neural interfaces. Small, 2006; 2: 89-94.

Norman J, Desai T. Methods for Fabrication of Nanoscale Topography for Tissue Engineering Scaffolds. Annals of Biomedical Engineering, 2006; 34: 89.

Novikova LN, Mosahebi A, Wiberg M, Terenghi G, Kellerth J, Novikov LN. Alginate hydrogel and matrigel as potential cell carriers for neurotransplantation. Journal of Biomedical Materials Research Part A, 2006; 77A: 242-52.

O'Connor SM, Stenger DA, Shaffer KM, Ma W. Survival and neurite outgrowth of rat cortical neurons in three-dimensional agarose and collagen gel matrices. Neuroscience Letters, 2001; 304: 189.

O'Connor SM, Stenger DA, Shaffer KM, Maric D, Barker JL, Ma W. Primary neural precursor cell expansion, differentiation and cytosolic Ca2+ response in three-dimensional collagen gel. Journal of Neuroscience Methods, 2000; 102: 187.

Offenhausser A, Bocker-Meffert S, Decker T, Helpenstein R, Gasteier P, Groll J, Moller M, Reska A, Schafer S, Schulte P, Vogt-Eisele A. Microcontact printing of proteins for neuronal cell guidance. Soft Matter, 2007; 3: 290-8.

Oliva AA, James CD, Kingman CE, Craighead HG, Banker GA. Patterning Axonal Guidance Molecules Using a Novel Strategy for Microcontact Printing. Neurochemical Research, 2003; 28: 1639.

Patel N, Poo MM. Orientation of neurite growth by extracellular electric fields. J. Neurosci., 1982; 2: 483-96.

Phillips JB, Bunting SC, Hall SM, Brown RA. Neural tissue engineering: a self-organizing collagen guidance conduit. Tissue Eng, 2005; 11: 1611-7.

Polleux F, Morrow T, Ghosh A. Semaphorin 3A is a chemoattractant for cortical apical dendrites. Nature, 2000; 404: 567-73.

Raivich G, Makwana M. The making of successful axonal regeneration: genes, molecules and signal transduction pathways. Brain Res Rev, 2007; 53: 287-311.

Pittier R, Sauthier F, Hubbell JA, Hall H. Neurite extension and *in vitro* myelination within three-dimensional modified fibrin matrices. Journal of Neurobiology, 2005; 63: 1-14.

Rose D, Chiba A. A Single Growth Cone is Capable of Integrating Simultaneously Presented and Functionally Distinct Molecular Cues during Target Recognition. J. Neurosci., 1999; 19: 4899-906.

Rosentreter SM, Davenport RW, Loschinger J, Huf J, Jung J, Bonhoeffer F. Response of retinal ganglion cell axons to striped linear gradients of repellent guidance molecules. J Neurobiol, 1998; 37: 541-62.

Rosoff WJ, McAllister R, Esrick MA, Goodhill GJ, Urbach JS. Generating controlled molecular gradients in 3D gels. Biotechnol Bioeng, 2005; 91: 754-9.

Rosoff WJ, Urbach JS, Esrick MA, McAllister RG, Richards LJ, Goodhill GJ. A new chemotaxis assay shows the extreme sensitivity of axons to molecular gradients. Nat Neurosci, 2004a; 7: 678-82.

Schense JC, Hubbell JA. Three-dimensional Migration of Neurites Is Mediated by Adhesion Site Density and Affinity. J. Biol. Chem., 2000; 275: 6813-8.

Schmidt CE, Leach JB. Neural tissue engineering: strategies for repair and regeneration. Annu Rev Biomed Eng, 2003; 5: 293-347.

Schmidt CE, Shastri VR, Vacanti JP, Langer R. Stimulation of neurite outgrowth using an electrically conducting polymer. PNAS, 1997; 94: 8948-53.

Serini G, Bussolino F. Common Cues in Vascular and Axon Guidance. Physiology, 2004; 19: 348-54.

Silva GA, Czeisler C, Niece KL, Beniash E, Harrington DA, Kessler JA, Stupp SI. Selective Differentiation of Neural Progenitor Cells byHigh-Epitope Density Nanofibers. Science, 2004; 303: 1352.

Silver J, Miller JH. Regeneration beyond the glial scar. Nat Rev Neurosci, 2004; 5: 146-56.

Song H, Ming G, He Z, Lehmann M, McKerracher L, Tessier-Lavigne M, Poo M. Conversion of neuronal growth cone responses from repulsion to attraction by cyclic nucleotides. Science, 1998; 281: 1515-8.

Song HK, Toste B, Ahmann K, Hoffman-Kim D, Palmore GT. Micropatterns of positive guidance cues anchored to polypyrrole doped with polyglutamic acid: a new platform for characterizing neurite extension in complex environments. Biomaterials, 2006; 27: 473-84.

Sperry RW. Chemoaffinity In The Orderly Growth Of Nerve Fiber Patterns And Connections. Proc Natl Acad Sci U S A, 1963; 50: 703-10.

Stein E, Tessier-Lavigne M. Hierarchical organization of guidance receptors: silencing of netrin attraction by slit through a Robo/DCC receptor complex. Science, 2001; 291: 1928-38.

Stroock AD, Dertinger SK, Ajdari A, Mezic I, Stone HA, Whitesides GM. Chaotic mixer for microchannels. Science, 2002a; 295: 647-51.

Stroock AD, Dertinger SK, Whitesides GM, Ajdari A. Patterning flows using grooved surfaces. Anal Chem, 2002b; 74: 5306-12.

Tashiro K-I, Sephel GC, Greatorex D, Sasaki M, Shirashi N, Martin GR, Kleinman HK, Yamada Y. The RGD containing site of the mouse laminin A chain is active for cell attachment, spreading, migration and neurite outgrowth. Journal of Cellular Physiology, 1991; 146: 451-9.

Tashiro K, Sephel GC, Weeks B, Sasaki M, Martin GR, Kleinman HK, Yamada Y. A synthetic peptide containing the IKVAV sequence from the A chain of laminin mediates cell attachment, migration, and neurite outgrowth. J. Biol. Chem., 1989; 264: 16174-82.

Taylor L, Jones L, Tuszynski MH, Blesch A. Neurotrophin-3 Gradients Established by Lentiviral Gene Delivery Promote Short-Distance Axonal Bridging beyond Cellular Grafts in the Injured Spinal Cord. J. Neurosci., 2006; 26: 9713-21.

Tessier-Lavigne M, Goodman CS. The molecular biology of axon guidance. Science, 1996; 274: 1123-33.

Thompson DM, Buettner HM. Neurite outgrowth is directed by schwann cell alignment in the absence of other guidance cues. Ann Biomed Eng, 2006; 34: 161-8.

Tom VJ, Steinmetz MP, Miller JH, Doller CM, Silver J. Studies on the Development and Behavior of the Dystrophic Growth Cone, the Hallmark of Regeneration Failure, in an In Vitro Model of the Glial Scar and after Spinal Cord Injury. J. Neurosci., 2004; 24: 6531-9.

Vogt AK, Wrobel G, Meyer W, Knoll W, Offenhausser A. Synaptic plasticity in micropatterned neuronal networks. Biomaterials, 2005; 26: 2549-57.

von Philipsborn AC, Lang S, Loeschinger J, Bernard A, David C, Lehnert D, Bonhoeffer F, Bastmeyer M. Growth cone navigation in substrate-bound ephrin gradients. Development, 2006; 133: 2487-95.

Waid MC, McKenzie JL, Price RL, Ejiofor JU, Webster TJ. Nano-biotechnology: carbon nanofibres as improved neural and orthopaedic implants. Nanotechnology, 2004; 15: 48-54.

Walsh JF, Manwaring ME, Tresco PA. Directional neurite outgrowth is enhanced by engineered meningeal cell-coated substrates. Tissue Eng, 2005; 11: 1085-94.

Wang H, Iovenitti P, Harvey E, Masood S. Numerical investigation of mixing in microchannels with patterned grooves. Journal of Micromechanics and Microengineering, 2003; 13: 801.

Wang K, Fishman HA, Dai H, Harris JS. Neural Stimulation with a Carbon Nanotube Microelectrode Array. Nano Lett., 2006; 6: 2043-8.

Wen X, Tresco PA. Effect of filament diameter and extracellular matrix molecule precoating on neurite outgrowth and Schwann cell behavior on multifilament entubulation bridging device *in vitro*. J Biomed Mater Res A, 2006; 76: 626-37.

Whitesides GMS, Abraham D. Flexible methods for microfluidics. Physics Today, Vol. 54 Issue 6, p42, , Jun2001, .

Willits RK, Skornia SL. Effect of collagen gel stiffness on neurite extension. J Biomater Sci Polym Ed, 2004; 15: 1521-31.

Winberg ML, Mitchell KJ, Goodman CS. Genetic analysis of the mechanisms controlling target selection: complementary and combinatorial functions of netrins, semaphorins, and IgCAMs. Cell, 1998; 93: 581-91.

Yang F, Murugan R, Wang S, Ramakrishna S. Electrospinning of nano/micro scale poly(L-lactic acid) aligned fibers and their potential in neural tissue engineering. Biomaterials, 2005a; 26: 2603.

Yang IH, Co CC, Ho C-C. Alteration of human neuroblastoma cell morphology and neurite extension with micropatterns. Biomaterials, 2005b; 26: 6599.

Yeung CK, Lauer L, Offenhausser A, Knoll W. Modulation of the growth and guidance of rat brain stem neurons using patterned extracellular matrix proteins. Neuroscience Letters, 2001; 301: 147.

Yu TW, Bargmann CI. Dynamic regulation of axon guidance. Nat Neurosci, 2001; 4 Suppl: 1169-76.

Yu X, Bellamkonda RV. Dorsal root ganglia neurite extension is inhibited by mechanical and chondroitin sulfate-rich interfaces. J Neurosci Res, 2001; 66: 303-10.

Zhang J, Venkataramani S, Xu H, Song Y-K, Song H-K, Palmore GTR, Fallon J, Nurmikko AV. Combined topographical and chemical micropatterns for templating neuronal networks. Biomaterials, 2006; 27: 5734.

Zhang N, Yan H, Wen X. Tissue-engineering approaches for axonal guidance. Brain Res Brain Res Rev, 2005a; 49: 48-64.

Zhang Z, Yoo R, Wells M, Beebe TP, Biran R, Tresco P. Neurite outgrowth on well-characterized surfaces: preparation and characterization of chemically and spatially controlled fibronectin and RGD substrates with good bioactivity. Biomaterials, 2005b; 26: 47.

Chapter 2

Evaluation of neurite outgrowth using a novel application of circular analysis

Precise axon growth is required for making proper connections in development and after injury. One method of studying axon guidance and growth is through *in vitro* outgrowth assays that present controlled microenvironments. In this study, we applied circular statistical methods to evaluate directional neurite response. Specifically, the direction of neurite outgrowth from dorsal root ganglia derived neurons on different substrate types was quantitatively measured. Further, simulations of datasets with known circular parameters reflecting expected neurite angle distributions from different substrate types were generated. Circular statistical methods were utilized and compared to linear statistical models widely used in the neuroscience literature. These analysis methods represent a useful tool for evaluation of directionality of neurite outgrowth with applications that include: (1) assessment of neurite outgrowth potential; (2) determination of isotropy of cellular responses to single and multiple cues and (3) determination of the relative strengths of cues present in a complex environment.

2.1 Introduction

Axon guidance during development and after injury has been studied in traditional cell culture and in increasingly complex *in vitro* environments generated with tissue engineering and other biomedical engineering techniques. One approach has been to manipulate the cells' local microenvironment and observe neurite outgrowth in microenvironments containing cues of interest. Studies of axon guidance often use *in vitro* neurite outgrowth assays (Ronn et al., 2000; Smit et al., 2003; Thompson and Buettner, 2006; Weaver et al., 2003) as models to elucidate the growth potential of neurons, the effects of the environment, and the mechanisms underlying the axon growth process.

Quantitative assessment of neurite outgrowth in these assays represents a critical step in gaining specific information on axon growth. Quantitative morphometric analyses depend heavily on microscopy techniques (Meijering et al., 2004; Mitchell et al., 2007) and automated (Karlon et al., 1998; Price et al., 2006; Weaver et al., 2003) or semi-automated (Bilsland et al., 1999; Hynds and Snow, 2002; Thompson and Buettner, 2006) image analysis tools which allow researchers to accurately assess neuronal and neurite growth. Parameters that provide information on neuronal response may include the area of the neuron or neurite (Abosch and Lagenaur, 1993), number of neurites (Abosch and Lagenaur, 1993; Le Roux and Reh, 1994), neurite orientation, neurite length (Abosch and Lagenaur, 1993) and path of migration. One widely used measure for the strength of a guidance cue is the direction of neurite outgrowth following some underlying directional stimulus (Alexander et al., 2006; Bruder et al., 2007; Deumens et al., 2004; Mahoney et al., 2005; Thompson and Buettner, 2006).

The geometry of neurite outgrowth is most meaningfully parameterized in a circular coordinate system centered on the cell and rotationally aligned to the stimulus applied. The distribution of neurite angles in culture can be described by circular statistical parameters, such as mean (μc) and concentration ($\varkappa$), in an analogous manner to linear statistical parameters mean (μ) and variance (ς). Circular variables have values that fall along a circle and hence have specific properties related to the cyclic nature of the circular scale. The ap-

plication of these methods to neurite direction is analogous to the application of population biology measures to cellular function.

Statistical analysis of circular variables differs from analysis of linear variables as there are several properties of circular variables that need to be taken into account. Because circular variables are finite and closed when a circular data set comes back on itself (at 0° and 360°), the zero direction, the designation of magnitude, and the number and size of groups (in the case of grouped data) are arbitrary. In addition, the mean angle of orientation cannot be found by the simple summation of measured values and division by the sample size. The sums of circular variables must be taken either modulo 360° if the sample is circular, or taken modulo 180° if the sample is axial, i.e. where data occur as an undirected line as in the example of geological fractures (Tran, 2007). For axial data in the present study, there is symmetry about the y-axis hence there is no distinction between the north-south directions. Analysis for linear variables approximates randomness by using a Poisson distribution; this distribution does not translate to circular variables. In circular statistics, the null hypothesis describing a random distribution is taken to be a uniform distribution, where all directions may occur at equal probability, approximating randomness and reflecting the finite closure of a circle (Fisher, 1993).

Neurite outgrowth angles are generally simple distributions, requiring display of data and summary of a single random sample usually with single or bimodal groups. As such, a null hypothesis of uniformity and randomness is generally appropriate, with the objective to assess the uniformity of a given distribution of neurite angles cultured in different environmental conditions. When the comparison of two or more samples of neurites cultured in different conditions is of interest, regression analysis and statistical models may be useful for description and prediction of cell response. Circular statistical methods complement traditional linear statistical methods to describe and draw inferences about the population of neurons and neurites being studied (Batschelet, 1981; Fisher, 1993). We propose in this study that in many cases, circular statistical methods allow us to more robustly describe the complexity of neurite outgrowth phenomena.

In this work, we employed circular statistical models to evaluate directional growth in a variety of representative *in vitro* neurite outgrowth assays. Multiple statistical methods were used to evaluate *in vitro* neurite outgrowth ranging from Gaussian based models and nonparametric methods to hypothesis testing for circular samples. Here we report a comparison of circular and linear data presentation and statistical methods for evaluation of several types of neurite outgrowth patterns.

2.2 Methods

2.2.1 Substrate preparation

Three types of substrates were used to evaluate the use of circular statistical methods on directionality of neurite outgrowth: adsorbed uniform protein coating on glass, adsorbed protein stripes and adsorbed protein gradients. Uniform protein coating was performed by incubating protein solution for one hour on acid washed glass coverslips, washing twice with sterile water and air drying.

Micropatterned laminin (LN, 50μg/mL) and chondroitin sulfate proteoglycans (CSPG, 10μg/mL) stripes of 10 mm length, 50 μm width and 50 μm pitch were stamped onto glass coverslips via micro-contact printing techniques as described in Bruder et al. (Bruder et al., 2006). Briefly, grooved polydimethyl siloxane (PDMS) stamps fabricated using the method described in Goldner et al. (Goldner et al., 2006), were submerged in 10% sodium dodecyl sulfate in deionized water, rinsed in water, and incubated with 50μg/mL mouse LN in Hank's balanced salt solution without calcium or magnesium (HBSS-CMF) for 1 h. Glass coverslips were plasma activated with a plasma cleaner/sterilizer (PDC-32 G, Med RF level), and incubated in contact with stamps overnight to achieve adsorbed alternating stripes of either LN or CSPG.

Protein gradients were generated with the use of a microfluidic gradient mixer, fabricated using soft lithography techniques in a modification of the method of Dertinger et al. (Dertinger

et al., 2002), described in Li et al. (Li et al., 2007). Briefly, the gradient mixer pattern was designed in AutoCAD and transferred to a silicon wafer using photolithography. Using the silicon wafer as a template and PDMS as an elastomeric replica, soft lithography was used to fabricate the gradient mixer. The polymeric gradient mixer and a glass slide were irreversibly bonded by plasma activation of both surfaces for 1 min. Single cue gradients of LN or CSPG opposite bovine serum albumin (BSA, 3%, a neutral molecule for neurite guidance), were generated as substrates to evaluate neurite directionality. Protein solutions of LN or CSPG and BSA were pumped through the gradient mixer, at 0.2µL/min and allowed to interdiffuse and adsorb overnight. The glass substrates containing the adsorbed protein gradients were used as the substrates on which to culture dorsal root ganglia (DRG) neurons.

2.2.2 Cell culture

DRG were dissected from the spinal columns of postnatal (P0-P4) rat pups and cleaned of axons, blood, and connective tissue. DRG were incubated in 0.05% trypsin-EDTA in HBSS-CMF at 37 $^{\circ}$C for 60 min and dissociated by trituration. Cells were plated onto substrates in Dulbecco's modified eagle's medium (DMEM) with 10% fetal bovine serum (FBS), 4 mM L-glutamine, 100 U/ml penicillin, and 100 µg/ml streptomycin with 50 ng/ml nerve growth factor (NGF). Cells were seeded at a density of 100,000 cells/mL, on uniformly coated glass or micropatterned substrates and 12,500 cells/mL on gradient substrates. Phase contrast microscopy at 100x magnification was performed using a Nikon Eclipse TE2000-S, and images were captured with Hamamatsu-ORCA outputting to Openlab v.4.05 after 24 hours in culture.

2.2.3 Image analysis

To evaluate direction of neurite outgrowth on uniform substrates and micropatterned protein stripes, the angles of all neurites in at least 6 fields of view were measured as the angle between the vector from the cell body to the tip of the neurite and the vertical axis (0°,

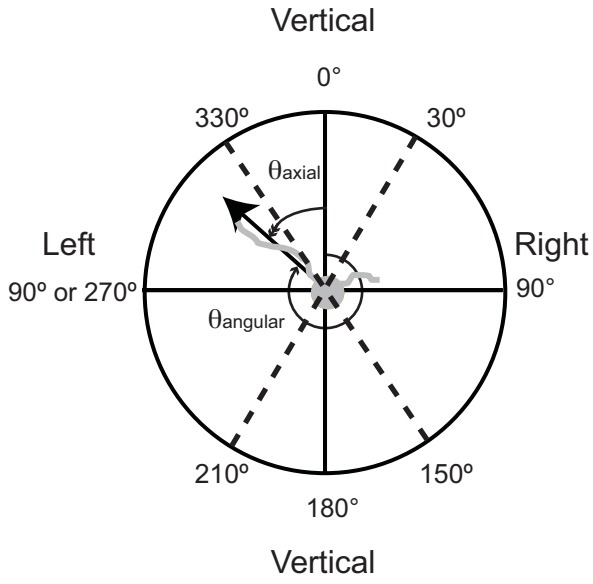

Figure 2.1: Measurement of neurite angles.
Schematic showing neurite angles measured in this study (ϑangular). Note that for alignment to protein stripes, the data (ϑaxial) is taken as axial data and the circular scale extends from 0-180°.

Figure 2.1), using the measure tool in OpenLab software on phase contrast images. To evaluate directional bias of neurites on gradient substrates, the angles (ϑ) of the longest neurites of all neurons adhered to the gradient channel were measured as described above.

2.2.4 Linear statistical analysis

Linear descriptive statistics such as mean and standard deviation were calculated by equations described in Table I. Conventional statistical tests were performed using SPSS 14. Linear probability density functions were tested against circular data as comparison (SPSS 14; listed in Table II). For the $\chi 2$ test, the angle data was grouped into three groups: neurites growing towards the left (210^{o}-330^{o}), right (30^{o}-150^{o}) and vertical (0^{o}-30^{o}, 150^{o}-210^{o}, 330^{o}-360^{o}). For the KS test, the angles of neurite outgrowth were grouped into 10^{o} bins.

2.2.5 Circular data presentation

Circular data was plotted as a frequency distribution with neurites binned in ten degree bins, and "wrapped" around a circle. Circular histograms were plotted using circular statistical software package Oriana v2.02.

2.2.6 Circular Statistics

A common aim for analysis of directional data is to estimate the preferred direction and distribution of data. To describe circular distributions, measures have been developed such as circular mean angle (μ),the length of vector (R) and the concentration parameter ($\varkappa$) (Batschelet, 1981; Fisher, 1993). These parameters take into account the periodicity in angular data by using trigonometric functions, and the equations describing the calculations are listed in Table 2.1.

Six one-sample goodness-of-fit tests were compared in this paper, to test against the null hypothesis of uniformity of neurite angle distributions: Rayleigh's test, Rao's spacing test, Kuiper's test, Watson's U2 test, chi-squared ($\chi 2$) test, and V-test, a modification of Rayleigh's test. The $\chi 2$ goodness of fit tests are not strictly circular, but are generally accepted to be appropriate for circular variables under certain conditions (listed in Table 1, (Batschelet, 1981; Fisher, 1993; Zar, 1996)). Equations for each circular goodness-of-fit test are listed in Table II. Each type of test was developed for different data distributions. These tests differ in their alternate hypotheses, where Rao's and Kuiper's test for randomness in the sample against any alternative, and Rayleigh's and Watson's test against a unimodal alternative. The V-test tests against a specified mean direction and was only performed for alignment studies and computer simulations as these were the only cases in which an external direction was applied.

Two multisample tests were performed in this study, to compare two datasets and determine whether their distributions are different: Mardia-Watson-Wheeler test and Watson's U2 test. Equations for each multisample test are listed in Table 2.2. Both tests determine

Statistic	Equation
CIRCULAR	
Vector components	$S = \sum_{i=1}^{n} \sin(\theta_i); C = \sum_{i=1}^{n} \cos(\theta_i)$
Mean direction(μ_c)	$\mu_c = \begin{cases} \tan^{-1} (S/C), & S > 0, C > 0 \\ \tan^{-1} (S/C) + \pi, & C < 0 \\ \tan^{-1} (S/C) + 2\pi, & S < 0, C > 0 \end{cases}$
Length of mean vector(R)	$R = \sqrt{C^2 + S^2}$
Variance(Var_c)	$Var_c = -2 \ln R$
Standard deviation(σ_c)	$\sigma_c = \sqrt{Var_c}$
LINEAR	
Mean direction(μ)	$\mu = \frac{1}{n} \sum_{i-1}^{n} \theta_i$
Variance(Var)	$Var = \frac{1}{n} \sum_{i-1}^{n} (\theta_i - \mu)^2$
Standard deviation(σ)	$\sigma = \sqrt{Var}$

Table 2.1: Equations of calculations of mean and standard deviation to determine preferred direction and spread of data.

Where ϑi = angular data for the ith observation as i= 1,. . . , n and n = number of observations. Variance calculations performed by Oriana, according to Zar (Zar, 1999).

Test	Data type	Null hypothesis	Formula for test statistic	Notes
CIRCULAR ONE-SAMPLE TESTS				
Rayleigh's	Continuous	Uniform	$Z = \frac{R}{n}$	unimodal von Mises alternative
Rao's Spacing	Continuous	Uniform	$\theta_1 \leq \theta_2 \leq ... \leq \theta_n$ $T_{i-1} = \theta_i - \theta_{i-1}$ $T_n = 360 + \theta_1 - \theta_n$ $U = \frac{1}{2}\sum_i = 1^n(\lvert T_i - \frac{360}{n} \rvert)$	$n \geq 5$ where T_i is the arclength between consecutive angles
Watson's U^2	Continuous	Uniform	$\theta_1 \leq \theta_2 \leq ... \leq \theta_n$ $v_i = F(\theta_i), \bar{v} = \frac{1}{n}\sum v_i, c_i = 2i - 1$ $U^2 = \sum v_i^2 - \sum[\frac{c_i v_i}{n}) + n(\frac{1}{3} - (\bar{v} - \frac{1}{2})^2]$	where $F(\theta)$ is the function of (uniform) theoretical distribution suitable for unimodal and multimodal distributions
Kuiper's	Continuous	Uniform	$V_n = D^+ + D^-$ $K = \sqrt{n}V_n$	where D is the deviation from (uniform) theoretical distribution for small n, more powerful than χ^2 test circular goodness-of-fit test corresponding to Kolmogorov-Smirnov
V-test	Continuous	Uniform	$V = R\cos(\mu_c - \mu_0), u = V\sqrt{\frac{2}{n}}$	external direction (μ_0) specified a priori
CIRCULAR MULTISAMPLE TESTS				
Mardia-Watson-Wheeler	Continuous	Two samples have same distributions	$W = 2\sum_{i=1}^{k}[\frac{C_i^2 + S_i^2}{n_i}]$	data is ungrouped
Watson's U^2	Continuous	Two samples have same distributions	$U^2 = \frac{n_1 n_2}{N^2}[\sum_{k=1}^{N} d_k^2 - \frac{(\sum_{k=1}^{N} d_k)^2}{N}]$	where $N = n_1 + n_2$ no ties between samples
LINEAR TESTS				
χ^2	Grouped	Uniform	$\chi^2 = \sum_i^k = 1^k \frac{(O_i - e_i)^2}{e_i}$	where e_i = expected value for ith term distribution based on approximation, need large n suitable for both unimodal and multimodal distributions
Kolmogorov-Smirnov	Grouped	Uniform	$D_{max} = \max[\lvert d_i \rvert)$ where $\lvert d_i \rvert = \lvert F_i - \bar{F}_i \rvert$	where $\bar{F}_i$ is the function of (uniform) theoretical distribution distribution more powerful than χ^2 when n is small distribution dependent on starting point, more sensitive near median than at tails
Student's t-test	Continuous	Two samples have same means	$t = \frac{\bar{x}_1 - \bar{x}_2}{s_{\bar{x}_1 - \bar{x}_2}}$ where $s_{\bar{x}_1 - \bar{x}_2} = \sqrt{\frac{s_1^2 + s_2^2}{n}}$	where $\bar{x}$ is the sample mean and s is the sample standard deviation assuming equal variances

Table 2.2: Equations of test statistical parameters used in circular and linear tests. Where ϑi = angular data for the ith observation as i= 1,. . . , n and n = number of observations. Tables providing critical values of each test statistic are available from Batschelet (Batschelet, 1981) or from circular statistical software programs such as Oriana. Refer to Table 2.1 for definitions of variables.

whether the two samples differ significantly from each other in mean angle, angular variance or both measures. Neurite angles on LN and CSPG striped substrates, LN striped and gradient substrates, and LN and CSPG gradient substrates were compared against each other to test if neurite outgrowth directions differed significantly on these substrates. Mardia-Watson-Wheeler compares the resultant vector lengths (R), and Watson's U2 test compares the deviation between the cumulative density functions of the two populations (Batschelet, 1981). All circular data analysis was performed using Oriana v2.02c. Student t-test was performed on the same datasets to compare circular methods to linear methods of comparing means between two samples.

2.2.7 Simulations of circular distributions

Simulations approximating various circular distributions were performed using a custom MATLAB program that generates circular random numbers from a specified distribution with input parameters. Algorithms for simulation of data types (uniform, unimodal von Mises (VM), and bimodal (BM) distributions with corresponding probability density func-

Theoretical distribution	Probability density function	n	Mean(μ) (°)	Concentration(κ)	Dispersion (°)
Uniform, U	$f(\theta) = \frac{1}{2\pi}, 0 \leq \theta \leq 2\pi$	5, 30, 100	0	0	
von Mises, VM(μ, κ)	$f(\theta) = [2\pi I_0(\kappa)]^{-1} \exp[\kappa \cos(\theta - \mu)], 0 \leq \theta \leq \infty$ where $I_0\kappa = (2\pi)^{-1} \int_0^{2\pi} \exp[\kappa \cos(\theta - \mu)] d\phi$	5, 30, 100	0	0.85, 1, 1.5, 3	180, 120, 60, 20
Bimodal, VM(μ_1, κ_1),VM(μ_2, κ_2)	$f(\theta) = [2\pi I_0(\kappa)]^{-1} \exp[\kappa \cos 2(\theta - \mu)], 0 \leq \theta \leq \infty$	5, 30, 100	0	0.85, 1, 1.5, 3	180, 120, 60, 20

Table 2.3: Equations of probability density functions and parameters of statistical models used in simulation of neurite outgrowth.

tions described in Table 2.3) were taken from Fisher (Fisher, 1993). In each simulation, random numbers were generated (n=5, 30, 100), input parameters included mean (μc), and concentration (ϰ) corresponding to angular dispersion and simulation of each distribution was run 100 times. Simulated uniform data were generated by transforming linear random numbers in the range of 0 to 1 into degrees by using the RAND function in MATLAB modulo 360. Random numbers from VM and BM distributions were generated according to Fisher (Fisher, 1993). BM distributions consisted of data drawn from two subsets of proportions p and (1-p), with parameters (μc1, R1, ϰ1) and (μc2, R2, ϰ2) corresponding to each subset. In this case, bimodal distributions were simulated as an equal mixture of two subpopulations with VM distribution (p1=p2=0.5).

Two linear and four circular goodness-of-fit tests were performed on each experimental condition similar to the experimental data described in section 2.5 to assess the probability density function that would best describe the data. The percentage of significant simulations ($p<0.05$) was determined for each experimental condition and Type I error was determined for each experimental condition in the simulation (Table 2.7).

2.3 Results

Here we describe the evaluation of directional neurite outgrowth using linear and circular statistics of two types of data: experimental data with unknown population parameters and simulated data with known (user defined) population parameters.

2.3.1 Experimental Results

Experimental data of three different types of DRG neurite behavior were elicited from three differently micropatterned substrates and simulations of established uniform, unimodal and bimodal datasets were performed. Experimental neurite angle data were presented in circular histograms customary for circular data, and also in more conventional ways of presenting alignment, by bar graphs of neurites categorized in aligned and unaligned groups.

By varying micropatterns of proteins presented in culture using multiple substrates (uniform, striped, gradient), neurite outgrowth could be directed towards different directions. Comparison of mean neurite angles and deviations from the vertical axis calculated both with linear and with circular methods revealed differences in the abilities of linear and circular approaches to accurately reflect the complex distributions of neurites. The large linear standard deviations reflected how linear methods fail to account for data clustering around 0°. Deviation from the vertical axis 0° or 180°, on a circular or angular scale, (Figure 2.2; Table IV), showed that the circular mean angle avoided the convergence to 180°, providing a better estimate of mean angle. For striped samples that aligned to the vertical axis, linear methods yielded means of 135.01° and 182.93° for LN and CSPG respectively, while circular statistical methods yielded corresponding means that aligned with the vertical axis for striped substrates (1.90° and 178.61° for LN and CSPG respectively). For gradient samples, circular mean angles showed directed growth towards more permissive or less inhibitory regions on gradient substrates (293.89° and 300.90° for LN and CSPG respectively). Corresponding linear mean angles converged towards 180°, showing little directionality (197.58° and 183.09° for LN and CSPG respectively).

Phase contrast images of neurons on uniformly coated LN (Figure 2.3) show neurite outgrowth in all directions. A grouped bar graph poorly reflects the uniformity of the dataset, where more neurites appear to have grown in the “left” direction than in all others. A linear histogram of neurite data appears to show four modal groups (0-80°, 90-170°, 190-290°, 300-360°) and reveals the poor fit of a normal distribution. Data plotted on a circular axis reflects the variability of the angular data and most clearly shows that angular data falls in

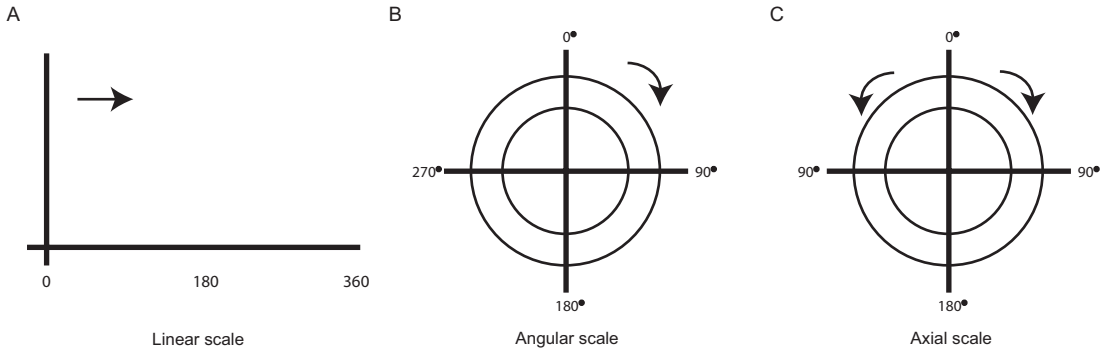

Figure 2.2: Visualization of linear and circular scales.
(a) Linear data fall in a straight line with values increasing along the axes. (b) Angular data is shown on a circular scale where 0-360° wraps around on a circle. Scale used in this study for neurite angles on gradient substrates. (c) Axial data is shown on a circular scale with an axis of symmetry about the y-axis such that the scale extends from 0-180°. Scale used in this study for neurite angles on striped substrates. Note that for circular histograms, concentric circles about the axes denote frequency of data.

even spacing around a circular scale.

When permissive LN and inhibitory CSPG were presented on substrates, DRG neurons adhered to LN coated regions and avoided CSPG coated regions (Figure 2.4). DRG neurites extended and aligned to LN stripes (Figure 4a) and to uncoated regions between CSPG stripes (Figure 4e). Qualitative and quantitative analysis of the data show a larger population and density of neurons and aligned neurites on LN striped substrates, as compared to CSPG striped substrates, but the mean neurite outgrowth direction (the parameter of interest) was similar for DRG neurons on both LN and CSPG striped substrates. Grouped bar graphs, with groups defined as left: 210-330°, right: 30-150°, and aligned: 330-30° and 150-210°) are able to show that the data cluster around the vertical direction which is set to correspond to alignment to the underlying pattern (Figure 4b, f). Linear histograms split the data clusters, fail to recognize the relationship between 0-10° and 350-360°, and reveal a poor fit to a normal distribution around the linear mean of 180° (Figure 4c, g). Data plotted on circular axes show that the majority of the data falls within a 30° interval around the vertical 0° direction (Figure 4d, h).

Analysis of neurite growth on gradient substrates illustrates how circular statistics can be used to analyze neurite outgrowth patterns that are more complex (Figure 2.5). Phase

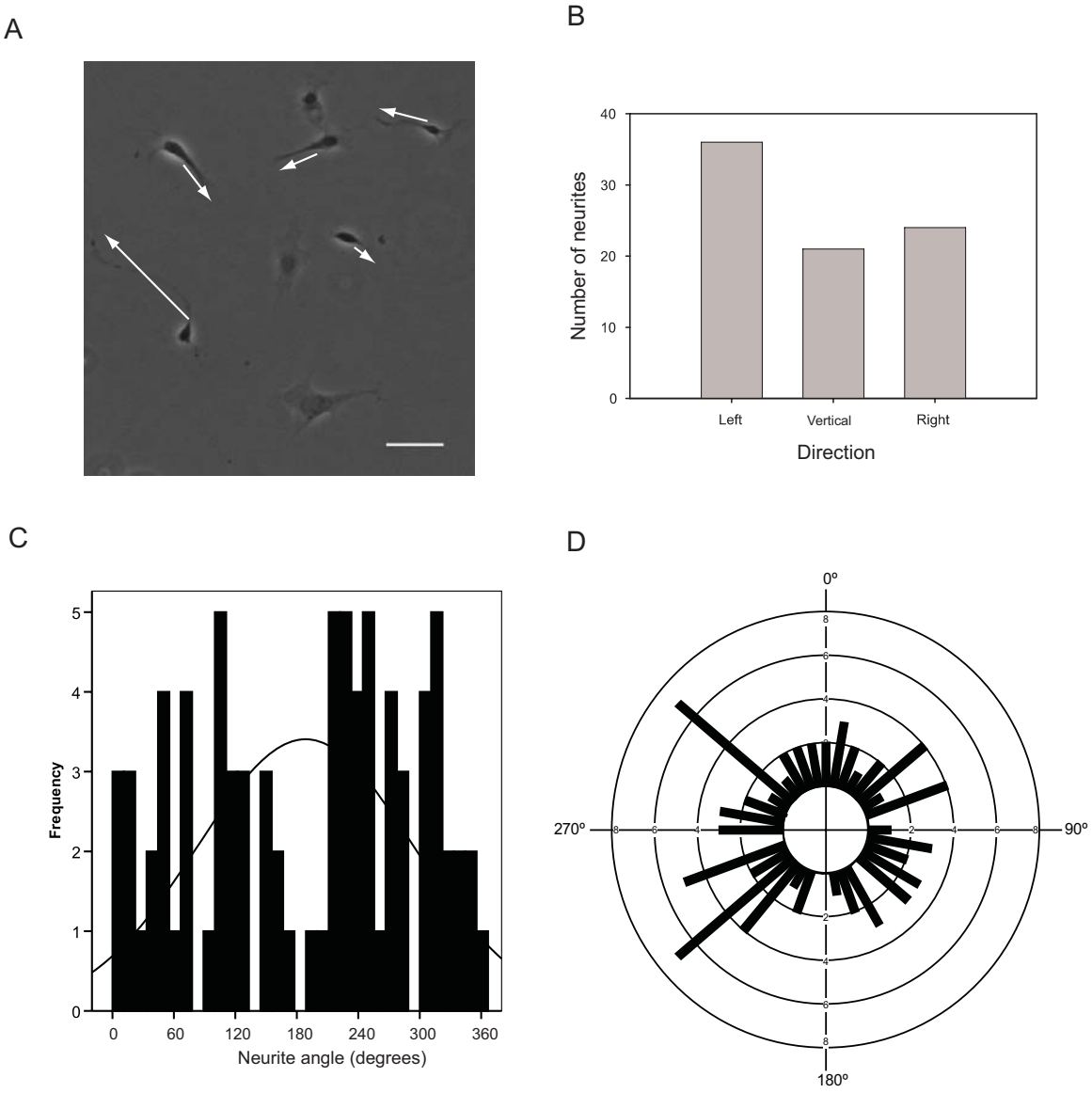

Figure 2.3: Distribution of neurites after 24 hours in culture on uniformly coated LN substrates shows uniformity in neurite outgrowth angles.
(a) Phase contrast image of DRG neurons on uniform LN coated glass surface. Bar = 50μm. Arrows show the vectors that were used to evaluate the neurites. (b) Bar graph shows the corresponding grouped neurite outgrowth angle data. (c) Linear histogram shows corresponding distribution of neurite angles where each angle presented is the angle of the longest neurite per neuron. Normal curve is fitted to the linear histogram around the linear sample mean and standard deviation. (d) Circular histogram shows the corresponding distributions of neurite angles where each angle presented is the angle of the longest neurite per neuron.

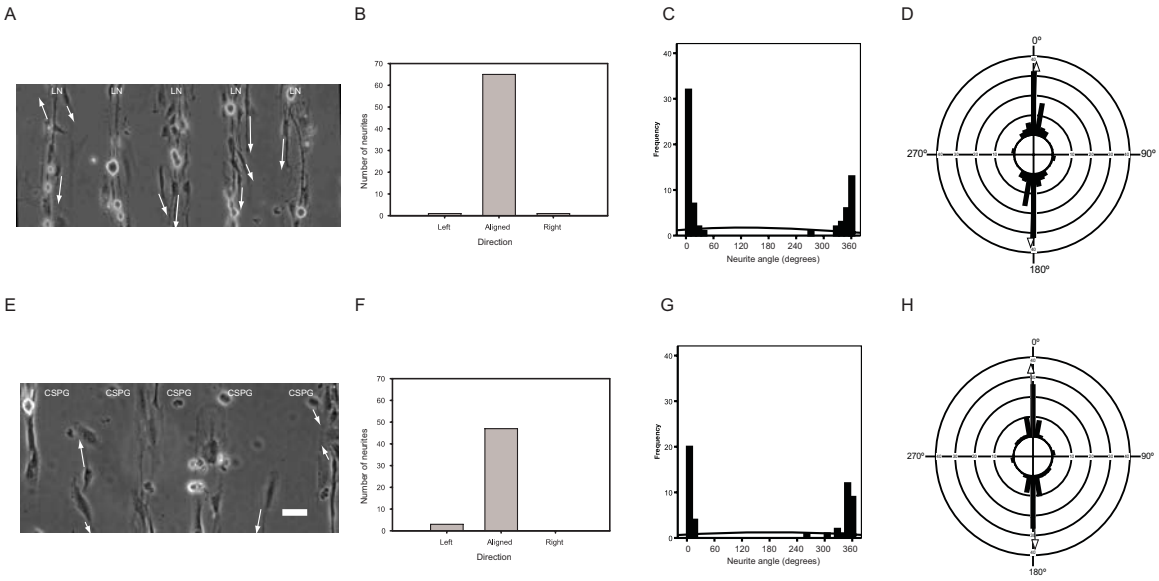

Figure 2.4: Distribution of neurites after 24 hours in culture on micropatterned LN or CSPG stripes shows clustered and directed neurite outgrowth angles.
Phase contrast images of DRG neurons on micropatterned LN (a) and CSPG (e) stripes respectively on glass surface. Bar = 50μm. Arrows show the vectors that were used to evaluate the neurites. (b, f) Bar graphs show the corresponding grouped neurite outgrowth angle data. (c, g) Linear histograms show corresponding distributions of neurite angles where each angle presented is the angle of the longest neurite per neuron. Normal curve is fitted to the linear histogram around the linear sample mean and standard deviation. Circular histograms show the corresponding distributions of neurite angles on LN (d) and CSPG (h) striped substrates, where each angle presented is the angle of the longest neurite per neuron. White arrows indicate mean neurite angles for directed distributions.

contrast images of DRGs plated on a LN gradient (Figure 5a) and a CSPG gradient (Figure 5e) show an overall trend of neurite growth toward the permissive LN and away from the inhibitory CSPG, but the neurite response to the underlying substrate is not nearly as obvious as that of DRGs cultured on protein stripes in Figure 4. Grouped bar graphs (Figure 5b, f) are able to show the bias towards the "left" edge of the channel, which was the more permissive or the less inhibitory direction. Linear histograms appear to show three modal groups (0-70°, 70-250°, 250-360°) for neurite growth on LN gradients (Figure 5c). For DRG neurites on a CSPG gradient however, the neurite angle distribution is flattened and appears more uniform (Fig 5g). Data plotted on circular axes show a similar trend to the grouped bar graphs, where growth appears to be towards the more permissive or less inhibitory regions (Figs. 5d, h). Similar to DRG response on protein stripes, the permissiveness of the substrate is reflected by the number of neurons and neurites present, whereas the directional guidance potential of the substrate is reflected by the angles at which the neurites extend.

Several circular and linear goodness-of-fit tests were performed for all experimental data conditions with the null hypothesis of uniformity (Table 2.5). For neurites cultured on uniform LN substrates, patterned LN and CSPG stripes, and LN gradients, circular and linear tests exhibited similar results. On uniform substrates, all circular and linear tests showed no significant difference from a uniform distribution. On striped substrates and LN gradients, all circular and linear tests showed significant difference from a uniform distribution. However, on CSPG gradients, a common linear test, KS, showed no significant difference from uniformity whereas Rayleigh's, Watson's, Rao's and Kuiper's circular tests showed significant difference from uniformity. Surprisingly, $\chi 2$ tests for grouped data with 3 groups were in better agreement with other circular tests than $\chi 2$ tests for grouped data with 36 groups.

Multisample analysis showed no difference in neurite angles between LN striped and CSPG striped samples. It also showed no difference in angles between LN gradient and CSPG gradient samples. Both Mardia-Watson-Wheeler and Watson's U2 test showed no significant differences with p-values greater than 0.49 (Table 2.6). Student t-test was performed as a comparison and also found neurite angles to be not significantly different on these substrates

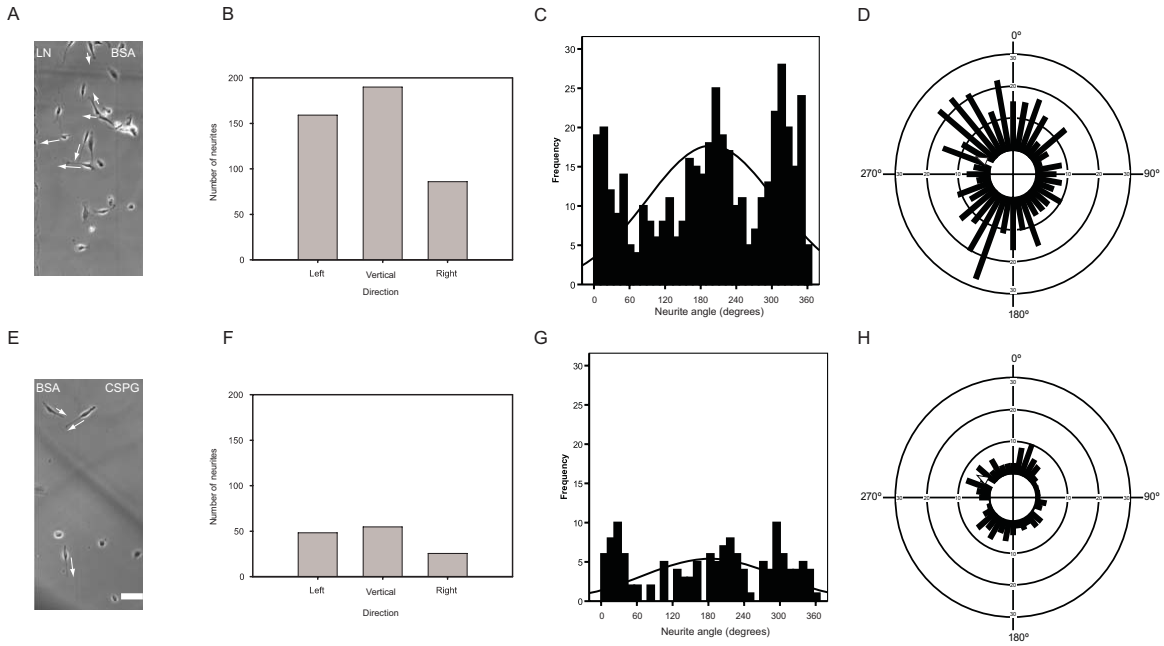

Figure 2.5: Distribution of neurites after 24 hours in culture on micropatterned LN or CSPG gradients shows dispersed but directed neurite outgrowth angles.
Phase contrast images of DRG neurons on micropatterned LN (a) and CSPG (e) gradients respectively on glass surface. Bar = 50μm. Arrows show the vectors that were used to evaluate the neurites. (b, f) Bar graphs show the corresponding grouped neurite outgrowth angle data. (c, g) Linear histograms show corresponding distributions of neurite angles where each angle presented is the angle of the longest neurite per neuron. Normal curve is fitted to the linear histogram around the linear sample mean and standard deviation. Circular histograms show the corresponding distributions of neurite angles on LN (d) and CSPG (h) gradient substrates, where each angle presented is the angle of the longest neurite per neuron. White arrows indicate mean neurite angles for directed distributions.

	LN Uniform	LN Stripe	CSPG Stripe	LN Gradient	CSPG Gradient
n	81	67	50	435	136
CIRCULAR					
Mean angle (°)	290.21	1.90	178.61	293.78	300.90
Length of mean vector	0.11	0.90	0.89	0.15	0.16
Circular Standard Deviation (°)	120.78	13.363	14.038	112.18	109.873
Deviation from vertical axis	69.79	1.9	1.39	66.22	59.1
Corresponding figure	3d	4d	4h	5d	5h
LINEAR					
Mean (°)	188.55	135.01	182.93	197.58	183.09
Standard deviation (°)	105.43	166.43	173.01	109.04	111.47
Deviation from vertical axis	8.55	44.99	2.93	17.58	3.09
Corresponding figure	3c	4c	4g	5c	5g

Table 2.4: Comparison of circular and linear descriptive statistics for all experimental conditions tested.

	LN Uniform	LN Stripe	CSPG Stripe	LN Gradient	CSPG Gradient
CIRCULAR					
Rayleigh's	0.386	< 1E-12	< 1E-12	8.18E-05	0.032
Rao's Spacing	0.50 > p > 0.10	< 0.01	< 0.01	< 0.01	< 0.05
Watson's U^2	0.5 > p > 0.25	< 0.005	< 0.005	< 0.005	< 0.01
Kuiper's	> 0.15	< 0.01	< 0.01	< 0.01	< 0.01
LINEAR					
Chi squared (36 groups)	0.317	< 1E-12	1	0.04	0.089
Chi squared (3 groups)	0.097	0	0	0	0.006
Kolmogorov-Smirnov (Ha=uniform)	0.185	0	0	0	0.122

Table 2.5: Comparison of circular and linear goodness-of-fit statistical tests for all experimental conditions tested.

One sample uniformity tests developed for circular variables were performed for all experimental samples, including Rayleigh's, Rao's Spacing, Watson's U2 and Kuiper's test. Linear non-parametric one sample tests were also performed for all experimental samples including chi-squared (performed on data grouped in 3 bins) and KS tests (performed on ungrouped data). Significance levels taken to be $p<0.05$. Ha indicates the alternate hypothesis used.

at $p<0.05$ significance level, but p-values were much lower ($p<0.1$). Further examination of data shows similar mean angles on LN and CSPG striped substrates and on LN and CSPG gradient substrates (Table 2.4). Multisample analysis with Mardia-Watson-Wheeler and Watson's U2 test showed that neurites on striped LN and LN gradient substrates were significantly different from each other. Comparison with Student t-test shows that linear methods also show significant difference between neurite angles on LN stripe and gradient substrates (Table 2.6). Further examination of data shows differences in both mean angles and circular standard deviation (Table 2.4. For CSPG striped versus CSPG gradient substrates, Student t-test comparison shows no significant difference in neurite growth. However, circular analysis does show significant differences in neurite angles (Table 2.4). Further examination of the data shows that this distinction is due to the convergence of the linear mean towards 180° (Table 2.4).

2.3.2 Simulation Results

Simulations of circular data were performed to compare the results of circular and linear goodness-of-fit tests for one sample statistical analysis of known distributions. Simulations

Substrate	CIRCULAR Mardia-Watson Wheeler W	p	Watson's U^2	U^2 p	LINEAR Student t t	p
LN versus CSPG stripe	1.409	0.494	0.079	0.5 > p > 0.2	-1.515	0.066
LN versus CSPG gradient	0.056	> 0.5	0.021	0.989	1.345	0.090
LN stripe versus gradient	33.867	0.000	1.385	< 0.001	-4.033	0.000
CSPG stripe versus gradient	9.479	0.009	0.721	< 0.001	-0.007	0.497

Table 2.6: Comparison of circular and linear multisample tests for all experimental conditions tested.
Circular multisample tests Mardia-Watson-Wheeler and Watson's U2 test were performed to determine differences between neurite outgrowth on pairs of substrate types. Linear comparisons were performed using Student t-tests. Significance levels taken to be $p<0.05$.

of neurite angles were drawn from established circular statistical models such as uniform distribution to model the experimental condition of applying no directional cue, VM distribution to model the condition of applying one unidirectional cue and BM distribution to model the condition of applying two cues from two different directions. Because the sample size of neurite angles obtained from experimental data is variable based on the permissivity of the substrate, the sample size in simulated data was varied from n=5 to n=100 to cover a range of sample sizes used in neurite outgrowth analysis. Simulated circular data was only presented in circular histograms (Figure 2.6).

For uniform distributions, all directions between 0° and 360° are equally likely to occur, and μc is undefined as R=0. VM distribution is the most commonly used model for unimodal samples of circular data. As κ approaches 0, the distribution converges to a uniform distribution, and as κ approaches infinity, the distribution tends to concentration around the direction μc. Sample means of VM based data approached the population means (user-defined μc=0). Circular means were better approximated for simulated samples with tighter distributions, μc=11° where κ =0.85 and μc=5° where κ =3 (Figure 6b, c). Circular histograms of BM data highlight the difficulty in graphically assessing multimodality in data (Figure 6d, e). The means calculated for a BM distribution of (μ1=0°, μ2=90°) were 79° and 61°. For BM distributions, histograms do not show a clear distinction between the two subpopulations of data.

Table 2.7 shows the number of statistically significant (non-uniform) simulations out of 100

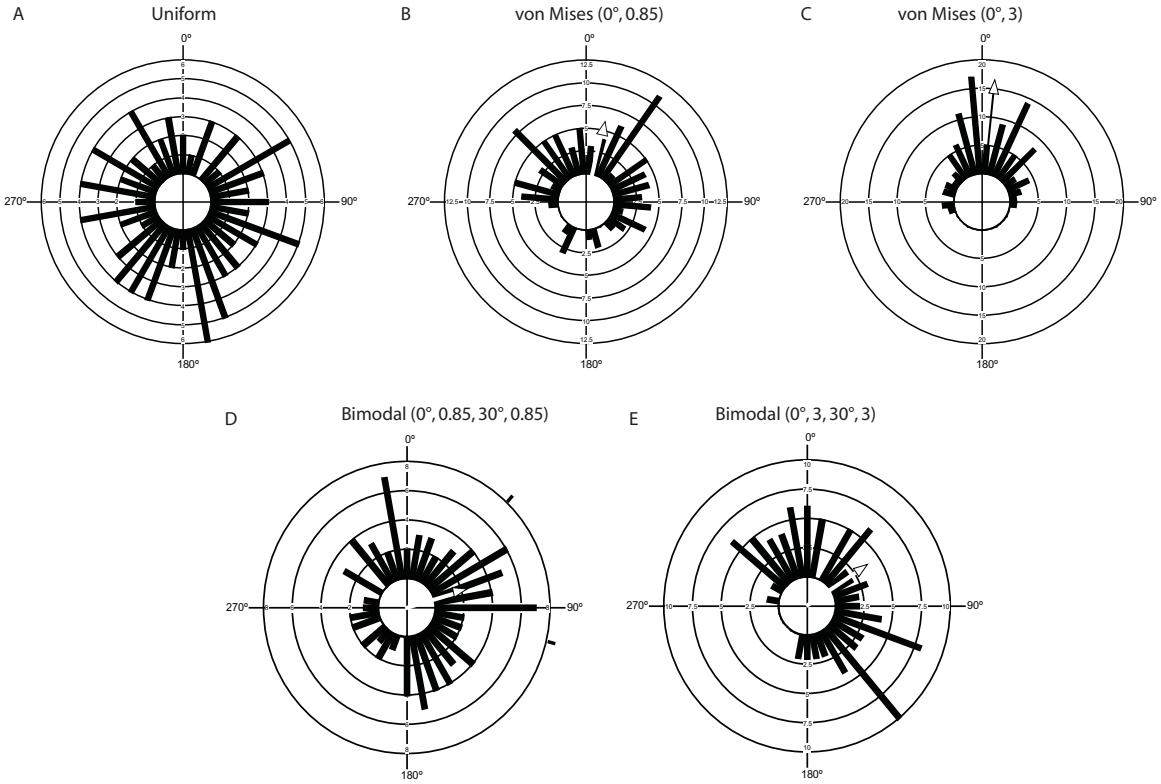

Figure 2.6: Representative circular histograms of simulated data generated by MATLAB algorithm.

Circular histograms of representative runs with n=100 angles generated from a (a) uniform circular distribution, (b) dispersed VM distribution ($\varkappa$=0.85) with a mean of 0^{o}, (c) tight VM distribution ($\varkappa$ =3) with a mean of 0^{o}, (d) dispersed BM distribution ($\varkappa$ =0.85) with means 0^{o} and 30^{o} and (e) tight BM distribution ($\varkappa$ =3) with means 0^{o} and 30^{o}.

trials, from each type of uniformity test listed in rows (Rayleigh, Rao's spacing, Watson's U2, Kuiper's and V-test). Watson's U2 test was unavailable for n=5 samples as the test's assumptions require n=10 for analysis using this method. Simulated data is listed in columns, with the type of distribution (uniform, VM and BM) described by its parameters (μ, $\varkappa$).

For uniform distributions, the number presented in Table VII when taken as a percentage corresponds to the Type I error of the given test. Type I error occurs when the null hypothesis (in this case, distribution is uniform) is rejected by the test when the null hypothesis is in fact true. A lower Type I error value indicates a better test for this type of data, as the test is wrong less often. As expected, for all tests, as n increases, Type I error decreases. Linear goodness-of-fit tests showed low Type I error for uniform distributions, indicating that nonparametric tests against a null hypothesis of uniformity such as KS tests are effective for determining uniformity. For circular tests, where n is small, Rao's spacing test has the lowest Type I error, which is consistent with other studies comparing one sample statistical tests (Bergin, 1991). For VM and BM distributions, the number of significant trials out of 100 corresponded to the power of the statistical test of interest. The expectation was that the tests would find the data significantly different from the null hypothesis of uniformity. Power is defined as the probability at which the null hypothesis will be rejected if it is false. As expected, increasing sample size corresponded to increasing power of each test.

For VM and BM distributions with large sample sizes (approaching n=100) K-S tests found VM and BM distributions to be significantly different from a Gaussian distribution. Overall circular tests performed similarly for VM distributions, although Rao's Spacing test was less powerful than other circular statistical one-sample tests. V-test had the highest power for VM datasets with small sample size and higher dispersion. For simulated data, the hypothesized mean direction was known as it was user defined. It is important to note that this hypothesized direction ($\vartheta 0$) must be assigned in advance of experimentation and if the null hypothesis is not rejected by the V-test, it is unknown whether the population is distributed uniformly or whether the distribution has a mean direction other than $\vartheta 0$. For one-sample data with an unknown external directional component, the Rayleigh test is usually recommended for unimodal data. (Batschelet, 1981; Fisher, 1993) Both the Rayleigh

	n	Uniform	VM (0,0.85)	VM (0,1)	VM (0,1.5)	VM (0,3)	BM(0, 90, 0.85, 0.85)	BM(0, 90, 1, 1)	BM(0, 90, 1.5, 1.5)	BM(0, 90, 3, 3)
CIRCULAR										
Rayleigh	5	10	17	24	34	75	13	22	46	79
	30	3	85	92	100	100	21	29	56	98
	100	6	100	100	100	100	69	87	97	100
Rao's Spacing	5	8	15	19	36	65	13	22	41	65
	30	6	39	45	83	100	6	14	17	85
	100	4	71	92	98	100	16	15	55	100
Watson's U^2	5									
	30	4	86	93	100	100	19	31	55	100
	100	6	100	100	100	100	67	88	98	100
Kuiper's	5	10	16	23	38	70	15	22	43	67
	30	3	80	92	100	100	20	32	56	98
	100	3	100	100	100	100	59	82	97	100
V-test	5	10	34	57	63	94	12	17	35	49
	30	3	95	97	100	100	33	54	76	100
	100	4	100	100	100	100	85	93	98	100
LINEAR										
Kolmogorov-Smirnov	5	0	0	0	0	0	0	0	0	0
Ha=normal	30	0	6	4	33	93	0	0	1	0
	100	2	99	99	100	100	7	0	47	97
Kolmogorov-Smirnov	5	4	12	6	13	21	0	5	2	9
Ha=uniform	30	1	38	59	86	100	0	28	49	94
	100	5	97	98	10	100	59	76	90	100

Table 2.7: Comparison of circular and linear goodness-of-fit statistical tests for simulated data of known distribution.
Each simulation in each condition was run 100 times, and each one-sample goodness of fit test listed in Table II was run for each simulation. Type I errors are listed for all conditions and for all tests performed. Ha indicates the alternate hypothesis used.

test and Kuiper's test yielded similar power levels for unimodal VM distributions, even for distributions with relatively high angular dispersion (corresponding to a lower κ value). The power of all circular statistical tests were higher than the corresponding linear K-S test against uniformity for simulated VM and BM distributions, except in the case where n=100. However, the power of the same test against a null hypothesis of a normal distribution is very low, such that most simulations showed that a K-S test did not find the simulated uniform distribution to be significantly different from a normal distribution.

As expected, one-sample uniformity tests exhibited low power when tested on BM distributions, as the cluster of data around two peaks began to resemble uniform data when both distributions had low concentration values. V-test showed the highest power when testing BM data against a null hypothesis. When the BM distribution was relatively clustered (at the highest concentration value tested κ=3), all tests showed higher power in detecting non-uniformity.

2.4 Discussion

The present study demonstrates that circular statistical methods may be used to analyze biological data containing directional biases and anisotropy, particularly to quantify neurite outgrowth. To analyze the direct effects of the underlying substratum of the culture surface on neuronal outgrowth, we plated and cultured neurons at low density for 24 hours and imaged the cultures for analysis. In the absence of directional cues, on uniform substrates, neurites were randomly oriented. The neurons on substrates with patterned protein stripes were highly aligned to the underlying stripe geometry. The neurons on substrates with graded anisotropy in protein concentration were directed towards the more permissive regions of the substrate.

In this report, we demonstrated the utility of an analysis procedure that we have found to be useful for evaluating a wide range of neurite outgrowth phenomena. First, circular histograms were plotted to visualize the data about a circular axis. The descriptive statistics were calculated for each distribution, including the mean angle, length of the mean vector, and the circular standard deviation. We then ran circular one-sample goodness-of-fit tests against uniformity and compared the circular methods to commonly used linear statistical methods. We simulated data with known distribution parameters to test the power of the circular and linear goodness-of-fit tests.

We have shown that circular statistical methods show sufficient power and are a better model than linear statistical methods to analyze directional neurite outgrowth on micropatterned substrates. Circular histograms and categorization allow easy visualization of data clustering, as demonstrated by histograms of neurite angles grouped around the direction of alignment. Circular data presentation avoids observational and truncation biases which occur in linear statistical analyses, for more accurate characterization of data. Circular statistical tests are more sensitive for smaller sample sizes, as shown by higher power of circular tests for simulations containing low n's. Further, they are more sensitive to complex distributions, as shown by the performance of multisample tests in comparing neurite angles on CSPG stripes versus CSPG gradients. The approximate linearity of a small arc,

in the case when data is clustered, is sometimes used to justify the application of linear models to simplify data analysis; however, different degrees of dispersion depending on the variability of the data can strongly affect the validity of this assumption. If there is any appreciable variability of circular data, it has been noted that the average of the dataset is better described by a resultant vector rather than the arithmetic mean (Fisher, 1993).

Evaluation of neurite outgrowth *in vitro* have included qualitative scoring systems with grouped categorical quantification (Dertinger et al., 2002; Sonigra et al., 1999; Sorensen et al., 2007), and measurement of neurite characteristics such as neurite length, area, number and branching patterns (Kim et al., 2006; Mann et al., 1998; Recknor et al., 2004). A number of studies initially demonstrated the ability of patterned striped substrates to support directional neurite outgrowth *in vitro* (Clark et al., 1993; Gomez and Letourneau, 1994) and the ability of concentration gradients to direct neuronal growth up concentration gradients (Walsh et al., 2005) by using traditional linear statistical methods. Categorization of circular data prior to using linear statistical methods has been a common approach to analyzing directional data. After the categorization of angular data into bins for plotting histograms (generally in bins of 10-20°), or into categories of "aligned" versus "unaligned," linear statistical tests can be applied to the groups of categorical data. ANOVAs are commonly used to test the differences between the degrees of neurite alignment over different substrates or experimental conditions (Macias et al., 2000; Sorensen et al., 2007). It is important to note that ANOVAs assume a Gaussian model for the distribution of angles which may not be accurate, depending on the population. Previous studies of neurite growth and orientation have used nonparametric statistical tests such as the $\chi 2$ test (Biran et al., 2003; Dertinger et al., 2002; Manwaring et al., 2004; Smeal et al., 2005) and the Kolmogorov-Smirnov (KS) test (Ming et al., 2001; Thompson and Buettner, 2006; Yuan et al., 2003). A rational for using nonparametric tests is that circular data of neurite outgrowth angles are rarely expected to approach a normal distribution (in a linear presentation) or a VM distribution (in a circular presentation). The $\chi 2$ and KS tests were also performed in this study and shown in some cases to perform differently from circular tests. One limitation of linear statistical methods for the application of directional neurite outgrowth in culture systems is that there may

be an overemphasis on the tails of the linear scale, in this case 0° and 180° or 360°. This overemphasis can result in artificially inflating the calculated variance of the data.

Other studies that analyze cellular phenomenon, particularly of cell migration, have recognized the need to present data in a nonlinear fashion in order to most appropriately visualize and analyze movement data which is usually highly complex, with cell trajectories tracing a relatively noisy path. If the nature of the path in response to a directional stimulus is of interest, the migration angle is usually an important aspect of analysis. Recent studies have utilized circular visualizations for data presentation, most commonly using Rose diagrams, where the frequency of migration angles are plotted around a circular axis with the area of each bar corresponding to frequency (Frevert et al., 2006; Papakonstanti et al., 2007; Saadi et al., 2006). In neuroscience literature, examples of visualization of angular data using circular methods have included neuronal migration (Ward et al., 2003), neurite outgrowth (Tailby et al., 2005), response to magnetic stimulation (Macias et al., 2000), and mitochondrial organization in axonal transport (Miller and Sheetz, 2004).

2.5 Conclusion

In conclusion, we have applied a statistical method for graphically representing and analyzing directional data pertaining to neurite growth that can be used to investigate neuronal cultures and their interactions with their microenvironment *in vitro*. Despite recent advances, current approaches to nerve repair fall short of restoring complete function, and *in vitro* systems that have been developed to more systematically study parameters affecting neurite growth have become more specific and quantitative. The techniques described here are useful in identifying directional neurite outgrowth patterns on *in vitro* platforms, allowing us to better evaluate neurite growth trajectories that exhibit circular geometry. Statistical methods such as uniformity tests provide a formal means to test hypotheses relating to neuronal responses to complex microenvironments, and circular histograms provide a visualization tool to investigate neuronal processes exhibiting circular geometries. This

approach offers a more informative way to probe the mechanisms of neurite outgrowth and guidance.

2.6 Acknowledgements

The authors thank Elizabeth Deweerd for assistance with alignment and gradient experiments, and Michael Sherback for assistance with MATLAB programming and for helpful discussion of the manuscript. This work was funded by an NSF CAREER grant to DHK and a Robert and Susan Kaplan Fellowship to GNL.

2.7 References

Abosch A, Lagenaur C. Sensitivity of neurite outgrowth to microfilament disruption varies with adhesion molecule substrate. Journal of Neurobiology, 1993; 24: 344-55.

Alexander JK, Fuss B, Colello RJ. Electric field-induced astrocyte alignment directs neurite outgrowth. Neuron Glia Biology, 2006; 2: 93.

Batschelet E. Circular statistics in biology. Academic Press: London, 1981. Bergin TM. A Comparison Of Goodness-Of-Fit Tests For Analysis Of Nest Orientation In Western Kingbirds (Tyrannus-Verticalis). Condor, 1991; 93: 164-71.

Bilsland J, Rigby M, Young L, Harper S. A rapid method for semi-quantitative analysis of neurite outgrowth from chick DRG explants using image analysis. Journal of neuroscience methods, 1999; 92: 75-85.

Biran R, Noble MD, Tresco PA. Directed nerve outgrowth is enhanced by engineered glial substrates. Experimental Neurology, 2003; 184: 141-52.

Bruder JM, Lee AP, Hoffman-Kim D. Biomimetic materials replicating Schwann cell topography enhance neuronal adhesion and neurite alignment *in vitro*. J Biomater Sci Polym Ed, 2007; 18: 967-82.

Bruder JM, Monu NC, Harrison MW, Hoffman-Kim D. Fabrication of Polymeric Replicas of Cell Surfaces with Nanoscale Resolution. Langmuir, 2006; 22: 8266-70.

Clark P, Britland S, Connolly P. Growth cone guidance and neuron morphology on micropatterned laminin surfaces. J Cell Sci, 1993; 105: 203-12.

Dertinger SK, Jiang X, Li Z, Murthy VN, Whitesides GM. Gradients of substrate-bound laminin orient axonal specification of neurons. Proc Natl Acad Sci U S A, 2002; 99: 12542-7.

Deumens R, Koopmans GC, den Bakker CGJ, Maquet V, Blacher S, Honig WMM, Jerome R, Pirard JP, Steinbusch HWM, Joosten EAJ. Alignment of glial cells stimulates directional neurite growth of CNS neurons *in vitro*. Neuroscience, 2004; 125: 591.

Fisher NI. Statistical Analysis of Circular Data. Cambridge University Press: Cambridge, U.K, 1993.

Frevert CW, Boggy G, Keenan TM, Folch A. Measurement of cell migration in response to an evolving radial chemokine gradient triggered by a microvalve. Lab Chip, 2006; 6: 849-56.

Goldner JS, Bruder JM, Li G, Gazzola D, Hoffman-Kim D. Neurite bridging across micropatterned grooves. Biomaterials, 2006; 27: 460-72.

Gomez TM, Letourneau PC. Filopodia initiate choices made by sensory neuron growth cones at laminin/fibronectin borders *in vitro*. J. Neurosci., 1994; 14: 5959-72.

Hynds DL, Snow DM. A semi-automated image analysis method to quantify neurite preference/axon guidance on a patterned substratum. Journal of Neuroscience Methods, 2002; 121: 53.

Karlon WJ, Covell JW, McCulloch AD, Hunter JJ, Omens JH. Automated measurement of myofiber disarray in transgenic mice with ventricular expression of ras. Anat Rec, 1998; 252: 612-25.

Kim IA, Park SA, Kim YJ, Kim SH, Shin HJ, Lee YJ, Kang SG, Shin JW. Effects of mechanical stimuli and microfiber-based substrate on neurite outgrowth and guidance. J Biosci Bioeng, 2006; 101: 120-6.

Le Roux PD, Reh TA. Regional differences in glial-derived factors that promote dendritic outgrowth from mouse cortical neurons *in vitro*. J. Neurosci., 1994; 14: 4639-55.

Li G, Liu J, Hoffman-Kim D. Multi-Molecular Gradients of Permissive and Inhibitory Cues Direct Neurite Outgrowth. Annals of Biomedical Engineering, 2007.

Macias MY, Battocletti JH, Sutton CH, Pintar FA, Maiman DJ. Directed and enhanced neurite growth with pulsed magnetic field stimulation. Bioelectromagnetics, 2000; 21: 272-86.

Mahoney MJ, Chen RR, Tan J, Saltzman WM. The influence of microchannels on neurite growth and architecture. Biomaterials, 2005; 26: 771-8.

Mann F, Zhukareva V, Pimenta A, Levitt P, Bolz J. Membrane-Associated Molecules Guide Limbic and Nonlimbic Thalamocortical Projections. J. Neurosci., 1998; 18: 9409-19.

Manwaring ME, Walsh JF, Tresco PA. Contact guidance induced organization of extracellular matrix. Biomaterials, 2004; 25: 3631-8.

Meijering E, Jacob M, Sarria JC, Steiner P, Hirling H, Unser M. Design and validation of a tool for neurite tracing and analysis in fluorescence microscopy images. Cytometry A, 2004; 58: 167-76.

Miller KE, Sheetz MP. Axonal mitochondrial transport and potential are correlated. J Cell Sci, 2004; 117: 2791-804.

Ming G-l, Henley J, Tessier-Lavigne M, Song H-j, Poo M-m. Electrical Activity Modulates Growth Cone Guidance by Diffusible Factors. Neuron, 2001; 29: 441-52.

Mitchell PJ, Hanson JC, Quets-Nguyen AT, Bergeron M, Smith RC. A quantitative method for analysis of *in vitro* neurite outgrowth. Journal of neuroscience methods, 2007; 164: 350-62.

Papakonstanti EA, Ridley AJ, Vanhaesebroeck B. The p110delta isoform of PI 3-kinase negatively controls RhoA and PTEN. EMBO J, 2007; 26: 3050-61.

Price RD, Oe T, Yamaji T, Matsuoka N. A simple, flexible, nonfluorescent system for the automated screening of neurite outgrowth. J Biomol Screen, 2006; 11: 155-64.

Recknor JB, Recknor JC, Sakaguchi DS, Mallapragada SK. Oriented astroglial cell growth on micropatterned polystyrene substrates. Biomaterials, 2004; 25: 2753-67.

Ronn LC, Ralets I, Hartz BP, Bech M, Berezin A, Berezin V, Moller A, Bock E. A simple procedure for quantification of neurite outgrowth based on stereological principles. Journal of neuroscience methods, 2000; 100: 25-32.

Saadi W, Wang S-J, Lin F, Jeon N. A parallel-gradient microfluidic chamber for quantitative analysis of breast cancer cell chemotaxis. Biomedical Microdevices, 2006; 8: 109-18.

Smeal RM, Rabbitt R, Biran R, Tresco PA. Substrate Curvature Influences the Direction of Nerve Outgrowth. Annals of Biomedical Engineering, 2005; 33: 376.

Smit M, Leng J, Klemke RL. Assay for neurite outgrowth quantification. BioTechniques, 2003; 35: 254-6.

Sonigra RJ, Brighton PC, Jacoby J, Hall S, Wigley CB. Adult rat olfactory nerve ensheathing cells are effective promoters of adult central nervous system neurite outgrowth in coculture. Glia, 1999; 25: 256-69.

Sorensen A, Alekseeva T, Katechia K, Robertson M, Riehle MO, Barnett SC. Long-term neurite orientation on astrocyte monolayers aligned by microtopography. Biomaterials, 2007; 28: 5498-508.

Tailby C, Wright LL, Metha AB, Calford MB. Activity-dependent maintenance and growth of dendrites in adult cortex. Proc Natl Acad Sci U S A, 2005; 102: 4631-6.

Thompson DM, Buettner HM. Neurite outgrowth is directed by schwann cell alignment in the absence of other guidance cues. Ann Biomed Eng, 2006; 34: 161-8.

Tran NH. Fracture orientation characterization: Minimizing statistical modelling errors. Computational Statistics & Data Analysis, 2007; 51: 3187-96.

Walsh JF, Manwaring ME, Tresco PA. Directional Neurite Outgrowth Is Enhanced by Engineered Meningeal Cell-Coated Substrates. Tissue Engineering, 2005; 11: 1085-94.

Ward M, McCann C, DeWulf M, Wu JY, Rao Y. Distinguishing between directional guidance and motility regulation in neuronal migration. J Neurosci, 2003; 23: 5170-7.

Weaver CM, Pinezich JD, Lindquist WB, Vazquez ME. An algorithm for neurite outgrowth reconstruction. Journal of neuroscience methods, 2003; 124: 197-205.

Yuan X-B, Jin M, Xu X, Song Y-Q, Wu C-P, Poo M-M, Duan S. Signalling and crosstalk of Rho GTPases in mediating axon guidance. Nat Cell Biol, 2003; 5: 38-45.

Zar JH. Biostatistical Analysis. Prentice-Hall: Englewood Cliffs, NJ, 1996.

Chapter 3

Multi-Molecular Gradients of Permissive and Inhibitory Cues Direct Neurite Outgrowth

Correct development of neuronal tracts requires the coordination of multiple permissive and inhibitory signals. By generating an *in vitro* microenvironment using soft lithography and microfluidic techniques, multiple guidance cues can be presented in a spatially defined way. Here we evaluated how neurites of dorsal root ganglia neurons responded to permissive and inhibitory cues presented by substrate-bound molecular gradients. Linear gradients containing inhibitory chondroitin sulfate proteoglycan (CSPG) and/or permissive laminin-1 (LN) were generated as single-cue gradients, parallel double-cue gradients, and opposing double-cue gradients with varying slopes. Neurite growth was analyzed using circular statistical methods, and for all gradients examined, neurons extended neurites toward regions of lower CSPG and higher LN concentrations. Single-cue gradients elicited similarly directed neurite growth responses at the higher concentrations tested for both LN and CSPG, and both gradient slope and fractional concentration change affected neurite growth. When the two contrasting molecular cues were presented together, neurites responded differently depending on the directions of the gradients. Neurite growth on LN-CSPG double gradients of oppo-

site direction was strongly directed, while neurite growth on LN-CSPG double gradients of parallel direction was uniform. These results represent an important step towards understanding how neurite growth is guided by complex microenvironments containing multiple molecular cues.

3.1 Introduction

A fundamental issue in developmental neuroscience is how growing axons find their way to establish the myriad of specific connections of the nervous system. This question is also critical to efforts toward promoting regrowth after injury, since regenerating axons re-express many characteristics from development. Answers were initially suggested by Ramón y Cajal, who posited that axons navigate by chemotaxis (Ramon y Cajal, 1892), and later by Sperry, who suspected that gradients of specific molecules could guide axons (Sperry, 1963).

The existence of attractive and repulsive molecules in the nervous system has been established experimentally, and it is largely accepted that the graded expression of guidance molecules plays an important role in forming the precise wiring of the nervous system (Dickson, 2002; Tessier-Lavigne and Goodman, 1996). However, how growing axons respond to gradients of guidance cues and integrate this information into a functional response is less well understood. Theoretical models provide differing hypotheses on how axons read gradients to infer critical guidance characteristics, and experiments have found differing cellular responses depending on the cell type and range of concentrations and slopes tested (Goodhill and Baier, 1998; Goodhill and Urbach, 1999; Loschinger et al., 2000).

Experimental work has suggested that axons could be guided by a wide range of parameters including the absolute molecular concentration, the gradient sign or direction, the gradient shape, the gradient slope or slope, and the fractional change in concentration (Bagnard et al., 2000; Halfter, 1996; Isbister et al., 2003; Rosentreter et al., 1998; Song et al., 1998; von Philipsborn et al., 2006). Previous studies of axon guidance by gradients have largely focused on examining diffusible gradients of soluble molecules such as neurotrophic factors,

semaphorins, and netrins (Bagnard et al., 1998; Bagnard et al., 2000; Kennedy et al., 1994; MacLennan et al., 1997; Song et al., 1998). Recently, gradients of soluble cues have been deposited on the surfaces of three-dimensional collagen gels (Rosoff et al., 2004). Many diffusible molecules reside *in vivo* largely bound within tissues and matrix (Kennedy et al., 1994; MacLennan et al., 1997). Thus, it is important to consider the direction of axon growth by surface-bound gradients, including gradients of soluble molecules, extracellular matrix molecules, and cell surface molecules. While axon guidance by discontinuous surface-bound molecules has been characterized for a number of systems, typically using variations of the stripe assay (Rosentreter et al., 1998; Snow and Letourneau, 1992), until recently it has been difficult to generate reproducible continuous gradients of surface-bound molecules *in vitro*. Recent studies have demonstrated the fabrication of molecular gradients with high degrees of resolution and control over gradient parameters through microfluidic techniques, achieving definition on the scale of hundreds of microns (Dertinger et al., 2002).

In this study, we used microfluidic techniques to create substrate-bound gradients of laminin-1 (LN), of chondroitin sulfate proteoglycan (CSPG), and of the two cues presented simultaneously. LN is a well-established permissive guidance cue that is present in developing and regenerating axonal tracts, and that can influence neurite direction and speed and reduce neurite retraction (Luckenbill-Edds, 1997). CSPGs are strong inhibitors of neurite growth that are present in boundary regions of the developing brain and in the glial scar and degenerating nerve after injury (Hoke and Silver, 1996). We analyzed the growth of postnatal rat dorsal root ganglion (DRG) neurons in response to permissive versus inhibitory cues, to single versus multi-cue gradients, to changes in absolute versus fractional molecular concentration, and to changes in gradient direction. The motivation for these studies is to gain a more rigorous comprehension of how growing neurons interpret their complex extracellular environment in which permissive and repulsive guidance molecules act in combination to direct axonal growth.

3.2 Materials and Methods

3.2.1 Fabrication of gradient mixer

The microfluidic gradient mixers used to generate patterns of protein gradients (Figure 3.1a) were fabricated using soft lithography and rapid prototyping. Gradient mixer masks were designed using patterns modified from Dertinger et al. (Dertinger et al., 2002), and patterns were transferred onto silicon wafers using photolithography. Gradient mixers were made by fabricating poly(dimethylsiloxane) (PDMS) impression replicas of the pattern from the silicon wafer masters. Gradient mixers were then assembled by adhesion of PDMS microchannels to glass surfaces. Patterns for photolithography were designed with AutoCAD LT 2004 (Autodesk Inc, San Rafael, CA) and printed on high resolution transparent film at 10,000 dpi (CAD/Art Services, Inc., Bandon, OR). Standard photolithography techniques were used to pattern substrates. Silicon wafers (Silicon Sense Inc, Nashua, NH) were coated with a layer of negative tone Nano SU-8 50 photoresist (MicroChem, Newton, MA) by spin coating with a CEE100 spinner (Brewer Science, Rolla, MO) in a two stage process: 1) spinning at 500rpm for 10sec with a ramp of 100rpm/sec, and 2) spinning at 2000rpm for 30sec with a ramp of 300rpm/sec. Wafers were baked at 65°C for 6min, baked at 95°C for 20min, and slowly cooled to 22°C. Photoresist was polymerized by UV exposure through the patterned film with a Karl Suss mask aligner (MJB3 UV300) at 5.3 mW/cm2 for 1.1min. Wafers were baked at 65°C for 2min, 95°C for 5min, and slowly cooled. Non-crosslinked photoresist was dissolved with SU-8 Developer (MicroChem), and wafers were rinsed with isopropyl alcohol (IPA) and dried under nitrogen. Tridecafluoro-1,1,2,2-tetrahydrooctyl-1-trichlorosilane (silane, United Chemical Technologies, Bristol, PA) was deposited under vacuum onto the micropatterned wafers to prevent adhesion of the photoresist to the polydimethylsiloxane (PDMS) during casting. Sylgard 184 PDMS elastomer base (Dow Corning, Midland, MI) was mixed with Sylgard 184 PDMS curing agent at a 10:1 wt/wt ratio, degassed, poured onto micropatterned wafers to a thickness of 1-2 mm, and cured at 95°C for 60min. PDMS replicas of gradient mixer patterns were cut out and inlet and outlet holes were made using a steel punch. PDMS substrate and a clean glass slide were plasma activated at 10.5 W for

60 sec with a plasma cleaner/sterilizer (PDC – 32 G, Med RF level, Harrick, Pleasantville, NY), and brought together immediately after activation to form an irreversible seal. To prevent the final gradient channel from bonding irreversibly to the glass slide, the final channel was covered with a piece of PDMS while plasma activation occurred. Immediately following plasma activation and bonding of the PDMS and glass, the microchannels were filled with poly-L-lysine (pLL) solution (1mg/mL, MW 30-70kDa, Sigma, St. Louis, MO) and allowed to adsorb for 4 hours. Channels were rinsed with dH2O to remove excess pLL, and protein solutions to generate gradients were applied and stored hydrated at 4^{o}C overnight.

3.2.2 Generation of protein gradients

Table 3.1 lists the types of gradients generated for this study. Polyethylene tubes inserted into the inlet and outlet ports were attached to 1mL syringes containing varying mouse LN solutions (10μg/mL or 50μg/mL, Invitrogen, Carlsbad, CA) varying CSPG solutions from embryonic chick brain (10μg/mL or 20μg/mL; Chemicon, Temecula, CA), and 3% bovine serum albumin (BSA) in phosphate buffered saline (PBS). Single-cue gradients of LN and CSPG were generated by delivering either protein solution into one inlet of the microchannels, and BSA, a neutral molecule, into the second inlet of the microchannels with a syringe pump set to a constant flow rate of 0.2μL/min. Double contrasting gradients were generated in a similar manner using LN and CSPG solutions in the respective inlets to the gradient mixer. Double parallel gradients were generated by adding both LN and CSPG solutions to one inlet, and BSA to the second inlet of the gradient mixer. The solutions were delivered over 12h to allow adsorption of the proteins onto the glass slide. After adsorption of the protein gradient, the PDMS covering the final gradient channel was cut and peeled from the substrate to expose the area over the final gradient channel for cell culture. Gradient-containing substrates were stored in PBS at 4°C overnight.

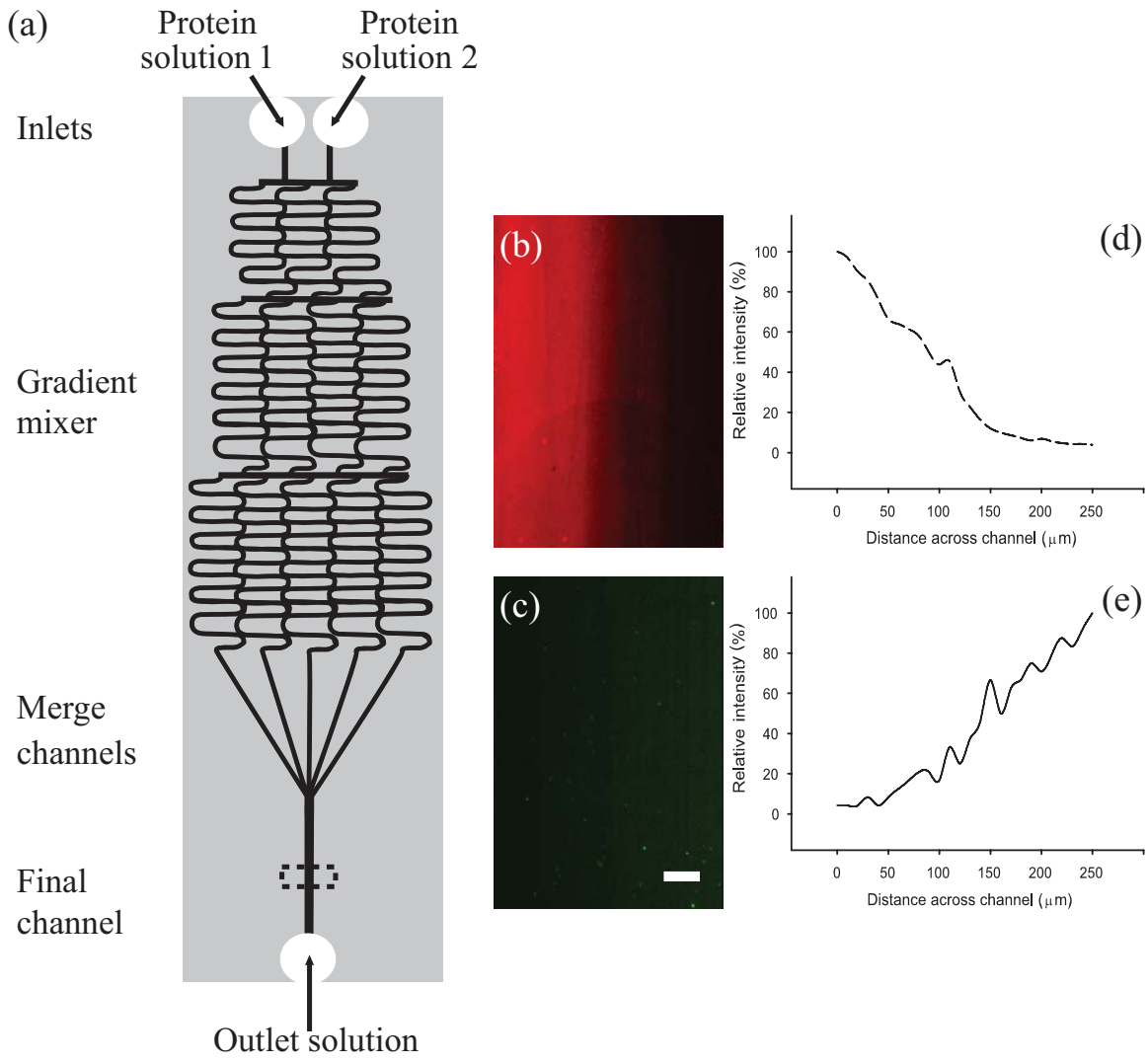

Figure 3.1: Microfluidic gradient mixer generates linear substrate-bound protein gradients. (a) Schematic diagram of gradient mixer used to generate multiple gradient types. Dashed rectangle shows the region analyzed in b-e. (b,c) Fluorescent micrographs of the double-cue opposing gradient (LN50/CSPG10) channel stained with anti-LN (b) and with anti-CSPG (c) immunohistochemistry. Bar = 50μm. (d) Corresponding densitometric analysis of pixel intensity of anti-LN (solid line) and anti-CSPG (dotted line) immunohistochemistry for LN50/CSPG10 gradients. r=0.96 for anti-LN, r=0.97 for anti-CSPG. (e) Densitometric analysis of double cue parallel gradient (LN50CSPG10/BSA) stained with anti-LN (solid line) and anti-CSPG (dotted line) immunohistochemistry. r=0.76 for both molecules.

Substrate name (Inlet 1/Inlet 2)	Gradient Type	Inlet 1 concentration (μg mL^{-1})	Inlet 2 concentration (μg mL^{-1})	Slope (LN) (μg mL^{-1}µm^{-1})	Slope (CSPG) (μgmL^{-1} μm^{-1})
LN50	Uniform permissive	50	50	0	N/A
LN10	Uniform permissive	10	10	0	N/A
LN50/BSA	Single permissive	50	30,000	0.2	N/A
LN10/BSA	Single permissive	10	30,000	0.04	N/A
LN50/LN40	Single permissive	50	40	0.2	N/A
BSA/CSPG10	Single inhibitory	30,000	10	N/A	0.08
BSA/CSPG20	Single inhibitory	30,000	20	N/A	0.08
LN50/CSPG10	Double opposing	50	10	0.2	0.04
LN10/CSPG10	Double opposing	10	10	0.04	0.04
LN10/CSPG20	Double opposing	10	20	0.04	0.08
LN50CSPG10/BSA	Double parallel	50, 10	30,000	0.2	0.04

Table 3.1: Gradients tested

3.2.3 DRG neuronal cell culture

All reagents were from Invitrogen unless otherwise specified. DRG were dissected from the spinal columns of postnatal (P0-P4) rat pups and cleaned of axons, blood, and connective tissue. DRG were incubated in 0.05% trypsin-EDTA in Hank's balanced salt solution without calcium or magnesium at 37 $^{\circ}$C for 60min and dissociated by trituration. Cells were plated at 2600 cells/cm2 in 2mL of serum-containing medium: Dulbecco's Modified Eagle's Medium, 10% fetal bovine serum, 4mM L-glutamine, penicillin (100U/ml)/streptomycin (100µg/ml) and 50ng/ml nerve growth factor (7S; Sigma). Cultures were incubated at 37°C with 5% CO2 in a humidified environment for 24h.

3.2.4 Visualization of gradients and DRG neurons

Samples were fixed with 2% paraformaldehyde (Sigma) in PBS for 20min at room temperature, then rinsed with PBS. Nonspecific staining was blocked by incubating for 1h at room temperature with 10% goat serum, 1% bovine serum albumin (Sigma), in PBS (blocking buffer) with the addition of 0.1% Triton X-100 (VWR) for permeabilization. Antibody

against neurofilament (mouse monoclonal RT97, 1:200, Developmental Studies Hybridoma Bank, Iowa City, IA) was used to visualize neurons, and antibodies against LN (rabbit polyclonal, 1:500, Biomedical Technologies Inc, Stoughton, MA) and against CSPG (mouse monoclonal CS56, 1:100, Sigma) were used to visualize the gradient. Following incubation with primary antibody, samples were rinsed in PBS, reacted for 1h at room temperature with appropriate secondary antibody (The Jackson Laboratory, Bar Harbor, ME) diluted 1:200 in blocking buffer, and rinsed in PBS. As a control, samples were processed without incubation with primary antibody. Samples were examined on a Nikon Eclipse TE2000-S microscope, equipped with phase-contrast and epifluorescence optics with appropriate filter cubes. Images were captured using a Hamamatsu Orca-ER camera and Orbit shutter controller (Improvision, Lexington, MA), outputting to OpenLab v4.0.2 (Improvision) running on Mac OS v10.2. Contrast adjustments for visualization were performed using the level function in Adobe Photoshop CS2.

3.2.5 Characterization of gradients

To quantify intensity changes across the gradients, comparative densitometry was performed for all samples. Intensity values for ten positions across the channel were measured using OpenLab. Intensity units were calibrated to a scale of 0-100% where 100% represents the highest intensity observed on the substrate corresponding to the highest concentration of molecule and 0% represents no fluorescence. Least-squares regression was used to fit a linear trend line to the data. For this analysis we defined each molecular concentration as a fraction of the initial concentration applied at the inlet of the gradient mixer, based on theoretical mixing in the microchannels as described by the following equation, where C(t,x) is the concentration at time t and at point x, D the diffusion coefficient in cm^2/s, t the time in s, l the width of the channel in μm, h the width of the initial distribution in μm, and C_0 the initial concentration in the channel in \mug/mL (Jeon et al., 2000). The slope of each molecular gradient was defined as the change in molecular concentration per micrometer, where the inlet concentration was taken to be the maximal protein concentration, according to the method of Dertinger et al. (Dertinger et al., 2002). Fractional concentration change

was defined as the percent concentration change (concentration change/initial maximum concentration) across the width of a typical DRG neuron growth cone, 10μm.

3.2.6 Quantification of cell response and statistical analysis

For quantification of cellular adhesion, each gradient substrate area was analyzed in five parallel, longitudinal regions across the width of the final microchannel. Each longitudinal region was 50μm wide and contained different concentrations of LN and CSPG. Cell adhesion was measured by counting the number of cells in each region for each substrate tested. A χ2 test was used to test for uniformity of the cell adhesion pattern. The length and angle of the longest neurite were measured for all neurons on the final gradient channel for which the neurite did not contact another neuron. This method was adapted from Dertinger et al., where the longest neurite was taken to represent the direction of neurite orientation, as the longest neurite eventually becomes the axon of a polarized cell (Dertinger et al., 2002). Kuiper's test for uniformity was used to evaluate if directionality of neurite growth occurred on gradient substrates, in contrast to the alternate hypothesis of random uniform outgrowth in all directions. Descriptive statistics such as circular mean vectors (with magnitude and direction components corresponding to clustering about the mean and mean direction respectively) and standard deviation were then determined to approximate the expected norm and spread in the neurite angle distribution. To characterize the overall direction of neurite outgrowth, neurite angles were further categorized into three categories: 1) growth towards the permissive cue, defined by angles in the range of 240-360° and 0-60°, 2) vertical growth, defined by angles in the range of 60-120° and 240-300°, 3) growth towards the inhibitory cue, defined by angles in the range of 120-240° (Figure 3.2c). To evaluate the effect of fractional concentration change on neurite orientation, the entire channel width was analyzed in 25 regions of 10 microns, the width of a typical growth cone, and the longest neurite of each neuron in each region was analyzed. To evaluate the effect of slope on neurite orientation, the angles of the longest neurites from neurons growing on protein gradients of different slopes were grouped. To evaluate the effect of regional adhesion on neurite orientation, the number of neurons adhered to each region of 10 microns was measured

and normalized to the total number of neurons on each substrate. To test for correlation between variables, i.e. neurite angle versus 25 regions for fractional concentration change, neurite angle versus inlet concentration for slope, and neurite angle versus regional adhesion, circular-linear coefficient and the associated significance were calculated. Oriana software (Anglesey, Wales) was used, and significance levels were taken to be $p<0.05$.

3.3 Results

3.3.1 Multi-molecular gradients generated

Protein gradients were first generated in solution by interdiffusion of adjacent laminar streams in microchannels, then the soluble gradients were adsorbed onto glass substrates coated with pLL to form substrate-bound gradients (Figure 3.1a). Laminar flow through the microchannels allowed for slow interdiffusion of the two proteins with even mixing and adsorption. Serial dilution and intermixing of multiple streams of varying concentrations gave rise to a step gradient at the convergence point of the streams, which formed a smooth gradient in the final channel. Gradients of varying slopes across the 250µm width of the channel were generated by changing the concentration of protein added to the inlet channels. Quantitative densitometry of immunofluorescence images of the gradient channel confirmed shapes of the adsorbed protein gradients generated (Figure 3.1b-e).

3.3.2 Molecular concentration and slope affect neurite growth

DRG neurons adhered and extended neurites on gradients, and were identified as neurons by immunocytochemistry for neurofilament (Figure 3.5d-f), which facilitated distinction of the neurons from the few DRG-derived Schwann cells in the cultures. As a control, DRG neurons cultured on uniformly coated LN coverslips were double immunostained with antibodies RT97 (anti-neurofilament) and S100 (a stain for glia), and imaged under confocal microscopy (Figure 3.2a). Distinct cell populations of neurons and glia were observed, as

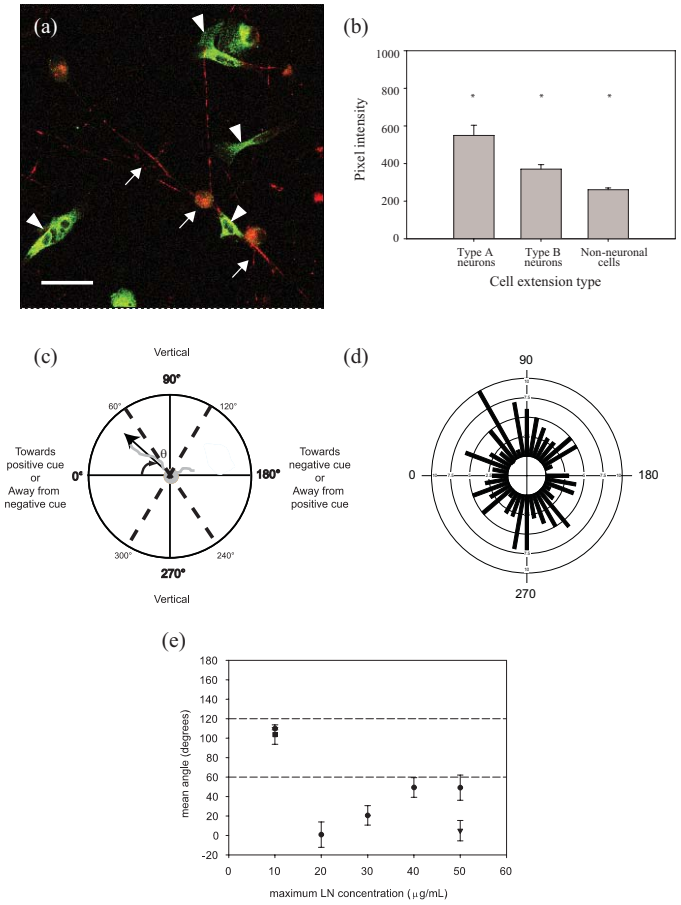

Figure 3.2: (a) Neurofilament and S100 double immunostaining allows identification of DRG neurons and non-neuronal cells in culture.
Overlaid confocal images of DRG cultures cultured on uniform LN substrates double stained with anti-neurofilament and Cy2 secondary antibody to identify neurons (red, indicated by arrows) and anti-S100 and Cy3 secondary antibody to stain for Schwann cells (green, indicated by arrowheads). Scale bar = 20μm. (b) Quantitative densitometry allows identification of DRG neuronal subtypes and non-neuronal cells. Histogram shows pixel intensities of anti-neurofilament stained DRG cultures on uniform LN substrates containing neuronal subtypes A, B and non-neuronal cells. *denotes statistical significance from all other groups at $p<0.05$. (c) Analysis of directional growth of neurites by quantifying the longest neurite per neuron. Schematic shows method of neurite angle measurement and the range of angles categorized as neurites growing "towards" or "away from" permissive/inhibitory cues presented, or growth in a "vertical" direction. (d) Concentration of LN affects neurite outgrowth. Dissociated DRG neurons were cultured on substrates with varied LN concentrations and corresponding slopes. Graph of mean neurite angles, rescaled from a 360^{o} scale to a 180^{o} scale for the linear plot, where mean angle of $0\text{-}60^{o}$ is defined as growth toward LN, $60\text{-}120^{o}$ is defined as vertical growth, and $120\text{-}180^{o}$ is defined as growth away from LN, as shown in (c). Square, LN10/BSA; Circle, LN50/BSA; Triangle, LN50/LN40.

shown by the minimal overlap between the neurofilament and S100 stains. Further, the morphology of the neurofilament positive cells was much different than that of the S100 positive cells, where the neurofilament positive cells were higher in the z-direction and S100 positive cells were flatter, showing that neurons were morphologically distinct from other cell populations in our culture system (data not shown). Comparative densitometry of neurofilament stained DRG images captured at constant exposure time showed that brightness of staining with anti-neurofilament is significantly different between the processes of neuronal subtypes A and B and non-neuronal cells (Figure 3.2b), allowing identification of neuronal versus non-neuronal populations in DRG cultures studied. A comparison of neuronal response to substrates presenting varying concentrations and slopes of LN showed that both these variables affected neurite growth (Table 3.2, Figure 3.2). When [LN]max applied was increased from 10 μg mL^{-1} to 50 μg mL^{-1} and slope was held constant at 0.04μg mL$^{-1}\mu$m^{-1}, neurite outgrowth was directed on both gradients (Kuiper's test; $p<0.05$), but neurite distributions were different. Where [LN]max applied was 50 μg mL^{-1} the angles were biased towards the direction of increasing [LN]. For the samples where the [LN]max applied was 10 µg mL-1 , neurites did not grow equally in all directions, but the mean of the distribution of neurite angles was 98°. Closer examination of the circular histogram of the LN10/BSA data (Figure 3.3e) revealed two clusters of neurites that contributed to this result, suggesting bimodality. One cluster of neurites grew at an angle between 50° and 70°, and a smaller cluster of neurites grew in the direction of 240°. Taken together with the entire distribution, these two clusters led to the nonuniform neurite angle distribution, with the corresponding mean vector of 98°. This distribution differed from the neurite angle distribution of LN50/BSA, where the majority of neurites grew towards the direction of higher [LN] (Figure 3.3c). When [LN]max was held constant at 50µg/ml and slope was increased from 0-0.04 μg mL$^{-1}\mu$m^{-1}„ the neurite angle distribution changed from uniform (Kuiper's test; $p>0.05$) to oriented toward higher [LN] (Kuiper's test; $p<0.05$). When the slope was increased further to 0.2 μg mL$^{-1}\mu$m^{-1}„ the neurite angles remained oriented toward higher [LN]. Examination of the mean neurite angles on gradients with varying [LN] shows that for [LN]max $>$ 20µg, neurite angles were directed toward higher [LN] (Figure 3.2d).

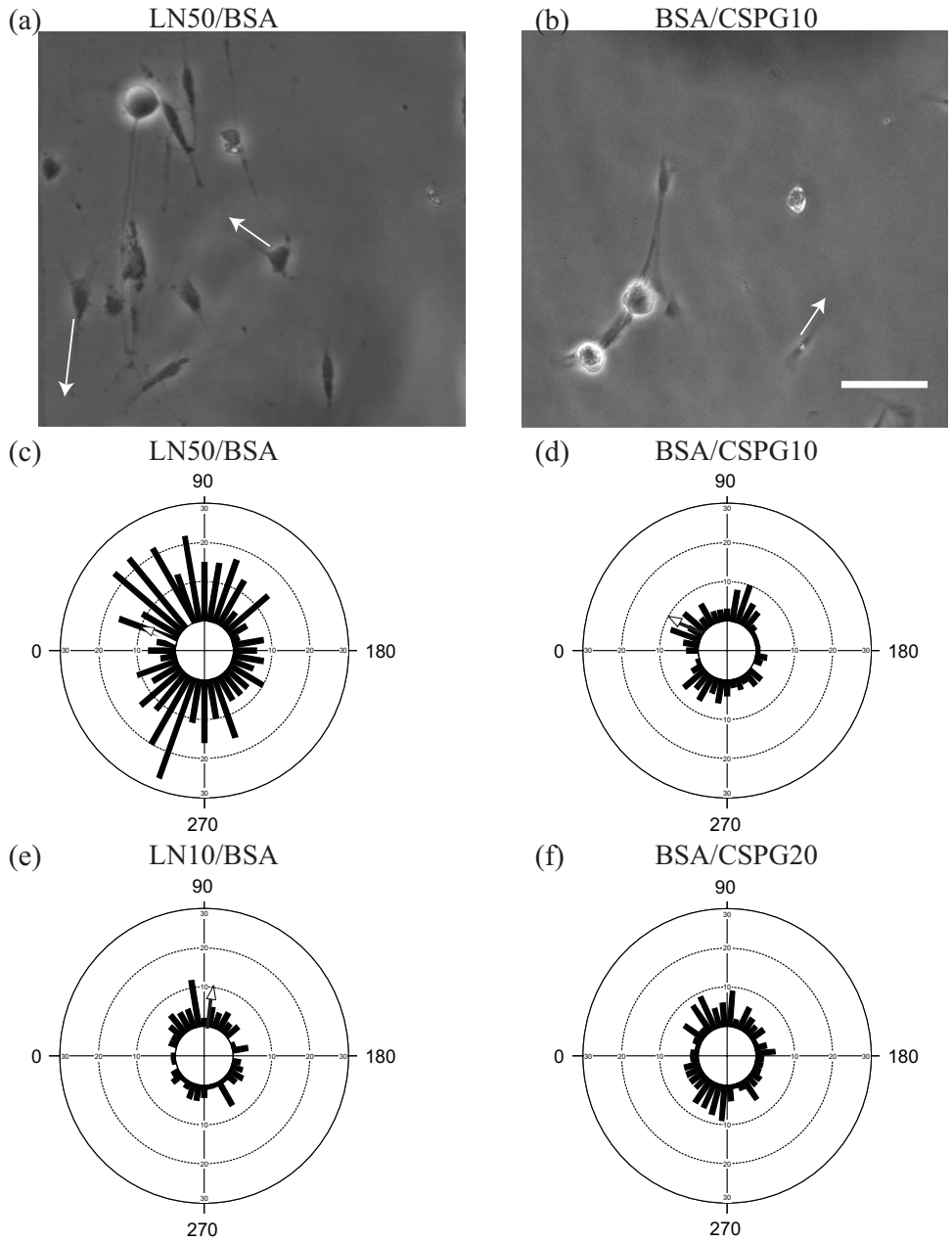

Figure 3.3: DRG neurite outgrowth on single-cue gradients is directed toward higher LN or lower CSPG concentration.

Phase contrast micrograph of dissociated DRG neurons cultured for 24 hours on single-cue LN50/BSA (a) or BSA/CSPG10 (b) gradients shown under phase contrast microscopy. Bar = 50μm. Arrows show the vectors that were used to evaluate the neurites. Circular histograms show the corresponding distributions of neurite angles on single-cue LN50/BSA (c), BSA/CSPG10 (d), LN10/BSA (e) or BSA/CSPG20 (f) gradients, where each angle presented is the angle of the longest neurite per neuron. White arrows indicate mean neurite angles for directed distributions; mean angles were not shown for uniform distributions.

	LN10 uniform	LN50 uniform	LN10/BSA	LN50/LN40	LN50/BSA
Slope (µg mL-1 µm-1)	0	0	0.04	0.04	0.2
[LN]max applied (µg mL-1)	10	50	10	50	50
Angle distribution	uniform	uniform	directed	directed	directed
Mean angle (º)	N/A	N/A	98	4	23

Table 3.2: Concentration and slope of LN gradients affect neurite outgrowth. Maximum applied LN concentration and slope characteristic of each type of substrate are shown, with resulting neurite angle distribution and mean neurite angle.

3.3.3 Neurite outgrowth on single-cue gradients of contrasting cues

Neuronal growth was compared on single-cue gradients whose maximum concentrations of guidance cues were previously shown to influence neuronal growth, i.e. 50µg/ml LN and 10µg/ml CSPG in the applied solution (Figure 3.3a-d). DRG neurons extended neurites on both LN and CSPG single-cue gradients, and Kuiper's uniformity test showed that in each case the distribution of neurite angles was directed, either toward higher concentrations of permissive LN on LN gradients, or toward lower concentrations of inhibitory CSPG on CSPG gradients. Comparison of the distributions of the neurite angles on LN gradients versus on CSPG gradients revealed that the two distributions were directed to a similar degree, and the distributions were not significantly different from each other (mean direction of 23.4° for LN gradient and 30.9° for CSPG gradient). Neurite growth was analyzed in response to the fractional concentration change (dC/C) across the width of an average DRG growth cone (10µm). On the LN single-cue gradients, as the concentration of LN decreased linearly from 100% on the left side of the gradient channel to 0% on the right side, the fractional concentration change increased exponentially from 0% on the left side to 100% on the right side (Figure 3.4a). The CSPG single-cue gradients contained similar absolute and fractional concentration profiles to the LN gradients, except that the left-to-right directions were reversed, since CSPG was infused through the right inlet and LN was infused through the left inlet for gradient generation (Figure 3.4b). On the LN gradient, more neurites were directed toward a higher LN concentration when they encountered the highest change in fractional concentration (100% change), whereas in contrast on the CSPG gradient, more neurites were directed toward a lower CSPG concentration when they encountered the lowest change in fractional concentration (4% change) (Figure 3.4c). This differential response on the gra-

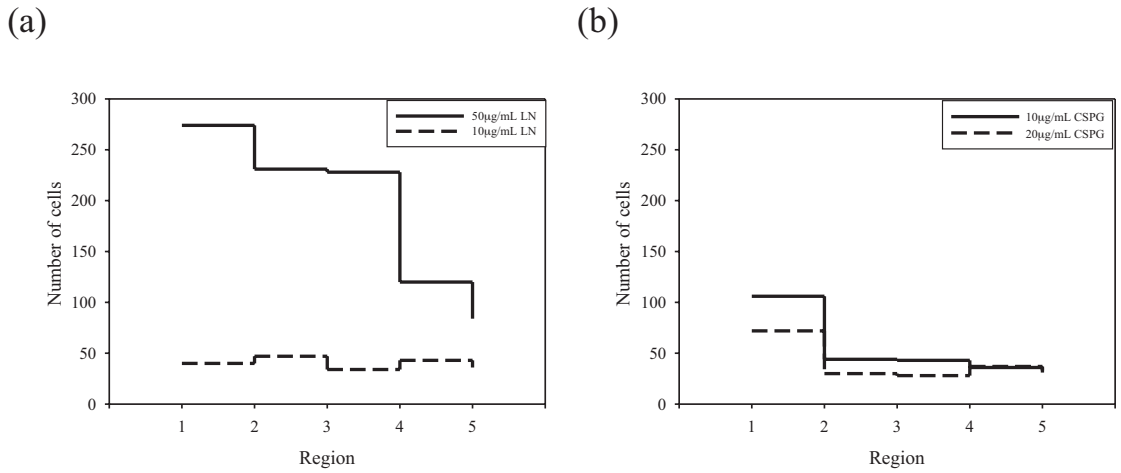

Figure 3.4: Growth evaluated in context of fractional concentration change.
(a,b) Fractional concentration change (dashed lines) is exponential for gradients of linear slope (solid lines). Change in concentration is expressed as the percent change in concentration over a 10μm region, across the channel width, for LN gradients with LN in inlet 1 (a) and for CSPG gradients with CSPG in inlet 2 (b). (c) Graph of neurite outgrowth direction in response to change in fractional concentration for single-cue gradients. Region 1 corresponds to a fractional concentration change of 4% in LN and 100% in CSPG, while region 25 corresponds to a fractional concentration change of 100% in LN and 4% in CSPG.

dient substrate may contribute to bimodality in neurite angle distributions when analyzed as a whole. The influence of the change in concentration of molecular cues was tested by varying inlet concentration, thus generating gradients of different maximum concentrations and corresponding different slopes. Neurite growth direction was affected by slope, such that when the LN gradient slope decreased from 0.2μg/mL μm-1 to 0.04μg/mL/μm, the mean direction of the distribution of neurite angles changed from 23.4° (toward increasing LN concentration) to 98° (oriented in a vertical, non-preferential direction) (Figure 3.3c, e). When the CSPG gradient slope was increased from 0.04μg/mL/μm, to 0.08μg/mL/μm, the neurite angle distribution changed from directed to not significantly directed ($0.05<p<0.1$) as tested by Kuiper's test; however, the mean direction changed from 30.9° (toward decreasing CSPG concentration) to 17.6° (more oriented toward decreasing CSPG concentration) (Figure 3.3d, f).

3.3.4 Neuronal adhesion and neurite elongation on single-cue gradients

Cell adhesion patterns were also influenced by the type of cue and the protein gradients presented. Higher total numbers of DRG neurons adhered to LN gradients than to CSPG gradients. DRG neurons adhered preferentially to regions of the substrates that contained higher permissive LN and lower inhibitory CSPG concentrations. A χ^2 test for uniformity demonstrated that DRG neuronal adhesion patterns were non-uniform on the LN and the CSPG gradients ($p<0.05$), and there was a graded increase in adhesion along the LN gradient in the direction of increasing LN concentration. In contrast, there was a threshold response in adhesion along the CSPG gradient with relatively small increases in adhesion in the direction of decreasing CSPG concentration until the final 1/5 of the channel width, where the frequency of adhered cells doubled in the region containing the lowest CSPG concentration (Figure **??**). Varying the slope of concentration gradients across the width of the channel of the LN gradient elicited different cellular adhesion responses, but changes were not seen in response to varying the slope of the CSPG gradient. Decreasing the slope of the LN gradient from 0.2μg/mL/μm to 0.04μg/mL/μm, changed the DRG neuronal adhesion pattern from non-uniform to uniform, but increasing the slope of the CSPG gradient from 0.04μg/mL/μm to 0.08μg/mL/μm, did not alter the cell adhesion patterns. Neurite elongation on single-cue gradients was evaluated by measuring the mean length of the longest neurite for all neurons observed. No significant difference in length of the longest neurite was found between substrates of different slopes or different types of cues (Table 4). To ensure that directional neurite outgrowth and adhesion patterns were not a consequence of the physical dimensions of the microchannels or of residual flow patterns during the gradient generation step, neuronal response on uniformly coated substrates of the same dimensions were tested. The distributions of neurite angles and neuronal adhesion were uniform across the channel width of uniform substrates.

Variables	r	p-value
Angle v. Slope (LN)	0.13	1.21E-04*
Angle v. Fractional LN change	0.247	8.12E-09*
Angle v. Regional adhesion (LN)	0.257	1.61E-09*
Angle v. Slope (CSPG)	0.014	0.983
Angle v. Fractional CSPG change	0.17	0.033*
Angle v. Regional adhesion (CSPG)	0.269	2.11E-4*

Table 3.3: Effects of slope, fractional concentration change, and regional adhesion on neurite angles.
Circular-linear correlation coefficients (r) and associated significance (p-value), shown for both LN50/BSA and CSPG10/BSA gradients. Slope affects direction of neurite outgrowth on LN gradients, but not on CSPG gradients. Fractional change affects neurite orientation on both gradient types tested. Regional adhesion affects neurite orientation on both gradient types tested. *Significance level taken to be $p<0.05$.

3.3.5 Multiple parameters affect neurite outgrowth on single-cue gradients

To test the relative effects of fractional concentration change and slope on neurite orientation, the correlation between neurite angles measured per substrate or neurite angles per 10μm region were calculated. Because neurite angle is a circular variable whereas the slope is a linear variable, a circular-linear coefficient and the significance of the correlation were determined (Mardia and Jupp, 2000) (Table 3.3). For both LN and CSPG gradients, circular-linear correlation analysis demonstrated a significant correlation between the fractional concentration change and the angles of the neurites growing over that change in concentration. LN gradients showed a significant correlation between the neurite angle and slope whereas CSPG gradients did not yield a significant correlation between the two variables. To test the effects of regional adhesion on neurite orientation, correlations between neurite angles and the number of neurons per 10µm region (normalized to the total number of neurons per substrate) were calculated. For both LN and CSPG gradients, circular-linear analysis showed a significant correlation between regional adhesion and the angles of the neurites growing in the region.

Substrate	n	Mean length (μm)	Standard deviation (μm)
LN 10	163	27.93	18.25
LN50	135	45.03	44.12
LN10/BSA	107	24.51	12.33
LN50/BSA	434	28.74	18.71
LN50/LN40	147	35.39	31.39
BSA/CSPG10	136	16.36	6.89
BSA/CSPG20	83	22.78	12.57
LN10/CSPG10	31	41.70	63.42
LN50/CSPG10	363	32.70	28.48
LN50/CSPG20	75	27.73	32.46
LN50CSPG10/BSA	82	30.44	16.21

Table 3.4: Neurite length is not affected by type of cue or by gradient slope. Mean and standard deviation of length of longest neurite measured on all gradient substrates tested.

3.3.6 Neurite outgrowth on double-cue opposing gradients

Double-cue gradients were generated in which LN increased in concentration linearly from right to left, and simultaneously, CSPG increased in concentration linearly from left to right across the final channel width, by infusing LN into the left inlet and CSPG into the right inlet of the same gradient mixer (Figure 3.1b-d). The DRG neuronal growth responses to these double-cue opposing gradients were similar in orientation to the responses to single-cue gradients of identical concentrations (Figure 3.5b, e, h, k – LN50/CSPG10). Mean neurite direction was 340.6°, which was more directed toward increasing LN concentration and decreasing CSPG concentration than the mean directions for neurite growth on the single-cue LN50/BSA and BSA/CSPG10 gradients (23.4° and 30.9°, respectively, see Figure 3.3c, d). On double-cue opposing gradients of different slopes, DRG neuronal responses were also similar to those on single-cue gradients, where neurite growth was vertical and non-preferential on gradients with either decreased LN slope (from 0.2μg/mL/μm to 0.04μg/mL/μm) or increased CSPG slope (from 0.2μg/mL/μm to 0.04μg/mL/μm) (Figure 3.5g-i). Similar to neurite behavior on single-cue gradients, neurite length was not significantly different for the double contrasting gradients tested (Table 3.4).

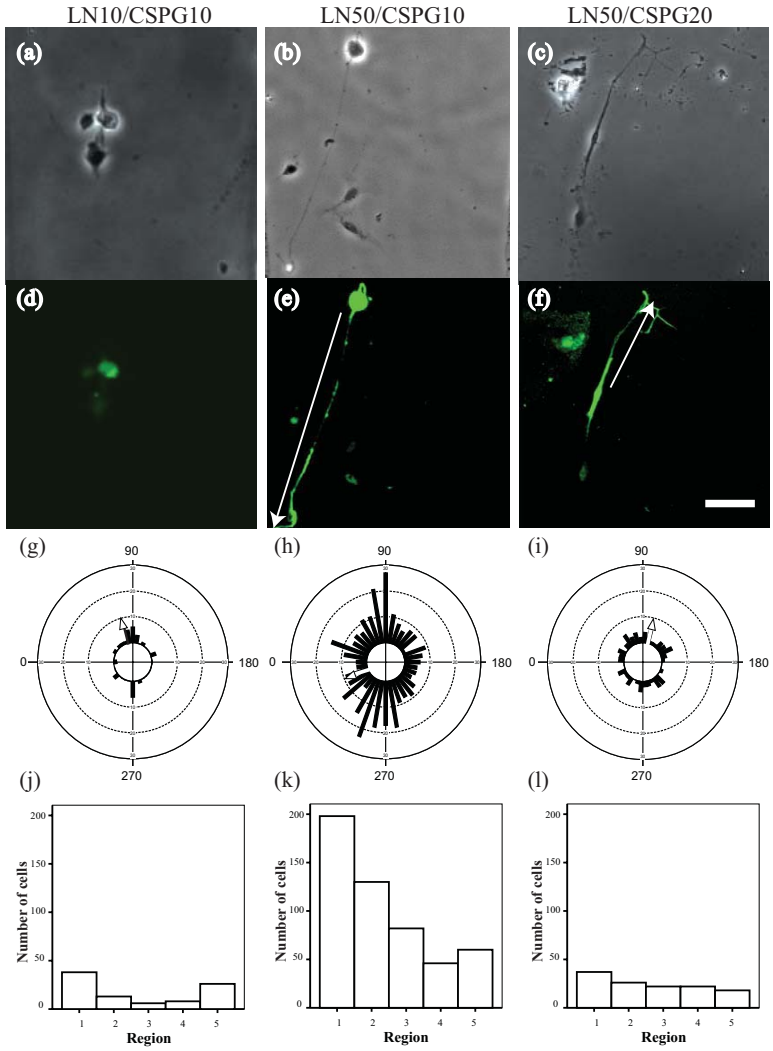

Figure 3.5: Neuronal response to double-cue opposing gradients.
DRG neurons show preference for higher LN and lower CSPG concentrations on opposing double-cue gradients in both neurite outgrowth and adhesion patterns. (a-c) Phase contrast and (d-f) fluorescent images of DRG neurons stained with anti-neurofilament immunocytochemistry after 24 hours in culture on LN10/CSPG10 gradients (a, d), LN50/CSPG10 gradients (b, e) and LN50/CSPG20 gradients (c, f). Arrows show vectors by which neurites are evaluated. (g, i) Mean neurite angles (arrows) on circular histograms of neurite angles on LN10/CSPG10, LN50/CSPG20 gradients indicate angles directed toward the vertical axis of the gradient channel (i.e. no directional preference). (h) Neurite angle distribution on LN50/CSPG10 gradient indicates preference towards direction of higher LN and lower CSPG concentration. (j-k) Histogram of cell adhesion patterns analyzed in 5 regions of 50µm width across the channel of LN10/CSPG10 (j), LN50/CSPG10 (k) and LN50/CSPG 20(l) gradients. Cell adhesion patterns across opposing double-cue gradients changed when slope was varied. Bar = 50µm.

3.3.7 Neuron adhesion patterns on double-cue opposing gradients

Adhesion patterns on LN50/CSPG10 gradient substrates were similar to those on single-cue LN50/BSA gradient substrates, with a non-uniform distribution of cells across the microchannel width ($p<0.05$ by chi-squared test) and a graded decrease in cell number as the concentration of LN decreased and the concentration of CSPG increased. By decreasing the maximal concentration of LN applied or increasing the maximal concentration of CSPG applied, (50μg/mL to 10µg/ml LN and 10µg/ml to 20μg/mL CSPG), cell adhesion was dramatically reduced (516 versus 91 cells and 516 versus 126 cells respectively). Decreasing only the slope of the LN gradient (from 0.2μg/mL/μm to 0.04μg/mL/μm) resulted in similar cell adhesion patterns across the microchannel, where a gradual decrease in cell number was observed as the concentration of LN decreased and the concentration of CSPG increased (Figure 3.5j-l). Increasing only the slope of the CSPG gradient (from 0.04μg/mL/μm to 0.08μg/mL/μm) changed the DRG neuronal adhesion pattern from uniform to non-uniform ($p=0.075$).

3.3.8 Neuronal response to double-cue parallel gradient

A double-cue gradient was generated in which LN and CSPG both increased in concentration from right to left across the final channel width, by infusing LN and CSPG into the left inlet and the neutral molecule BSA into the right inlet of the same gradient mixer. These gradients were somewhat less linear than the double-cue opposing gradients (Figure 3.1e). The DRG neuronal growth response to the double-cue parallel gradient (Figure 3.6) was different from that to the double-cue opposing gradient (Figure 3.5). The neurite angle distribution was not directed on the parallel gradient (Figure 3.6b), in contrast to the directed distribution on the opposing gradient. Neurite length was unaffected by the direction of the protein gradients, with no significant difference between the two substrates tested (Table 3.4). Cellular adhesion was lower on the double-cue parallel gradient than on the double-cue opposing gradient, even when the concentrations of the respective proteins were the same at 50μg/mL maximum LN and 10μg/mL maximum CSPG (141 cells on the parallel gradient

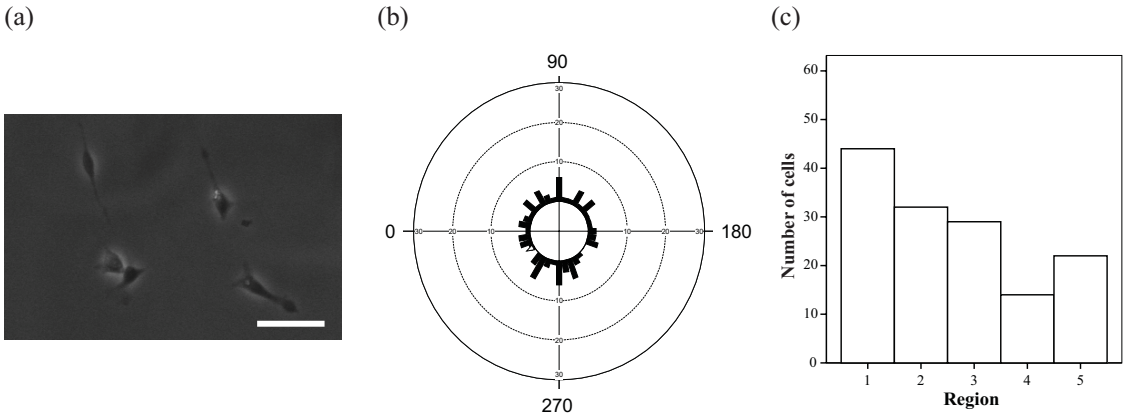

Figure 3.6: Change in direction of gradients influences neurite angle and neuronal adhesion patterns.
(a) Phase contrast images of DRG neurons on double-cue parallel gradients of LN50CSPG10/BSA after 24 hours in culture. Bar = 50μm. (b) The distribution of neurite angles on parallel double-cue gradients is uniform as tested by Kuiper's test for uniformity. (c) Adhesion patterns across the gradient channel width for LN50CSPG10/BSA double-cue parallel gradient are non-uniform.

versus 516 cells on the opposing gradient). The adhesion patterns were similar between the two types of double-cue gradients, with a gradual decrease in cell adhesion across the width of the microchannel toward region 5. Both distributions were non-uniform as determined by a chi-squared uniformity test (Figure 3.6c).

3.4 Discussion

The main objective of this study was to analyze neurite outgrowth on molecular gradients that varied in molecular type, molecular concentration, gradient direction, and gradient slope. In previous studies, gradients containing a single guidance cue were generated by diffusion from various source reservoirs over a given distance of a substrate, such as polymeric membrane filter (Bagnard et al., 2000; Halfter, 1996) or hydrogels (Cao and Shoichet, 2001), and most recently from patterned nanoliter sources (Rosoff et al., 2004). These methods have been modified for covalent immobilization of the protein after gradient generation, by photoimmobilization methods on hydrogels (Dodla and Bellamkonda, 2006). Our microfluidic approach, modified from the method developed by Dertinger et al. (Dertinger et al., 2002),

provided several advantages in this study; (1) substrates were generated that contained reproducible, linear gradients of protein concentration with micron-scale dimensions; (2) by simply changing the types and concentrations of the inlet solutions, a wide variety of gradients were produced, including spatially well defined double-cue gradients, whose influence on neurite outgrowth has not previously been investigated, and (3) exploiting the versatility of this approach, we compared for the first time the effects of multiple molecular and gradient parameters in the same study. Linear gradients over a distance of 250µm were generated that contained specific combinations of the following molecules in substrate-bound form: permissive LN, neutral BSA, and inhibitory CSPG. The single permissive, single inhibitory, and double opposing gradients all directed the outgrowth of neurites from DRG neurons in the direction of increasing LN concentration and of decreasing CSPG concentration. Neuronal adhesion trends displayed corresponding preferences for higher LN and lower CSPG concentrations. The single-cue gradients demonstrated similar strengths in their neurite guidance abilities, regardless of the type of cue. The double opposing gradient displayed a slightly stronger ability to direct neurites than the single gradients suggesting the possibility that this gradient presentation may facilitate a slight synergism of the effects of these two contrasting molecular cues. In contrast, when LN and CSPG were presented as a double parallel gradient, the gradient did not direct neurite outgrowth, suggesting that the contrasting guidance effects of the permissive and inhibitory molecular cues counteracted each other when concentrations of similar relative "strengths" were present in the same regions for a parallel presentation.

Previous studies have suggested that neurite growth on gradients could be guided by numerous parameters including the absolute molecular concentration, the gradient slope, the fractional molecular concentration, and the gradient direction (Baier and Bonhoeffer, 1992; Britland et al., 1996; Isbister et al., 2003; Rosentreter et al., 1998; Song et al., 1998). We analyzed our data from single-cue gradient experiments in the context of the two models of gradient detection: absolute change (to which we refer as slope) and fractional change in concentration. Within our system, the molecular concentration varied linearly across the 250µm width of each gradient channel, as confirmed by immunofluorescence. Molecular concentra-

tion also varied between gradients of differing slopes. Fractional concentration change was defined as the change in concentration over 10µm, the width of a typical DRG growth cone, divided by the maximum molecular concentration along the gradient. Comparing growth on single-cue gradients of permissive and inhibitory cues has shown that neurite orientation is influenced by both slope and fractional change in concentration. Correlations between neurite angle and the relative change in protein concentration of both models suggest that fractional concentration change may play a larger role in orienting neurites, perhaps in part through effects on adhesion.

The inclusion of an opposing cue in our system allowed us to determine whether additive effects or synergism occurs when both permissive and inhibitory gradients are interpreted simultaneously by a growth cone. Neuronal responses to the variations in relative gradient directions between the double-cue opposing gradients and double-cue parallel gradients showed that the same combination of cues can elicit different neurite guidance and orientation responses when spatially patterned in different ways. Statistically significant differences in neurite outgrowth direction and neuronal adhesion patterns in response to the concentration, the gradient slope, and the gradient direction provide evidence that DRG neurons respond to multiple substrate bound molecular cues by utilizing concentration, slope, and directional information to make directional growth decisions.

Both LN and CSPG are present in the nervous system during development and after injury, are co-localized in many regions (Kuecherer-Ehret et al., 1990; Tona et al., 1993), and are important molecules for study because they play key roles in axon guidance. LN is a glycoprotein localized in basement membrane and extracellular matrix. It can strongly stimulate neuronal migration and neurite outgrowth, and its patterned expression during development suggests its importance in axon guidance (Liesi et al., 1995; McLoon et al., 1988). CSPGs are expressed in many regions of the developing nervous system that axons avoid (Landolt et al., 1995; Oakley and Tosney, 1991; Snow et al., 1990), and CSPGs can inhibit neurite growth *in vitro* (Condic, 2001; Snow and Letourneau, 1992; Tom et al., 2004). The post-injury environment of the glial scar has been shown to express both LN and CSPG, and the interactions of damaged axons with both molecules likely provide key

information to influence the potential for regeneration (Davies et al., 1999; Fitch et al., 1999). Specifically, both growth-inhibiting and growth-promoting ECM molecules increase simultaneously in reactive astroglia, thus the double cue parallel gradients mimic this *in vivo* post-injury environment.

Early studies evaluated the effects of sharp borders of LN and CSPG on neurite growth (Snow et al., 1990); subsequent work has presented the cues in gradient form, which is relevant to their spatial distribution within the nervous system. Previous work has examined the effect of single-cue LN gradients on axon guidance and neurite growth, with varying results. Neurites from sympathetic neurons and DRG neurons have been demonstrated to not orient in the direction of LN gradients (Dodla and Bellamkonda, 2006; McKenna and Raper, 1988). Dertinger et al. found that LN gradients could orient initial axon polarization from hippocampal neurons, but suggested that the gradient did not play a significant role in guiding neurite outgrowth (Dertinger et al., 2002). In contrast, studies have shown guidance of retinal axons by gradients of merosin (Halfter, 1996) and of neurites from DRG explants by gradients of the IKVAV peptide (Adams et al., 2005). Our results for neurons plated on single-cue LN gradients suggest that the graded presentation of substrate bound LN can direct neurite growth. In the present study, the protein concentration ranges were chosen from concentrations shown to affect neurite outgrowth after adsorption to a substrate. The gradient shapes were linear, yielding varying fractional concentration changes across the substrate. A larger range of fractional concentration changes was tested than in previous studies: in the range of 0% change, corresponding to no gradient to 100% change where the concentration doubles over the width of a growth cone. Other studies have reported neurite turning and increased neurite outgrowth from culture on gradients with fractional changes of 0.35-3.5% (Dodla and Bellamkonda, 2006; McKenna and Raper, 1988) and 10%(Adams et al., 2005). For LN gradients in this study, the magnitude of fractional concentration change affected the direction of neurite growth such that when the fractional concentration change was 4% (Region 1 in our system), fewer neurites grew in the direction of higher LN concentration, whereas when the fractional concentration change was 100% (Region 25 in our system), more neurites grew toward higher LN concentration. In general, neurites

on more shallow fractional concentration changes have been reported to be not oriented by underlying LN gradients, while steeper fractional concentration changes resulted in growth cone turning up a gradient.

Previous studies of axon guidance by proteoglycans have typically presented CSPG in combination with a low concentration of LN, as CSPG is highly inhibitory to neurite outgrowth. LN was excluded from the present experimental setup with a graded presentation of CSPG, on which the neurite outgrowth response could be analyzed systematically. DRG neurons showed preferential neurite outgrowth and adhesion patterns on single-cue CSPG gradients that are consistent with the chemorepulsion associated with CSPG, i.e. directed away from regions of higher CSPG concentration. CSPG functions can vary depending on what other molecules are present in the surrounding local environment (Snow DM, 2002), i.e., the inhibitory effects of CSPG are reduced when CSPG is presented simultaneously with LN. In response to simple parallel gradients of LN and the CSPG aggrecan, dystrophic endbulbs were shown to enter regions containing LN and lower aggrecan concentration (Tom et al., 2004). Snow et al. have reported that growth cones can grow onto and up increasing concentration steps of CSPG on a substrate (combined with a uniform low concentration of LN) at concentrations that inhibit neurite growth when presented as a border (Snow and Letourneau, 1992). Previously demonstrated effects of CSPG on LN conformation as well as the increased expression of integrin receptors by neurons in response to CSPG speak to the complexity of the interactions of these molecules as they influence neurite outgrowth (Snow DM, 2002; Tom et al., 2004; Tona et al., 1993). In this study and others that include two cues, the conformational presentation of the cues is expected to be influenced by steric interactions, as both molecules are relatively large and CSPGs have an uneven negative charge distribution depending on the structure of their GAG chains. However, while CSPG has been hypothesized to inhibit axon growth by modulating the effects of LN by binding to GAG binding sites (Snow DM, 2002), previous biochemical studies have suggested that LN does not have a strong interaction with CSPGs, particularly when compared to heparin sulfate proteoglycans (Herndon et al., 1999). In the present study, the orientation and adhesion patterns of neurites and neurons of opposing double-cue gradients were consistent with

those on single-cue LN gradients, but the number of cells that adhered to the substrate was lower when CSPG was introduced onto the substrates. For double-cue parallel gradients, cell numbers were further reduced and the preference in directionality that neurites showed for single permissive cue gradients and double opposing cue gradients was lost. These results suggest that the addition of CSPG modulates the guidance by LN but that the spatial arrangement of these proteins is important in how this occurs.

The findings presented here provide new insights into the basic mechanisms of haptotactic guidance and the neuronal mechanisms involved in sensing directional gradients of guidance cues. These results show that DRG neurons can detect substrate bound gradients using two gradient detection mechanisms that are the topics of much study: slope and fractional concentration change. This study shows that in response to double-cue gradients, DRG neurons can incorporate information that includes the concentration, the gradient direction, and the gradient slope and suggests that the growth cone may have a shifting internal baseline for comparing more than one cue to the external environment. Many studies have focused on response to single guidance cues to evaluate the mechanisms by which neurons read gradients; this work indicates that the introduction of more than one cue likely presents complex interactions between cues that further affect neurite outgrowth. Studying both single cue and double cue gradients allows us to conceptually deconstruct the complex environment of the glial scar to study the individual and combined effects of the cues present in concentration gradients. In future studies it will be of interest to investigate how the parameters in a complex system of multiple molecular, spatially defined, overlapping gradients are integrated and are transduced through downstream signaling pathways. The roles of such factors as neuron type and protein type will also be important to evaluate. This work is important for understanding the mechanisms of growth cone navigation and directed axon growth and guidance to enhance strategies for neurite growth promotion for nerve regeneration.

3.5 Acknowledgements

The authors thank Elise Cheng and Julie Richardson for assistance with gradient experiments, and Elizabeth Deweerd and Helen Buettner for helpful discussion of the manuscript. This work was funded by the Charles H. Hood Foundation and an NSF CAREER grant to DHK.

3.6 References

Adams DN, Kao EYC, Hypolite CL, Distefano MD, Hu W, Letourneau PC. Growth cones turn and migrate up an immobilized gradient of the laminin IKVAV peptide. Journal of Neurobiology, 2005; 62: 134-47.

Bagnard D, Lohrum M, Uziel D, Puschel AW, Bolz J. Semaphorins act as attractive and repulsive guidance signals during the development of cortical projections. Development, 1998; 125: 5043-53.

Bagnard D, Thomasset N, Lohrum M, Puschel AW, Bolz J. Spatial distributions of guidance molecules regulate chemorepulsion and chemoattraction of growth cones. J Neurosci, 2000; 20: 1030-5.

Baier H, Bonhoeffer F. Axon guidance by gradients of a target-derived component. Science, 1992; 255: 472-5.

Britland S, Perridge C, Denyer M, Morgan H, Curtis A, Wilkinson C. Morphogenetic guidance cues can interact synergistically and hierarchically in steering nerve cell growth. Exp Biol Online, 1996; 1.

Cao X, Shoichet MS. Defining the concentration gradient of nerve growth factor for guided neurite outgrowth. Neuroscience, 2001; 103: 831-40.

Condic ML. Adult Neuronal Regeneration Induced by Transgenic Integrin Expression. J. Neurosci., 2001; 21: 4782-8.

Davies Y, Lewis D, Fullwood NJ, Nieduszynski IA, Marcyniuk B, Albon J, Tullo A. Proteoglycans on normal and migrating human corneal endothelium. Exp Eye Res, 1999; 68: 303-11.

Dertinger SKW, Jiang X, Li Z, Murthy VN, Whitesides GM. Gradients of substrate-bound laminin orient axonal specification of neurons. PNAS, 2002; 99: 12542-7.

Dickson BJ. Molecular mechanisms of axon guidance. Science, 2002; 298: 1959-64.

Dodla MC, Bellamkonda RV. Anisotropic scaffolds facilitate enhanced neurite extension *in vitro*. J Biomed Mater Res A, 2006; 78: 213-21.

Fitch MT, Doller C, Combs CK, Landreth GE, Silver J. Cellular and molecular mechanisms of glial scarring and progressive cavitation: *in vivo* and *in vitro* analysis of inflammation-induced secondary injury after CNS trauma. J Neurosci, 1999; 19: 8182-98.

Goodhill GJ, Baier H. Axon guidance: stretching gradients to the limit. Neural Comput, 1998; 10: 521-7.

Goodhill GJ, Urbach JS. Theoretical analysis of gradient detection by growth cones. J Neurobiol, 1999; 41: 230-41.

Halfter W. The Behavior of Optic Axons on Substrate Gradients of Retinal Basal Lamina Proteins and Merosin. J. Neurosci., 1996; 16: 4389-401.

Herndon ME, Stipp CS, Lander AD. Interactions of neural glycosaminoglycans and proteoglycans with protein ligands: assessment of selectivity, heterogeneity and the participation of core proteins in binding. Glycobiology, 1999; 9: 143-55.

Hoke A, Silver J. Proteoglycans and other repulsive molecules in glial boundaries during development and regeneration of the nervous system. Prog Brain Res, 1996; 108: 149-63.

Isbister CM, Mackenzie PJ, To KC, O'Connor TP. Gradient slope influences the pathfinding decisions of neuronal growth cones *in vivo*. J Neurosci, 2003; 23: 193-202.

Kennedy TE, Serafini T, de la Torre JR, Tessier-Lavigne M. Netrins are diffusible chemotrophic factors for commissural axons in the embryonic spinal cord. Cell, 1994; 78: 425-35.

Kuecherer-Ehret A, Graeber MB, Edgar D, Thoenen H, Kreutzberg GW. Immunoelectron microscopic localization of laminin in normal and regenerating mouse sciatic nerve. J Neurocytol, 1990; 19: 101-9.

Landolt RM, Vaughan L, Winterhalter KH, Zimmermann DR. Versican is selectively expressed in embryonic tissues that act as barriers to neural crest cell migration and axon outgrowth. Development, 1995; 121: 2303-12.

Liesi P, Hager G, Dodt HU, Seppala I, Zieglgansberger W. Domain-specific antibodies against the B2 chain of laminin inhibit neuronal migration in the neonatal rat cerebellum. J Neurosci Res, 1995; 40: 199-206.

Loschinger J, Weth F, Bonhoeffer F. Reading of concentration gradients by axonal growth cones. Philos Trans R Soc Lond B Biol Sci, 2000; 355: 971-82.

Luckenbill-Edds L. Laminin and the mechanism of neuronal outgrowth. Brain Res Brain Res Rev, 1997; 23: 1-27.

MacLennan AJ, McLaurin DL, Marks L, Vinson EN, Pfeifer M, Szulc SV, Heaton MB, Lee N. Immunohistochemical localization of netrin-1 in the embryonic chick nervous system. J Neurosci, 1997; 17: 5466-79.

Mardia K, Jupp P. Directional Statistics 2nd ed. John Wiley and Sons Ltd: Chichester, England, 2000.

McKenna MP, Raper JA. Growth cone behavior on gradients of substratum bound laminin. Dev Biol, 1988; 130: 232-6.

McLoon SC, McLoon LK, Palm SL, Furcht LT. Transient expression of laminin in the optic nerve of the developing rat. J. Neurosci., 1988; 8: 1981-90.

Oakley RA, Tosney KW. Peanut agglutinin and chondroitin-6-sulfate are molecular markers for tissues that act as barriers to axon advance in the avian embryo. Dev Biol, 1991; 147: 187-206.

Ramon y Cajal S. La rétine des vertébrés. Van In: Lierre, Belgium, 1892.

Rosentreter SM, Davenport RW, Loschinger J, Huf J, Jung J, Bonhoeffer F. Response of retinal ganglion cell axons to striped linear gradients of repellent guidance molecules. J Neurobiol, 1998; 37: 541-62.

Rosoff WJ, Urbach JS, Esrick MA, McAllister RG, Richards LJ, Goodhill GJ. A new chemotaxis assay shows the extreme sensitivity of axons to molecular gradients. Nat Neurosci, 2004; 7: 678-82.

Snow DM, Lemmon V, Carrino DA, Caplan AI, Silver J. Sulfated proteoglycans in astroglial barriers inhibit neurite outgrowth *in vitro*. Experimental Neurology, 1990; 109: 111.

Snow DM, Letourneau PC. Neurite outgrowth on a step gradient of chondroitin sulfate proteoglycan (CS-PG). J Neurobiol, 1992; 23: 322-36.

Snow DM SJ, Gurwell JA. Binding characteristics of chondroitin sulfate proteoglycans and laminin-1, and correlative neurite outgrowth behaviors in a standard tissue culture choice assay. Journal of Neurobiology, 2002; 51: 285-301.

Song H, Ming G, He Z, Lehmann M, McKerracher L, Tessier-Lavigne M, Poo M. Conversion of neuronal growth cone responses from repulsion to attraction by cyclic nucleotides. Science, 1998; 281: 1515-8.

Sperry RW. Chemoaffinity In The Orderly Growth Of Nerve Fiber Patterns And Connections. Proc Natl Acad Sci U S A, 1963; 50: 703-10.

Tessier-Lavigne M, Goodman CS. The molecular biology of axon guidance. Science, 1996; 274: 1123-33.

Tom VJ, Steinmetz MP, Miller JH, Doller CM, Silver J. Studies on the Development and Behavior of the Dystrophic Growth Cone, the Hallmark of Regeneration Failure, in an In Vitro Model of the Glial Scar and after Spinal Cord Injury. J. Neurosci., 2004; 24: 6531-9.

Tona A, Perides G, Rahemtulla F, Dahl D. Extracellular matrix in regenerating rat sciatic nerve: a comparative study on the localization of laminin, hyaluronic acid, and chondroitin sulfate proteoglycans, including versican. J Histochem Cytochem, 1993; 41: 593-9.

von Philipsborn AC, Lang S, Loeschinger J, Bernard A, David C, Lehnert D, Bonhoeffer F, Bastmeyer M. Growth cone navigation in substrate-bound ephrin gradients. Development, 2006; 133: 2487-95.

Chapter 4

Optimization of combinatorial protein gradients for neurite outgrowth

Presentation of guidance molecules in an anisotropic manner has been shown to guide growing axons by chemotaxis. Here we evaluated the influence of specific parameters such as molecular concentration, slope and direction of combinatorial laminin (LN) and chondroitin sulfate proteoglycan (CSPG) gradients on dorsal root ganglia neurons. Linear combinatorial gradients were generated using a microfluidic gradient mixing device. We analyzed the growth of postnatal rat dorsal root ganglion neurons in response to permissive versus inhibitory cues in multiple spatial presentations of gradients. Neuronal adhesion and neurite growth were analyzed after 24 hour culture on various double-cue gradients. Slopes were shown to exhibit a nonlinear relationship with cellular adhesion. Slope of LN showed a linear correlation with neurite length while the slope of CSPG showed nonlinear correlations with neurite length. The directionality of neurite outgrowth was evaluated using circular statistical methods to determine the influence of the underlying gradients on neurite angles of outgrowth. Optimization of inlet concentrations of molecular gradients was performed, and maximizing LN while minimizing CSPG concentrations over the concentration ranges tested was shown to maximize cellular adhesion and length. Addition of Rho kinase inhibitor Y27632 significantly increased neurite length as compared to controls on opposing double

cue LN/CSPG gradients. The motivation for these studies is to gain a more rigorous comprehension of how growing neurons interpret their complex extracellular environment in which permissive and repulsive guidance molecules act in combination to direct axonal growth. These results represent an important step towards understanding how neurite growth is guided by complex microenvironments containing multiple molecular cues.

4.1 Introduction

Promotion of neuron growth and direction of neurite outgrowth are primary goals in the development of strategies for nerve repair. These goals also address a fundamental issue in developmental neurobiology to understand how neurons sense and respond to changes in their extracellular environment. Anisotropic distribution of guidance cues has been identified as one important way in which guidance cues can direct growth, by exploiting the differential response of growth cones (Bellamkonda, 2006). The existence of attractive and repulsive guidance molecules in a graded fashion has been observed *in vivo* both in the developing nervous system and the glial scar after injury. In addition, the response of neurons to these gradients has been studied in *in vivo* and *in vitro* models, and it is largely accepted that the graded expression of guidance molecules plays an important role in forming the precise wiring of the nervous system (Gurdon and Bourillot, 2001), and can be used as a possible strategy to overcome the inhibition of the post-injury environment.

However, the specific gradient parameters that strongly influence neurite growth are less well understood. Previous theoretical (Goodhill and Urbach, 1999) and experimental studies (Bagnard et al., 2000; von Philipsborn et al., 2006) have suggested that a range of gradient parameters influence neurite growth including: direction, shape, slope or relative changes in concentration, and absolute molecular concentration. Gradients generated by microfluidic methods offer greater levels of precision, spatial and temporal control, the ability to quantify gradient parameters, and the ability for quantitative cellular analysis on the single cell level, which allow us to better investigate these gradient parameters (reviewed by Keenan and Folch (Keenan and Folch, 2008)).

Combinatorial gradients have been studied previously as it was recognized that these exist *in vivo*. Experimental work with combinatorial gradients of nerve growth factor (NGF), neurotrophin-3 (NT-3) and brain-derived neurotrophic factor (BDNF) (Cao and Shoichet, 2003), semaphorins 3A and 3C (Bagnard et al., 2000), BDNF and LN (Wang et al., 2008), and aggrecan and LN (Tom et al., 2004) have shown that combinatorial gradients are able to elicit differential growth responses depending on the combinations of proteins presented.

In this study we examine the effects of multiple combinatorial protein gradients on DRG neuron and neurite growth to determine the optimal spatial presentations of protein gradients to direct neurite outgrowth and promote cellular adhesion and neurite outgrowth. The two molecules used in this study are LN, a well-established permissive guidance cue that is present in developing and regenerating axonal tracts (Buettner and Pittman, 1991) and CSPGs, strong inhibitors of neurite growth that are present in boundary regions of the developing brain and in the glial scar (Lemons et al., 2005). These molecules were chosen as strong promoters and inhibitors of neurite growth in the post-injury microenvironment. Here we show that DRG adhesion and neurite outgrowth respond differentially to different features of protein gradients presented, showing complex responses to substrate bound combinatorial protein gradients.

Further, strategies to overcome the inhibition present in the glial scar primarily from proteoglycans, were also explored in this study, including enzymatic digestion of inhibitory chondroitin sulfate chains with chondroitinase ABC (chABC) and the application of a pharmacological inhibitor to Rho kinase, Y27632. Digestion of glycosaminoglycan chains (Lemons et al., 2003) and inhibition of glycosaminoglycan chain polymerization (Laabs et al., 2007) have been shown to decrease the inhibition of CSPG. Modulating Rho kinase activity has been shown to modulate neurite outgrowth on CSPG substrates(Jain et al., 2004). In this study we show that inhibition of Rho kinase can affect neurite outgrowth, mitigating the inhibitory effects of CSPG, on opposing LN/CSPG gradients.

4.2 Materials and methods

Unless otherwise stated, all materials were purchased from Sigma-Aldrich (St. Louis, MO).

4.2.1 Substrate fabrication

Microfluidic gradient mixers were used to generate patterns of protein gradients. These devices were fabricated using photolithography and soft lithography. Masks containing patterns of gradient mixers were designed with modifications from Dertinger et al. (Dertinger et al., 2002), and described further in Li et al. (Li et al., 2008). Patterns were transferred to silicon wafers using photolithography. Poly dimethyl siloxane (PDMS; Dow Corning) was mixed 10:1 elastomer:curing agent and cast onto silicon wafers to produce a replica. Gradient mixers were then assembled by adhesion of PDMS microchannel molds to glass surfaces after plasma activation (PDC-32 G, High RF level, Harrick, Pleasantville, NY). Gradient mixers were coated with poly-L-lysine (100μg/mL, MW 30-70kDa) and incubated at 4°C overnight.

Protein solutions were prepared for injection by syringe pump through the gradient mixer. Mouse LN solutions (10μg/mL to 50μg/mL, Invitrogen, Carlsbad, CA), CSPG solutions from embryonic chick brain (1μg/mL to 20μg/mL; Chemicon, Temecula, CA), and/or 3% bovine serum albumin (BSA) in 0.1M phosphate buffered saline (PBS) were applied at the inlets of the gradient mixer.

To test the effects of the core protein of the proteoglycans on neurite outgrowth, enzymatic treatment of CSPG with chABC was performed to digest the chondroitin sulfate chains of CSPG, leaving the core protein. CSPG solutions (10μg) were treated with 0.05U chABC (units defined as the quantity of the enzyme that catalyzes the formation of 1 µmol of unsaturated disaccharide from chondroitin sulfate C per minute) in 50mM Tris-HCl, 0.15M NaCl, 3uM aprotinin, 20mM benzamidine, 1mM leupeptin, 1mM pepstatin A (Tris buffer) by incubation at 37°C for 3 hours prior to injection into the gradient mixer. Enzymatically

digested solutions of 10μg/mL CSPG and 50μg/mL LN were applied in gradient mixer inlets to generate opposing gradients, as described above.

Protein solutions were delivered over 12h to allow adsorption of the proteins onto the glass slide. After adsorption of the protein gradient, the PDMS covering the final gradient channel was cut and peeled from the substrate to expose the area over the final gradient channel for cell culture. Gradient-containing substrates were stored in PBS at 4°C overnight.

4.2.2 DRG cell culture

DRG were dissected from the spinal columns of postnatal (P0-P4) rat pups and cleaned of axons, blood, and connective tissue. DRG were incubated in 0.05% trypsin-EDTA in Hank's balanced salt solution without calcium or magnesium (Invitrogen, Carlsbad, CA) at 37 $^\circ$C for 60min and dissociated by trituration. Cells were plated at 2600 cells/cm^2 in 2mL of serum-containing medium: Dulbecco's Modified Eagle's Medium, 10% fetal bovine serum, 4mM L-glutamine, penicillin (100U/ml)/streptomycin (100µg/ml) (Invitrogen, Carlsbad, CA) and 50ng/ml nerve growth factor (7S). Cultures were incubated at 37°C with 5% CO2 in a humidified environment for 24h.

To test the effects of Rho kinase activity on modulating the inhibition of neurite outgrowth by CSPG gradients, Y27632 was added to DRG cultures on double cue gradients containing LN gradients of -0.2µg/mL/µm and CSPG gradients of 0.04µg/mL/µm. After an initial incubation time of 1 hour for plating (37°C, 5% CO2), 50μl of either pharmacological inhibitor or culture media was added to the DRG cultures. ROCK inhibitor Y27632 was used at a concentration of 10μM (Borisoff et al., 2003; Fournier et al., 2003; Yuan et al., 2003). Cells were incubated (37°C, 5% CO2) for an additional 23 hours for a total of 24 hours.

4.2.3 Microscopy and Image analysis

Samples were examined on a Nikon Eclipse TE2000-S microscope, images were captured using a Hamamatsu Orca-ER camera and Orbit shutter controller (Improvision, Lexington,

MA), outputting to OpenLab v4.0.2 (Improvision) running on Mac OS v10.2. Contrast adjustments for visualization were performed using the level function in Adobe Photoshop CS2.

Total cellular adhesion on the final microchannel presenting the protein gradients was analyzed. All cell bodies fixed and imaged at 24 hours after cell seeding were counted. Duplicate samples were performed and analyzed. Neurite outgrowth was analyzed by evaluation of the length of the longest neurite. Neurites longer than the length of a soma, and that did not come into contact with another cell were included in this analysis. OpenLab software was used to determine the average longest neurite length. The ruler tool was used to measure the length of the process from the point on the soma where the process began to the tip of the neurite visible under phase contrast microscopy. The direction of neurite outgrowth was analyzed by the angle of the process outgrowth from the vertical (y) axis as measured by the ruler tool in the OpenLab software.

4.2.4 Data analysis

Each experimental group contained duplicate samples, with a minimum of 10 measures per condition. Results are shown as the mean ± standard error.

Gradient slope was calculated for each protein gradient generated by calculating the concentration change across the gradient channel and dividing by the width of the gradient channel. To test the influence of the slope of LN and CSPG gradients on DRG responses, the slope of either LN or CSPG was held constant in magnitude, while the slope of the other protein gradient was varied. Each dataset thus has gradients of both molecules present, but for comparison across the dataset, slope of only one molecular gradient is varied to determine the individual effects of the molecular gradient of interest.

Experimentally, LN solutions were applied from the left inlet port of the gradient mixer, whereas CSPG solutions were applied from either the left or right inlet port. For analysis of DRGs on constant CSPG slope with varying LN slope, the magnitude of CSPG slope

was held constant, and for the substrates where CSPG solutions were applied from the left inlet port, the gradient calculations and neurite angle measurements were transformed to allow our reference frame to denote a positive CSPG slope of 0.04µg/mL/µm. The gradient mixer design is symmetrical, and as the magnitude of CSPG does not change, and the serial dilution and mixing undergone by the CSPG solutions are the same, the gradient calculations only reflect a change in sign.

To test the effects of gradient slope on cellular adhesion and neurite length, statistical analysis was performed using one-way ANOVA testing and post-hoc analysis using Tukey's test for multiple comparison using SPSS 14.0 (SPSS, Inc., Chicago, IL). Data were plotted on bar graphs and differences between substrates tested within each dataset were analyzed for statistical significance.

To test the effects of gradient substrates on directional neurite growth, statistical analysis was performed with circular statistical methods. Circular histograms are presented that wrap a linear 0°-180° scale around a circle, and show the mean direction. To determine if the substrates elicited directional growth versus random uniform outgrowth, Rao's spacing tests were performed. To determine if direction of neurite outgrowth differed between substrates, the multisample Mardia-Watson-Wheeler test was performed. All circular tests were performed with Oriana 2.0 (Kovach Computing Services).

To test the effects of gradient direction on DRG response, data was grouped into the substrate types that we defined as "opposing" or "parallel" (Li et al., 2008), where opposing gradients presented LN and CSPG gradients in opposite directions, and parallel gradients presented LN and CSPG gradients in the same direction. Statistical analysis was performed on Design-Expert 7 (Stat-Ease). Input factors of LN and CSPG slopes for opposing and parallel gradients were used at two levels (high/low) in a statistical model based on two-way ANOVA, with response factors of cellular adhesion and neurite length.

Optimization with the ANOVA statistical model was also performed to determine the optimal input values of LN and CSPG slopes within the experimental range for maximal cellular adhesion and maximal neurite length using Design-Expert 7. As the statistical model for

a) cellular adhesion for opposing gradients and b) neurite length for parallel gradients were found to be significant in the analysis described above, optimization was only performed for those datasets. Cellular adhesion and neurite length as a result of the input slopes of LN and CSPG as predicted by the statistical model are presented in contour plots.

To test the effects of exogenous factors on modulating DRG response to CSPG gradients, data from untreated, chABC and Y27632 treated samples were compared using ANOVA for cellular adhesion and neurite length.

4.3 Results

Three measurements were made from each sample to evaluate the effects of protein gradients on DRG neurite growth. The total number of cells over the area of the final gradient channel was counted as a measure of overall permissiveness to neurons. The lengths of the longest neurites were determined and averaged to generate a measure to evaluate the permissiveness to outgrowth potential. The angles of the longest neurites were measured to determine the directionality of neurite outgrowth cultured with anisotropic molecular cues. An ideal treatment would be highly permissive to neuronal adhesion, and stimulate long neurite growth in a specified direction.

4.3.1 Cellular adhesion is affected by LN concentration and slope in double cue LN and CSPG gradients

We investigated the effects of the inlet concentration and slope of LN gradients when presented concurrently with a constant CSPG gradient, on DRG neuronal adhesion and neurite outgrowth. The inlet concentration of CSPG applied was kept constant at 10µg/mL, to present a linear slope of 0.04µg/mL/µm. For analysis, the slopes of LN and CSPG were transformed to reorient the reference frame so that all CSPG slopes were -0.04µg/mL/µm, as described in section 2.4. By varying the inlet concentrations to the gradient mixer, varying LN slopes were generated in the range of -0.04µg/mL/µm to 0.2µg/mL/µm.

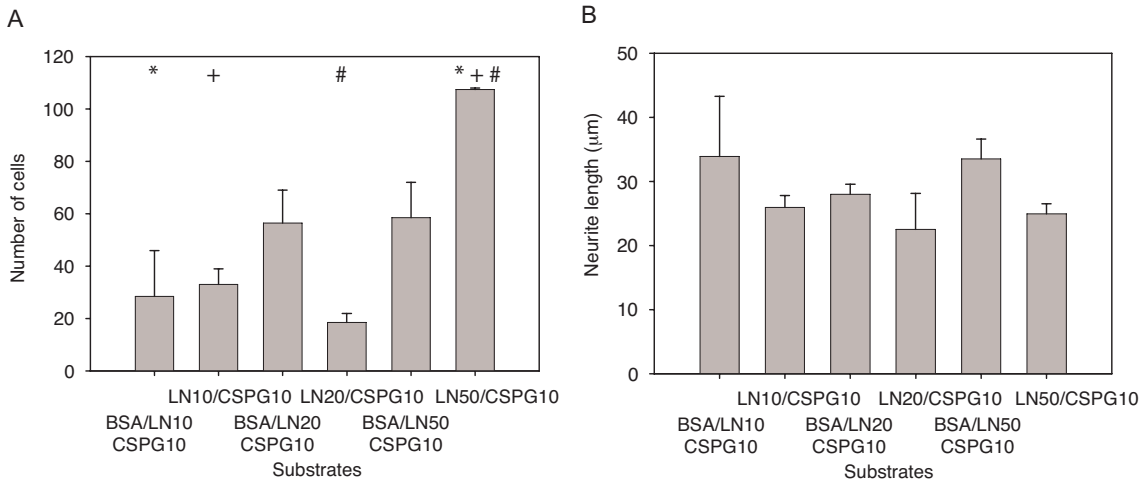

Figure 4.1: Effects of varyng LN concentration (LN10-50) and slope (-0.04 to 0.2µg/mL/µm) presented simulataneously with -0.04µg/mL/µm CSPG gradients (CSPG10) on cellular adhesion
(A) and neurite length (B). *, +, # denote significantly different groups ($p<0.05$). Data represents mean ±SEM for n=2 samples.

The inlet concentrations and slope of LN significantly affected cellular adhesion as tested by ANOVA ($p<0.05$). Cellular adhesion was maximized, at 107 cells, on LN50/CSPG10 substrates, corresponding to the steepest negative slope tested, -0.2 µg/mL/µm (Figure 4.1a). Post-hoc analysis with Tukey's test showed that the number of cells adhered onto the LN50/CSPG10 substrate was significantly different from cell numbers on BSA/LN10CS10, LN10/CSPG10 and LN20/CSPG10. Neurite length was not found to be significantly different on substrates with varying CSPG slope using ANOVA ($p=0.512$), with all neurite lengths in the range of 22.9 µm to 33.5µm (Figure 4.1b).

A comparison of the neurite angle distributions of the longest neurites on substrates with varying LN slopes and constant CSPG slope, showed that negative LN slopes (0.04, 0.08 and 0.2µg/mL/µm) elicited directed neurite outgrowth (Figure 4.2). A transformed positive LN slope of 0.08µg/mL/µm was also able to direct neurites to a vertical orientation (6°).

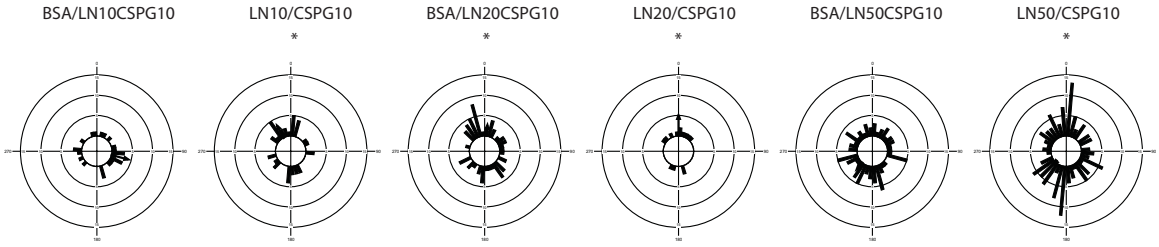

Figure 4.2: Effects of varyng LN concentration (10-50μg/mL) and slope (-0.04 to 0.2µg/mL/µm) presented simulataneously with -0.04µg/mL/µm CSPG gradients (CSPG10) on neurite outgrowth direction.

* denotes directed neurite outgrowth ($p<0.05$)

4.3.2 Cellular adhesion is affected by CSPG inlet concentration and slope in double cue LN and CSPG gradients presenting a shallow LN gradient

We investigated the effects of inlet concentrations of CSPG gradients on double cue gradients with LN slope of -0.04µg/mL/µm. The slope of CSPG was varied from -0.004µg/mL/µm to 0.08µg/mL/µm, and data is presented by increasing CSPG concentrations (Figure 4.3). Cell adhesion numbers ranged from 33 to 121. Inlet concentration of CSPG was a significant factor influencing the number of cells adhered when presented concurrently with a LN gradient of -0.04µg/mL/µm, as tested by one-way ANOVA ($p<0.05$). Post-hoc analysis showed that the number of cells on LN10CS1/BSA was significantly different from the number on LN10/CSPG10 (Tukey's test, $p<0.05$). The inlet concentrations of CSPG did not significantly influence neurite length as tested by one-way ANOVA, although the longest mean neurites observed were on LN10CS10/BSA, substrates with the highest input LN concentration and lowest input concentration of CSPG tested.

Neurite angle distributions of the longest neurites cultured on double cue LN and CSPG gradients with varying CSPG slopes at a constant LN slope of -0.04µg/mL/µm show directed neurite growth on CSPG slopes of -0.004µg/mL/µm and 0.04µg/mLum (Figure 4.4). Neurite angles in both cases were directed toward the direction of increasing LN concentration (220°, 331° on substrates with -0.004µg/mL/µm and 0.04µg/mL/µm respectively).

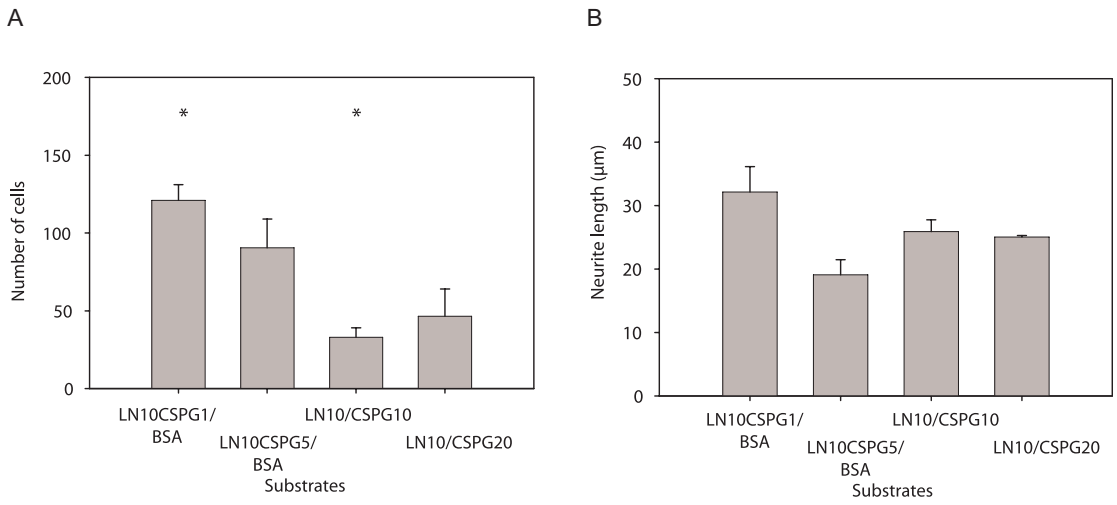

Figure 4.3: Effects of varyng CSPG concentration (CSPG1-20) and slope (-0.004 to 0.08µg/mL/µm) presented simulataneously with -0.04µg/mL/µm LN gradients (LN10) on cellular adhesion

(A) and neurite length (B). * denotes significantly different groups ($p<0.05$). Data represents mean ±SEM for n=2 samples.

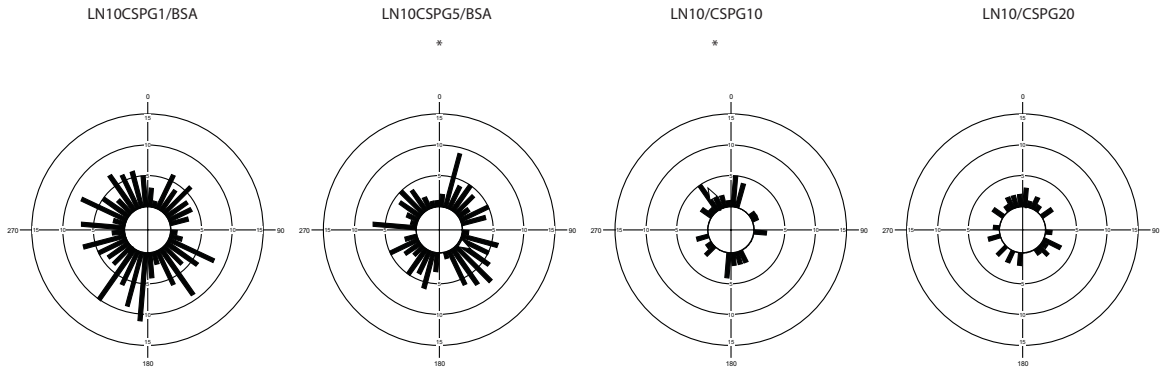

Figure 4.4: Effects of varyng CSPG concentration (CSPG1-20) and slope (-0.004 to 0.08µg/mL/µm) presented simulataneously with -0.04$\mu g/mL$ LN gradients (LN10) on neurite outgrowth direction.

* denotes directed neurite outgrowth ($p<0.05$)

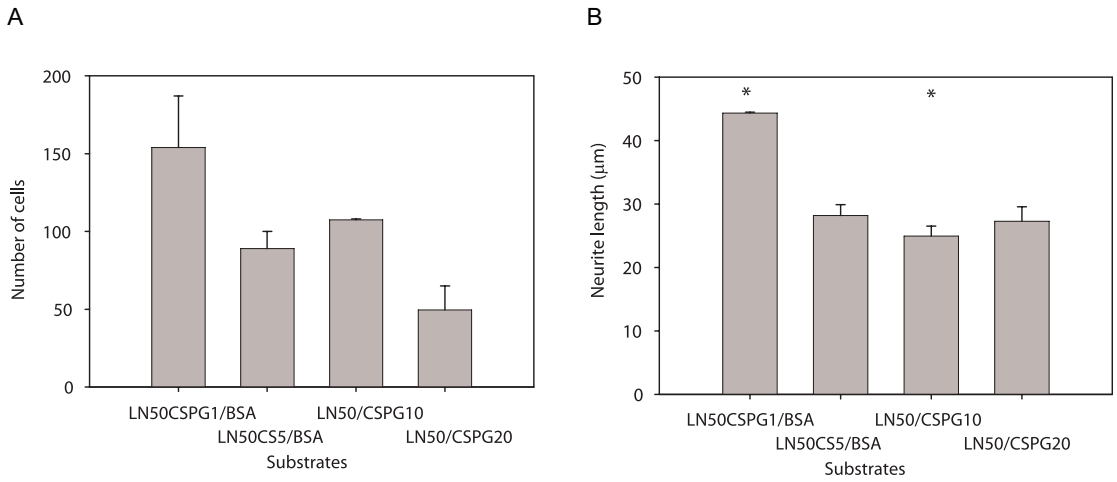

Figure 4.5: Effects of varyng CSPG concentration (1-20μg/mL) and slope (-0.004 to 0.08µg/mL/µm) presented simulataneously with -0.2$\mu g/mL$ LN gradients (LN50) on cellular adhesion
(A) and neurite length (B). * denotes significantly different groups ($p<0.05$). Data represents mean ±SEM for n=2 samples.

4.3.3 Neurite length is affected by CSPG inlet concentration and slope in double cue LN and CSPG gradients presenting a steep LN gradient

We investigated the effects of inlet concentration of CSPG on double cue gradients with LN slope of -0.2µg/mL/µm. The slope of CSPG was varied from -0.004µg/mL/µm to 0.08 µg/mL/µm and data is presented by increasing CSPG concentrations. The effect of CSPG inlet concentrations on cellular adhesion was not significant, as tested by one-way ANOVA. CSPG inlet concentrations significantly affected neurite length when presented concurrently with a LN gradient of -0.2µg/mL/µm (Figure 4.5) as tested by one-way ANOVA ($p<0.05$). Post-hoc analysis showed that mean neurite length on CSPG gradients with slopes of -0.004µg/mL/µm was significantly different from neurite length on substrates with CSPG slopes of 0.2µg/mL/µm on substrates presenting steep LN gradients (Tukey, $p<0.05$).

Neurite angle distribution on substrates with CSPG slope of -0.02µg/mL/µm to 0.04µg/mL/µm was directed as shown from Rao's spacing test (Figure 4.6). These correspond to double cue parallel gradients and lower CSPG inlet concentrations applied, suggesting that slope of CSPG gradients play a role in directing neurite outgrowth. Neurite outgrowth was directed either vertically or toward higher LN concentrations.

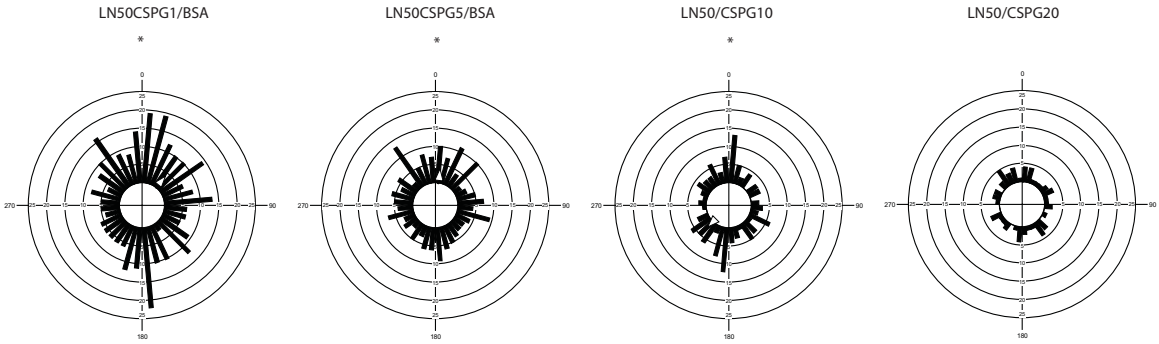

Figure 4.6: Effects of varyng CSPG concentration (1-20μg/mL) and slope (-0.004 to 0.08µg/mL/µm) presented simulataneously with -0.2µg/mL/µm LN gradients (LN50) on neurite outgrowth direction.

* denotes directed neurite outgrowth ($p<0.05$)

4.3.4 The relationship between cellular adhesion and neurite length

To optimize the presentation of protein gradients, the goal is to maximize both cellular adhesion and neurite length. Figure 4.7 shows adhesion and length normalized as a percentage of the maximal value in the dataset. By varying the inlet concentrations and slopes of LN, cellular adhesion was maximized on LN50/CSPG10, whereas neurite length was maximized on LN10CSPG10/BSA substrates. As cellular adhesion was found to be significantly affected by slope and neurite length was not from previous analysis, LN50/CSPG10 appeared to be the optimal substrate for neurite outgrowth when the CSPG slope is presented at -0.04µg/mL/µm. By varying the inlet concentrations and slopes of CSPG, with both LN gradients tested (-0.04µg/mL/µm and -0.2µg/mL/µm), the lowest CSPG concentration applied yielded maximal cellular adhesion and longest neurite outgrowth.

Presenting the data as a scatterplot enabled curve fitting to interpolate local maxima and minima of responses with given input parameters (Figures 4.8). Cellular adhesion showed similar and non-linear responses to the slope of protein gradients, with regression lines described by third-order equations showing the best fit. Local maximum of cellular adhesion for substrates with CSPG slope of 0.04µg/mL/µm was found for a LN slope 0.18µg/mL/µm. Local minimum of cellular adhesion for the same substrate was found for a LN slope of -0.05µg/mL/µm. The absolute maximum of cellular adhesion on this substrate over the slopes tested was on the LN slope of -0.2µg/mL/µm. For substrates with LN slopes of -0.04

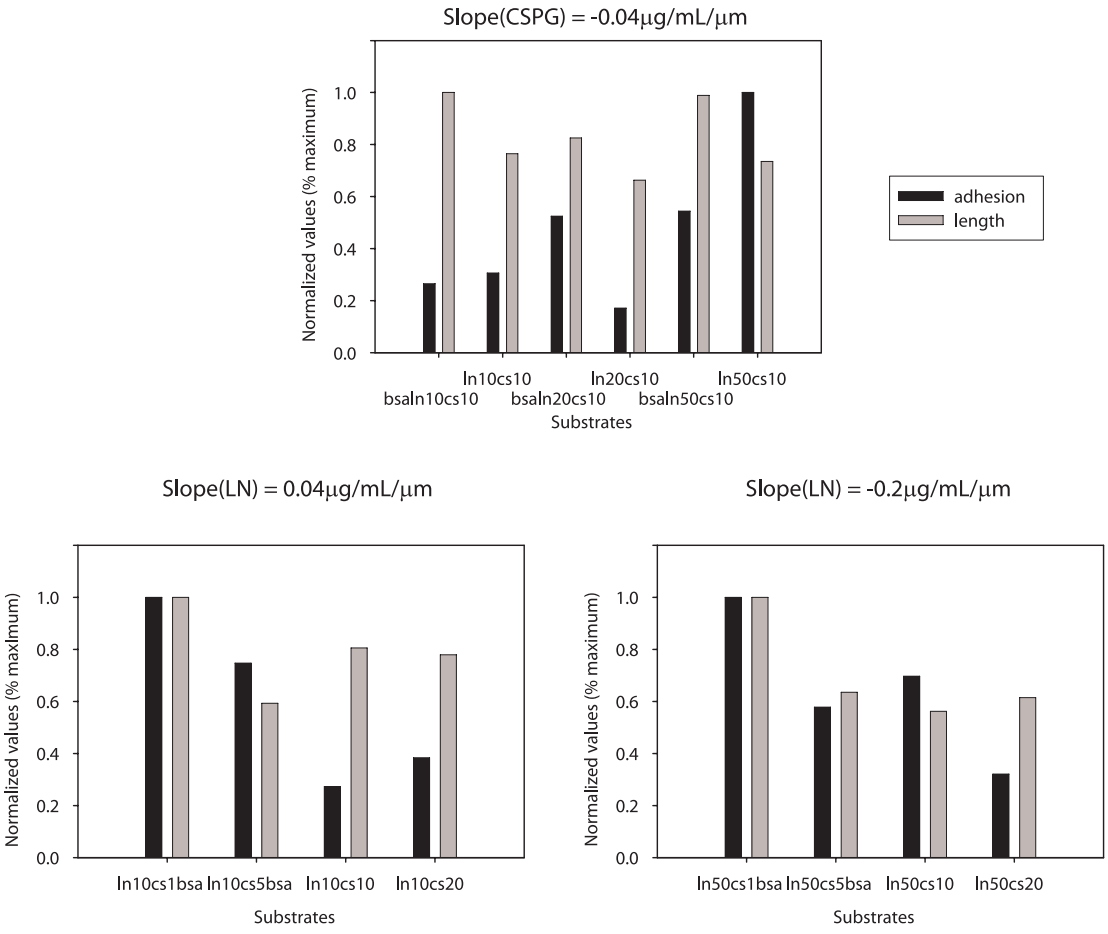

Figure 4.7: Comparison of cellular adhesion and neurite length as a normalized fraction of maximum adhesion and outgrowth of each dataset

(A) varied LN slope, (B) varied CSPG slope on -0.04µg/mL/µm LN (LN10), (C) varied CSPG slope on -0.2µg/mL/µm LN (LN50). Black bars denote adhesion and gray bars denote length of longest neurite.

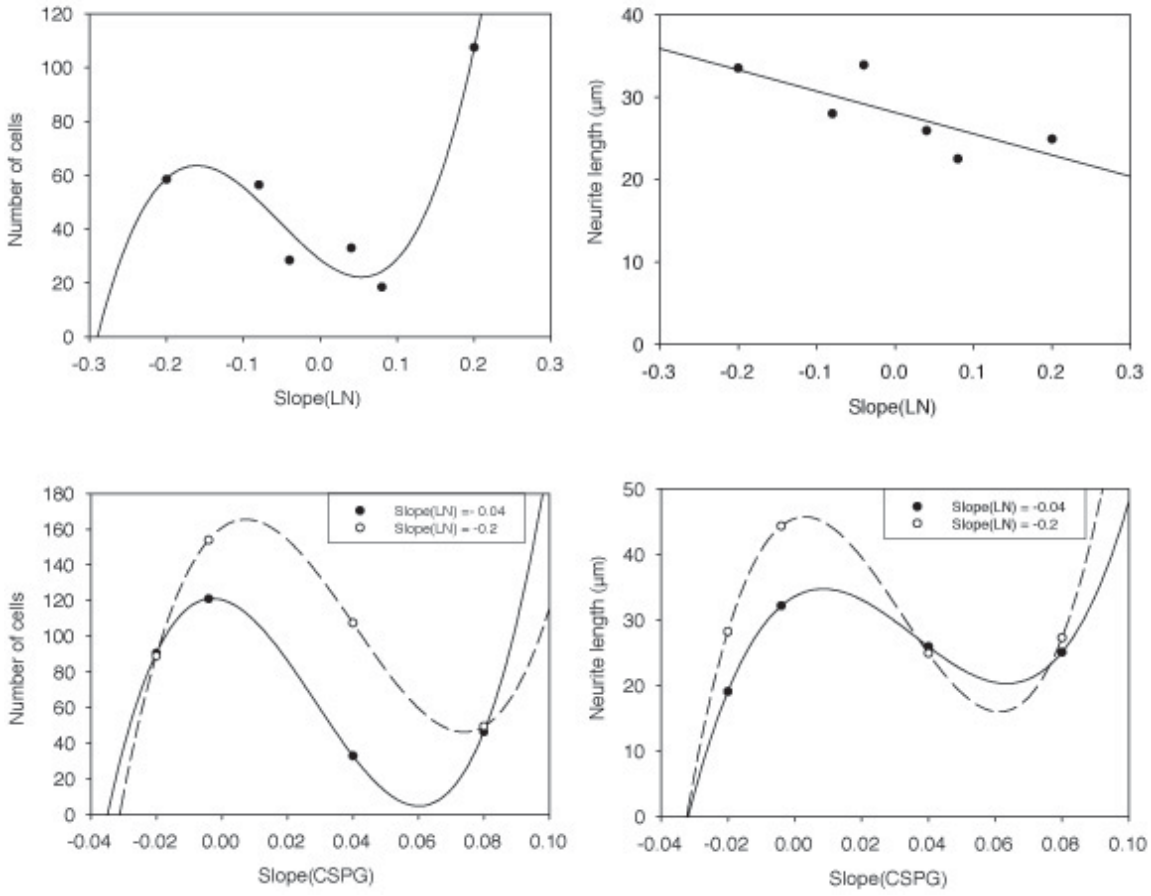

Figure 4.8: Scatterplot of slope versus adhesion or length to show non-linear relationship between these variables. Complex third order equations were found to best fit these datasets in A, C, D.

and -0.2µg/mL/µm, local maxima and minima largely overlapped, where cell adhesion was maximized on the CSPG slope of 0.01µg/mL/µm and minimized on the CSPG slope of 0.07µg/mL/µm.

Neurite length showed a differential response to protein slope depending on the molecule presented. Varying LN slope showed a linear correlation with neurite length, with a positive correlation. Varying CSPG slope at both LN slopes tested showed local maxima of neurite lengths on 0.01µg/mL/µm CSPG slope and local minima of neurite lengths on 0.06µg/mL/µm, as described by third-order equations.

Term	Opposing gradients Cellular adhesion % Contribution	p-value	Parallel gradients Neurite length %Contribution	p-value
ANOVA	100	0.0406	100	0.0024
A-LN	38.92642	0.0326	32.43936	0.0080
B-CSPG	12.83397	0.1390	58.622	0.0023
AB	33.13242	0.0415	not selected	N/A

Table 4.1: Contribution of each input parameter (LN or CSPG) to ANOVA model

4.3.5 LN and CSPG concentrations elicit differential effects on neurite outgrowth dependent on gradient direction

Substrates tested could also be sorted by the direction of the gradient presented. For these double cue gradients, opposing gradients or parallel gradients can be generated. Cellular adhesion was significantly affected by the inlet concentrations of LN and CSPG on substrates presenting opposing gradients, and was not significantly affected by these concentrations on parallel gradients. Neurite length was significantly affected by the inlet concentrations of LN and CSPG on substrates presenting parallel gradients, as tested by ANOVA, and was not significantly affected by these concentrations on opposing gradients. Equations below show the multiple regression model used to describe the relationship between inlet concentration and cellular adhesion on opposing gradients (Equation 4.1) and inlet concentration and neurite length on parallel gradients (Equation 4.2). Table 4.1 shows the contributions of each molecule to DRG responses.

$$Adhesion = 59.13 + 19.38A - 11.13B - 17.88(A * B) \tag{4.1}$$

$$\ln(Length) = 3.38 + 0.18A - 0.24B \tag{4.2}$$

	Opposing gradients	Parallel gradients
LN (µg/mL)	50	50
CSPG (µg/mL)	10	1
Adhesion	87.07	154
Length (μm)	25.76	45.12
Desirability (average of % maximum of adhesion and length)	0.537	0.844

Table 4.2: Optimized double cue gradients

4.3.6 Optimization of LN and CSPG slope to maximize cellular adhesion and neurite outgrowth

Using the solver function in Design Expert 7, the solutions that maximize cellular adhesion and neurite length from the ANOVA model were found by an iterative process and plotted on a contour plot over the ranges of input parameters bound by the high/low levels tested in the screening model. The optimal inlet concentrations are listed in Table 4.2. The contour plots show the predicted number of cells and neurite length for all given ranges of LN and CSPG slope, from interpolation of the ANOVA model. Figure 4.9A shows the nonlinear response of cellular adhesion to double cue opposing gradients of LN and CSPG, where over the ranges of LN concentrations tested (10µg/mL to 50µg/mL), 20µg/mL LN slope appears to be a threshold below which cellular adhesion is unresponsive to CSPG slope presented, and above which the slope of CSPG has a much larger effect on adhesion. Figure 4.9B shows the linear response of neurite length on double cue parallel gradients of LN and CSPG, where as LN slope is maximized and CSPG slope is minimized, neurite length is maximized.

4.3.7 Effects of treatments against inhibitory CSPG on neurite outgrowth on double cue LN and CSPG gradients

In comparisons between untreated, chABC, and Y27632 treated cultures of DRG on LN50/CSPG10 gradients, cellular adhesion on these substrates were not significant different from each other (Figure 4.10). Neurite length on Y27632 treated samples was significantly greater than neurite lengths on untreated and chABC treated samples, as tested by oneway ANOVA (57.64µm versus 24.93 µm on untreated controls). The untreated controls elicited directed

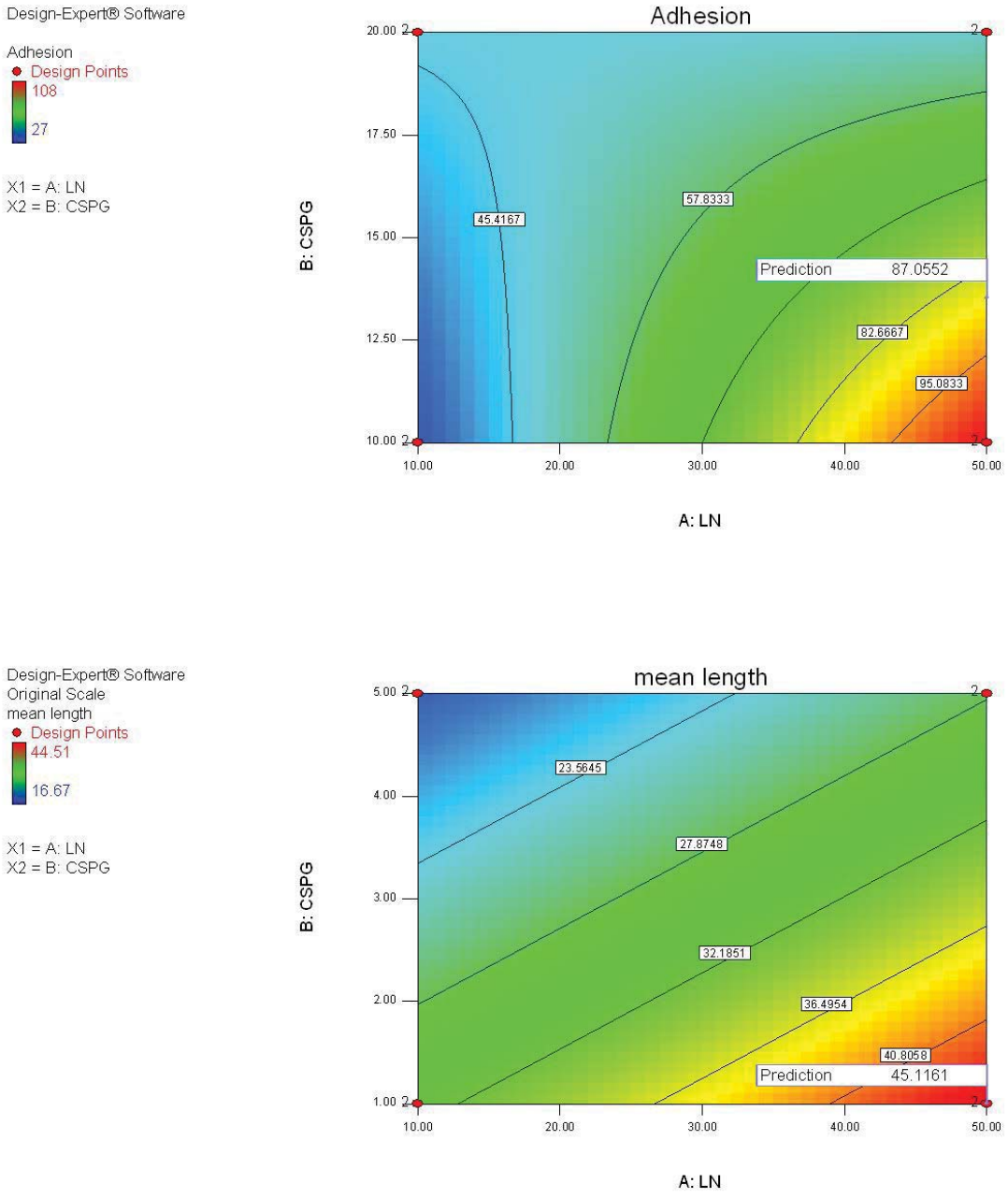

Figure 4.9: Contour plots of optimization within multiple regression model described in Equations 1 and 2.

Red dots indicate design points of experimental data, color maps correspond to low (blue) to high (red) response ranges. (A) represents 3D response surface of cellular adhesion to inlet concentrations of LN and CSPG of opposing gradients, (B) represents 3D response surface of neurite length to inlet concentration of LN and CSPG of parallel gradients.

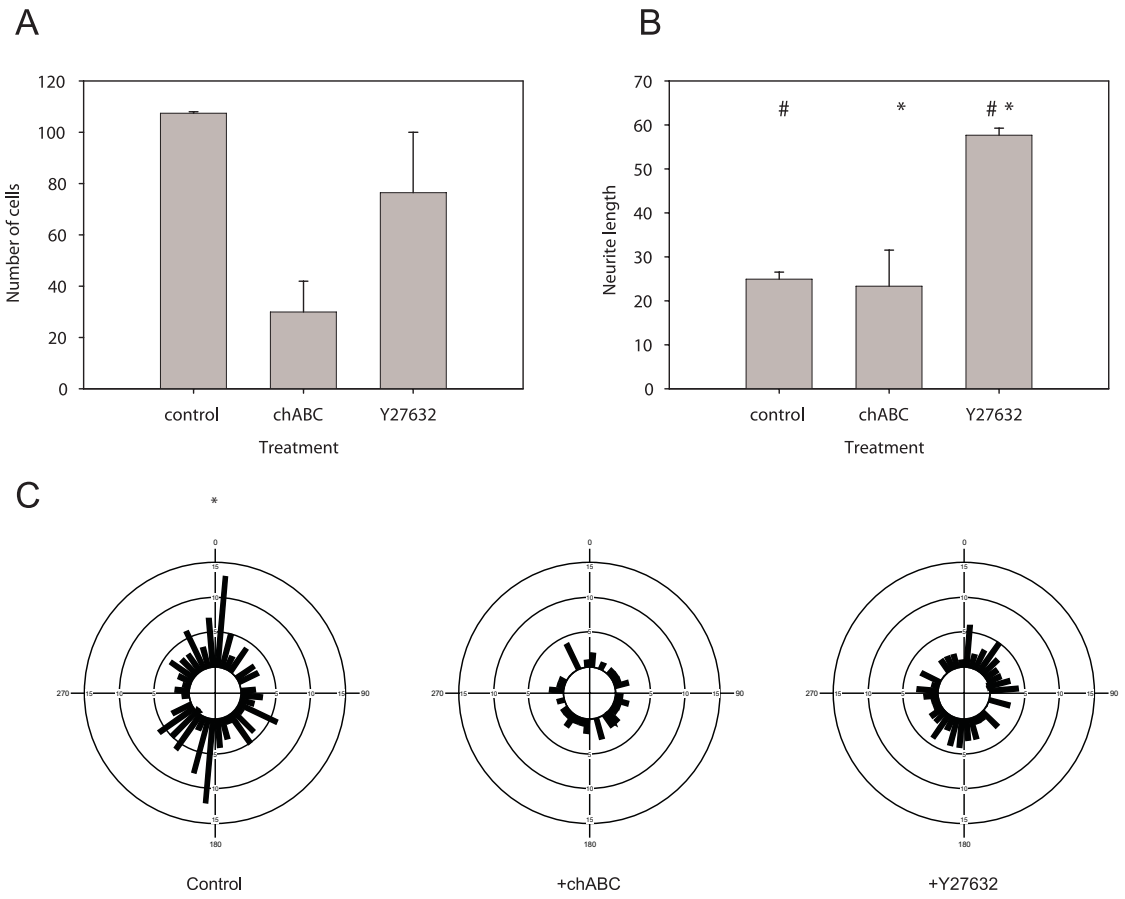

Figure 4.10: Addition of exogenous factors chABC and Y27632 affects neurite length on multimolecular gradients.

Cellular adhesion (A) and neurite length (B) on opposing LN50/CSPG10 gradients after the enzymatic digestion of CSPG with chABC, and addition of Y27632, a Rho kinase inhibitor. Untreated controls are included as a comparison. (C) shows neurite angle distribution on chABC, Y7632 treated samples and untreated controls. Data represents mean ±SEM for n=2 samples.

neurite growth towards the areas of higher LN concentration, while samples treated with chABC and Y27632 showed neurite outgrowth in all random directions.

4.4 Discussion

The present study uses combinations of substrate bound linear gradients of LN and CSPG to examine the neurite promoting effects of specific features of protein gradients such as molecular concentration, and concentration change, corresponding to slope and gradient

direction. Gradients generated by microfluidic methods offer several advantages, the most useful being the ability to create predictable, reproducible linear protein gradients with precise spatial control over the scale of hundreds of microns (reviewed in (Keenan and Folch, 2008)). Gradient parameters are easily controlled by varying inlet concentrations and ports used during the solution injection process through the microfluidic device. Linear adsorbed gradients do not change over the timescale of cell culture used in these studies. DRG cells were seeded at low density and analyzed only if they were not in contact with other cells in order to isolate the effects of the gradients from other cell-cell guidance mechanisms.

Previous studies have used LN concentrations ranging from 1µg/cm2 (Buettner and Pittman, 1991) to 100µg/mL (Hammarback et al., 1985), and CSPG concentrations ranging from 3-5µg/mL (Snow et al, 2000) to 100 µg/mL (Hynds and Snow, 2001) in studies investigating selective adhesion of neurons to substrates. Laminin, a basement membrane associated glycoprotein, was chosen as a candidate molecule for neurite guidance, found in embryonic development and peripheral nerve. CSPG, a heterogeneous class of extracellular matrix molecules, have a complex role in the development of the nervous system, with both stimulatory and inhibitory effects (Lemons et al., 2005). CSPGs from embryonic chick brain used in this study, have been shown to be inhibitory *in vitro* to DRG growth (Snow, 1994; Snow et al., 2003).

The purpose of this study was to determine if key measures of growth promotion: adhesion, neurite length and direction, were affected by molecular concentration, slope of each molecular gradient, or gradient direction in combinatorial gradients of LN and CSPG. The data show that for cellular adhesion, slope of LN and CSPG gradients appeared to have a large effect. For neurite extension, the slope of CSPG had an effect only when steep LN gradients were concurrently presented. This suggests that CSPG gradients play a larger role in adhesion than extension, where inhibition occurs regardless of the slope of LN presented. For the direction of neurite outgrowth, molecular concentration appeared to have a large effect, showing that a combination of molecular concentration and anisotropy is most effective for directing neurite growth in a particular direction. A comparison of the relationship between neurite adhesion and length showed that for combinatorial gradients, optimal values

of slope and direction do not necessarily coincide to maximize both adhesion and length. This suggests that promoting adhesion and neurite extension may be regulated by different guidance mechanisms. This is also supported by findings from Dou and Levine (Dou and Levine, 1995), where cerebellar granule neurons were observed to attach equally well to the LN coated surfaces and the LN-glycosaminoglycan coatings, but neurite outgrowth was largely inhibited. Local maxima and minima for adhesion and neurite length were identified to find the optimal LN and CSPG slopes individually over the ranges tested in this study. Non-linear relationships between slope of LN and CSPG and adhesion showed a complex relationship.

Combinations of guidance molecules have been tested and shown to have synergistic effects on neurite outgrowth. Neurotrophic factor combinations of NGF, GDNF and CNTF were found to have a synergistic effect on neurite extension (Deister and Schmidt, 2006). The optimal concentration of all three factors applied in combination corresponded to the optimum concentration of individual factors (50ng/mL NGF and 10ng/mL GDNF and CNTF) resulted in increased neurite outgrowth compared to individually applied neurotrophic factors. Coating of substrates with different combinations of LN and CSPG has been shown to elicit differential neurite outgrowth patterns. When the concentration of LN is low in comparison to CSPG concentration, CSPGs inhibit neurite growth and induce growth cone collapse or turning away from CSPG. When LN concentration is high in comparison to CSPG concentration, neurites are able to grow on the substrate (Snow, 1994).

Multimolecular gradients have been studied, and the additive effects of each molecule have been found to be nonlinear. Multimolecular soluble gradients of NGF and NT-3 gradients have been found to work synergistically (Cao and Shoichet, 2003), and BDNF and LN gradients have been observed to direct growth cone turning (Wang et al., 2008). Double cue gradients of LN and CSPGs have been studied as models of the glial scar, where LN and aggrecan gradients have been observed to elicit neuronal morphologies with dystrophic endbulbs in adult axons consistent with regenerating axons through the glial scar *in vivo* (Tom et al., 2004). In a previous study from this laboratory (Li et al. 2008) the effects of multi-molecular gradients of permissive and inhibitory cues, LN and CSPG were explored,

which suggested that gradients presenting only one cue, either permissive or inhibitory, were able to direct neurite growth in a similar manner, but there were large differences in cellular adhesion. For double cue gradients, it was shown that neuronal responses were dependent on gradient directions and elicited different neurite guidance and orientation responses when spatially patterned in different ways.

Treatment using chABC and Y27632 were hypothesized to modulate response to CSPG on double cue LN and CSPG gradients, as the addition of these exogenous factors modulate response to CSPG stripes *in vitro* (Jain et al., 2004; Lemons et al., 2003; Monnier et al., 2003; Snow et al., 1990). In this study, there was no reduction in inhibition when CSPGs were enzymatically digested by chABC prior to generating the gradient. This may be due to ABC digestion leaving behind digested sugar chain "stubs," which may have biological activity (Lemons et al., 2003), as the “stubs” are not removed before the solution is injected into the gradient mixer. Adsorption of these “stubs” to the substrate surface may be inhibitory to neurite growth. Previous studies on the effect of Y27632 have shown that neurite length is greatly increased by the addition of Y27632 to DRG cultures on CSPG substrates (Jain et al., 2004; Monnier et al., 2003). Our results agree with these studies.

Neurons may respond differentially to the local environment if multiple complex cues present conflicting information. Hence, it is important to consider combinatorial gradients separately from single cue gradients as interactions between the molecules presented may add additional complexity to the microenvironment. In this study, cellular responses have been shown to correlate to molecular gradients in a non-linear fashion, with differential response to specific gradient parameters such as slope or direction. Treatment using strategies such as enzymatic digestion or pharmacological inhibition of downstream signaling pathways may also elicit more complex cell responses when combinations of cues are presented, and further investigations would clarify and elucidate how cells integrate such iniformation to make growth decisions.

4.5 References

Bagnard D, Thomasset N, Lohrum M, Puschel AW, Bolz J. Spatial Distributions of Guidance Molecules Regulate Chemorepulsion and Chemoattraction of Growth Cones. J. Neurosci., 2000; 20: 1030-5.

Bellamkonda RV. Peripheral nerve regeneration: An opinion on channels, scaffolds and anisotropy. Biomaterials, 2006; 27: 3515-8.

Buettner HM, Pittman RN. Quantitative effects of laminin concentration on neurite outgrowth *in vitro*. Developmental Biology, 1991; 145: 266-76.

Cao X, Shoichet MS. Investigating the synergistic effect of combined neurotrophic factor concentration gradients to guide axonal growth. Neuroscience, 2003; 122: 381-9.

Deister C, Schmidt CE. Optimizing neurotrophic factor combinations for neurite outgrowth. J Neural Eng, 2006; 3: 172-9.

Dertinger SK, Jiang X, Li Z, Murthy VN, Whitesides GM. Gradients of substrate-bound laminin orient axonal specification of neurons. Proc Natl Acad Sci U S A, 2002; 99: 12542-7.

Dou CL, Levine JM. Differential effects of glycosaminoglycans on neurite growth on laminin and L1 substrates. J. Neurosci., 1995; 15: 8053-66.

Goodhill GJ, Urbach JS. Theoretical analysis of gradient detection by growth cones. J Neurobiol, 1999; 41: 230-41. Gurdon JB, Bourillot PY. Morphogen gradient interpretation. Nature, 2001; 413: 797-803.

Hammarback JA, Palm SL, Furcht LT, Letourneau PC. Guidance of neurite outgrowth by pathways of substratum-adsorbed laminin. Journal of Neuroscience Research, 1985; 13: 213-20.

Hynds DL, Snow DM. Fibronectin and laminin elicit differential behaviors from SH-SY5Y growth cones contacting inhibitory chondroitin sulfate proteoglycans. Journal of Neuroscience Research, 2001; 66: 630-42.

Jain A, Brady-Kalnay SM, Bellamkonda RV. Modulation of Rho GTPase activity alleviates chondroitin sulfate proteoglycan-dependent inhibition of neurite extension. J Neurosci Res, 2004; 77: 299-307.

Keenan TM, Folch A. Biomolecular gradients in cell culture systems. Lab on a Chip, 2008; 8: 34-57.

Laabs TL, Wang H, Katagiri Y, McCann T, Fawcett JW, Geller HM. Inhibiting Glycosaminoglycan Chain Polymerization Decreases the Inhibitory Activity of Astrocyte-Derived Chondroitin Sulfate Proteoglycans. J. Neurosci., 2007; 27: 14494-501.

Lemons ML, Barua S, Abanto ML, Halfter W, Condic ML. Adaptation of Sensory Neurons to Hyalectin and Decorin Proteoglycans. J. Neurosci., 2005; 25: 4964-73.

Lemons ML, Sandy JD, Anderson DK, Howland DR. Intact aggrecan and chondroitin sulfate-depleted aggrecan core glycoprotein inhibit axon growth in the adult rat spinal cord. Experimental Neurology, 2003; 184: 981-90.

Li G, Liu J, Hoffman-Kim D. Multi-Molecular Gradients of Permissive and Inhibitory Cues Direct Neurite Outgrowth. Annals of Biomedical Engineering, 2008; [Epub ahead of print].

Monnier PP, Sierra A, Schwab JM, Henke-Fahle S, Mueller BK. The Rho/ROCK pathway mediates neurite growth-inhibitory activity associated with the chondroitin sulfate proteoglycans of the CNS glial scar. Mol Cell Neurosci, 2003; 22: 319-30.

Snow DM. Neurite Outgrowth in Response to Patterns of Chondroitin Sulfate Proteoglycan: Inhibition and Adaptation. Neuroprotocols, 1994; 4: 146-57.

Snow DM, Lemmon V, Carrino DA, Caplan AI, Silver J. Sulfated proteoglycans in astroglial barriers inhibit neurite outgrowth *in vitro*. Exp Neurol, 1990; 109: 111-30.

Snow DM, Smith JD, Cunningham AT, McFarlin J, Goshorn EC. Neurite elongation on chondroitin sulfate proteoglycans is characterized by axonal fasciculation. Experimental Neurology, 2003; 182: 310-21.

Tom VJ, Steinmetz MP, Miller JH, Doller CM, Silver J. Studies on the Development and Behavior of the Dystrophic Growth Cone, the Hallmark of Regeneration Failure, in an In Vitro Model of the Glial Scar and after Spinal Cord Injury. J. Neurosci., 2004; 24: 6531-9.

von Philipsborn AC, Lang S, Loeschinger J, Bernard A, David C, Lehnert D, Bonhoeffer F, Bastmeyer M. Growth cone navigation in substrate-bound ephrin gradients. Development, 2006; 133: 2487-95.

Wang CJ, Li X, Lin B, Shim S, Ming G-l, Levchenko A. A microfluidics-based turning assay reveals complex growth cone responses to integrated gradients of substrate-bound ECM molecules and diffusible guidance cues. Lab on a Chip, 2008; 8: 227-37.

Chapter 5

Genomic and Morphological Changes of Neuroblastoma Cells in Response to Three-Dimensional Matrices

Advances in neural tissue engineering require a comprehensive understanding of neuronal growth in three dimensions. This study investigated the gene expression of SH-SY5Y human neuroblastoma cells when cultured in three-dimensional (3D) versus two-dimensional (2D) environments. Microarray analysis demonstrated that in response to varying matrix geometry, SH-SY5Y cells exhibited differential expression of 1766 genes in collagen I, including those relevant to cytoskeleton, extracellular matrix, and neurite outgrowth. Cells extended longer neurites in 3D versus 2D collagen I cultures. Real-time RT-PCR experiments and morphological analysis comparing collagen I and Matrigel tested whether the differential growth and gene expression reflected influences of culture dimension or culture material. SH-SY5Y neuroblastoma cells responded to geometry by differentially regulating cell spreading and genes associated with actin in similar patterns for both materials; however, neurite outgrowth and the expression of the gene encoding for neurofilament varied with the type of material. Electron microscopy and mechanical analysis showed that collagen I was more fibrillar than Matrigel, with larger interfiber distance and higher stiff-

ness. Taken together, these results suggest complex cell-material interactions, in which the dimension of the culture material influences gene expression and cell spreading, and the structural and mechanical properties of the culture material influence gene expression and neurite outgrowth.

5.1 Introduction

Current goals for neural tissue engineering include replacing damaged or degenerated neural tissue with a matrix containing neural progenitor cells, promoting the ingrowth of host neurons into an acellular matrix, and generating *in vitro* systems in which to study neuronal growth under conditions that mimic the *in vivo* nervous system environment. Neurons *in vivo* adhere to and interact with the extracellular matrix (ECM); in tissue engineering, hydrogels and other polymer matrices have been utilized to perform ECM functions. Recent efforts have focused on promoting neuronal growth and directing neurite extension in three-dimensional (3D) environments.

A variety of 3D matrices have been shown to support neuronal growth and neurite extension, including microporous polystyrene scaffolds (Hayman et al., 2004), fibrin matrices (Pittier et al., 2005), agarose hydrogels (Balgude et al., 2001), Matrigel hydrogels (Khan et al., 2002), and collagen hydrogels (Ma et al., 2004; O'Connor et al., 2001). While studies have begun to characterize these matrices with regard to their chemical composition and mechanical properties, the underlying physiologic response of the neuron to the 3D environment is not completely understood. Comparisons of neuronal growth as well as comparisons of the growth of nonneuronal cells, in standard two-dimensional (2D) monolayer cultures as compared to 3D matrix cultures that more closely resemble *in vivo* environments, have shown clear phenotypic differences. For example, previous studies have revealed differences in cellular surface area, stress fiber distribution, cellular migration, focal adhesions, neurite and growth cone dimensions, and protein and gene expression (Balgude et al., 2001; Even-Ram and Yamada, 2005; Hayman et al., 2004; Jaworski and Klapperich, 2006; Klapperich and Bertozzi, 2004; Li et al., 2003; Pittier et al., 2005; Wang et al., 2003).

A powerful approach to investigate these differences is to examine the neuron's global gene expression profile. In this study, we used oligonucleotide microarrays to compare the gene expression patterns of SH-SY5Y neuroblastoma cells grown in 3D versus 2D culture environments, with the aim of identifying molecules with putative roles in differentially interpreting 3D guidance cues and promoting neurite outgrowth. Neuroblastoma cells were initially cultured in collagen hydrogel matrices and on collagen substrates. Matrigel was subsequently utilized as an additional hydrogel matrix and substrate material, to determine if material type influenced neuroblastoma growth response.

The motivation for these studies is to gain a more rigorous comprehension of the cellular and molecular mechanisms underlying axon growth in a matrix that is physiologically relevant in its three-dimensional geometry. The overarching goal is to combine materials design requirements with knowledge of the physiological response of the neuron, in order to optimize the development of biomaterials for neural tissue engineering.

5.2 Materials and Methods

5.2.1 Cell culture

All materials were purchased from Invitrogen (Carlsbad, CA) unless otherwise specified.

The human neuroblastoma cell line SH-SY5Y, ATCC#CRL-2266 (American Type Culture Collection, Manassas, VA) was cultured in a 1:1 mixture of Eagle's MEM Minimum Essential Medium (ATCC) and Ham's F12 Medium (containing 2mM L-glutamine and 1.5g/l of sodium bicarbonate) supplemented with 10% fetal bovine serum and 100 U/ml penicillin-streptomycin. To further differentiate the cell line toward a neuronal phenotype, cell media was supplemented with 10µM retinoic acid (RA) for three days. Cells cease proliferation and 70% of cells are differentiated following this treatment (Navone et al., 2001; Rebhan et al., 1994; Sidell, 1982).

Cell culture for RNA studies was performed using six-well plates as described below. Cell

culture for microscopy studies utilized donut dishes. For donut dish assembly, sterile, acid-washed (sulfuric and nitric acid (5:1)) glass coverslips were affixed to 35x10mm tissue culture dishes with 20 mm holes (Willco Wells, Amsterdam, Netherlands). For 2D cell culture on collagen I substrates, dishes or wells were coated with 3 mg/ml of purified bovine dermal type I collagen in 0.012 N HCl according to the manufacturer's instructions (PureCol, Inamed Co., Fremont, CA; also marketed as Vitrogen 100, Cohesion Technologies, Palo Alto, CA and referred to hereafter as collagen I). SH-SY5Y cells (106 cells per well for 2D and 3D RNA studies; 6.5 x 104 cells per dish for 2D and 1.3 x105 cells per dish for 3D microscopy studies) cultured in RA-supplemented media were plated onto the collagen-coated wells or dishes. For culture in 3D collagen I, matrices of 2ml final volume were prepared with a mixture of 5X Dulbecco's Modified Eagle's Media (DMEM), collagen I, and SH-SY5Y cell suspension in a ratio of 2:7:1, and the pH was adjusted to 7.3-7.4. This solution was plated on wells or dishes and gelled at 37^{o}C with 5% CO2. RA-supplemented media was added 1 hour after plating. Cells were cultured for 24h in a humidified environment at 37^{o}C with 5% CO2.

For 2D culture on growth factor reduced MatrigelTM (BD Biosciences, Franklin Lakes, NJ, referred to hereafter as Matrigel), wells or dishes were coated with 0.5ml Matrigel, and incubated at 37^{o}C for 30 minutes. SH-SY5Y cells cultured in RA-supplemented media were plated onto the gelled Matrigel. For culture in 3D Matrigel, matrices of 1.5ml final volume were made with a mixture of Matrigel and cell suspension (SH-SY5Y cells in 50-100 µl DMEM; 0.5-0.8 x 106 cells per well for 2D and 1-1.6 x 106 cells per well for 3D RNA studies; 2 x 104 cells per dish for 2D and 4 x 104 cells per dish for 3D microscopy studies), plated on wells or dishes and incubated at 37^{o}C for 30 minutes. RA-supplemented media was added 30 minutes after plating. Cells were cultured for 24h in a humidified environment at 37^{o}C with 5% CO2.

5.2.2 RNA isolation

Cells grown in collagen I were treated with 0.5% collagenase (Sigma, St. Louis, MO) at 37^{o}C for 20-40 minutes, washed with 0.1M phosphate buffered saline, pH 7.4 (PBS), and suspended in 100 µl of PBS. One ml of RNAlater stabilization reagent (Qiagen Inc. Valencia, CA) was added and the cells were stored at 4^{o}C. Cells grown in Matrigel were treated with MatriSperse Cell Recovery Solution (BD Biosciences) according to the manufacturer's instructions. The cells were resuspended in 100ul of PBS, one ml of RNAlater was added, and the cells were stored at 4^{o}C. RNA was isolated with the RNAeasy Mini Kit (Qiagen). RNA purity was determined by spectrophotometry, with an A260/A280 ratio of 1.9-2.1 indicating pure RNA.

5.2.3 Microarray analysis

RNA from collagen I cultures was converted into double stranded cDNA using a Super-Script Double Stranded cDNA Synthesis Kit. Double stranded cDNA was converted into cRNA using the BioArray High Yield RNA Transcript Labeling Kit (Enzo Diagnostics, New York, NY). The cRNA was fragmented for target preparation according to the GeneChip Expression Analysis Technical Manual (Affymetrix, Santa Clara, CA). Fragmented biotin-labeled cRNA samples were hybridized for 16 h to U133A Human GeneChips (Affymetrix). Chips were washed and labeled with streptavidin-phycoerythrin according to the Affymetrix 2 Stain Protocol. Chips were scanned using an Agilent Technologies G2500A GeneArray scanner and Affymetrix MicroArray Suite (MAS) 5.0 software. Data analysis was performed using MAS 5.0, Affymetrix Micro DB, and Data Mining Tool 3.0 software.

5.2.4 Real-time RT-PCR

RNA was prepared as described above and total RNA concentration was determined by absorbance at 260 nm. Serial dilutions of RNA were made for RT-PCR reactions containing 100 ng, 10 ng, 1 ng, 0.5 ng, 0.25 ng or 0.125 ng of total RNA. All reactions were performed

in triplicate. The primers and probes were designed with QuantiProbe Design Software (Qiagen, Valencia, CA). Reactions also contained 1X Quantitect Probe RT-PCR Master mix, 1X Quantitect specific PCR primers and dual-labeled specific probe mix with a CarboxyFluorescein FAM fluorophore at the 3' end of the specific probe and an Eclipse Dark Quencher at the 5' end. Reactions were carried out using an Applied Biosystems 7300 Real Time PCR system using the following protocol: reverse transcription (30 minutes at 500^oC), initial activation step (15 minutes at 950C), and amplification (45 cycles of 15 seconds denaturation at 940C, 30 seconds annealing at 560^oC and 30 seconds of extension at 760C). Fluorescence data was collected during the annealing step.

5.2.5 Real-time RT-PCR analysis

Fold changes in gene expression were calculated relative to the level of glyceraldehyde-3-phosphate dehydrogenase (GAPDH) mRNA in the samples. GAPDH was chosen as the reference gene because microarray analysis indicated that its expression level did not change when cells were plated on 2D versus 3D collagen. The efficiency calibrated model(Pfaffl et al., 2002) was applied to the data to calculate relative expression of genes of interest (target genes) as compared to GAPDH (reference gene) for each condition tested (2D or 3D) in each matrix (collagen or Matrigel). Cycle threshold (Ct) values for a dilution series of 2D and 3D RNA were determined for reference and target genes. Ct values were plotted against log of RNA concentration and efficiencies were calculated according to $E = 10^{-\frac{1}{Slope}}$.

For each gene at each condition and matrix tested, three replicates of six serially diluted concentrations were performed. These exceed the minimum requirement of three replicates at three concentrations in order to yield data with sufficient statistical power, and the minimum requirement of two replicates of three concentrations to yield data with an appropriate dynamic range and reproducibility(Yuan et al., 2006). The mean Ct values for each input concentration and each condition were used to calculate ΔCt values. ΔCts for each gene were calculated by subtracting the Ct value of the 3D sample from that of the 2D sample. Expression ratios between the conditions were calculated from the ΔCts for each gene in each

matrix using the following equation, with fold change corresponding to the expression ratio for upregulated genes in 3D, and the reciprocal of the expression ratio for downregulated genes in 3D: Expression ratio = $\frac{E_{target}^{\Delta Ct_{target}}}{E_{reference}^{\Delta Ct_{reference}}}$

5.2.6 Quantification of neurite growth

After 24h of culture, 2D samples were examined on a Nikon Eclipse TE2000-S microscope under phase-contrast optics using a 20X objective and 10X projection lens. Images were captured using a Hamamatsu Orca-ER camera and Orbit shutter controller (Improvision, Lexington, MA), outputting to OpenLab v4.0.2 (Improvision). Neurite lengths were measured using OpenLab software. Cells cultured in 3D were examined at multiple focal planes under phase-contrast optics using a Zeiss Axiovert microscope using a 20X objective and 10X projection lens. Images were captured using a Hamamatsu Orca-ER camera and neurite length segments were measured along the plane of focus using the ruler tool in Zeiss Axiovision software, that allowed for continuous measurements between slices in a z-stack, yielding a summation of length segments. The height of a stack was measured by counting the number of focal planes, with an intra-plane distance of 1µm. The 3D neurite length was then calculated using the Pythagorean theorem as the hypotenuse of a triangle with the horizontal projection of neurite trajectory (x) and height of z-stacks (z) as the sides . A neurite was defined as an extension exceeding the length of a cell body, and was included in the analysis only if the neurite was the longest neurite of the neuron examined and did not contact other cells (Wu et al., 2004; Yamashita et al., 2002; Yip et al., 1998). Neurons with neurites that did not meet these criteria were not included in analysis of cell morphology. A total of 90 neurites per condition, taken from 3 replicate samples for each condition, were measured to determine the average neurite length.

5.2.7 Confocal microscopy

Confocal microscopy was used to view neurite extension on 2D substrates and in 3D gels. SH-SY5Y cells were plated and labeled with phalloidin as described below. After 24h in

culture, samples were analyzed using a Leica TCS SP2 AOBS spectral confocal microscope. A krypton-argon laser was used to excite at 488nm and cells were viewed using a 63X objective lens. Multiple z scans were obtained and Voxx software or Leica confocal software was used for image analysis.

5.2.8 Phalloidin staining

Cells grown on 2D substrates were fixed with 2% paraformaldehyde for 20 minutes, washed with PBS, treated with 0.1% Triton X-100 for 5 minutes, washed twice with PBS, incubated for 20 minutes with 1% bovine serum albumin (BSA) in PBS, stained for 20 minutes with 1 unit of Alexa Fluor 546 phalloidin (Molecular probes, Invitrogen, Carlsbad, CA), washed with PBS, and visualized under epifluorescence and confocal microscopy. For cells grown in 3D gels, the staining protocol was the same, except that incubation periods were 2 hours for paraformaldehyde, 30 minutes for Triton X-100, one hour for BSA, and one hour for fluorescent phalloidin.

5.2.9 Mechanical characterization of gels using dynamic mechanical analysis

The storage modulus and loss modulus of the hydrogels were measured using a DMA 7e Dynamic Mechanical Analyzer (Perkin Elmer, Wellesley, MA). Parallel plate geometry was employed with 15 mm diameter plates. Acellular hydrogel samples, with thickness varying from 2-4 mm, were subjected to static force of 11mN and an oscillating dynamic force of 10mN at 2.6 Hz at room temperature. The modulus of a sample was determined by averaging data points between 1 and 3 minutes of a sample's run on the DMA. Triplicate samples were tested for each type of hydrogel.

5.2.10 Scanning electron microscopy

For examination under scanning electron microscopy (SEM), acellular samples were fixed in Karnovsky's fixative (Electron Microscopy Sciences, Hatfield, PA) for 3h and rinsed in 0.1M cacodylate buffer (Sigma). Samples were washed with dH2O and dehydrated with graded ethanols to 100% ethanol. Samples were dried by incubation with hexamethyldisilazane (HMDS; Sigma) for 10min and a further incubation with fresh HMDS overnight. Samples were examined with a Hitachi S-2700 scanning electron microscope using an acceleration voltage of 3kV.

5.2.11 Transmission electron microscopy

For examination under transmission electron microscopy (TEM), acellular samples were fixed in Karnovsky's fixative for 3h and rinsed in 0.1M cacodylate buffer. Samples were postfixed with 1% osmium tetroxide for 3h, washed with dH2O, and dehydrated with graded ethanol washes to 100% ethanol. Samples of 1mm3 in size were cut from the original sample, infiltrated with Spurr's resin, and 85nm sections were cut with a diamond knife on a Reichert-Jung Ultracut E. Sections were mounted on copper mesh grids and examined with a Phillips EM 410 using a voltage of 80kV. TEM micrographs were analyzed to determine pore size as approximated by inter-fibril distance, using Adobe Photoshop CS2. The distance between fibrillar structures was measured in pixels using the line tool and converted to microns. Ten measurements per image were taken with n=3 images for Matrigel and n=5 images for collagen.

5.2.12 Statistical analysis

Statistics were performed on all quantitative measurements. To evaluate the effect of matrix material on gene expression, Student t-tests were performed on calculated gene expression fold changes for each gene in each matrix material for n=4 samples. To evaluate the significance of dimensionality and materials on cell spreading and neurite outgrowth, one-way

analysis of variance (ANOVA) was performed in the between-subject design. Post-hoc multiple comparison analysis was done using the Bonferroni test. To evaluate the difference in mechanical properties of the two gels tested, the Student t-test was used. SPSS 11.5 software (SPSS, Inc., Chicago, IL) was used, and significance levels were taken to be p=0.05.

5.3 Results

5.3.1 SH-SY5Y cells exhibited differential gene expression in 3D versus 2D cultures

SH-SY5Y cells grown in 2D and 3D collagen I were recovered after 24h, RNA was extracted, and 30-40 μg of total RNA was obtained from 0.5-1.0x107 cells. RNA was confirmed to be free of degradation or DNA contamination. A total of 14,564 genes and expressed sequence tags were screened by microarray analysis. Concordance analysis identified 1766 probesets that were significantly differentially expressed with $p \leq 0.05$. Of these, 919 known and 12 unknown genes were up-regulated in 3D cultures, and 823 known and 12 unknown genes were down-regulated in 3D cultures. Fold changes of 1.5 fold or greater and found to be significantly different by MAS 5 algorithms with $p < 0.05$ were taken to be differentially expressed genes of interest (Costigan et al., 2002; Li and Wong, 2001). Known genes that were differentially expressed in neuroblastoma cells cultured in 3D collagen I gels included those encoding proteins involved in cytoskeleton, extracellular matrix, RNA metabolism, protein metabolism, signal transduction, and other functions (fold change > 1.5 and $p < 0.05$; Table 5.1). Genes up-regulated in 3D cultures included those encoding cytoskeletal-associated proteins such as actin filament α2 capping protein and signal transduction factors such as midkine. Among the genes that were down-regulated in 3D cultures were genes encoding the cytoskeletal proteins filamin A, actinin 1-α1, and talin 1, and genes encoding extracellular matrix molecules such as fibronectin 1, collagen IIIα1 and versican.

Because initial pilot studies showed difference in neuronal morphology (see below), we selected for further evaluation seven genes differentially expressed in 3D versus 2D that en-

TABLE 1. DIFFERENTIAL GENE EXPRESSION OF SH-SY5Y NEUROBLASTOMA CELLS WHEN GROWN IN 3-DIMENSIONAL (3D) AND 2-DIMENSIONAL (2D) COLLAGEN I

Genbank	Description	Fold change ± SD
CYTOSKELETON		
NM_006289.1	talin 1	−1.9 ± 0.3
AW051856	filaminin A, a-actin binding protein	−1.7 ± 0.1
AI082078	actinin 1, a1	−1.6 ± 0.1
NM006158.1	neurofilament	1.3 ± 0.1
AV685920	capping protein (actin filament) muscle Z-line, a2	1.7 ± 0.3
EXTRACELLULAR MATRIX		
AF130095.1	fibronectin 1	−3.5 ± 1.0
AU144167	highly similar procollagen a1 (III) chain precursor	−3.1 ± 1.1
AI813758	collagen, type III, a1	−3.0 ± 0.8
AF130082.1	collagen, type III, a1	−2.5 ± 0.8
NM_004385.1	chondroitin sulfate proteoglycan 2 (versican)	−1.9 ± 0.2
RNA METABOLISM		
AW103422	poly(rC)-binding protein 2	−2.3 ± 0.7
AI655799	RNA binding protein; AT-rich element binding factor	−2.2 ± 0.5
BG026366	KH-type splicing regulatory protein (FUSE binding protein 2)	−1.8 ± 0.3
NM_004643.1	poly(A)-binding protein, nuclear 1	−1.6 ± 0.2
NM_005105.1	RNA binding motif protein 8A	1.7 ± 0.2
AI800983	cleavage and polyadenylation specific factor 5, 25 kDa	1.7 ± 0.2
PROTEIN METABOLISM		
AW772056	dopa decarboxylase (aromatic L-amino acid decarboxylase)	1.6 ± 0.3
NM_002539.1	ornithine decarboxylase 1	2.1 ± 0.5
NM_001415.2	eukaryotic translation initiation factor 2, subunit 3 (Y 52kD)	2.4 ± 0.5
OTHER		
NM_004039.2	annexin A2	−2.0 ± 0.4
D21254.1	cadherin 11, type 2 (osteoblast specific)	−1.9 ± 0.3
NM_024555.1	f-box and leucine-rich repeat protein 6	−1.6 ± 0.3
NM_005413.1	sine oculis homeobox (Drosophila) homolog 3	−1.5 ± 0.2
NM_016127	HSPC035 protein (hematopoietic stem/progenitor cell)	1.5 ± 0.1
M69148.1	midkine (neurite growth promoting factor 2)	1.6 ± 0.2
BG288007	lysophospholipase	1.7 ± 0.2
AF180519.1	GABA-A receptor-associated protein	1.8 ± 0.1
AW138159	H3 histone, family 3B/FL ¼ gb:NM_005324.1	1.9 ± 0.5
NM_005461.1	Kreisler (mouse) maf-related leucine zipper homolog	2.3 ± 0.4
UNKNOWN		
AK024108.1	Homo sapiens cDNA FLJ14046 fis, clone HEMBA1006461	−1.9 ± 0.4
AW238632	KIAA1096 protein	−1.6 ± 0.1
BG256504	KIAA0220 protein	−1.8 ± 0.3
NM_014392.1	neuron-specific protein	1.5 ± 0.1
NM_024034.1	hypothetical protein MGC3129	1.5 ± 0.1
BC005807.1	clone MGC:10264, mRNA, complete cds	1.6 ± 0.1
BE881590	Homo sapiens clone 24421 mRNA sequence	1.7 ± 0.2
AI890972	hypothetical protein PRO2730	2.0 ± 0.2

SH-SY5Y cells were cultured on 2D collagen I substrates or in 3D collagen matrices for 24 h and subjected to microarray analysis. Fold change is the average 3D/2D ratio from three independent microarray experiments ($p \leq 0.05$). Genes reported were upregulated (þ) or downregulated (−) in 3D and had fold changes ≥ 1.5 in all runs with the exception of neurofilament

Table 5.1: Microarray results of 2D versus 3D

coded for proteins relevant to the cytoskeleton, extracellular matrix, and neurite growth. The gene for neurofilament was included in light of its relevance to neurite growth, even though its fold change between 3D and 2D cultures was less than 1.5 by microarray analysis. Fold changes for the RT-PCR experiments were calculated relative to the level of GAPDH mRNA. The differential gene expression results from the microarray data were confirmed by real time RT-PCR using samples from the same samples that had been used for the microarray experiments. The RT-PCR experiments confirmed the differential expression of three genes that had been shown by microarray to be up-regulated in 3D cultures: neurofilament, midkine, and actin filament capping protein; and four genes that had been shown by microarray to be down-regulated in 3D cultures: collagen IIIα1, actinin 1-α1, fibronectin 1 and filamin A (compare Table 1 and Table 2 – collagen I column). The sign of the average fold change for each gene tested was identical between the RT-PCR and microarray results.

These experiments were extended to include a second type of hydrogel material, Matrigel, in order to test whether the gene expression changes observed in cells cultured in 3D versus 2D collagen reflected influences of culture dimension or culture material. Matrigel is composed of 56% laminin, 31% collagen IV, and 8% entactin. The sign of the average 2D versus 3D fold change for each gene tested was identical between the collagen and Matrigel results (Table 5.2). For five of the seven genes tested (filamin A, actinin 1 alpha 1, capping protein alpha 2, fibronectin 1 and midkine), the magnitudes of the average fold changes were similar between collagen and Matrigel cultures ($p > 0.05$; Table 5.2). The fold change for neurofilament was significantly higher in collagen ($p < 0.01$), and the fold change for collagen III alpha 1 was significantly higher in Matrigel ($p < 0.001$).

5.3.2 SH-SY5Y cells displayed different morphologies when grown in 3D versus 2D cultures

SH-SY5Y neuroblastoma cells exhibited healthy growth with neurite extension on control 2D tissue culture plastic as well as under all four culture conditions tested – 2D collagen I, 3D collagen I, 2D Matrigel, and 3D Matrigel. For all culture conditions, after 24 hours in

TABLE 2. DIFFERENTIAL 3-DIMENSIONAL (3D)/2-DIMENSIONAL (2D) EXPRESSION OF SELECTED SH-SY5Y GENES IN COLLAGEN I AND MATRIGEL

Gene	CollagenI	MatrigeI	p-value
CYTOSKELETON			
filaminin A	−1.69± 0.43	−1.68± 0.21	0.94
actinin1, a1	−1.16± 0.11	−1.63± 0.51	0.12
neurofilament	1.66± 0.22	1.18± 0.10	0.01
cappingprotein a2	1.66± 0.54	2.19± 0.70	0.28
EXTRACELLULARMATRIX			
fibronectin1	−2.01± 0.26	−2.17± 0.24	0.39
collagenIII, a1	−1.40± 0.17	−2.86± 0.18	< 0.001
SIGNALTRANSDUCTION			
midkine	1.70± 0.58	2.18± 0.59	0.29

Table 5.2: qPCR results

culture, some somata and neurites touched neighboring cells while other cells did not contact adjacent cells. Neuronal morphology varied with the dimension of the substrate/matrix and the type of material (Figures 5.15.25.3). After 24 hours in culture, the somata of SH-SY5Y cells cultured in 3D matrices were globular in appearance (Figure 1B, 1D, 3B, 3D) while cells on 2D substrates exhibited a flatter, more spread morphology (Figure 1A, 1C, 3A, 3C). Quantitative image analysis of cell morphology supported these observations and showed that neuroblastoma cells grown on 2D substrates had longer somata than cells grown in 3D matrices ($p < 0.001$; Figure 2A). Cells grown on 2D Matrigel substrates tended to aggregate into cell clusters (Figure 1C). Cell spreading was prominent in cells growing on 2D substrates stained with phalloidin, showing a flat, angular morphology. Staining with phalloidin showed that while actin was present in cells growing in both 2D (Figure 3A, C) and 3D (Figure 3B, D), the filament organization of actin was not visible in 3D.

5.3.3 SH-SY5Y neurite outgrowth varied with type and dimension of material

Quantitative analysis showed that SH-SY5Y cells grown with collagen I as the culture material extended neurites that were longer in 3D cultures than in 2D cultures (47.2 + 1.5µm versus 26.0 + 0.57µm, $p<0.001$, Figure 2B). Cells grown with Matrigel as the culture material extended neurites with somewhat longer average lengths in 2D cultures than in 3D

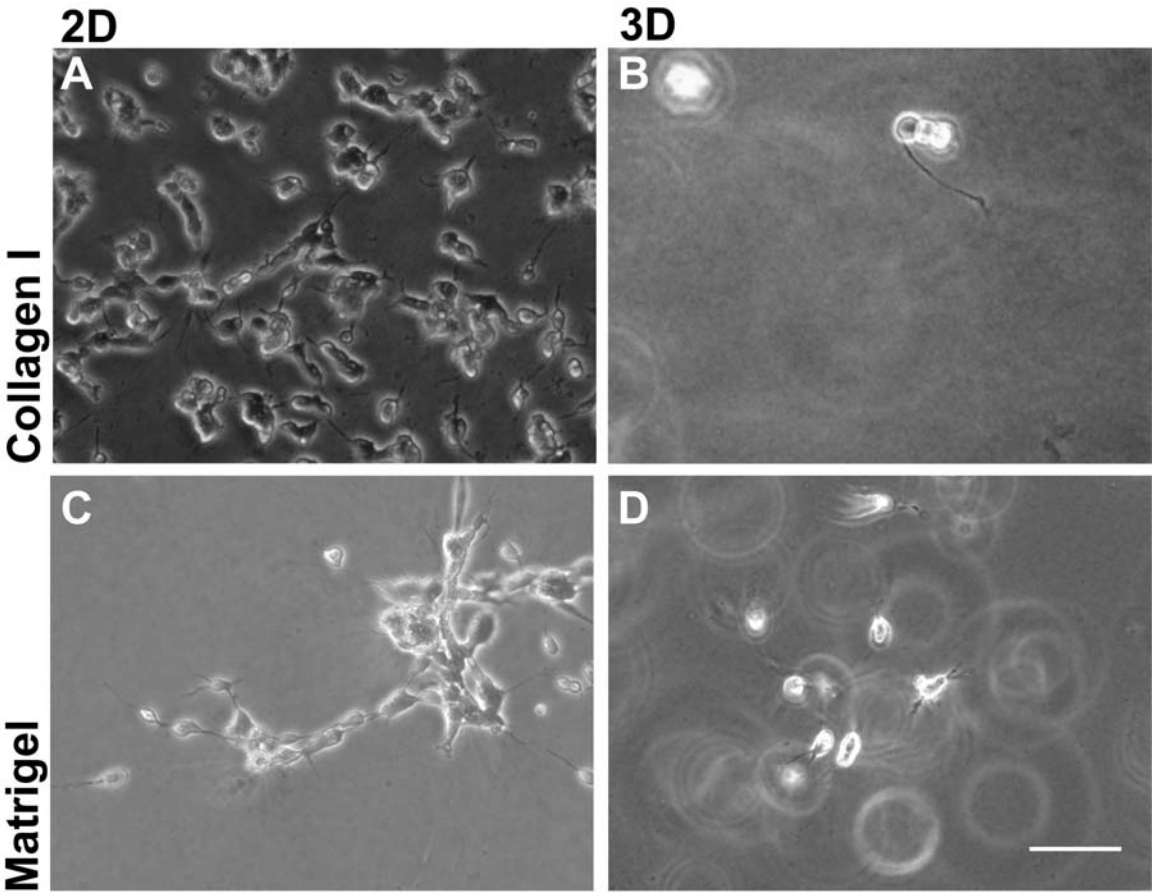

Figure 5.1: Different morphologies of SH-SY5Y neuroblastoma cells in 3-dimensional (3D) and 2-dimensional (2D) cultures.
Phase contrast micrographs of SH-SY5Y cells cultured for 24 h on 2D collagen I substrates (A), on 2D Matrigel substrates (C), in 3D collagen I matrices (B), and in 3D Matrigel matrices (D). Scale bar, 50 mm.

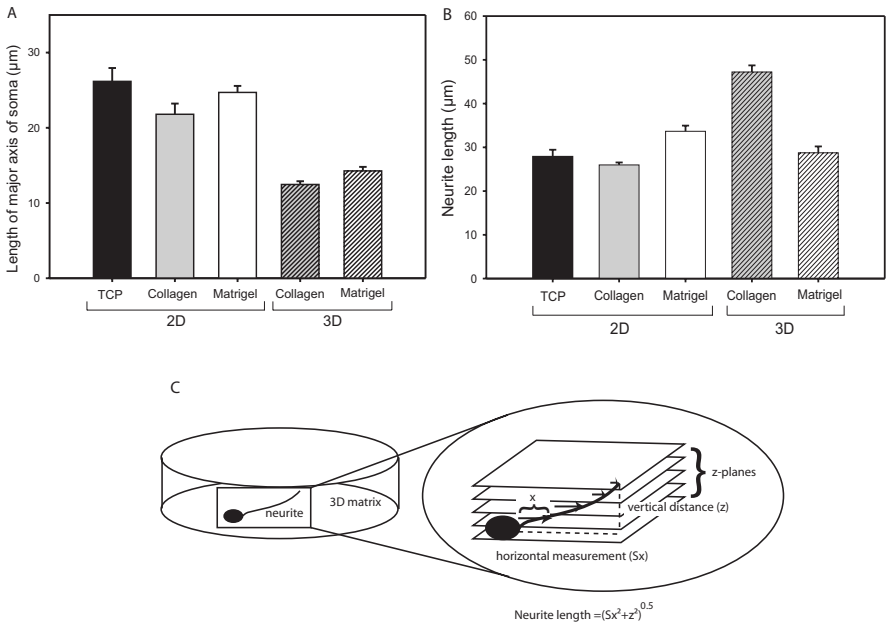

p-values		2D			3D	
		TCP	Collagen I	Matrigel	Collagen I	Matrigel
2D	TCP	X	0.06	1	< 0.001	< 0.001
	Collagen I		X	0.41	< 0.001	< 0.001
	Matrigel			X	< 0.001	< 0.001
3D	Collagen I				X	1
	Matrigel					X

p-values		2D			3D	
		TCP	Collagen I	Matrigel	Collagen I	Matrigel
2D	TCP	X	1	< 0.05	< 0.001	1
	Collagen I		X	< 0.001	< 0.001	1
	Matrigel			X	< 0.001	0.06
3D	Collagen I				X	< 0.001
	Matrigel					X

Figure 5.2: SH-SY5Y neuroblastoma cell spreading and neurite outgrowth varied with material type and geometry.

Quantification of the length of the major axis of the soma (A) and neurite length (B) of SH-SY5Y cells cultured for 24h on tissue culture plastic (TCP), on 2D collagen I substrates, on 2D Matrigel substrates, in 3D collagen I matrices, or in 3D Matrigel matrices. Data are mean ± SEM. Cells were chosen for evaluation randomly across 3 samples for each condition. n=82 for somata in 3D collagen I; n=90 for all other conditions. Tables indicate p values for each pair-wise comparison. Figure 2C shows the method of quantifying neurite length in 3D. A cartoon of a neuron grown in a 3D matrix in a typical orientation of soma and neurites spanning multiple focal planes. The inset is a zoomed in view of the neuron and neurite in multiple z-planes taken using a Zeiss Axiovert microscope. The horizontal projection of each neurite segment in focus at each focal plane is measured and summed (Σx), the vertical projection of the entire neurite is approximated to the nearest 1µm by taking the total of the z-stack height, and the resultant neurite length is calculated using the Pythagorean theorem to determine the length of the hypotenuse.

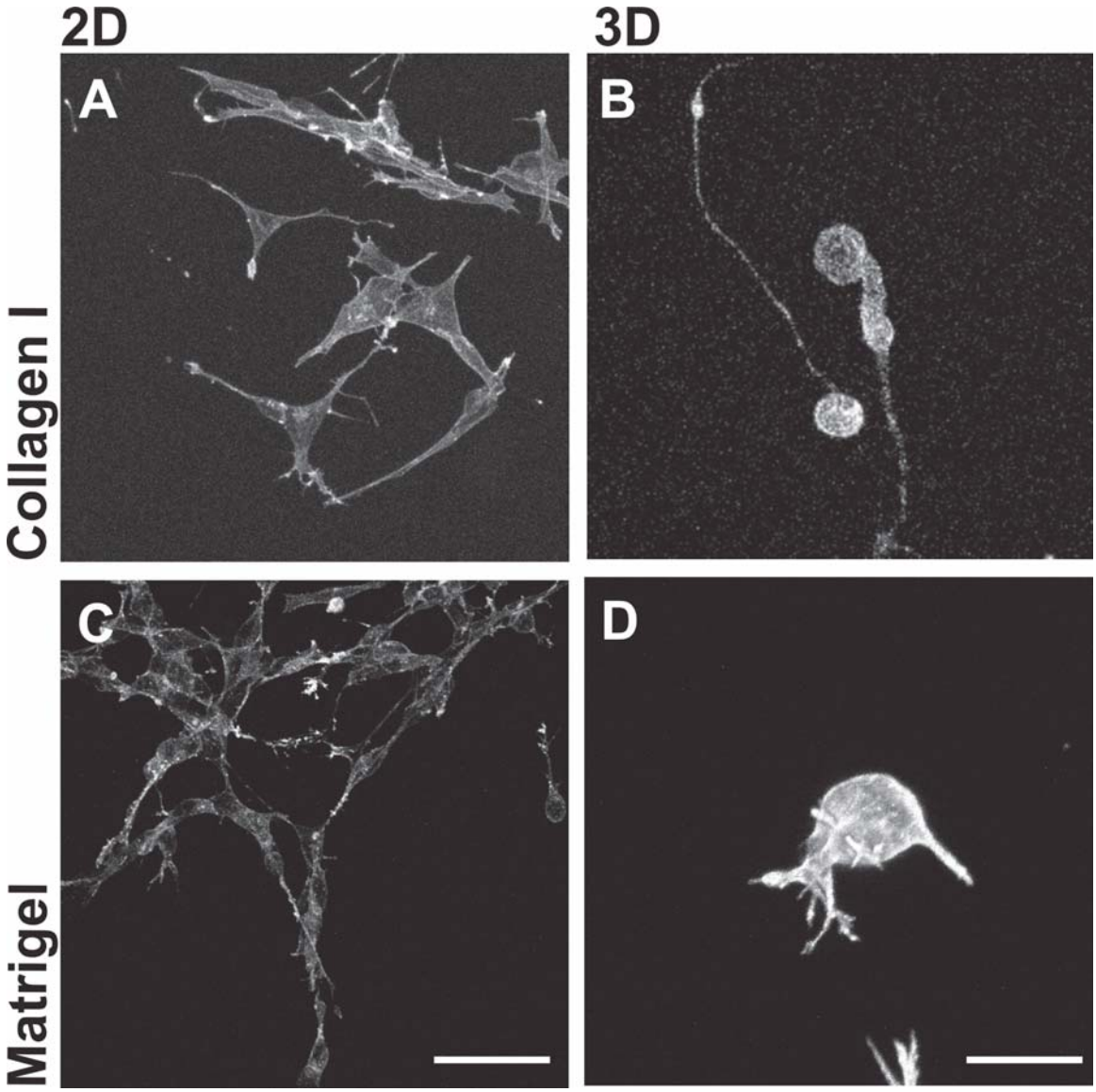

Figure 5.3: Visualization of actin in SH-SY5Y neuroblastoma cells in 3-dimensional (3D) and 2-dimensional (2D) cultures.

Confocal micrographs of SH-SY5Y cells stained with phalloidin after culture for 24h on 2D collagen I substrates (A), on 2D Matrigel substrates (C), in 3D collagen I matrices (B), and in 3D Matrigel matrices (D). In cells cultured in 2D, filaments were visible, whereas staining was more diffuse in cells in 3D. Scale bars, 50 mm (A,C) and 25 mm (B,D).

cultures (33.7 + 1.3µm versus 28.7 + 1.5µm), but this difference was not significant ($p=0.06$). When neuroblastoma cells were cultured on 2D substrates, Matrigel supported the growth of longer neurites than both collagen I ($p<0.001$) and tissue culture plastic ($p<0.05$). In contrast, when cells were cultured in 3D matrices, collagen I supported longer neurites than Matrigel ($p<0.001$). SH-SY5Y cells in 3D collagen I matrices often extended a single long neurite, while cells in 3D Matrigel matrices typically extended several shorter neurites, including one that could be easily observed to be the longest. Neurite diameters were similar for all samples tested.

5.3.4 Collagen I and Matrigel differ in structure and mechanical properties

In light of the observed differences in the two matrices to support neurite outgrowth, we compared the structures of collagen I and Matrigel by examination under scanning and transmission electron microscopy (Figure 5.4). Scanning electron microscopy analysis of 3D collagen I and Matrigel matrices showed distinct structural differences between the two matrices (Figure 4A, 4C). Collagen I matrices contained an intertwined fibrillar network, while Matrigel surfaces contained a more dense, non-fibrillar structure with clustered ECM molecules and tighter pores. These observations were extended to the internal structure of the matrices upon examination with transmission electron microscopy (TEM; Figure 4B, 4D). Quantitative analysis was performed on the TEM images, since the incorporation of resin during the processing helped to preserve the relative dimensions of the two matrices. Collagen I matrices were more fibrillar in structure with fibrils of approximately 80-300nm in diameter, and were more porous with inter-fiber distances of 3.9 + 0.7µm, as compared to the more dense Matrigel matrices, with inter-fiber distances of 0.4 + 0.2µm.

Collagen I and Matrigel matrices also displayed different mechanical properties (Figure 5.5). Dynamic mechanical analysis demonstrated that the storage modulus of the collagen I matrices was larger than that for Matrigel matrices of the same volume and geometry (14.26 ± 0.34 versus 2.43 ± 0.44, $p<0.001$), indicating that the collagen I matrices were stiffer than

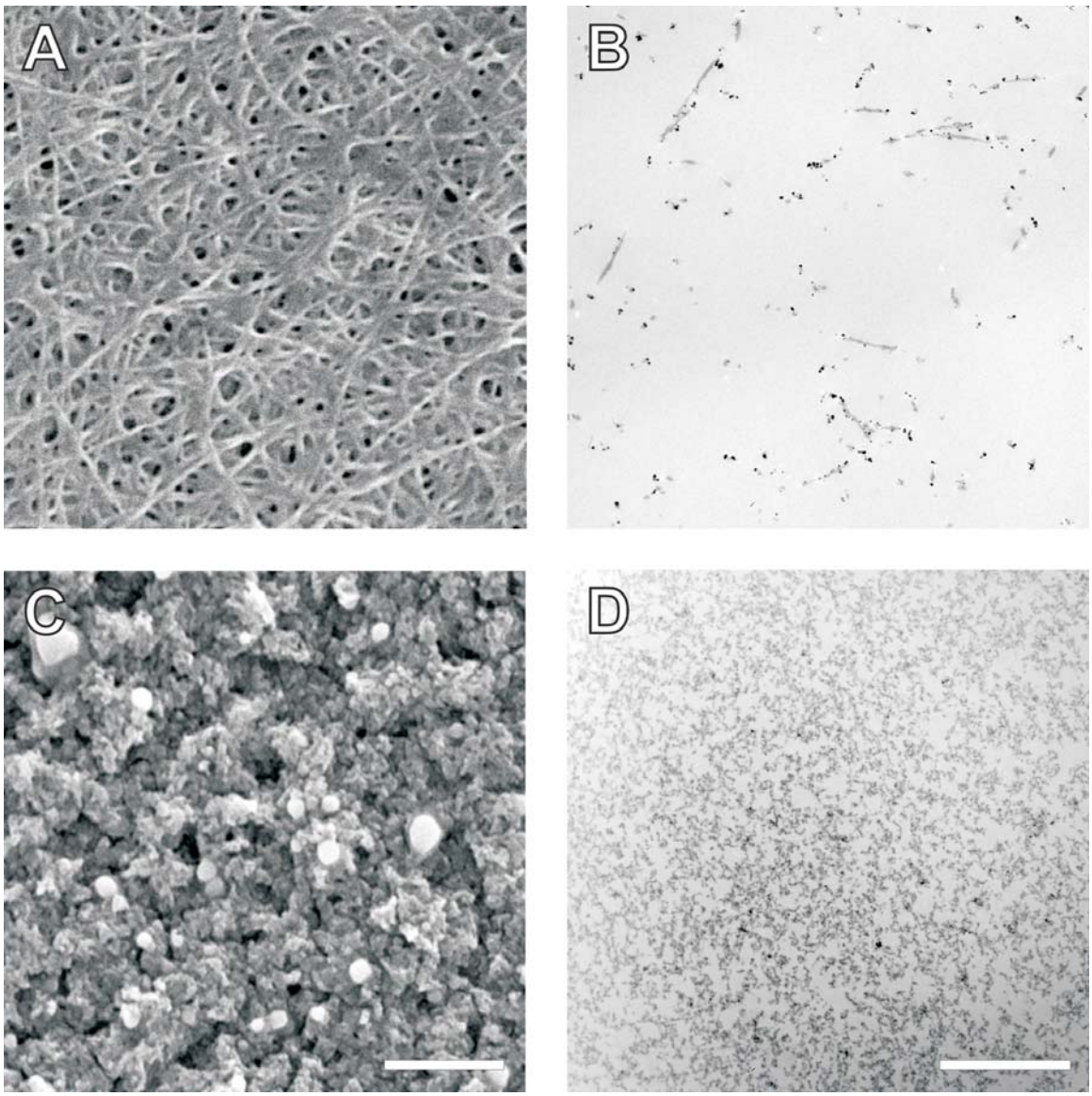

Figure 5.4: Distinct structural properties of collagen I and Matrigel matrices. Scanning electron micrographs of collagen I (A) and Matrigel (C) matrices and transmission electron micrographs of collagen I (B) and Matrigel (D) matrices. Note the more fibrillar and porous structure of collagen I and the denser structure of Matrigel. Scale bars, 5μm.

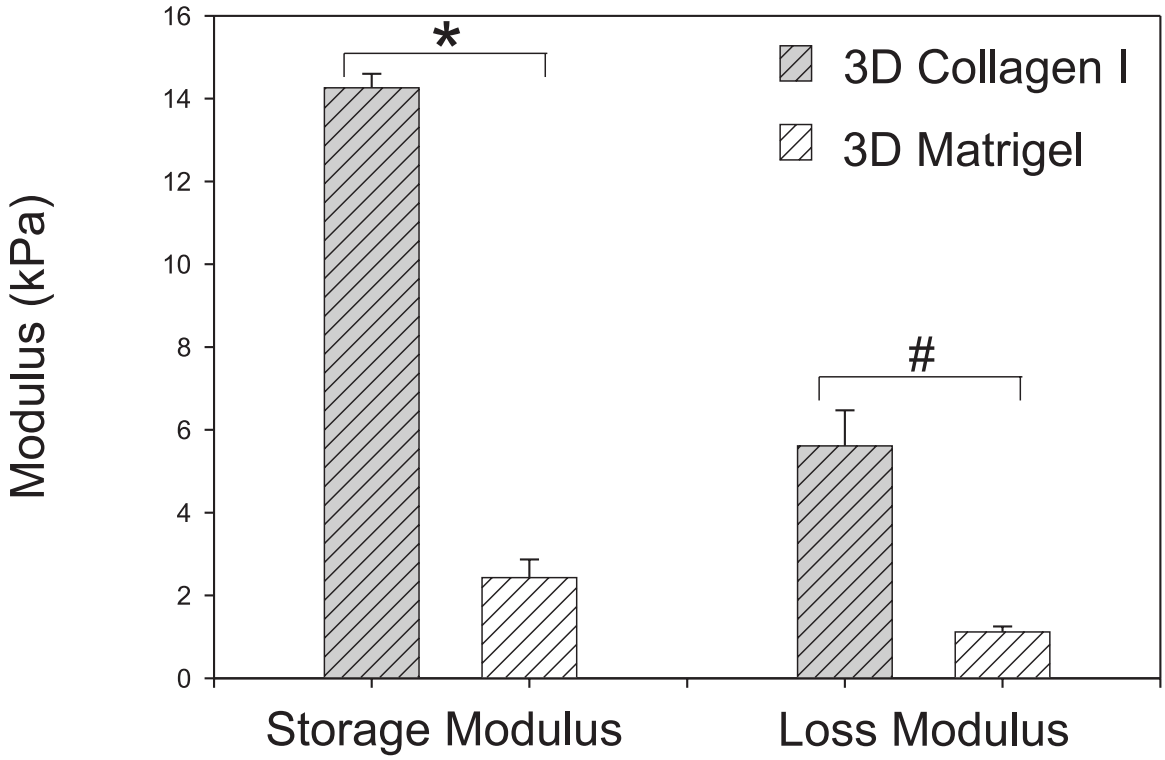

Figure 5.5: Distinct mechanical properties of collagen I and Matrigel matrices. Storage and loss modulus for collagen I and Matrigel matrices as measured using dynamic mechanical analysis. *p $<$ 0.001; #p $<$ 0.01. Data are mean $\pm$ standard error of the mean, n = 3 for each condition.

the Matrigel matrices. The loss modulus for collagen I matrices was also larger than that for Matrigel matrices (5.61 $\pm$ 0.86 versus 1.12 $\pm$ 0.13, p$<$0.01), suggesting that collagen I matrices have a larger damping capacity than Matrigel matrices. By dividing the loss modulus by the storage modulus we obtain the tangent of the loss angle (tan delta), which is a measure of viscosity, where a smaller tan delta corresponds to a more viscous material. Collagen I has a slightly higher tan delta value (0.39) than Matrigel (0.35), reflecting a slightly lower viscosity of the collagen I matrices. Thus, in 3D cultures, SH-SY5Y neuroblastoma cells extended longer neurites in an environment composed of a stiffer material with a slightly lower viscosity and a higher damping capacity.

5.4 Discussion

The main objective of this study was to analyze the growth response of human neuroblastoma cells in a 3D as compared to a 2D environment. Toward this end, we compared the gene expression of SH-SY5Y cells grown in 3D collagen I matrices to that of SH-SY5Y cells grown on 2D collagen I substrates. Microarray analysis identified over 1700 genes that were differentially regulated. The study was focused in light of observed differences in neuronal morphology and neurite outgrowth; seven genes with roles in cytoskeleton, ECM, and neurite growth were selected for further analysis, and their differential expression in 3D versus 2D culture conditions in two distinct matrices was confirmed by RT-PCR. We hypothesized that the differences in gene expression were related to differences in the geometry of the culture and were independent of the type of ECM material used. RT-PCR experiments tested this hypothesis and confirmed that genes for filamin A, actinin 1 alpha 1, capping protein alpha 2, fibronectin 1 and midkine were differentially regulated in response to culture geometry, and expression patterns were similar between collagen I and Matrigel. Neuroblastoma cell soma morphology also varied with culture geometry; in both collagen I and Matrigel, cells were more round in 3D and more spread in 2D cultures.

More complex results were seen for patterns of neurite outgrowth, which varied between the two types of materials. Growth of neuroblastoma cells in collagen I cultures resulted in a 3D/2D neurite length ratio of 1.8, while growth in Matrigel cultures resulted in a 3D/2D neurite length ratio of 0.85. We hypothesized that neurite growth could be correlated with material properties. To gain insight into the cell-material interactions that underly the observed material-specific variations in neurite growth, we compared the structural and mechanical properties of collagen I and Matrigel. Collagen I matrices, which were more supportive of neurite outgrowth than Matrigel matrices, were found also to be more fibrillar, more stiff, and more porous. These results suggest that neuronal cells preferentially extend their neurites in microenvironments that provide the requisite structure, space, and traction.

In the experimental design of this study SH-SY5Y neuroblastoma cells were utilized since they have been used in previous studies of neurite outgrowth (Ferrari-Toninelli et al., 2004;

Sheehan et al., 2006; Shiraishi et al., 2006; Soumyanath et al., 2005), neuronal function (Arun et al., 2006; Gutala et al., 2006; Navone et al., 2001), and gene expression (Dunckley and Lukas, 2006; Gutala et al., 2006; Lee et al., 2006). They also contain a single cell type as compared to primary neuronal cultures that typically contain multiple cell types, making the cell line well suited for gene profiling experiments. Collagen was selected as a biomaterial because it is a biological hydrogel, and its highly hydrated and porous structure is supportive for cellular adhesion and neurite outgrowth (Lin et al., 2005; O'Connor et al., 2001). Cells were seeded with similar cell numbers per condition, which required the use of unequal cell densities between conditions. A pilot study testing changes in gene expression of fibronectin in 2D versus 3D collagen under three different cell density conditions showed similar down-regulation of the gene and similar fold changes between the three conditions, suggesting that the different plating densities did not significantly influence the results of this study. Gene expression was evaluated after 24 hours in culture, since at this time, neuroblastoma cells have attached to their substrates and extended neurites; this timepoint is often used for assessment of neurite outgrowth (Balgude et al., 2001) and gene expression (Jaworski and Klapperich, 2006; Lafrenie et al., 1998; Li et al., 2003). The use of triplicate samples and the combination of the fold-change (> 1.5) and p-value (< 0.05) criteria facilitated a rigorous analysis of the changes observed in the microarray experiments, as described in previous studies (Costigan et al., 2002; Li and Wong, 2001), and real-time RT-PCR with analysis developed by Pfaffl(Pfaffl, 2001; Pfaffl et al., 2002) verified changes in selected genes.

A 3D culture environment surrounds cells with matrix material, providing structural support and matrix-derived molecular and chemical cues, and exerting physical forces from all directions. This environment contrasts with a conventional 2D culture substrate on which cells form adhesions and receive support only on their ventral surfaces. Matrix geometry can influence cell migration (Even-Ram and Yamada, 2005; Friedl and Brocker, 2000; Friedl et al., 1998; Lutolf and Hubbell, 2005; Vicente-Manzanares et al., 2005), signaling events and other cellular functions (Bottaro et al., 2002; Cukierman et al., 2002; Geiger, 2001; Rong et al., 2002; Stevens and George, 2005). In this study, SH-SY5Y neuroblastoma cells displayed a more spread morphology with more prominent actin filaments when cultured

on 2D substrates, while they were more globular with more diffuse actin when cultured in 3D matrices. Similar 3D/2D differences in actin staining and morphology have been observed for smooth muscle cells in collagen cultures (Li et al., 2003). Correlated with the SH-SY5Y cells' globular morphology in 3D was the downregulation of the actin crosslinking proteins filamin A and actinin 1-α1 and the focal adhesion protein talin, which function as connector proteins between the cytoskeleton and integrins, and thus are important in mediating cell-matrix adhesions during cell spreading(Alberts et al., 2002a, b; Even-Ram and Yamada, 2005; Feng and Walsh, 2004; Small et al., 2002; van der Flier and Sonnenberg, 2001; Vicente-Manzanares et al., 2005). Interestingly, kidney cells down-regulated talin protein when cultured on 3D versus 2D Matrigel and collagen (Wang et al., 2003). Also correlated with the reduced prominence of actin filaments was the upregulation in 3D cultures of the gene for actin capping protein, that binds the growing plus ends of actin filaments and regulates their growth. Taking these results together, we hypothesize that the differences in cellular surface area could be mediated by restrictions from the surrounding matrix in 3D.

These results have shown that both the dimension and type of material influence neurite outgrowth. Both neuroblastoma cells (this study) and dorsal root ganglion neurons (preliminary studies from our laboratory) extended longer neurites in 3D versus 2D collagen. In other studies comparing growth in 3D and 2D cultures, shorter neurites have been found in 3D versus 2D fibrin cultures (Pittier et al., 2005), and the growth cones of neurons grown in 3D agarose have been observed to be more globular than growth cones of neurons on 2D agarose (Balgude et al., 2001). These variations in neurite outgrowth among different culture materials suggest important roles for material-associated properties. In the present study, neurite outgrowth and the correlated 3D upregulation of neurofilament gene expression were enhanced by the stiffer, more fibrillar, and more porous collagen I matrix, as compared to Matrigel. Interestingly, neurofilament protein has also been found to be increased by neural cells derived from human embryonic stem cells, when these cells were cultured in 3D polystyrene scaffolds (Hayman et al., 2004). Collagen and fibrin gels have been shown to promote neurite extension and neuron viability, particularly when aligned (Ceballos et al.,

1999; Dubey et al., 1999) and when compared to agarose gels (Lin et al., 2005; O'Connor et al., 2001). Other studies have suggested that stiffness is inversely correlated and pore size is positively correlated to neurite outgrowth (Balgude et al., 2001; Bellamkonda et al., 1995; Dillon et al., 1998; Flanagan et al., 2002; Gunn et al., 2005; Krewson et al., 1994; Yu and Bellamkonda, 2001). Future studies will be needed to elucidate the respective contributions of material properties such as stiffness, porosity and surface energy, as well as chemical composition, to cell-material interactions, and to further our comprehension of how the multifaceted microenvironment influences cell function.

The 3D environment in which cells reside and function *in vivo* and that tissue engineers aim to replicate, provides physical support and matrix-associated cues to cells from all directions. Neuroblastoma cells respond to a 3D environment by regulating their gene expression and changing their morphology and neurite outgrowth. The findings of this study suggest that the regulation of these responses is complex, and depends on the geometry of the matrix as well as on its composition, structure, and mechanical properties. The connection of these material parameters and cellular responses is an important step toward the development of tailored matrices for neural tissue engineering.

5.5 Acknowledgements

The authors thank Pilar Gil for help with initial RT-PCR experiments; Jan Bruder, Johnathon Rollo, Beverly See, and Carl Simkevich for help with experimental analysis; Geoff Williams for help with TEM and SEM; and Edwin Edwards for help with DMA. This work was funded by the NIH COBRE Center for Genetics and Genomics (NIH P20 RR 15578-04).

5.6 References

Alberts B, Johnson A, Lewis J, Raff M, Roberts K, Walter P. Cell Junctions, Cell Adhesion, and the Extracellular Matrix. In Gibbs S, editor. Molecular Biology of the Cell. Garland Science: New York, 2002a: 1065-126.

Alberts B, Johnson A, Lewis J, Raff M, Roberts K, Walter P. The Cytoskeleton. In Gibbs S, editor. Molecular Biology of the Cell. Garland Science: New York, 2002b: 907-82.

Arun P, Madhavarao CN, Moffett JR, Namboodiri MA. Regulation of N-acetylaspartate and N-acetylaspartylglutamate biosynthesis by protein kinase activators. J Neurochem, 2006; 98: 2034-42.

Balgude AP, Yu X, Szymanski A, Bellamkonda RV. Agarose gel stiffness determines rate of DRG neurite extension in 3D cultures. Biomaterials, 2001; 22: 1077-84.

Bellamkonda R, Ranieri JP, Bouche N, Aebischer P. Hydrogel-based three-dimensional matrix for neural cells. J Biomed Mater Res, 1995; 29: 663-71.

Bottaro DP, Liebmann-Vinson A, Heidaran MA. Molecular signaling in bioengineered tissue microenvironments. Ann N Y Acad Sci, 2002; 961: 143-53.

Ceballos D, Navarro X, Dubey N, Wendelschafer-Crabb G, Kennedy WR, Tranquillo RT. Magnetically aligned collagen gel filling a collagen nerve guide improves peripheral nerve regeneration. Exp Neurol, 1999; 158: 290-300.

Costigan M, Befort K, Karchewski L, Griffin RS, D'Urso D, Allchorne A, Sitarski J, Mannion JW, Pratt RE, Woolf CJ. Replicate high-density rat genome oligonucleotide microarrays reveal hundreds of regulated genes in the dorsal root ganglion after peripheral nerve injury. BMC Neurosci, 2002; 3: 16.

Cukierman E, Pankov R, Yamada KM. Cell interactions with three-dimensional matrices. Curr Opin Cell Biol, 2002; 14: 633-9.

Dillon GP, Yu X, Sridharan A, Ranieri JP, Bellamkonda RV. The influence of physical structure and charge on neurite extension in a 3D hydrogel scaffold. J Biomater Sci Polym Ed, 1998; 9: 1049-69.

Dubey N, Letourneau PC, Tranquillo RT. Guided neurite elongation and schwann cell invasion into magnetically aligned collagen in simulated peripheral nerve regeneration. Exp Neurol, 1999; 158: 338-50.

Dunckley T, Lukas RJ. Nicotinic modulation of gene expression in SH-SY5Y neuroblastoma cells. Brain Res, 2006; 1116: 39-49.

Even-Ram S, Yamada KM. Cell migration in 3D matrix. Curr Opin Cell Biol, 2005; 17: 524-32.

Feng Y, Walsh CA. The many faces of filamin: a versatile molecular scaffold for cell motility and signalling. Nat Cell Biol, 2004; 6: 1034-8.

Ferrari-Toninelli G, Paccioretti S, Francisconi S, Uberti D, Memo M. TorsinA negatively controls neurite outgrowth of SH-SY5Y human neuronal cell line. Brain Res, 2004; 1012: 75-81.

Flanagan LA, Ju YE, Marg B, Osterfield M, Janmey PA. Neurite branching on deformable substrates. Neuroreport, 2002; 13: 2411-5.

Friedl P, Brocker EB. The biology of cell locomotion within three-dimensional extracellular matrix. Cell Mol Life Sci, 2000; 57: 41-64.

Friedl P, Zanker KS, Brocker EB. Cell migration strategies in 3-D extracellular matrix: differences in morphology, cell matrix interactions, and integrin function. Microsc Res Tech, 1998; 43: 369-78.

Geiger B. Cell biology. Encounters in space. Science, 2001; 294: 1661-3.

Gunn JW, Turner SD, Mann BK. Adhesive and mechanical properties of hydrogels influence neurite extension. J Biomed Mater Res A, 2005; 72: 91-7.

Gutala R, Wang J, Hwang YY, Haq R, Li MD. Nicotine modulates expression of amyloid precursor protein and amyloid precursor-like protein 2 in mouse brain and in SH-SY5Y neuroblastoma cells. Brain Res, 2006; 1093: 12-9.

Hayman MW, Smith KH, Cameron NR, Przyborski SA. Enhanced neurite outgrowth by human neurons grown on solid three-dimensional scaffolds. Biochem Biophys Res Commun, 2004; 314: 483-8.

Jaworski J, Klapperich CM. Fibroblast remodeling activity at two- and three-dimensional collagen-glycosaminoglycan interfaces. Biomaterials, 2006; 27: 4212-20.

Khan Z, Ferrari G, Kasper M, Tonge DA, Steiner JP, Hamilton GS, Gordon-Weeks PR. The non-immunosuppressive immunophilin ligand GPI-1046 potently stimulates regenerating axon growth from adult mouse dorsal root ganglia cultured in Matrigel. Neuroscience, 2002; 114: 601-9.

Klapperich CM, Bertozzi CR. Global gene expression of cells attached to a tissue engineering scaffold. Biomaterials, 2004; 25: 5631-41.

Krewson CE, Chung SW, Dai W, Saltzman WM. Cell Aggregation and Neurite Growth in Gels of Extracellular Matrix Molecules. Biotechnology and Bioengineering, 1994; 43: 555-62.

Lafrenie RM, Bernier SM, Yamada KM. Adhesion to fibronectin or collagen I gel induces rapid, extensive, biosynthetic alterations in epithelial cells. J Cell Physiol, 1998; 175: 163-73.

Lee JS, Kim IH, Kim SY. Changes in gene expression with increased transglutaminase 2 in a SH-SY5Y cell line. Front Biosci, 2006; 11: 2774-81.

Li C, Wong WH. Model-based analysis of oligonucleotide arrays: expression index computation and outlier detection. Proc Natl Acad Sci U S A, 2001; 98: 31-6.

Li S, Lao J, Chen BP, Li YS, Zhao Y, Chu J, Chen KD, Tsou TC, Peck K, Chien S. Genomic analysis of smooth muscle cells in 3-dimensional collagen matrix. Faseb J, 2003; 17: 97-9.

Lin PW, Wu CC, Chen CH, Ho HO, Chen YC, Sheu MT. Characterization of cortical neuron outgrowth in two- and three-dimensional culture systems. J Biomed Mater Res B Appl Biomater, 2005; 75: 146-57.

Lutolf MP, Hubbell JA. Synthetic biomaterials as instructive extracellular microenvironments for morphogenesis in tissue engineering. Nat Biotechnol, 2005; 23: 47-55.

Ma W, Fitzgerald W, Liu QY, O'Shaughnessy TJ, Maric D, Lin HJ, Alkon DL, Barker JL. CNS stem and progenitor cell differentiation into functional neuronal circuits in three-dimensional collagen gels. Exp Neurol, 2004; 190: 276-88.

Navone F, Consalez GG, Sardella M, Caspani E, Pozzoli O, Frassoni C, Morlacchi E, Sitia R, Sprocati T, Cabibbo A. Expression of KIF3C kinesin during neural development and *in vitro* neuronal differentiation. Journal of Neurochemistry, 2001; 77: 741-53.

O'Connor SM, Stenger DA, Shaffer KM, Ma W. Survival and neurite outgrowth of rat cortical neurons in three-dimensional agarose and collagen gel matrices. Neurosci Lett, 2001; 304: 189-93.

Pfaffl MW. A new mathematical model for relative quantification in real-time RT-PCR. Nucleic Acids Res, 2001; 29: e45.

Pfaffl MW, Horgan GW, Dempfle L. Relative expression software tool (REST) for group-wise comparison and statistical analysis of relative expression results in real-time PCR. Nucleic Acids Res, 2002; 30: e36.

Pittier R, Sauthier F, Hubbell JA, Hall H. Neurite extension and *in vitro* myelination within three-dimensional modified fibrin matrices. J Neurobiol, 2005; 63: 1-14.

Rebhan M, Vacun G, Bayreuther K, Rosner H. Altered ganglioside expression by SH-SY5Y cells upon retinoic acid-induced neuronal differentiation. Neuroreport, 1994; 5: 941-4.

Rong Y, Sugumaran G, Silbert JE, Spector M. Proteoglycans synthesized by canine intervertebral disc cells grown in a type I collagen-glycosaminoglycan matrix. Tissue Eng, 2002; 8: 1037-47.

Sheehan J, Eischeid A, Saunders R, Pouratian N. Potentiation of neurite outgrowth and reduction of apoptosis by immunosuppressive agents: implications for neuronal injury and transplantation. Neurosurg Focus, 2006; 20: E9.

Shiraishi M, Tanabe A, Saito N, Sasaki Y. Unphosphorylated MARCKS is involved in neurite

initiation induced by insulin-like growth factor-I in SH-SY5Y cells. J Cell Physiol, 2006; 209: 1029-38.

Sidell N. Retinoic acid-induced growth inhibition and morphologic differentiation of human neuroblastoma cells *in vitro*. J Natl Cancer Inst, 1982; 68: 589-96.

Small JV, Stradal T, Vignal E, Rottner K. The lamellipodium: where motility begins. Trends Cell Biol, 2002; 12: 112-20.

Soumyanath A, Zhong YP, Gold SA, Yu X, Koop DR, Bourdette D, Gold BG. Centella asiatica accelerates nerve regeneration upon oral administration and contains multiple active fractions increasing neurite elongation in-vitro. J Pharm Pharmacol, 2005; 57: 1221-9.

Stevens MM, George JH. Exploring and engineering the cell surface interface. Science, 2005; 310: 1135-8.

van der Flier A, Sonnenberg A. Function and interactions of integrins. Cell Tissue Res, 2001; 305: 285-98.

Vicente-Manzanares M, Webb DJ, Horwitz AR. Cell migration at a glance. J Cell Sci, 2005; 118: 4917-9.

Wang YK, Wang YH, Wang CZ, Sung JM, Chiu WT, Lin SH, Chang YH, Tang MJ. Rigidity of collagen fibrils controls collagen gel-induced down-regulation of focal adhesion complex proteins mediated by alpha2beta1 integrin. J Biol Chem, 2003; 278: 21886-92.

Wu Y, Sheng W, Chen L, Dong H, Lee V, Lu F, Wong CS, Lu WY, Yang BB. Versican V1 isoform induces neuronal differentiation and promotes neurite outgrowth. Mol Biol Cell, 2004; 15: 2093-104.

Yamashita T, Higuchi H, Tohyama M. The p75 receptor transduces the signal from myelin-associated glycoprotein to Rho. J Cell Biol, 2002; 157: 565-70.

Yip PM, Zhao X, Montgomery AM, Siu CH. The Arg-Gly-Asp motif in the cell adhesion molecule L1 promotes neurite outgrowth via interaction with the alphavbeta3 integrin. Mol Biol Cell, 1998; 9: 277-90.

Yu X, Bellamkonda RV. Dorsal root ganglia neurite extension is inhibited by mechanical and chondroitin sulfate-rich interfaces. J Neurosci Res, 2001; 66: 303-10.

Yuan JS, Reed A, Chen F, Stewart CN, Jr. Statistical analysis of real-time PCR data. BMC Bioinformatics, 2006; 7: 85.

Chapter 6

Conclusions and Future Directions

In this thesis, the main objective was to determine the contributions of different classes of guidance cues individually or in combination to neurite growth, with particular focus on molecular and topographical guidance cues. The interaction between a cell and its microenvironment involves a complex mixture of many cues, and no single guidance cue has been able to elicit directed and functional nerve regeneration. The objective of this thesis was approached using three strategies: (1) to determine the salient and optimal parameters for neurite guidance by anisotropic presentation of the extracellular matrix molecules, laminin (LN) and chondroitin sulfate proteoglycans (CSPG), (2) to determine relationships between physical three-dimensional (3D) cues and global changes in neuronal behavior, and (3) to determine the important intracellular and extracellular events necessary for cellular bridging.

Chapter 1 provided a brief overview of the fundamental science behind the development of nerve repair technologies, with a focus on *in vitro* studies that have both described cellular phenomena and elucidated some mechanisms behind these phenomena. As highlighted in Chapter 1, many *in vitro* biomaterials platforms have been studied that incorporate cues with varying molecular cues and micropatterning, topographical features and dimensions, and microstructural and architectural features, and many of these guidance features have been included in the design of nerve guidance channels for the application of nerve repair. The move to using *in vitro* platforms to further study the mechanisms of nerve growth and

neuronal interactions with their microenvironments after the observation of promising *in vivo* results has given investigators a way to more precisely control the cues presented to growing or regenerating axons to quantify the resulting cellular behavior. The use of microfabrication techniques also marks an improvement in our ability to control the microscale features incorporated in the substrates that are used to conduct these studies. Microfabrication techniques allow very precise spatiotemporal presentation of both molecules and geometries of interest. The experimental work in this thesis has made extensive use of microfabrication techniques such as photolithography, soft lithography, microfluidics and micro contact printing to deposit precise protein patterns and generate templates with microscale topographical features.

An underlying goal of this thesis was to select the most appropriate analysis methods for quantitative evaluation of neurite outgrowth in response to cues presented by *in vitro* biomaterial platforms. Statistical methods to summarize and describe distributions of cellular responses have been critical for the analysis of the response of single cells in a population. Inferential statistics have been heavily used in the present studies to take observed patterns of neuronal responses and build statistical models that take into account randomness and uncertainties to draw inferences about the process of neurite guidance by molecular and topographical cues.

One particular application of circular statistics for the analysis of directional data, in this case, neurite outgrowth angles, has been described in Chapter 2. Because neurite angles are directional in nature, where the most suitable presentation of the data is on a circular scale between 0° and 360°, which wraps upon itself, linear statistical methods that treat the scale as a unidirectional line forever increasing are not appropriate for analysis of this type of data. Instead, circular statistical methods have been developed where directional data is broken down into their vector components and operations for statistical analyses are performed in the polar coordinate system to account for geometry of the scale. These methods that include one-sample uniformity tests such as Rayleigh's, Rao's and Kuiper's tests, and multisample comparison tests such as Watson's U^2 and Mardia-Watson-Wheeler test have been described and applied to experimental neurite outgrowth data on different

substrate types (uniform, striped and gradient) and simulated directional data with known parameters (mean direction and dispersion).

Future directions for applying directional analysis methods to neurite outgrowth studies are to apply spherical statistical methods and models developed for datasets in geology and crystallography to directional neurite outgrowth in 3D cultures. In the case of neurite growth in 3D cultures, the polar coordinate system would not be sufficient to describe positional and directional information. The application of spherical statistical models would allow for better descriptive, correlation and regression methods for analysis of the spatial response of neurite growth to the spatial organization of the 3D environment.

The first objective of this thesis was to understand which parameters of molecular gradients would be optimal to promote and guide neurite growth. Anisotropy in molecular concentration had been shown to be able to better guide neurite growth in previous studies, with the hypothesis that anisotropic presentation of cues is able to exploit a geometry-dependent differential response in the growth cone that would establish polarity or induce a directional change in trajectory of growth.

Chapter 3 demonstrated that absolute and relative concentration changes across the growth cone affect neurite directional growth, and slopes of protein gradients have differential effects on dorsal root ganglia (DRG) cellular adhesion and neurite growth depending on the presence of other proteins and protein gradients. Both absolute and relative concentration changes were found to have an effect on the direction of neurite outgrowth on single cue gradients. Differential adhesion across the gradient channel was seen for single cue gradients and double cue contrasting gradients. This response was mainly due to concentration differences over the channel area. Neurite length was not significantly changed on the substrates tested, which suggested that these molecules do not play a large role in neurite extension. The main finding of this chapter was that directional neurite growth was achieved with single cue and double cue opposing LN and CSPG concentration gradients. Uniformly coated LN and double cue parallel gradients did not elicit directional growth.

Chapter 4 demonstrated that gradient slope and direction of LN and CSPG had differential

effects on cellular adhesion and neurite growth. Cellular addhesion and parallel gradients responded non linearly to slope of LN and CSPG, as expressed by μg/mL/μm. Opposing gradients were shown to influence cellular adhesion, and parallel gradients were shown to influence neurite length. Further analylsis with the ANOVA model showed that LN and CSPG did not act independently on opposing gradients. Optimization of inlet concentrations to maximize cellular adhesion and neurite length showed that increasing LN concentration and decreasing CSPG concentrations were optimal for neurite outgrowth. Appendix B also demonstrated the effects of Rho GTPases on neurite outgrowth on parallel gradients, which starts to address the question of the mechanism of cellular response and neurite outgrowth to these multimolecular gradients.

Future directions for this project include studying the effects of different molecular gradients and combinations of molecular gradients. Of particular interest would be the optimization of gradient parameters of both substrate bound factors such as the extracellular matrix molecules studied here in combination with concentration gradients of soluble growth factors or chemotropic factors such as nerve growth factor (NGF), brain derived neurotrophic factors or other neurotrophins. These molecules act on neurons through different signal transduction pathways and investigation of the intersection of these pathways may provide more insight into the optimal microenvironments for neurite growth.

Another objective of this thesis was to study the influence of mechanical and physical cues in 3D on neuron gene expression and morphology. Microarray analysis showed that for SH-SY5Y neuroblastoma cells, RNA and protein metabolism were upregulated in 3D cultures, and extracellular matrix gene expression was generally downregulated. Genes regulating the cytoskeleton were differentially regulated with genes important for cell spreading such as actinin α1 dependent on dimensionality. Gene expression for neurofilament and the corresponding neurite lengths in 2D versus 3D culture were material-specific, with upregulation of neurofilament and longer neurites in 3D collagen I cultures, and no change in neurofilament expression and shorter neurites in 3D Matrigel. Characterization of the biomatrices showed that collagen I was stiffer and more fibrillar than Matrigel which may have contributed to these changes.

Future directions for this project include testing the effect of 3D culture in different biomatrices and synthetic matrices with more controllable chemical, mechanical and structural properties. By precisely controlling specific mechanical and structural features in the microenvironment, more specific correlations can be made between structural features with neuronal growth characteristics.

Microgrooves are another geometric feature that can impart directional information to the growing neurite. When presented in combination with directional molecular cues such as stripes, they present a very strong guidance cue for both neurons and glial cells such as Schwann cells (SCs). Appendix C compares adhesion, bridge formation and dynamics of DRG and SC across micropatterned grooves. For the formation of SC bridges, LN coating appears to be necessary for the distal anchoring of process on plateaus. Dynamics of the SC bridging process is also highly variable over a wide timescale, showing a wide range of inherent motility of SCs that can form SC bridges.

Future directions for studying specific parameters of SC bridging include the inclusion of other extracellular matrix molecule coatings that may be able to direct SC adhesion and alignment. Experimental data can also be compared to theoretical models regarding force generation and bridge formation, with input variables of cell motility, geometry, process extension and retraction and density of cells.

The results from this thesis will allow for greater understanding of cellular and molecular mechanisms involved in axon guidance and neuron growth, particularly after injury. These results contribute to elucidation of mechanisms that underlie axon growth and guidance that can be applied to translational research. The cues under investigation in this thesis can be incorporated into a nerve guidance channel construct to enhance regeneration of peripheral nerves across a large gap, as well as in more complex glial scar models to evaluate growth potential in the central nervous system. This thesis investigates the growth promoting potential of several different classes of guidance cues individually and in combination, as it is widely accepted that no single approach will prove sufficient for successful regeneration — a methodology combining the most effective individual therapies is required (Harel and

Strittmatter, 2006; Schwab, 2002).

In specific aim 1, neurite growth responses to specific parameters of molecular concentration, slope and direction were quantified *in vitro*. From a basic science perspective, understanding the specific contributions of two important molecules present in the glial scar in combination may inform applications in nerve tissue engineering that aim to direct neurites in a particular direction. From an application perspective, using these optimized parameters in more complex glial scar models would allow more direct evaluation of the regenerative potential of externally applying concentration gradients in a post-injury environment. Translational research that uses anisotropic presentations of molecules in the context of peripheral nerve repair are discussed in Bellamkonda (Bellamkonda, 2006), where distribution of permissive factors such as substrates (hydrogels/fibers), extracellular matrix (ECM) proteins or peptides (LN), trophic factors (NGF), and glial cells were identified as essential components of grafts. The specific parameters identified in specific aim 1 would suggest optimal ranges and presentations of these essential components.

In specific aim 2, global changes in gene expression and morphology in response to dimension were quantitatively assessed. From a basic science perspective, we have identified several hundreds of genes that were up or down regulated simply by the change in the dimension of culture conditions. These genes can be further investigated to address the question of how 2D *in vitro* studies may relate to 3D *in vivo* studies. *In vitro* studies in 2D offer the advantage of simplicity in experimental design, operation and analysis, but parallels cannot be drawn directly. By identifying and understanding the specific differences between 2D and 3D on a global scale, better platforms using tissue engineered approaches in 2D and 3D can be developed for the study of axon growth and guidance. From an application perspective, all *in vivo* experiments are by necessity in 3D, but understanding the specific effects of 2D versus 3D on neurons may allow for the design of substrates that exploit the permissiveness of both types of geometry by distributing 2D-like substrates/surfaces in 3D space, as suggested by Bellamkonda (Bellamkonda, 2006).

In specific aim 3, molecular and topographical cues were able to affect cellular bridging.

From an axon guidance perspective, cellular bridging appears to be a side effect of contact guidance, where a subset of cells does not extend in the direction of the longitudinal axis of grooves, but rather perpendicular it. From a basic science perspective, characterization of the cellular bridges and their associated cell functions such as process extension, cellular motility and force generation allows us to understand how this process occurs. From an application perspective, spinal cord lesions have shown cysts and scars (Schwab, 2002) and bridging may be useful to span areas of cysts, as there is no underlying support available for cellular growth in those injured areas.

The studies described in this thesis have quantified cellular responses to specific extracellular guidance cues. This information can be used both to add to the body of knowledge of how axons grow and make growth decisions, both in development and after and injury, and also applied to translational research as more precise methods of presenting guidance cues become available. More generally, future directions for studying the specific effects of protein gradients on neurite outgrowth include the investigation of focal adhesions to specific ligands on the single cell level. Quantitative information on the spatial and temporal interactions of specific receptors on the cell surface with the molecules presented, and intracellular organization would elucidate the mechanisms by which gradient sensing occurred. The investigation of ligand-target patterns such as integrin clustering and activity and organization of cytoskeletal elements such as actin or microtubules and the activity of key signaling molecules such as Rho kinase would provide more detailed information on how neurons respond to these molecular cues. By understanding the specific roles of these intracellular signaling elements, we can begin to build a model of how a cell responds to a complex environment such as the *in vivo* environment. Currently the studies in this thesis contribute to the body of basic science knowledge regarding axon growth and guidance. Future studies with a goal towards informing translational research using similar presentations of guidance cues in more complex injury models can provide quantitive information to the problem of nerve regeneration.

References

Bellamkonda RV. Peripheral nerve regeneration: an opinion on channels, scaffolds and anisotropy. Biomaterials, 2006; 27: 3515-8.

Harel N, Strittmatter S. Can regenerating axons recapitulate developmental guidance during recovery from spinal cord injury? Nat Rev Neurosci. 2006; 7(8): 603–616.

Schwab M., Repairing the Injured Spinal Cord. Science. 2002: 295(5557): 1029 - 1031

Appendix A

Tissue Engineered Platforms of Axon Guidance

The following appendix has been published as shown in Tissue Engineering, Part B.

TISSUE ENGINEERING: Part B
Volume 14, Number 1, 2008

DOI: 10.1089/teb.2007.0181

Tissue-Engineered Platforms of Axon Guidance

GRACE N. LI, M.Eng., and DIANE HOFFMAN-KIM, Ph.D.

ABSTRACT

Tissue engineering provides a valuable tool for *in vitro* investigation of complex *in vivo* environments. A particular application of tissue-engineered *in vitro* platforms in neuroscience and regenerative medicine is the fabrication of controlled microenvironments for the study of axon guidance, with the goal of informing strategies to overcome nerve injury. The innovative design of tissue-engineered scaffolds that incorporate multiple guidance cues and cell types into various environments is advancing the understanding of how neurons integrate guidance information to make growth decisions. This review focuses on recent strategies that present neurons with multiple cues with micro- and nanoscale resolution in order to study the interactions between neurons and their local environment during axon guidance.

INTRODUCTION

AXON GUIDANCE HAS BEEN a topic of study in neuroscience for many decades in developmental neurobiology and in nerve regeneration, and many cues have been identified that influence axon pathfinding. A number of these guidance cues are soluble factors such as ephrins, netrins, and semaphorins.[1–5] Other categories of guidance cues include bound factors that guide through neuron–matrix interactions,[6–9] topographical cues that influence nerve growth through contact guidance,[10–15] and electrical cues that affect the rate and direction of nerve growth.[16–18] Experimental research using traditional biological techniques has provided valuable information regarding the neuronal response to individual guidance cues. However, the local environment that growing nerves face is inherently complex and contains a rich mixture of cues whose collective influence on growing nerves is not completely understood. Biomedical engineers and neuroscientists have employed tissue engineering techniques to model the complex *in vivo* environment of the nervous system as a means of isolating and studying the specific interactions between these cues and the neurons on which they act.

Historically, tissue engineering strategies have been used in efforts to develop therapies for peripheral nerve and spinal cord injury, combining biomaterials, cell therapy, and drug delivery approaches.[19–23] Strategies for nervous system repair include preventing cell death by delivering anti-inflammatory agents and neuroprotective agents and promoting axonal growth to appropriate targets. The intrinsic growth capacity of cells and the extracellular environment contribute to the capability of axon regeneration. Manipulating the cells' local microenvironment has been a particular focus of much research, from nerve grafts to engineered constructs. Regenerative repair in the peripheral nervous system (PNS) is thought to be possible because of the presence of growth-promoting cues provided by supportive glia (i.e., Schwann cells; SCs), macrophages, and monocytes. More serious injuries to the PNS require surgical intervention, most commonly autologous nerve grafts (reviewed in[24,25]). The central nervous system (CNS) has much poorer regenerative capacity because of the inhibitory post-injury environment composed of degenerating myelin and the glial scar, formed by hypertrophic reactive astrocytes. Similar transplantation strategies for CNS injuries using embryonic spinal cord[26] or peripheral nerve tissue have met with limited success (reviewed in [27]). The conventional paradigm of tissue engineering, in which cells and scaffold materials are combined to replace or regenerate diseased or injured tissue, initially seemed particularly applicable to the problems of nerve injury. However, it has been found that successful nerve regeneration with complex, precise connections requires more than the substitution of engineered tissue for

Department of Molecular Pharmacology, Physiology, and Biotechnology, Brown University, Providence, Rhode Island.

injured tissue. A consensus has emerged that it will ultimately require the coordinated presentation of multiple permissive signals to be incorporated into tissue-engineered biomaterial platforms designed to promote regrowth.

Hence, understanding the mechanisms underlying axon guidance by multiple cues is a critical aspect of nerve regeneration and one that can best be addressed using tissue engineering approaches. Evans[28] has reviewed the strategies for traditional tissue-engineered constructs for nerve repair according to component: scaffolds, support cells, growth factors, and extracellular matrix (ECM). Scaffolds are biomaterials-based and can be biological or synthetic.[29] Support cells include glial cells of the CNS and PNS, neural progenitor cells (NPCs), and cells genetically modified to secrete growth-promoting molecules.[30–32] Growth factors can improve neuronal viability and increase neurite initiation and outgrowth. ECM can increase cellular adhesion, migration, and neurite initiation and extension. Incorporation of these permissive molecules is one way of promoting axogenesis and neurite growth.

In 1993, Langer and Vacanti described tissue engineering as "an interdisciplinary field that applies the principles of engineering and life sciences toward the development of biological substitutes that restore, maintain, or improve tissue function or a whole organ."[33] More recently, MacArthur and Oreffo defined tissue engineering as "understanding the principles of tissue growth, and applying this to produce functional replacement tissue for clinical use."[34] Here we employ both these descriptions in combination to provide the context for this review.

Tissue engineering approaches can be used to create more *in vivo*–like platforms for studies of axon guidance, because they allow the generation of precisely controlled microenvironments that mimic specific features of the local *in vivo* environment. These platforms can incorporate 3 dimensions, cocultures of different cell types, and defined presentation of molecules to enable the study of key neuronal functions. One particular advantage of tissue-engineered platforms of neural microenvironments is that they can present several types of cues in a synergistic or a competitive manner to elucidate their relative importance (Fig. 1). This article will review studies from the past 5 years that employ tissue-engineering approaches to advance the understanding of the effects of the local microenvironment on axon guidance. (See Table 1 for overview.)

PRESENTATION OF MOLECULAR CUES AS GRADIENTS AND MICROPATTERNS

Axon guidance by concentration gradients of soluble guidance cues has been studied extensively *in vitro.* Trophic factors such as nerve growth factor (NGF), brain-derived neurotrophic factor (BDNF), insulin-like growth factor (IGF-1, IGF-2), and fibroblast growth factor (FGF) have been found to elicit turning of growth cones toward the molecule of interest.[35–37] Gene therapy experiments using lentiviral vectors expressing NT-3[38] have shown that greater growth through and beyond the inhibitory glial scar region is achievable, but longer distance growth was not obtainable with the trophic stimulus alone, because the presence of a continuing growth factor gradient beyond the lesion did not stimulate growth into those areas. The complexity of the local post-injury CNS environment has motivated the development of *in vitro* models of the glial scar, which have largely focused on patterning the chemical cues present, particularly permissive laminins (LNs) and inhibitory chondroitin sulfate proteoglycans (CSPGs[39,40]). More recently, neurite outgrowth assays have also incorporated peptides that correspond to locations of cell-binding sites on permissive extracellular molecules such as LN or fibronectin (FN). These key peptides include arg-gly-asp (RGD),[41] ile-lys-val-ala-val (IKVAV),[42] and tyr-ile-gly-ser-arg (YIGSR),[43,44] which have been shown to mediate cell attachment, spreading, migration, and neurite outgrowth; they have been incorporated into assays evaluating the effect of molecular

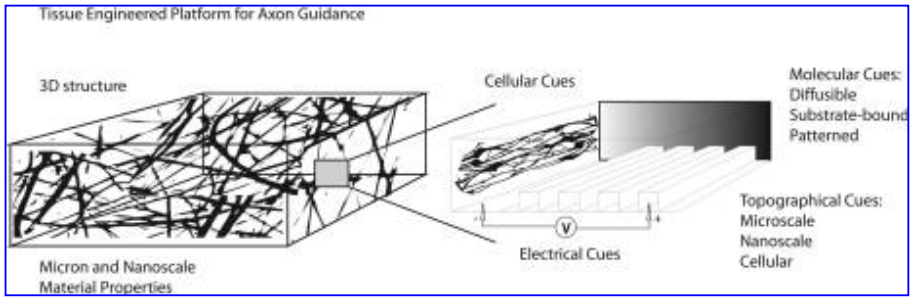

FIG. 1. Types of guidance cues incorporated into *in vitro* tissue-engineered platforms to investigate axon guidance and growth.

Table 1. Overview of Axon Guidance Cues

Cue	*Cellular response*	*Reference*
Molecular gradients		
CSPG	Growth towards [CSPG]	[49]
EphrinA5	Growth towards low [EphrinA5]	[48]
IKVAV	Growth towards high [IKVAV]	[7]
LN	Growth towards high [LN]	[8], [49], [98]
Molecular micropatterns		
Fibronectin	Neurite attachment dependent on stripe width	[54]
LN	Neurite extension on micropatterns only	[52], [59]
Electrical cues		
Endogenous	Migration, differentiation, wound healing, neurite extension	[60], [61]
Direct current	Increase branching, growth rate	[17], [66]
	Synchronize firing, induce polarity	[62], [63]
	Astrocyte alignment	[76]
Pulsed electromagnetic field	Enhanced differentiation of PC12, inhibited neurite extension	[67], [68]
Combined electrical and molecular cues		
Electrical stimulation with NGF	Longer neurite growth on substrates with pPy and NGF than pPy alone	[56]
Structural and mechanical cues		
Agarose	Synergy between NT-3 and NGF	[94]
	GRGDS channels preferred	[58]
Collagen	Longer neurites in 3D	[86]
	Increased neurite length and interfiber diameter on soft substrates	[85], [93]
Matrigel	Longer neurites in 2D	[86]
	Induced axogenesis	[92]
Polyacrylamide	Longer neurites formed on stiffer substrates	[103]
Topographical cues		
Microchannels	Neurites directed along grooves	[10]
Microchannels with NGF	Longest neurites observed with combined NGF and topography	[106]
	Neuritogenesis with sub-optimal [NGF] reduced on nanogrooves	[107]
Microchannels with pLL	Neurites extended only where pLL was present	[109]
Microgrooves coated with LN	Neurite alignment and "bridging"	[13]
SC topography	Neurite growth along SC topography pattern	[126]
Cellular cues		
Aligned astrocytes	Astrocyte monolayer directed progenitor cell growth	[122]
Aligned OEC/ONF	Neurites oriented and grew in the direction of glial cell culture	[124]
Aligned SC	DRG neurites aligned to SC monolayer	[31]
Nerve guidance channels		
Alginate gels	More myelinated axons and SC migration *in vivo*	[143]
Collagen	Gel contraction, uniaxial alignment of collagen fibrils *in vitro*	[84]
	Increase in myelinated axons in gels with RGD *in vivo*	[84], [140], [143]
Ethylene vinyl acetate with NGF or GDNF	Nerve cables, myelinated axons, motoneurons, and DRG neurons supported *in vivo*	[135]
Fibrin gels with NT-3	Cellular infiltration after 9 days *in vivo*	[38, 143]
PLA, PLGA	Stimulate DRG neurite outgrowth *in vitro*	[137]
	Cellular infiltration observed after 13 days *in vivo*	[148]

cues on axon guidance, the results of which will be described in a later section.

Bellamkonda[45] has discussed the concept of anisotropy in structural and molecular contexts of scaffold design, where anisotropy may facilitate faster and more robust regeneration by exploiting the sensitivity of the growth cone to elicit directional growth. For molecular cues, anisotropy translates to concentration gradients across the dimensions of a growth cone. Concentration gradients of soluble neurotrophic factors have been widely studied because they can be easily generated through diffusion,[46] and they have been shown to contribute to the process of chemotaxis. Concentration gradients of substrate-bound molecules have also been generated using techniques such as micropatterning,[47] microfluidics, and self-assembly of monolayers to covalently bind peptides.[7,8] von Philipsborn *et al.*[48] showed guidance of retinal ganglia growth cones using discontinuous ephrinA5 gradients generated using microcontact printing. Neurite stop decisions depended on gradient steepness, as well as the concentration of ephrinA5 present locally, where a decreasing slope and lower ephrinA5 concentrations allowed further growth onto the gradient area. Adams *et al.*[7] demonstrated guidance of dorsal root ganglia (DRG) explants using an increasing concentration gradient generated using photo-immobilization of the IKVAV peptide. On these substrates, growth cones were able to turn up a gradient with a 10% to 25% fractional difference in IKVAV concentration over 30 μm (Fig. 2). Li *et al.*[49] have shown changes in neuronal response over a larger range of fractional concentration difference; a 4% fractional difference in LN concentration over 25 μm resulted in fewer DRG neurites oriented toward higher LN concentration, whereas a 100% fractional concentration change over 25 μm resulted in more neurites oriented toward the higher LN concentration. Multimolecular opposing gradients fabricated to present high concentrations of LN intermixed with low concentrations of CSPG were able to direct DRG neurite orientation in a similar manner as single-cue LN gradients, guiding neurite outgrowth in the direction of higher LN and lower CSPG concentrations.

Many studies have used microfabrication techniques to provide patterns of molecular cues to direct neuronal growth and cell adhesion.[47,50,51] Neurons from rat brain stem and cortices preferentially adhered to regions coated with permissive guidance cues such as LN, and neurite outgrowth followed the micropatterned tracks.[52,53] Cellular adhesion and neurite extension onto underlying line- or grid-patterned microcontact-printed substrates have been observed in dissociated neurons[53] and brain slices.[52] Optimal dimensions of nodes for neuronal adhesion for cells were found to be in the range of 14 to 20 μm.[52] DRG neurite attachment was found to be dependent on FN stripe width, with a minimum width of approximately 30 μm required for cell attachment and neurite extension.[54] To direct neurite growth to specific patterns of the substrate, several micropatterning techniques have been used, including "inking" elastomeric stamps and using adsorption to transfer patterns,[55] covalent binding of "inked" elastomeric stamps using 1-ethyl-3-(3-dimethylaminopropyl) carbodiimide/N-hydroxysuccinimide (EDC/NHS) chemistry, photoimmobilization of molecules using polyallylamine conjugation to N-4-(azidobenzoyloxy)succinimide) (PAA-azido chemistry),[56–58] and other methods of protein immobilization using commercially available heterobifunctional crosslinkers.[54] Song *et al.* used photolithography and EDC/NHS chemistry to micropattern poly-L-lysine (pLL) and LN on regions of conductive polypyrrole (pPy). Hippocampal neurons adhered to and extended neurites only on the pattern of pLL or LN, demonstrating a method for fabricating micropatterns of molecular guidance cues in combination with conductive polymers[54] (Fig. 3). Micropatterned cues allow highly controlled directional guidance of neuronal adhesion and axonal growth.

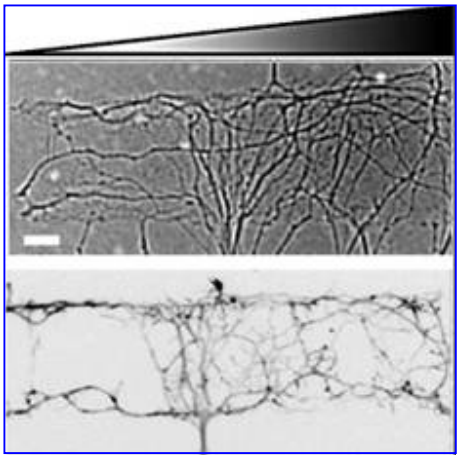

FIG. 2. Growth cones respond to immobilized gradients of ile-lys-val-ala-val (IKVAV) peptides. Greater neurite outgrowth occurs toward the regions of higher concentration of immobilized IKVAV peptide. Wedge indicates direction of concentration gradient. Phase contrast image shown on top; inverted grayscale image of phalloidin labeled f-actin shown in bottom panel. Scale bar = 50 μm. Figure from Adams *et al.*,[7] Journal of Neurobiology, Vol. 62, No. 1, 2005, pp. 134–147. Copyright (2004, Wiley Periodicals). Reprinted with permission of John Wiley & Sons, Inc.

The use of anisotropy in presenting chemical cues through gradients or stripes to provide directional bias has been largely successful *in vitro*. Recent advances in microfabrication techniques in microfluidics and microcontact printing have increased our capacity to present directional information on a biologically relevant scale. Optimal dimensions of features range from tens to hundreds of microns[8,52,59] and can be used in combination with other types of guidance cues for synergy in a more complex microenvironment.

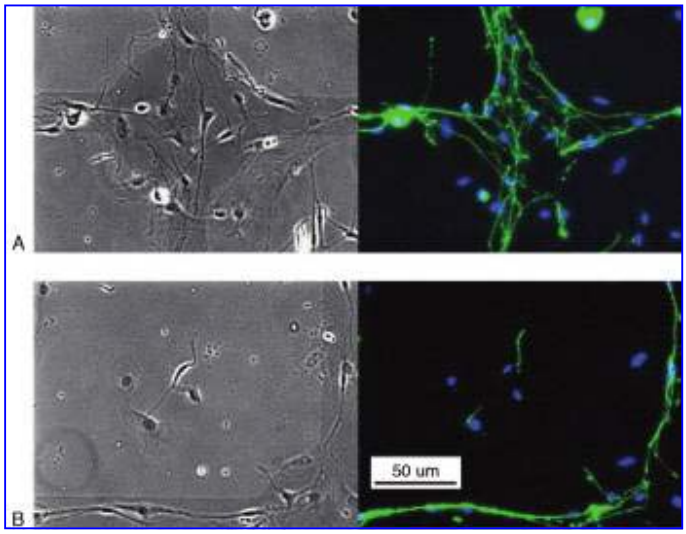

FIG. 3. Dorsal root ganglia neurons follow micropatterns of poly-L-lysine–laminin immobilized on polyglutamic acid–doped polypyrrole network at nodes (**A**) and on channels (**B**). Neurites stained positive for GAP-43 (green fluorescence). Cell nuclei were labeled with 4′,6-diamidino-2-phenylindole (blue fluorescence). Neurons preferentially adhere and neurites preferentially extend on micropatterns. Figure reprinted from Biomaterials, Vol. 27, No. 3, Song *et al.* Micropatterns of positive guidance cues anchored to polypyrrole doped with polyglutamic acid: A new platform for characterizing neurite extension in complex environments, pp. 473–484. Copyright (2005), with permission from Elsevier.[59] Color images available online at www.liebertpub.com/ten.

PRESENTATION OF ELECTRICAL CUES

Endogenous electric fields in the form of voltage gradients have been observed to polarize the nervous system along the rostral–caudal axis during development (5–18 mV/mm)[60] and direct nerve growth and accelerate wound healing in the rat cornea (+40 mV/0.5 mm).[61] Steady direct-current electric fields applied *in vitro* in solution (< 40 mV/mm) have been shown to synchronize neuronal firing patterns in hippocampal slices;[62] induce polarization of pyramidal neurons;[63] and affect neurite orientation, branching, and growth rate of Xenopus neurons *in vitro.*[17] Firing patterns in neuronal networks have been shown to respond to weaker electric fields (140 μV/mm rms, 295 μV/mm peak amplitude) than single neurons (185 μV/mm rms, 394 μV/mm peak amplitude).[62] Hence, electrical stimulation is thought to have a significant effect on neurite differentiation and extension. Parameters for optimization include frequency, orientation, flux density, and wave form (direct current or pulsed electromagnetic field).

Initial studies investigating the effect of electrical stimulation on neurons were performed on Xenopus neurons exposed to a steady direct current field. Extracellular electric fields (0.1–10 V/cm) applied in solution reversibly influenced the direction of neurite growth and increased neurite initiation and length in Xenopus.[17] Primary cell types such as embryonic chick DRGs were also used to assess the effects of electric fields; neurites grew faster, turned, and branched preferentially towards the cathode (25 V/m, 10 min duration).[64] PC12 cells, a culture line derived from a rat adrenal medulla pheochromocytoma, are widely used as a model system for neuronal differentiation and studying the mechanism of action of NGF,[65] particularly in studies of electrical stimulation. PC12 cells and their subline PC6 cells respond to NGF by shifting from a chromaffin cell-like phenotype to a neurite-bearing sympathetic neuron-like phenotype in a highly regular and dose-dependent manner,[66] and much research has been conducted to study the effects of electromagnetic fields on this particular type of NGF-stimulated neurite outgrowth of PC12 cells.

Magnetic fields have enhanced neuronal differentiation in PC12 cells, whereas they have inhibited neurite growth. Morgado-Valle *et al.*[67] have shown that low-frequency magnetic fields (0.7 mT, 2 h/day for 5 days, 60Hz) enhanced differentiation of PC12 cells to a neuronal phenotype, a process sensitive to modulation of L-Ca^{2+} channels by channel agonists and blockers. Blackman *et al.*[68] have shown that a direct action of magnetic fields (100 mT, sinusoidal,

50 Hz) inhibits NGF-stimulated neurite outgrowth of PC12 cells. Pulsed electromagnetic fields have been found to depress DRG neurite growth[69] (15 A, 20 μs pulse duration, 10–25 Hz) and PC6 cells[70] (0.3 mT, 20 ms pulse duration, 2 Hz) when cultured with NGF. The degree of pulsation (10–100% or direct current) had an effect on PC6 neurite initiation and extension, where low pulse duty (10%) results in a lower percentage of neurons with longer neurites, and conversely, direct current does not inhibit neurite initiation, although neurite lengths are decreased.[71] Varying experimental conditions investigating the effects of magnetic fields on neurite outgrowth have made direct comparisons across different studies difficult. Future work to standardize these parameters would allow better comparisons to enable optimization of these factors.

Molecules present in the environment under electrical stimulation can affect the cellular response to an applied electric field.[16,72,73] Novel biomaterial platforms have been developed to study the effects of electrical activity presented on conducting surfaces in combination with molecular cues. An applied constant current or constant voltage can enhance axonal extension *in vitro* from neurons adhered to substrates coated with the conductive polymer pPy.[18,72] Gomez and Schmidt[57] compared the effects of electrical stimulation on PC12 cell neurite growth when cultured on pPy alone and on pPy with NGF. They observed longer neurites on constant electrically stimulated (100 mV, 2 h) pPy–NGF substrates, than on pPy substrates without NGF. Electrical stimulation can also be incorporated into biomaterial platforms as a tool for drug delivery to deliver growth factors to promote nerve growth. Richardson *et al.* incorporated neurotrophin-3 (NT-3) in a film of pPy doped with *p*-toluene sulphonate galvanostatically grown on gold electrodes. NT-3 was released using electrical stimulation (1 mA, 100-μs pulse), and neurite outgrowth from auditory neurons (spiral ganglion neuron explants) was enhanced.[74] The development of these tailored biomaterial platforms allows systematic investigation of the contributions of different types of cues in the neuronal environment.

Electric fields have been found to influence the growth of other cell types. Electrical gradients (>10 mV/mm) direct neural crest cell migration toward the cathode.[75] Of interest for axon guidance is the effect of electrical stimulation on astrocytes.[76] On a cell culture platform that presented electrical current in solution to multiple culture chambers, astrocytes aligned after exposure to 1.63 mA for 24 h. These substrates were then used to direct DRG neurites, which will be discussed in a later section.

PRESENTATION OF CUES IN 3 DIMENSIONS

Comparisons of cellular growth in standard 2-dimensional (2D) monolayer cultures and 3-dimensional (3D) matrix cultures that more closely resemble *in vivo* environments have shown clear phenotypic differences. For example, previous studies have revealed differences in cell surface area, stress fiber distribution, cell migration, focal adhesions, neurite and growth cone dimensions, and protein and gene expression. Tissue engineering approaches have allowed the development of assay formats that include the third dimension as a controllable and defined parameter and are used to elucidate cell–material interactions between neurons and their ECM. Three-dimensional matrices that have been explored include biologically based matrices such as alginate,[77–79] collagen I,[80–86] Matrigel,[79,86] and fibrin,[87,88] as well as synthetic polymer-based scaffolds such as poly lactic acid (PLA),[89,90] poly lactic-co-glycolic acid (PLGA), and agarose.[91] Studies have characterized 3D matrices with regard to their chemical and mechanical properties and their ability to support neuronal growth. Collagen gels have been used successfully to differentiate neural stem cells[81] and NPCs[83] with FGF in the culture medium, and functional synapses have formed in the cultures.[81] Addition of Matrigel to rat sympathetic neurons plated on pLL substrates has been shown to induce rapid axogenesis with corresponding changes in microtubule organization. Another aspect of differential regulation of neuronal cell culture in 3D can be reflected in the global gene expression of neurons. Li *et al.*[86] showed, using microarray analysis, that differentially regulated genes between 2D and 3D culture of SH-SY5Y neuroblastoma cells included those involved in cytoskeletal reorganization, ECM, metabolism, and signaling. Gene expression trends were maintained over cultures in different matrices (collagen and Matrigel), but morphological differences in 2D and 3D cultures such as cell spreading and neurite growth appeared to be material-specific. The stiffer 3D matrix of collagen supported longer neurites than 2D collagen, whereas in the softer Matrigel, neurons in 3D extended shorter neurites than neurons in 2D.

Combining 3D environments with molecular guidance cues for neurite outgrowth to study the effects of cues in a more *in vivo*–like environment is a logical extension of neuronal assay formats in 3D. Neurotrophic factors can be incorporated into 3D cultures by the addition of growth factors to culture medium[92] or in a more controlled manner by covalent linkages between the growth factor and the matrix.[58,93–95] Steepness of NGF gradients was found to attract DRG[46] and PC12[95] neurite growth up the concentration gradient on collagen gels[46] and poly(2-hydroxyethylmethacrylate),[95] respectively. Cao and Shoichet[96] observed a synergistic effect on DRG outgrowth with NGF and NT-3 presented in 3D agarose. When NT-3 was applied individually, there was no directional growth. When the 2 growth factors were applied together, the guidance range of neurites toward higher concentrations of NGF and NT-3 exceeded the guidance range of an NGF gradient alone. Deister and Schmidt[92] adapted a DRG explant assay in a shallow collagen gel to study the combinations of neurotrophic factors in culture. After adding NGF, glial-derived neurotrophic factor (GDNF), and ciliary neurotrophic factor (CNTF) individually and in combination,

total neurite outgrowth and length were evaluated. The combination of 3 factors led to greater neurite outgrowth and length than in cultures containing individual factors at the optimal concentration, implying that interactions between neurotrophic factors can increase neuronal responsiveness in 3D.

Incorporation of ECM molecules in a 3D matrix has also been investigated.[91,93,97] Neuroblastoma cells showed greater cell adhesion on alginate gels that were coated with LN or covalently linked to YIGSR peptide and greater neurite number and length on YIGSR peptide–linked gels in a ligand density-dependent manner.[78] Luo and Shoichet[58] have demonstrated that DRG neurites will grow preferentially in channels modified to present GRGDS peptide in a 3D agarose gel. Dodla and Bellamkonda[91] have shown that concentration gradients of photo-immobilized LN-1 in 3D agarose gels can direct DRG neurite growth in the direction of higher LN-1 concentration. Furthermore, gels presenting concentration gradients of LN-1 promote faster neurite extension than gels presenting isotropic LN-1 concentrations, which implies that patterning of chemical cues may be a separate parameter to be optimized within the complexity of the 3D environment (Fig. 4). Embryonic cortical neurons have been challenged with choices between competing growth options of poly-D-lysine (PDL), 3D Matrigel, and microtopography. When presented with 2D PDL-adsorbed surfaces and an intermediate layer of 3D-gelled Matrigel, neurons appeared to prefer PDL-coated 2D surfaces. When presented with 2D PDL-adsorbed surfaces, 3D Matrigel, and grooved topography (3.5–15 μm), neurites preferred to extend into the 3D gel layer of Matrigel rather than along PDL surfaces (walls and grooves) of the topographical substrates, differing from the result of neurite turning into grooves in the absence of Matrigel. Growth cones therefore make growth decisions that balance permissiveness and obstacles in topography and 3D architecture, resulting in directional growth to minimize turning while remaining on the most permissive substrate available.[98]

The progression of tissue-engineering platforms from 2D to 3D has been widely noted. The capacity to integrate guidance cues of interest in a specific and controlled manner has enabled researchers to add a layer of complexity to *in vitro* systems for axon guidance to more closely mimic the local *in vivo* environment while maintaining the ability for quantitative analysis.

PRESENTATION OF MATERIAL AND PHYSICAL CUES

Physical and mechanical cues such as stiffness have been known to affect a multitude of cell functions such as adhesion, proliferation, migration, differentiation, and morphology. Durotaxis has been observed in many cell types, including neurons.[99] Neurite extension during development and after an injury requires mechanical interactions between growth cone and substrate. Parameters that have been shown to influence DRG neurite extension include substrate mechanical properties,[100] ligand concentration,[101] and geometry. Mechanical effects appear to be highly dependent on cell type and the range of moduli presented. Leach *et al.*[102] tested the NGF-dependent response of PC-12 cells on polyacrylamide substrates with varying stiffness, and by controlling the amount of FN present, kept the adhesive ligand concentration constant over the samples tested. The range of substrate stiffness tested (7–19 kPa) spanned the physiological range as well as "very soft" and "very stiff" substrates. A threshold response was observed in which the softest substrates supported fewer and shorter neurites but above a threshold of approximately 100 Pa, longer and more branched neurites were observed regardless of increasing shear modulus of the substrate. Willits and Skornia[85] studied the effects of mechanical stiffness on chick DRG neurons. By varying the concentration of collagen used to gel the matrix, varying stiffnesses (2.2–17 Pa) were generated. After 4 days in culture, softer matrices resulted in longer neurite lengths. In this experimental setup, it is interesting to note that an increase in interfiber diameter corresponds to a decrease in mechanical stiffness and collagen concentration, a geometric constraint that may contribute to the observed cellular response. Analysis and modeling suggested complex non-linear cell–material interactions.

Mechanical stiffness has been found to influence other cell types, including astrocytes.[103] On soft gels of polyacrylamide with a shear modulus of 200 Pa, suppression of astrocyte growth has been observed in monoculture and coculture experiments, with low attachment and spreading and disorganized F-actin. This behavior is in contrast to the growth of cortical neurons on the same soft substrates tested; coculture experiments show a significantly higher proportion of cortical neurons than astrocytes on the soft than on the hard (9 kPa shear modulus) substrates.[103] These studies point toward the development of materials tailored to support specific cell populations within the nervous system.

PRESENTATION OF TOPOGRAPHICAL CUES

A number of studies have drawn attention to the fact that interactions with a 3D extracellular microenvironment influence neuronal growth. Topographical cues influence nerve growth and regeneration using contact guidance and can be combined with adhesion molecules that also play a role in contact guidance. Neurons have the capacity to respond to topographical features in their microenvironments, and they have been shown to adhere, migrate, and orient their axons to navigate surface features such as grooves in substrates in the micro- and nanoscales. Using microfabrication techniques such as photolithography and soft lithography, topographic guidance of neurite outgrowth has been explored *in vitro* with culture substrates that contain well-defined micropatterned features. Mahoney *et al.*[10] studied the effects

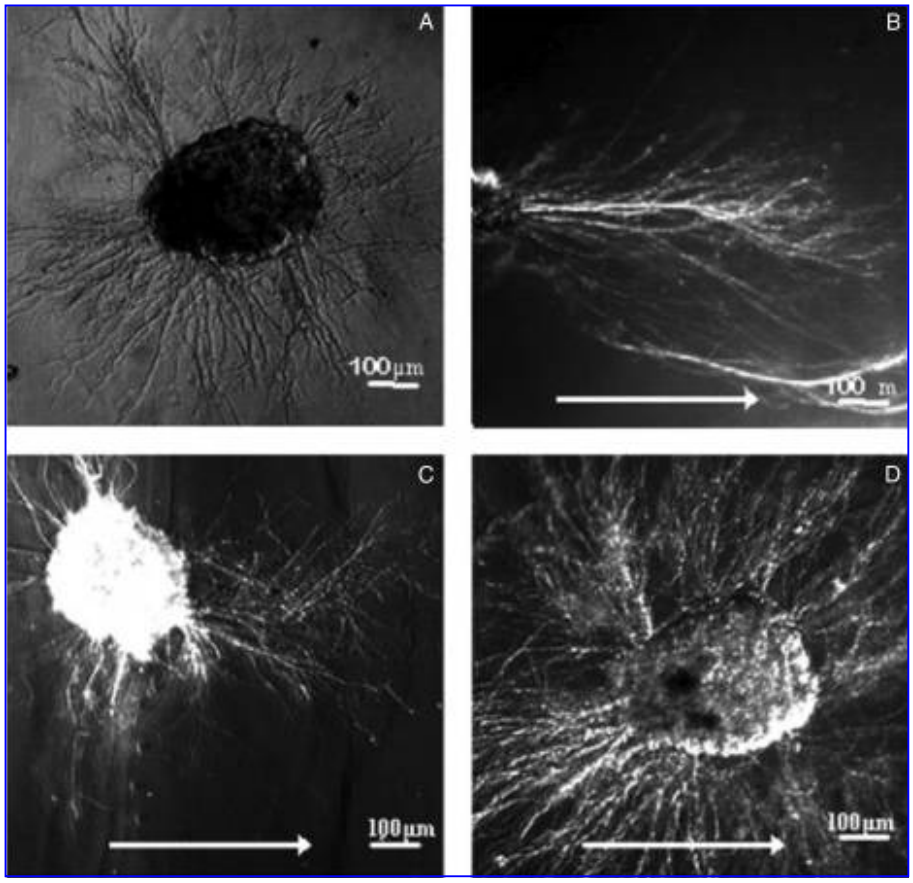

FIG. 4. Combination of 3-dimensional matrix with chemical cues: Anisotropy of laminin (LN) presentation in agarose gels can direct neurite outgrowth to regions of higher LN. Arrow indicates higher LN concentration. (**A**) Neurite outgrowth in unmodified agarose gel. (**B–D**) Neurite outgrowth in gels containing increasing steepness of LN concentration (0.017, 0.051, 0.121 µg/mL per mm respectively). Scale bar = 100 µm. Figure from Dodla and Bellamkonda,[91] Journal of Biomedical Materials Research Part A, Vol. 78A, No. 2, 2006, pp. 213–221, Copyright (2006, Wiley Periodicals, Inc). Reprinted with permission of John Wiley & Sons, Inc.

of microchannels of 20 to 60 µm in width and 11 µm in depth on PC12 cell cultures. Neurites were directed along the axis of the grooves, with microchannels of 20 to 30 µm being most effective at neurite direction. Polypropylene filaments have been found to direct DRG neurites and SCs from DRG explants along the long axis of the filaments tested with an optimal filament diameter of 5 µm. The addition of FN and LN coatings on the filaments led to greater maximal neurite lengths than with uncoated controls and resulted in neurite outgrowth that preceded migrating SCs.[104]

Combinations of defined topographical and molecular cues revealed synergies between cues. Gomez *et al.*[105] studied the combined effects of NGF and microtopography of microchannels on axon initiation, polarization and elongation of hippocampal neurons. When presented with microchannel substrates of 1- to 2-µm widths and 400- to 800-µm depths containing immobilized NGF on the surface, hippocampal neurons responded to the combination of molecular and topographical stimulation with the longest neurites. The observations that topography had a stronger

effect on polarization but no effect on elongation suggested that both cues are required for maximal neurite growth.[57,105] Foley *et al.*[106] observed that topographic feature size modulated neuritogenesis of PC12 cells cultured with suboptimal concentrations of NGF in media, with greater neuritogenesis when cells were cultured on ridges of 70 and 250 nm than on wider ridges (400–1900 nm) and flat surfaces. Synergy between topography and adsorbed ECM molecules of LN also promoted neurite alignment and outgrowth onto microgrooves.[107] DRGs cultured on substrates with groove depths of greater than 3 μm and groove widths of 10 μm in combination with 200 μg/mL of LN showed maximal neurite outgrowth and alignment of up to 95%. Zhang *et al.*[108] developed a hybrid template that combines topographical and molecular cues with channels 5 μm deep and 20 to 40 μm wide connecting to nodes of 50- to 100-μm widths and pLL to achieve geometric control over neurite connections for the application of microelectronic circuits. Hippocampal neurites extended on pLL tracks and avoided regions where no pLL was present. Studies such as these facilitate the investigation of hierarchies and synergies between cues.

Topographical cues have also generated unexpected neurite morphologies. Goldner *et al.*[13] have observed the phenomenon of neurite "bridging," in which a subset of DRG neurites can span grooves coated with LN varying from 30 to 200 μm wide and 50 μm deep with no underlying support (Fig. 5). Several cell types, including hippocampal neurons, rat B104 neuroblastoma cells, and SCs, were all shown to exhibit the bridging morphology. Neurites were observed to climb up the groove walls to generate such bridges, suggesting complex cell dynamics in response to micro-topography.

Nanotopography to promote cell growth has been a subject of interest for many biological applications and for axon guidance in particular. Nanotopography has been

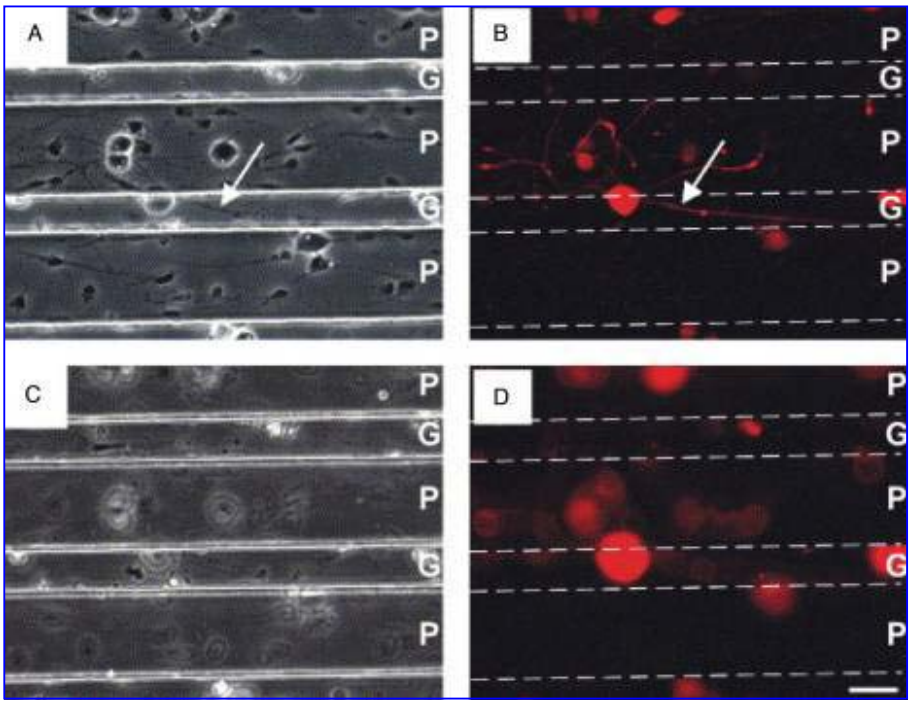

FIG. 5. Dorsal root ganglia neurites show unusual "bridging" morphology (arrows) over microgrooves 50 μm deep. (**A, C**) Phase contrast images at plateau and groove level, respectively. (**B, D**) Immunostained anti-neurofilament fluorescent images at plateau and groove level respectively. Scale bar = 50 μm. Figure reprinted from Biomaterials, Vol. 27, No. 3, Goldner *et al.* Neurite bridging across micropatterned grooves, pp. 460–472. Copyright (2005), with permission from Elsevier.[13] Color images available online at www.liebertpub.com/ten.

presented to cells *in vitro* via nanoscale etches into silicon wafers,[109,110] nanofibers on the surfaces of scaffolds,[111,112] and carbon nanotubes (CNTs) on flat surfaces.[113–116] Methods of fabrication have been reviewed in Norman and Desai,[117] including a list of ordered versus unordered nanotopographies that can be generated using methods such as chemical etching with hydrofluoric acid to generate unordered nanoscale grooves and more controllable electrospinning with well-studied polymeric materials such as PLA and PLGA, which may be aligned or unaligned.

Neuronal adhesion and viability on nanotopography have been most widely studied, and results vary depending on the type of nanoscale substrate presented. Chemical etching of silicon wafers found an optimal surface nano-roughness of 20 to 50 nm to be the most permissive for attachment of primary neurons isolated from the substantia nigra.[109] Electrospun polyamide nanofibers with a median diameter of 180 nm supported neuronal growth, and covalently linked tenascin-C–derived peptides increased the neurite outgrowth of a number of CNS primary neurons, including cerebellar granule, cerebral cortical, hippocampal, motor, and DRG neurons, indicating that nanotopography may act synergistically with molecular cues to promote neurite growth.[111] Nanofibrillar meshes presenting IKVAV peptides have also been fabricated using self assembly of amphiphilic peptides around cells in culture medium. These IKVAV-linked nanofibers differentiated NPCs more rapidly than the addition of soluble IKVAV peptide or LN[118] (Fig. 6). Cellular responses to substrates presenting CNTs have been evaluated; hippocampal cells have been stimulated using CNT microelectrodes,[116] PC12 neurite formation has been supported by 2% CNT containing polycarbonate urethane,[115] and astrocytes have been shown to have poorer adhesion to CNT–polycarbonate urethane substrates and lower alkaline phosphatase production on low-surface-energy nanophase fibers.[119] Using nanoscale fabrication methods, it will be exciting to generate biomaterial platforms that study combinations of nanoscale guidance cues with other important cues such as electrical stimulation and molecular cues.

Neurons have the capacity to respond to topographical features in their microenvironments, and grooves have been a widely studied geometry. The progression of guidance cues from micro- to nanoscale resolution has shown that the guidance range encompasses both length scales and can affect cell functions from cell differentiation of NPCs to neurite morphology such as orientation, direction, and length.

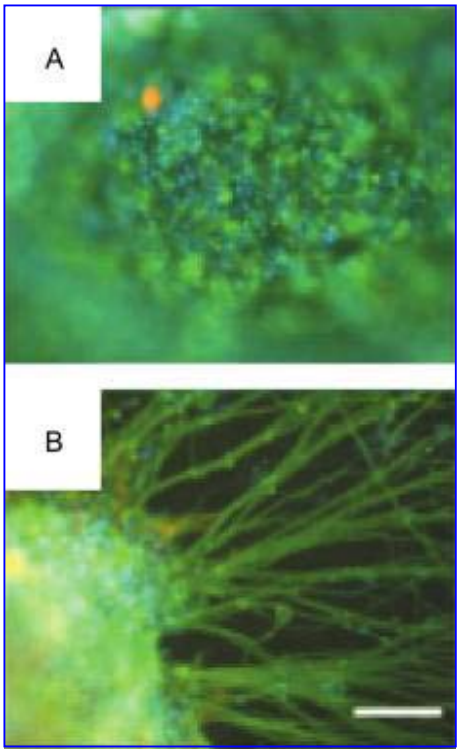

FIG. 6. Nanofibrillar gels presenting ile-lys-val-ala-val (IKVAV peptide are more effective at inducing differentiation of neural progenitor cells. Differentiated neurons were labeled for ß-tubulin (in green), and differentiated astrocytes (glial cells) were labeled for Glial fibrillary acidic protein (in orange). (**A**) No neurite formation from NPCs encapsulated in an IKVAV incorporated polyacrylamide gel. (**B**) Neurite formation from a neural progenitor cell (NPC) neurosphere cultured in a nanofibrillar gel presented with IKVAV on the surface. Scale bar = 100 µm. Figure from Silva *et al.,*[118] reprinted from Science, 27 February 2004: Vol. 303, no. 5662, pp. 1352–1355. Color images available online at www.liebertpub.com/ten.

PRESENTATION OF ALIGNMENT INFORMATION BY CELLS

Cocultures of neurons and glial cells have been investigated using primary cells and cell lines to study the influence of nonneuronal cells on axon guidance. Glial cells have been observed to bridge lesions and promote axon growth after injury in models of nerve damage.[32,120] SCs play an essential role in guiding neurites after injury in a transected nerve model, and the inhibition of SC proliferation and migration reduced axon growth.[32] Coculture studies have been performed to assess the effects of cell types present in the glial scar *in vivo,* and scar-in-a-dish experiments have explored injury environments *in vitro.*[31] Recently, these cocultures have been applied in novel biomaterials systems microfabricated to present cues in a more systematic manner, with cells from a more permissive environment being cocultured in an oriented manner or an unoriented manner where no

underlying directional cue is presented. Thompson and Buettner[121] have shown that, in cocultures of SC and DRG neurons, the underlying glial culture can direct neurite growth (Fig. 7). When DRG neurons were seeded onto SC monolayers oriented by microstamped LN stripes, neurites oriented to the direction of SC alignment.

Cultures of neurons on astrocyte monolayers have shown that astrocytes can direct neurite outgrowth in the direction of astrocyte orientation,[76] induce neurite turning to the underlying direction of astrocytes, and increase neurite length.[122] Recknor *et al.*[123] cocultured astrocytes with NPCs and observed that confluent, directed astrocyte monolayers can direct adult rat hippocampal progenitor cells and may contribute to the differentiation process of these neural progenitor cells. Deumens *et al.*[124] cultured neonatal cerebral cortical neurons with olfactory ensheathing cells (OECs), glial cells thought to be responsible for continuous growth of peripheral axons in the olfactory system, and their associated

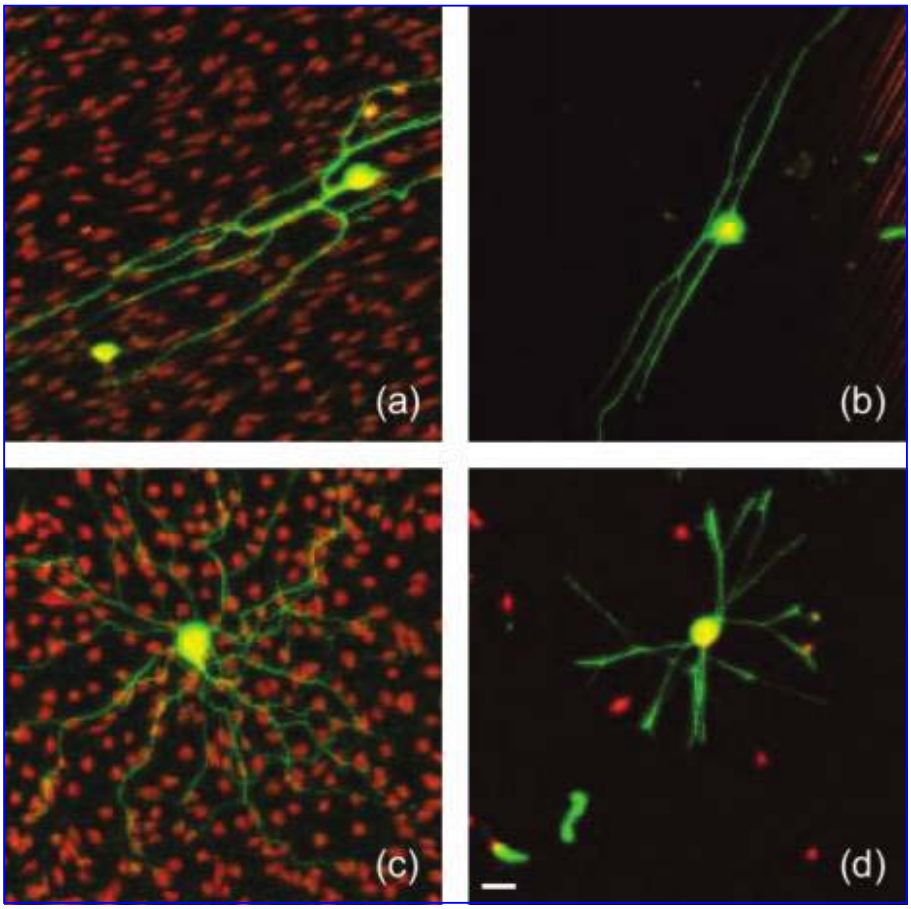

FIG. 7. Dorsal root ganglia cultured on aligned underlying Schwann cell (SC) monolayer culture are directed in the orientation of SCs. Fluorescent images of 4′,6-diamidino-2-phenylindole–stained SCs and neurofilament-stained DRGs on aligned (**A, B**) and unaligned (**C, D**) SC monolayers. Figure from Thompson and Buettner, 2006.[31] This figure first appeared in Annals of Biomedical Engineering Vol. 34, No. 1, 2006, pp. 161–168. Reprinted with permission from the authors. Color images available online at www.liebertpub.com/ten.

olfactory nerve fibroblasts (ONF) or neonatal astrocytes. Greater neurite elongation was observed on OEC/ONF cultures than on neonatal astrocyte cultures. OEC/ONF or astrocyte monolayers were aligned when cultured on aligned porous poly(D,L) lactide scaffolds. Cortical neurites were oriented in the direction of the underlying aligned OEC/ONF or astrocyte culture.

Neuron–glial interactions have been observed because glial cells are supportive cells in the CNS that can contribute to the modulation of neuronal responses to their environment. By including these cells in neuronal cultures that focus on guiding neurons and their extensions, a more complex mixture of cues can be presented in a time-dependent and feedback-dependent manner, which is much more similar to interactions *in vivo.*

PRESENTATION OF CELLULAR TOPOGRAPHY IN THE ABSENCE OF CELLS

Cells present a complex and dynamic set of cues that include their topography and their ability to produce permissive and inhibitory molecules. To understand how these cues affect neurons, it is useful to isolate the individual complex effects of neighboring cells. Until now, the difficulty in reproducing the complex shapes of cells without including molecular components has left the influence of cellular topography largely unexplored. To separate the contributions of molecular cues from cellular topographical cues, Bruder *et al.*[124] have recently developed transparent, biocompatible poly(dimethyl siloxane) substrates with biomimetic, SC-shaped relief topography. As a result, the contribution of cellular topography as an independent factor in cocultures and, in particular, the role of SC topography in axon guidance can be studied. Neurites have been found to respond to SC topography by following the underlying direction of SC alignment (Fig. 8).[125] This micromolding method can be extended to any cell type of interest, and polymeric templates of directed astrocyte monolayers have also been fabricated. In our laboratory, we have recently found that micromolded polymeric replicas of aligned astrocytes can direct DRG neurite growth to the orientation of astrocyte replicas.

NERVE GUIDANCE CHANNELS PRESENT COMBINATIONS OF CUES TO DIRECT AXON GROWTH

Nerve guidance channels (NGCs) are biomaterial-based devices that are designed to be transplanted experimentally for nerve repair, first studied as a possible alternative to nerve autografts. NGCs aim to provide a conduit through which regenerating axons can grow and connect to their

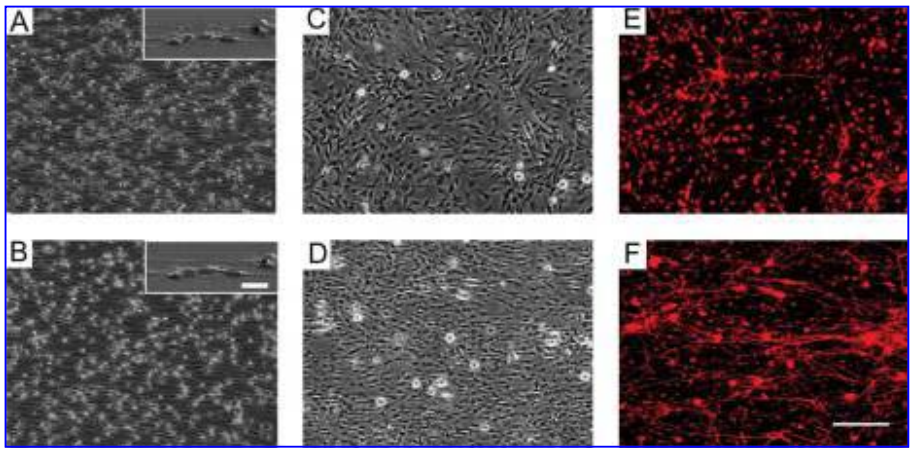

FIG. 8. Schwann cell (SC) replicas guide dorsal root ganglia (DRG) neurites. Phase contrast microscopy and scanning electron microscopy (SEM) (inset) of fixed SC templates (**A**) and polymeric replicates (**B**) of cells cultured at 120,000 cell/mL aligned onto 50-μm laminin stripes. DRG morphology visualized under phase contrast (**C, D**) and fluorescent micrographs (**E, F**) on flat polydimethylsiloxane (**C, E**) or replicas (**D, F**) and stained with neurofilament immunocytochemistry (**B, E**). Scale bars, 200 μm for phase contrast and fluorescent micrographs and 20 μm for SEM micrographs. Figure reprinted from Bruder *et al.,* Journal of Biomaterials Science, Polymer Edition, Vol. 18, No. 8, 2007, pp. 967–982, with permission from Koninklijke Brill N.V.[125] Color images available online at www.liebertpub.com/ten.

appropriate targets (reviewed in [23,126,127]). NGCs are an example of a tissue-engineering approach to axon guidance and nerve repair using cells and scaffolds to regenerate an injured nerve by incorporating features in the NGC to mimic the *in vivo* environment of a nerve autograft. By using information gained about guidance cues from *in vitro* studies as reviewed above, researchers are optimizing the incorporation of biological factors and generating biomaterials to present cues that stimulate the regeneration process. These cues have been incorporated into synthetic nerve grafts with the potential of increasing nerve growth after injury. NGCs are typically transplanted and then evaluated in a rat sciatic nerve model, a well-established *in vivo* model for peripheral nerve injury, with a gap distance of 10 to 15 mm and diameter of 1 to 2 mm. In this final section, we provide a brief review of recent advances in NGCs.

Topography of the NGC is a major component of guidance information. The tube structure itself provides a directional cue, providing a stronger topographical cue than unaligned degenerating fascicles that are present at the injury site.[128] Additional topography on the inner surfaces of the lumen can be incorporated by alignment of fibers,[11,89,129,130] membranes,[131] and surface roughness.[132] The curvature of a substrate has been found to provide relevant guidance information to growing neurites, where DRG neurites were found to align in directions of minimal curvature, and to increase branching on substrate areas with principal maximal curvature.[132] Microfilaments incorporated in NGCs can also provide topographical guidance, with PLA microfilament-containing conduits promoting tissue cable formation and SC migration *in vivo.* In 60- to 80-μm microfilament-incorporated poly-(L-lactide-co-DL-lactide), axon growth was greater toward the distal stump.[11] Higher packing density of PLA microfilaments has also been found to correlate with the number of successfully regenerated nerves.[89] Recently, microfilaments have been combined in NGCs with molecular cues such as heregulin-β1.[130] Synergism between heregulin (800 ng) and microfilaments (50–100 μm) was shown by more SCs in NGCs *in vivo* with both cues than in those presenting each cue separately.

Addition of growth factors to NGCs has been widely studied to enhance axon growth through the conduit. Controlled-release approaches have been used to fabricate polymeric devices that can deliver growth factors to the site of injury over time.[133–138] Yang *et al.*[136] fabricated a microporous conduit of PLGA with single or multiple lumens that incorporated NGF in encapsulated and unencapsulated formulations. Bioactive NGF release was measured up to 14 days in single- and multiple-channel NGCs; after subcutaneous implantation over 13 days, cellular infiltration was observed. NGF microspheres of degradable polymers have also been fabricated into NGCs by loading the microspheres into silicone or polyphosphoester tubes.[137] Addition of NGF into NGCs was found to increase nerve fiber diameter and density at the distal end of the injury site at the 3-month time point. Fine *et al.*[134] fabricated synthetic ethylene vinyl acetate copolymer NGCs with NGF or GDNF incorporated into the walls of the polymers to be released over 6 weeks. Addition of NGF or GDNF was found to support nerve cables, myelinated axons, motoneurons, and DRG neurons *in vivo.*

ECM molecules and gels can also be incorporated into NGCs to provide sites of adhesion, to attract permissive glia, and to promote axon growth.[84,139–141] Alginate, collagen, and fibrin sponges and gels have been used as materials to fill the inner volume of NGCs.[142] Hashimoto *et al.*[142] observed more myelinated axons and more SC migration from the distal stump into alginate gels than into collagen sponges or fibrin glues. By incorporating molecular cues, growth can be enhanced. Rafiuddin Ahmed and Jayakumar[139] incorporated RGD peptides into a collagen matrix with a NGC *in vivo* and showed more myelinated axons in RGD-incorporated gels than in collagen controls. SCs proliferated at early stages after implantation in proximity to RGD peptides. Taylor *et al.*[140] immobilized NT-3 into fibrin gels, thus combining a biological 3D matrix with trophic factors. Implantation of NT-3–loaded fibrin gels in an acute spinal cord suction ablation after 9 days showed cellular infiltration into the matrix and diminished glial fibrillary acidic protein-positive reactive astrocytes.

Combining NGCs with tubular structure, biological or polymeric matrices (collagen, fibrin, Matrigel, methylcellulose, or channels), and neurotrophic factors (FGF, NT-3) in a complete spinal cord transection allowed for comparison of matrices in NGCs.[143] Although addition of each matrix increased axon density, specific matrices elicited growth from different subpopulations in the spinal cord. Fibrin promoted growth from reticular neurons, and methylcellulose promoted growth from vestibular and red nucleus neurons, thus showing differential effects of matrix composition.

Mechanical properties of NGCs and incorporated matrices can affect neurite growth. Poly(2-hydroxyethyl methacrylate-co-methyl methacrylate) (PHEMA-MMA) channels with varying elastic moduli (177, 311 kPa) showed an increase in area and width of neural tissue within the stiffer NGCs.[144] In longer-term implantation studies, these PHEMA-MMA NGCs maintained their structural integrity for up to 8 weeks. Collapse of NGCs was observed in 29% of samples after 16 weeks, and the collapsed samples had significantly lower wall area than patent samples. To improve nerve graft patency, poly(caprolactone) coil-reinforced PHEMA-MMA tubes were fabricated to obtain NGCs with higher compressive strength, allowing NGCs with mechanical integrity from low modulus materials.[145]

Electrical guidance cues can also be incorporated into NGCs using pPy.[146] Electrical stimulation applied through the electrically conductive biodegradable polymers enhanced neurite outgrowth in a current-dependent fashion, promoting myelinated axons and SCs similar to those of the native sciatic nerve.

Addition of SCs to NGCs provides an additional cellular guidance cue. Philips *et al.*[84] incorporated SCs and

fibroblasts into collagen gels, which contracted and resulted in uniaxial alignment of collagen fibrils. This matrix was then loaded into silicone tubes for an implantable construct. Evans *et al.*[147] injected SCs into PLA conduits *in vivo,* and although axon density after 4 months was lower than that of isografts, mean sciatic function indices were comparable, suggesting promotion of functional recovery.

By taking lessons from *in vitro* studies such as those reviewed in this article and incorporating the cues that affect axon guidance into NGCs in a systematic manner, *in vivo* experiments can inform strategies to increase the effectiveness of nerve regeneration.[148] The biomaterial aspect of NGCs allows scientists to design and optimize physical parameters of the tube, including length, diameter, and wall thickness, which all contribute to the topographical information presented to growing neurons. Material properties of polymers such as permeability, degradability, interior surface morphology, and conductivity can also be modified for optimal ingrowth of cells and neurite extension. Incorporation of scaffolds or 3D matrices in the lumen of the NGCs allows a permissive substrate for cells to grow through, with appropriate mechanical and chemical cues such as exogenous trophic factors or ECM adhesion molecules dispersed or patterned within the matrices. Thus far, functional recovery over clinically relevant lengths has not been achieved with synthetic grafts, but these defined microenvironments allow for the careful study of the processes of axon guidance in a more controlled manner *in vivo.*

CONCLUSIONS

Tissue engineering approaches combine biomaterials, cells, molecules, and cutting-edge micro- and nanofabrication to develop new scaffolds, platforms, and experiments for the study of the key parameters in axon guidance. Major goals for nerve regeneration include prevention of secondary injury, compensation for demyelination, removal of inhibitors to growth, promotion of axonal growth, direction of newly growing axons to their proper targets, and replacement of dead cells to regain functional recovery.[149] These goals highlight the importance of a multi-factorial approach to tissue-engineering strategies for axon guidance and nerve repair. In addition to transplantation, in which nerve grafts[150–152] and cellular transplants[153,154] have been widely studied, strategies include anti-inflammatory and anti-apoptotic treatments (reviewed in [155,156]), drugs or antibodies that block the inhibitors of regeneration,[157] growth factors to promote axon sprouting,[35,150] gene therapy to deliver growth factors,[158,159] (and reviewed in[160]), and transplantation of stem cells with the potential to differentiate into new cell populations to replace the injured or dead cells.[161,162] One major approach with these strategies is to employ neural tissue–engineering principles to replace damaged or degenerated neural tissue with a matrix containing guidance cues including diffusible factors, substrate-bound factors, electrical gradients, and topographical cues, with the aim of incorporating these cues into nerve guidance channels to increase ingrowth and precise reconnection of host neurons. By using tissue engineering to present and examine multiple guidance cues in a precise and systematically composed manner *in vitro* and *in vivo,* we can gain critical information for a deeper understanding of how axon guidance occurs *in vivo.*

ACKNOWLEDGMENTS

This work was funded by National Science Foundation CAREER and National Institute of Biomedical Imaging and BioEngineering R21 grants to DHK and a Robert and Susan Kaplan Fellowship to GNL.

REFERENCES

1. David, S. and Lacroix, S. Molecular approaches to spinal cord repair. Annu Rev Neurosci **26,** 411, 2003.
2. Chilton, J. K. Molecular mechanisms of axon guidance. Dev Bio **292,** 13, 2006.
3. Mueller, B. K. Growth Cone guidance: first steps towards a deeper understanding. Annu Rev Neurosci **22,** 351, 1999.
4. Raivich, G. and Makwana, M. The making of successful axonal regeneration: genes, molecules and signal transduction pathways. Brain Res Rev **53,** 287, 2007.
5. Serini, G. and Bussolino, F. Common cues in vascular and axon guidance. Physiology **19,** 348, 2004.
6. Daniel M. and Suter, P. F. Substrate-cytoskeletal coupling as a mechanism for the regulation of growth cone motility and guidance. J Neurobiol **44,** 97, 2000.
7. Adams, D.N., Kao, E.Y.C., Hypolite, C.L., Distefano, M.D., Hu, W., and Letourneau, P.C. Growth cones turn and migrate up an immobilized gradient of the laminin IKVAV peptide. J Neurobiol **62,** 134, 2005.
8. Dertinger, S. K. W., Jiang, X., Li, Z., Murthy, V. N., and Whitesides, G. M. Gradients of substrate-bound laminin orient axonal specification of neurons. Proc Natl Acad Sci U S A **99,** 12542, 2002.
9. McFarlane, S. Metalloproteases: carving out a role in axon guidance. Neuron **37,** 559, 2003.
10. Mahoney, M. J., Chen, R. R., Tan, J., and Saltzman, W. M. The influence of microchannels on neurite growth and architecture. Biomaterials **26,** 771, 2005.
11. Cai, J., Peng, X., Nelson, K. D., Eberhart, R., and Smith, G. M. Permeable guidance channels containing microfilament scaffolds enhance axon growth and maturation. J Biomed Mater Res A **75,** 374, 2005.
12. Dowell-Mesfin, N. M., Abdul-Karim, M. A., Turner, A. M. P., Schanz, S., Craighead, H. G., Roysam, B., Turner, J. N., and Shain, W. Topographically modified surfaces affect orientation and growth of hippocampal neurons. J Neural Eng **1,** 78, 2004.

13. Goldner, J. S., Bruder, J. M., Li, G., Gazzola, D., and Hoffman-Kim, D. Neurite bridging across micropatterned grooves. Biomaterials **27,** 460, 2006.
14. Manwaring, M. E., Walsh, J. F., and Tresco, P. A. Contact guidance induced organization of extracellular matrix. Biomaterials **25,** 3631, 2004.
15. Walsh, J. F., Manwaring, M. E., and Tresco, P. A. Directional neurite outgrowth is enhanced by engineered meningeal cell-coated substrates. Tissue Eng **11,** 1085, 2005.
16. McCaig, C. D., Rajnicek, A. M., Song, B. and Zhao, M. Has electrical growth cone guidance found its potential? Trends Neurosci **25,** 354, 2002.
17. Patel, N. and Poo, M. M. Orientation of neurite growth by extracellular electric fields. J Neurosci **2,** 483, 1982.
18. Schmidt, C. E., Shastri, V. R., Vacanti, J. P. and Langer, R. Stimulation of neurite outgrowth using an electrically conducting polymer. Proc Natl Acad Sci U S A **94,** 8948, 1997.
19. Zhang, N., Yan, H., and Wen, X. Tissue-engineering approaches for axonal guidance. Brain Res Brain Res Rev **49,** 48, 2005.
20. Chalfoun, C. T., Wirth, G. A., and Evans, G. R. Tissue engineered nerve constructs: where do we stand? J Cell Mol Med **10,** 309, 2006.
21. Lavik, E. and Langer, R. Tissue engineering: current state and perspectives. Appl Microbiol Biotechnol **65,** 1, 2004.
22. Fry, E. J. Central nervous system regeneration: mission impossible? Clin Exp Pharmacol Physiol **28,** 253, 2001.
23. Schmidt, C. E. and Leach, J. B. Neural tissue engineering: strategies for repair and regeneration. Annu Rev Biomed Eng **5,** 293, 2003.
24. Meek, M. F. and Coert, J. H. Clinical use of nerve conduits in peripheral-nerve repair: review of the literature. J Reconstr Microsurg **18,** 097, 2002.
25. Fawcett, J. W. and Keynes, R. J. Peripheral nerve regeneration. Annu Rev Neurosci **13,** 4350, 1990.
26. McDonald, J. W., Liu, X.-Z., Qu, Y., Liu, S., Mickey, S. K., Turetsky, D., Gottlieb, D. I., and Choi, D. W. Transplanted embryonic stem cells survive, differentiate and promote recovery in injured rat spinal cord. Nat Med **5,** 1410, 1999.
27. Lakatos, A. and Franklin, R. J. M. Transplant mediated repair of the central nervous system: an imminent solution? Curr Opin Neurol **15,** 701, 2002.
28. Gregory, R. D. E. Peripheral nerve injury: a review and approach to tissue engineered constructs. Anat Rec **263,** 396, 2001.
29. Flaim, C. J., Chien, S., and Bhatia, S. N. An extracellular matrix microarray for probing cellular differentiation. Nat Meth **2,** 119, 2005.
30. Keilhoff, G., Goihl, A., Stang, F., Wolf, G., and Fansa, H. Peripheral nerve tissue engineering: autologous Schwann cells vs. transdifferentiated mesenchymal stem cells. Tissue Eng **12,** 1451, 2006.
31. Thompson, D. M. and Buettner, H. M. Neurite outgrowth is directed by Schwann cell alignment in the absence of other guidance cues. Ann Biomed Eng **34,** 161, 2006.
32. Chen, Y. Y., McDonald, D., Cheng, C., Magnowski, B., Durand, J., and Zochodne, D. W. Axon and Schwann cell partnership during nerve regrowth. J Neuropathol Exp Neurol **64,** 613, 2005.
33. Langer, R. and Vacanti, J. P. Tissue engineering. Science **260,** 920, 1993.
34. MacArthur, B. D. and Oreffo, R. O. Bridging the gap. Nature **433,** 19, 2005.
35. Boyd, J. G. and Gordon, T. Neurotrophic factors and their receptors in axonal regeneration and functional recovery after peripheral nerve injury. Mol Neurobiol **27,** 277, 2003.
36. Kato, A. C. and Lindsay, R. M. Overlapping and additive effects of neurotrophins and cntf on cultured human spinal cord neurons. Exp Neurol **130,** 196, 1994.
37. Jones, D. M., Tucker, B. A., Rahimtula, M., and Mearow, K. M. The synergistic effects of NGF and IGF-1 on neurite growth in adult sensory neurons: convergence on the PI 3-kinase signaling pathway. J Neurochem **86,** 1116, 2003.
38. Taylor, L., Jones, L., Tuszynski, M. H., and Blesch, A. Neurotrophin-3 gradients established by lentiviral gene delivery promote short-distance axonal bridging beyond cellular grafts in the injured spinal cord. J Neurosci **26,** 9713, 2006.
39. Tom, V. J., Steinmetz, M. P., Miller, J. H., Doller, C. M., and Silver, J. Studies on the development and behavior of the dystrophic growth cone, the hallmark of regeneration failure, in an *in vitro* model of the glial scar and after spinal cord injury. J Neurosci **24,** 6531, 2004.
40. Le Beau, J. M., Liuzzi, F. J., Depto, A. S., and Vinik, A. I. Up-regulation of laminin B2 gene expression in dorsal root ganglion neurons and nonneuronal cells during sciatic nerve regeneration. Exp Neurol **134,** 150, 1995.
41. Tashiro, K.-I., Sephel, G. C., Greatorex, D., Sasaki, M., Shirashi, N., Martin, G. R., Kleinman, H. K., and Yamada, Y. The RGD containing site of the mouse laminin A chain is active for cell attachment, spreading, migration and neurite outgrowth. J Cell Physiol **146,** 451, 1991.
42. Tashiro, K., Sephel, G. C., Weeks, B., Sasaki, M., Martin, G. R., Kleinman, H. K., and Yamada, Y. A synthetic peptide containing the IKVAV sequence from the A chain of laminin mediates cell attachment, migration, and neurite outgrowth. J Biol Chem **264,** 16174, 1989.
43. Graf, J., Ogle, R. C., Robey, F. A., Sasaki, M., Martin, G. R., Yamada, Y., and Kleinman, H. K. A pentapeptide from the laminin B1 chain mediates cell adhesion and binds to 67000 laminin receptor. Biochemistry **26,** 6896, 1987.
44. Massia, S. P., Rao, S. S., and Hubbell, J. A. Covalently immobilized laminin peptide Tyr-Ile-Gly-Ser-Arg (YIGSR) supports cell spreading and co-localization of the 67-kilodalton laminin receptor with alpha-actinin and vinculin. J Biol Chem **268,** 8053, 1993.
45. Bellamkonda, R. V. Peripheral nerve regeneration: an opinion on channels, scaffolds and anisotropy. Biomaterials **27,** 3515, 2006.
46. Rosoff, W. J., Urbach, J. S., Esrick, M. A., McAllister, R. G., Richards, L. J., and Goodhill, G. J. A new chemotaxis assay shows the extreme sensitivity of axons to molecular gradients. Nat Neurosci **7,** 678, 2004.
47. Cornish, T., Branch, D. W., Wheeler, B. C., and Campanelli, J. T. Microcontact printing: a versatile technique for the study of synaptogenic molecules. Mol Cell Neurosci **20,** 140, 2002.
48. von Philipsborn, A. C., Lang, S., Loeschinger, J., Bernard, A., David, C., Lehnert, D., Bonhoeffer, F., and Bastmeyer, M. Growth cone navigation in substrate-bound ephrin gradients. Development **133,** 2487, 2006.

49. Li, G., Liu, J., and Hoffman-Kim, D. Multi-molecular gradients of permissive and inhibitory cues direct neurite outgrowth. Ann Biomed Eng in press.
50. Offenhausser, A., Bocker-Meffert, S., Decker, T., Helpenstein, R., Gasteier, P., Groll, J., Moller, M., Reska, A., Schafer, S., Schulte, P., and Vogt-Eisele, A. Microcontact printing of proteins for neuronal cell guidance. Soft Matter **3,** 290, 2007.
51. Oliva, A. A., James, C. D., Kingman, C. E., Craighead, H. G., and Banker, G. A. patterning axonal guidance molecules using a novel strategy for microcontact printing. Neurochem Res **28,** 1639, 2003.
52. Yeung, C. K., Lauer, L., Offenhausser, A., and Knoll, W. Modulation of the growth and guidance of rat brain stem neurons using patterned extracellular matrix proteins. Neurosci Lett **301,** 147, 2001.
53. Vogt, A. K., Wrobel, G., Meyer, W., Knoll, W., and Offenhausser, A. Synaptic plasticity in micropatterned neuronal networks. Biomaterials **26,** 2549, 2005.
54. Zhang, Z., Yoo, R., Wells, M., Beebe, T. P., Biran, R., and Tresco, P. Neurite outgrowth on well-characterized surfaces: preparation and characterization of chemically and spatially controlled fibronectin and RGD substrates with good bioactivity. Biomaterials **26,** 47, 2005.
55. Yang, I. H., Co, C. C., and Ho, C.-C. Alteration of human neuroblastoma cell morphology and neurite extension with micropatterns. Biomaterials **26,** 6599, 2005.
56. Gomez, N., Chen, S., and Schmidt, C. E. Polarization of hippocampal neurons with competitive surface stimuli: contact guidance cues are preferred over chemical ligands. J R Soc Interface **4,** 223, 2007.
57. Gomez, N. and Schmidt, C. E. Nerve growth factor-immobilized polypyrrole: bioactive electrically conducting polymer for enhanced neurite extension. J Biomed Mater Res A **81,** 135, 2007.
58. Luo, Y. and Shoichet, M. S. A photolabile hydrogel for guided three-dimensional cell growth and migration. Nat Mater **3,** 249, 2004.
59. Song, H. K., Toste, B., Ahmann, K., Hoffman-Kim, D., and Palmore, G. T. Micropatterns of positive guidance cues anchored to polypyrrole doped with polyglutamic acid: a new platform for characterizing neurite extension in complex environments. Biomaterials **27,** 473, 2006.
60. Shi, R. and Borgens, R. Three-dimensional gradients of voltage during development of the nervous system as invisible coordinates for the establishment of embryonic pattern. Dev Dyn **202,** 101, 1995.
61. Song, B., Zhao, M., Forrester, J., and McCaig, C. Nerve regeneration and wound healing are stimulated and directed by an endogenous electrical field *in vivo*. J Cell Sci **117,** 4681, 2004.
62. Francis, J. T., Gluckman, B. J., and Schiff, S. J. Sensitivity of neurons to weak electric fields. J Neurosci **23,** 7255, 2003.
63. Bikson, M., Inoue, M., Akiyama, H., Deans, J. K., Fox, J. E., Miyakawa, H., and Jefferys, J. G. R. Effects of uniform extracellular DC electric fields on excitability in rat hippocampal slices *in vitro*. J Physiol **557,** 175, 2004.
64. Wood, M. and Willits, R. K. Short-duration, DC electrical stimulation increases chick embryo DRG neurite outgrowth. Bioelectromagnetics **27,** 328, 2006.
65. Greene, L. A. and Tischler, A. S. Establishment of a Noradrenergic clonal line of rat adrenal pheochromocytoma cells which respond to nerve growth factor. Proc Natl Acad Sci **73,** 2424, 1976.
66. Dichter, M. A., Tischler, A. S., and Greene, L. A. Nerve growth factor-induced increase in electrical excitability and acetylcholine sensitivity of a rat pheochromocytoma cell line. Nature **268,** 501, 1977.
67. Morgado-Valle, C., Verdugo-Díaz, L., García, D. E., Morales-Orozco, C., and Drucker-Colín, R. The role of voltage-gated Ca2+ channels in neurite growth of cultured chromaffin cells induced by extremely low frequency (ELF) magnetic field stimulation. Cell Tissue Res **291,** 217, 1998.
68. Blackman, C. F., Benane, S. G., and House, D. E. Evidence for direct effect of magnetic fields on neurite outgrowth. FASEB J. **7,** 801, 1993.
69. Macias, M., Battocletti, J., Sutton, C., Pintar, F., and Maiman, D. Directed and enhanced neurite growth with pulsed magnetic field stimulation. Bioelectromagnetics **21,** 272, 2000.
70. Shah, J. P., Midkiff, P., Brandt, P. C., and Sisken, B. F. Growth and differentiation of PC6 cells: the effects of pulsed electromagnetic fields (PEMF). Bioelectromagnetics **22,** 267, 2001.
71. Zhang, Y., Ding, J., Duan, W., and Fan, Y. W. Influence of pulsed electromagnetic field with different pulse duty cycles on neurite outgrowth in PC12 rat pheochromocytoma cells. Bioelectromagnetics **26,** 406, 2005.
72. Kotwal, A. and Schmidt, C. E. Electrical stimulation alters protein adsorption and nerve cell interactions with electrically conducting biomaterials. Biomaterials **22,** 1055, 2001.
73. Cui, X., Wiler, J., Dzaman, M., Altschuler, R. A., and Martin, D. C. *In vivo* studies of polypyrrole/peptide coated neural probes. Biomaterials **24,** 777, 2003.
74. Richardson, R. T., Thompson, B., Moulton, S., Newbold, C., Lum, M. G., Cameron, A., Wallace, G., Kapsa, R., Clark, G., and O'Leary, S. The effect of polypyrrole with incorporated neurotrophin-3 on the promotion of neurite outgrowth from auditory neurons. Biomaterials **28,** 513, 2007.
75. Stump, R. F. and Robinson, K. R. Xenopus neural crest cell migration in an applied electrical field. J Cell Biol **97,** 1226, 1983.
76. Alexander, J. K., Fuss, B., and Colello, R. J. Electric field-induced astrocyte alignment directs neurite outgrowth. Neuron Glia Biol **2,** 93, 2006.
77. Mosahebi, A., Simon, M., Wiberg, M., and Terenghi, G. A novel use of alginate hydrogel as Schwann cell matrix. Tissue Eng **7,** 525, 2001.
78. Dhoot, N. O., Tobias, C. A., Fischer, I., and Wheatley, M. A. Peptide-modified alginate surfaces as a growth permissive substrate for neurite outgrowth. J Biomed Mater Res A **71,** 191, 2004.
79. Novikova, L. N., Mosahebi, A., Wiberg, M., Terenghi, G., Kellerth, J., and Novikov, L. N. Alginate hydrogel and matrigel as potential cell carriers for neurotransplantation. J Biomed Mater Res A **77,** 242, 2006.
80. Cullen, D., Lessing, M., and LaPlaca, M. Collagen-dependent neurite outgrowth and response to dynamic deformation in three-dimensional neuronal cultures. Ann Biomed Eng **35,** 835, 2007.

81. Ma, W., Fitzgerald, W., Liu, Q. Y., O'shaughnessy, T. J., Maric, D., Lin, H. J., Alkon, D. L., and Barker, J. L. CNS stem and progenitor cell differentiation into functional neuronal circuits in three-dimensional collagen gels. Exp Neurol **190,** 276, 2004.
82. O'Connor, S. M., Stenger, D. A., Shaffer, K. M., and Ma, W. Survival and neurite outgrowth of rat cortical neurons in three-dimensional agarose and collagen gel matrices. Neurosci Lett **304,** 189, 2001.
83. O'Connor, S. M., Stenger, D. A., Shaffer, K. M., Maric, D., Barker, J. L., and Ma, W. Primary neural precursor cell expansion, differentiation and cytosolic Ca2+ response in three-dimensional collagen gel. J Neurosci Methods **102,** 187, 2000.
84. Phillips, J. B., Bunting, S. C., Hall, S. M., and Brown, R. A. Neural tissue engineering: a self-organizing collagen guidance conduit. Tissue Eng **11,** 1611, 2005.
85. Willits, R. K. and Skornia, S. L. Effect of collagen gel stiffness on neurite extension. J Biomater Sci Polym Ed **15,** 1521, 2004.
86. Li, G. N., Livi, L. L., Gourd, C. M., Deweerd, E. S., and Hoffman-Kim, D. Genomic and morphological changes of neuroblastoma cells in response to three-dimensional matrices. Tissue Eng **13,** 1035, 2007.
87. Ju, Y. E., Janmey, P. A., McCormick, M. E., Sawyer, E. S., and Flanagan, L. A. Enhanced neurite growth from mammalian neurons in three-dimensional salmon fibrin gels. Biomaterials **28,** 2097, 2007.
88. Pittier, R., Sautier, F, Hubbell, J.A., and Hall, H. Neurite extension and *in vitro* myelination within three-dimensional modified fibrin matrices. J Neurobiol **63,** 1, 2005.
89. Ngo, T. T. B., Waggoner, P. J., Romero, A. A., Nelson, K. D., Eberhart, R. C., and Smith, G. M. Poly(L-Lactide) microfilaments enhance peripheral nerve regeneration across extended nerve lesions. J Neurosci Res **72,** 227, 2003.
90. Bini, T.B., Gao, S., Xu, X., Wang, S., Ramakrishna, S., and Leong, K.W. Peripheral nerve regeneration by microbraided poly(L-lactide-co-glycolide) biodegradable polymer fibers. J Biomed Mater Res A **68,** 286, 2004.
91. Dodla, M. C. and Bellamkonda, R. V. Anisotropic scaffolds facilitate enhanced neurite extension *in vitro*. J Biomed Mater Res A **78,** 213, 2006.
92. Deister, C. and Schmidt, C. E. Optimizing neurotrophic factor combinations for neurite outgrowth. J Neural Eng **3,** 172, 2006.
93. Cao, X. and Shoichet, M. S. Photoimmobilization of biomolecules within a 3-dimensional hydrogel matrix. J Biomater Sci Polym Ed **13,** 623, 2002.
94. Kapur, T. A. and Shoichet, M. S. Chemically-bound nerve growth factor for neural tissue engineering applications. J Biomater Sci Polym Ed **14,** 383, 2003.
95. Kapur, T. A. and Shoichet, M. S. Immobilized concentration gradients of nerve growth factor guide neurite outgrowth. J Biomed Mater Res A **68,** 235, 2004.
96. Cao, X. and Shoichet, M. S. Investigating the synergistic effect of combined neurotrophic factor concentration gradients to guide axonal growth. Neuroscience **122,** 381, 2003.
97. Yu, X. and Bellamkonda, R. V. Dorsal root ganglia neurite extension is inhibited by mechanical and chondroitin sulfate-rich interfaces. J Neurosci Res **66,** 303, 2001.
98. Li, N. and Folch, A. Integration of topographical and biochemical cues by axons during growth on microfabricated 3-D substrates. Exp Cell Res **311,** 307, 2005.
99. Georges, P. C. and Janmey, P. A. Cell type-specific response to growth on soft materials. J Appl Physiol **98,** 1547, 2005.
100. Balgude, A. P., Yu, X., Szymanski, A., and Bellamkonda, R. V. Agarose gel stiffness determines rate of DRG neurite extension in 3D cultures. Biomaterials **22,** 1077, 2001.
101. Schense, J. C. and Hubbell, J. A. Three-dimensional migration of neurites is mediated by adhesion site density and affinity. J Biol Chem **275,** 6813, 2000.
102. Leach, J. B., Brown, X. Q., Jacot, J. G., DiMilla, P. A., and Wong, J. Y. Neurite outgrowth and branching of PC12 cells on very soft substrates sharply decreases below a threshold of substrate rigidity. J Neural Eng **4,** 26, 2007.
103. Georges, P. C., Miller, W. J., Meaney, D. F., Sawyer, E. S., and Janmey, P. A. Matrices with compliance comparable to that of brain tissue select neuronal over glial growth in mixed cortical cultures. Biophys J **90,** 3012, 2006.
104. Wen, X. and Tresco, P. A. Effect of filament diameter and extracellular matrix molecule precoating on neurite outgrowth and Schwann cell behavior on multifilament entubulation bridging device *in vitro*. J Biomed Mater Res A **76,** 626, 2006.
105. Gomez, N., Lu, Y., Chen, S., and Schmidt, C. E. Immobilized nerve growth factor and microtopography have distinct effects on polarization versus axon elongation in hippocampal cells in culture. Biomaterials **28,** 271, 2007.
106. Foley, J. D., Grunwald, E. W., Nealey, P. F., and Murphy, C. J. Cooperative modulation of neuritogenesis by PC12 cells by topography and nerve growth factor. Biomaterials **26,** 3639, 2005.
107. Miller, C., Jeftinija, S., and Mallapragada, S. Synergistic effects of physical and chemical guidance cues on neurite alignment and outgrowth on biodegradable polymer substrates. Tissue Eng **8,** 367, 2002.
108. Zhang, J., Venkataramani, S., Xu, H., Song, Y.-K., Song, H.-K., Palmore, G. T. R., Fallon, J., and Nurmikko, A. V. Combined topographical and chemical micropatterns for templating neuronal networks. Biomaterials **27,** 5734, 2006.
109. Fan, Y. W., Cui, F. Z., Chen, L. N., Zhai, Y., Xu, Q. Y., and Lee, I. S. Adhesion of neural cells on silicon wafer with nano-topographic surface. Appl Surf Sci **187,** 313, 2002.
110. Fan, Y. W., Cui, F. Z., Hou, S. P., Xu, Q. Y., Chen, L. N., and Lee, I. S. Culture of neural cells on silicon wafers with nano-scale surface topograph. J Neurosci Methods **120,** 17, 2002.
111. Ahmed, I., Liu, H. Y., Mamiya, P. C., Ponery, A. S., Babu, A. N., Weik, T., Schindler, M., and Meiners, S. Three-dimensional nanofibrillar surfaces covalently modified with tenascin-C-derived peptides enhance neuronal growth *in vitro*. J Biomed Mater Res A **76,** 851, 2006.
112. Yang, F., Murugan, R., Wang, S., and Ramakrishna, S. Electrospinning of nano/micro scale poly(L-lactic acid) aligned fibers and their potential in neural tissue engineering. Biomaterials **26,** 2603, 2005.
113. Lovat, V., Pantarotto, D., Lagostena, L., Cacciari, B., Grandolfo, M., Righi, M., Spalluto, G., Prato, M., and Ballerini, L. Carbon nanotube substrates boost neuronal electrical signaling. Nano Lett. **5,** 1107, 2005.

114. Nguyen-Vu, T. D., Chen, H., Cassell, A. M., Andrews, R., Meyyappan, M., and Li, J. Vertically aligned carbon nanofiber arrays: an advance toward electrical-neural interfaces. Small **2,** 89, 2006.
115. Waid, M. C., McKenzie, J. L., Price, R. L., Ejiofor, J. U., and Webster, T. J. Nano-biotechnology: carbon nanofibres as improved neural and orthopaedic implants. Nanotechnology **15,** 48, 2004.
116. Wang, K., Fishman, H. A., Dai, H., and Harris, J. S. Neural stimulation with a carbon nanotube microelectrode array. Nano Lett **6,** 2043, 2006.
117. Norman, J. and Desai, T. Methods for fabrication of nanoscale topography for tissue engineering scaffolds. Ann Biomed Eng **34,** 89, 2006.
118. Silva, G. A., Czeisler, C., Niece, K. L., Beniash, E., Harrington, D. A., Kessler, J. A., and Stupp, S. I. Selective differentiation of neural progenitor cells by high-epitope density nanofibers. Science **303,** 1352, 2004.
119. McKenzie, J. L., Waid, M. C., Shi, R., and Webster, T. J. Decreased functions of astrocytes on carbon nanofiber materials. Biomaterials **25,** 1309, 2004.
120. Hasegawa, K., Chang, Y.-W., Li, H., Berlin, Y., Ikeda, O., Kane-Goldsmith, N., and Grumet, M. Embryonic radial glia bridge spinal cord lesions and promote functional recovery following spinal cord injury. Exp Neurol **193,** 394, 2005.
121. Recknor, J. B., Sakaguchi, D. S., and Mallapragada, S. K. Growth and Differentiation of astrocytes and neural progenitor cells on micropatterned polymer films. Ann N Y Acad Sci **1049,** 24, 2005.
122. Biran, R., Noble, M. D., and Tresco, P. A. Directed nerve outgrowth is enhanced by engineered glial substrates. Exp Neurol **184,** 141, 2003.
123. Deumens, R., Koopmans, G. C., den Bakker, C. G. J., Maquet, V., Blacher, S., Honig, W. M. M., Jerome, R., Pirard, J. P., Steinbusch, H. W. M., and Joosten, E. A. J. Alignment of glial cells stimulates directional neurite growth of CNS neurons *in vitro*. Neuroscience **125,** 591, 2004.
124. Bruder, J. M., Monu, N. C., Harrison, M. W., and Hoffman-Kim, D. Fabrication of polymeric replicas of cell surfaces with nanoscale resolution. Langmuir **22,** 8266, 2006.
125. Bruder, J. M., Lee, A. P., and Hoffman-Kim, D. Biomimetic materials replicating Schwann cell topography enhance neuronal adhesion and neurite alignment *in vitro*. J Biomater Sci Polym Ed **18,** 967, 2007.
126. Belkas, J. S., Shoichet, M. S., and Midha, R. Axonal guidance channels in peripheral nerve regeneration. Oper Tech Orthop **14,** 190, 2004.
127. Battiston, B., Geuna, S. Ferrero, M., and Tos, P. Nerve repair by means of tubulization: literature review and personal clinical experience comparing biological and synthetic conduits for sensory nerve repair. Microsurgery **25,** 258, 2005.
128. Pearson, R. G., Molino, Y., Williams, P. M., Tendler, S. J. B., Davies, M. C., Roberts, C. J., and Shakesheff, K. M. Spatial confinement of neurite regrowth from dorsal root ganglia within nonporous microconduits. Tissue Eng **9,** 201, 2003.
129. Bini, T.B., Gao, S., Xu, X., Wang, S., Ramakrishna, S., and Leong, K.W. Peripheral nerve regeneration by microbraided poly(L-lactide-co-glycolide) biodegradable polymer fibers. J Biomed Mater Res A **68,** 286, 2004.
130. Cai, J., Peng, X., Nelson, K. D., Eberhart, R., and Smith, G. M. Synergistic improvements in cell and axonal migration across sciatic nerve lesion gaps using bioresorbable filaments and heregulin-beta1. J Biomed Mater Res A **69,** 247, 2004.
131. Ning Zhang, C. Z. X. W. Fabrication of semipermeable hollow fiber membranes with highly aligned texture for nerve guidance. J Biomed Mater Res A **75,** 941, 2005.
132. Smeal, R. M., Rabbitt, R., Biran, R., and Tresco, P. A. Substrate curvature influences the direction of nerve outgrowth. Ann Biomed Eng **33,** 376, 2005.
133. Patist, C. M., Mulder, M. B., Gautier, S. E., Maquet, V., Jerome, R., and Oudega, M. Freeze-dried poly(-lactic acid) macroporous guidance scaffolds impregnated with brain-derived neurotrophic factor in the transected adult rat thoracic spinal cord. Biomaterials **25,** 1569, 2004.
134. Fine, E. G., Decosterd, I., Papaloizos, M., Zurn, A. D., and Aebischer, P. GDNF and NGF released by synthetic guidance channels support sciatic nerve regeneration across a long gap. Eur J Neurosci **15,** 589, 2002.
135. Aszmann, O. C., Korak, K. J., Kropf, N., Fine, E., Aebischer, P., and Frey, M. Simultaneous GDNF and BDNF application leads to increased motoneuron survival and improved functional outcome in an experimental model for obstetric brachial plexus lesions. Plast Reconstr Surg **110,** 1066, 2002.
136. Yang, Y., De Laporte, L., Rives, C. B., Jang, J. H., Lin, W. C., Shull, K. R., and Shea, L. D. Neurotrophin releasing single and multiple lumen nerve conduits. J Control Release **104,** 433, 2005.
137. Xu, X., Yee, W.-C., Hwang, P. Y. K., Yu, H., Wan, A. C. A., Gao, S., Boon, K.-L., Mao, H.-Q., Leong, K. W., and Wang, S. Peripheral nerve regeneration with sustained release of poly(phosphoester) microencapsulated nerve growth factor within nerve guide conduits. Biomaterials **24,** 2405, 2003.
138. Mohanna, P. N., Young, R. C., Wiberg, M., and Terenghi, G. A composite poly-hydroxybutyrate-glial growth factor conduit for long nerve gap repairs. J Anat **203,** 553, 2003.
139. Rafiuddin Ahmed, M. and Jayakumar, R. Peripheral nerve regeneration in RGD peptide incorporated collagen tubes. Brain Res **993,** 208, 2003.
140. Taylor, S. J., McDonald, J. W., and Sakiyama-Elbert, S. E. Controlled release of neurotrophin-3 from fibrin gels for spinal cord injury. J Control Release **98,** 281, 2004.
141. Niere, M., Braun, B., Gass, R., Sturany, S., and Volkmer, H. Combination of engineered neural cell adhesion molecules and GDF-5 for improved neurite extension in nerve guide concepts. Biomaterials **27,** 3432, 2006.
142. Hashimoto, T., Suzuki, Y., Kitada, M., Kataoka, K., Wu, S., Suzuki, K., Endo, K., Nishimura, Y., and Ide, C. Peripheral nerve regeneration through alginate gel: analysis of early outgrowth and late increase in diameter of regenerating axons. Exp Brain Res **146,** 356, 2002.
143. Tsai, E. C., Dalton, P. D., Shoichet, M. S., and Tator, C. H. Matrix inclusion within synthetic hydrogel guidance channels improves specific supraspinal and local axonal regeneration after complete spinal cord transection. Biomaterials **27,** 519, 2006.
144. Tsai, E. C., Dalton, P. D., Shoichet, M. S., and Tator, C. H. Synthetic hydrogel guidance channels facilitate regeneration of adult rat brainstem motor axons after complete spinal cord transection. J Neurotrauma **21,** 789, 2004.

145. Katayama, Y., Montenegro, R., Freier, T., Midha, R., Belkas, J. S., and Shoichet, M. S. Coil-reinforced hydrogel tubes promote nerve regeneration equivalent to that of nerve autografts. Biomaterials **27,** 505, 2006.
146. Zhang, Z., Rouabhia, M., Wang, Z., Roberge, C., Shi, G., Roche, P., Li, J., and Dao, L. H. Electrically conductive biodegradable polymer composite for nerve regeneration: electricity-stimulated neurite outgrowth and axon regeneration. Artif Organs **31,** 13, 2007.
147. Evans, G. R. D., Brandt, K., Katz, S., Chauvin, P., Otto, L., Bogle, M., Wang, B., Meszlenyi, R. K., Lu, L., Mikos, A. G., and Patrick, C. W. Bioactive poly(-lactic acid) conduits seeded with Schwann cells for peripheral nerve regeneration. Biomaterials **23,** 841, 2002.
148. Geller, H. M. and Fawcett, J. W. Building a bridge: engineering spinal cord repair. Exp Neurol **174,** 125, 2002.
149. McDonald, J. W. and Sadowsky, C. Spinal-cord injury. Lancet **359,** 417, 2002.
150. Coumans, J. V., Lin, T. T.-S., Dai, H. N., MacArthur, L., McAtee, M., Nash, C., and Bregman, B. S. Axonal regeneration and functional recovery after complete spinal cord transection in rats by delayed treatment with transplants and neurotrophins. J Neurosci **21,** 9334, 2001.
151. Bregman, B. S., Coumans, J.-V., Dai, H. N., Kuhn, P. L., Lynskey, J., McAtee, M., Sandhu, F., and L. McKerracher, G. D. Transplants and neurotrophic factors increase regeneration and recovery of function after spinal cord injury. In: Heywood, C. A., ed. Progress in Brain Research. New York: Elsevier, 2002, pp. 257–273.
152. Cheng, H., Cao, Y., and Olson, L. Spinal cord repair in adult paraplegic rats: partial restoration of hind limb function. Science **273,** 510, 1996.
153. Rasouli, A., Bhatia, N., Suryadevara, S., Cahill, K., and Gupta, R. Transplantation of preconditioned schwann cells in peripheral nerve grafts after contusion in the adult spinal cord. Improvement of recovery in a rat model. J Bone Joint Surg Am **88,** 2400, 2006.
154. Jones, L. L., Oudega, M., Bunge, M. B., and Tuszynski, M. H. Neurotrophic factors, cellular bridges and gene therapy for spinal cord injury. J Physiol **533,** 83, 2001.
155. Hall, E. D. and Springer, J. E. Neuroprotection and Acute spinal cord injury: a reappraisal. NeuroRX **1,** 80, 2004.
156. Mattson, M. P. Apoptosis in neurodegenerative disorders. Nat Rev Mol Cell Biol **1,** 120, 2000.
157. Fouad, K., Schnell, L., Bunge, M. B., Schwab, M. E., Liebscher, T., and Pearse, D. D. Combining Schwann cell bridges and olfactory-ensheathing glia grafts with chondroitinase promotes locomotor recovery after complete transection of the spinal cord. J Neurosci **25,** 1169, 2005.
158. Ohori, Y., Yamamoto, S.-i., Nagao, M., Sugimori, M., Yamamoto, N., Nakamura, K., and Nakafuku, M. Growth factor treatment and genetic manipulation stimulate neurogenesis and oligodendrogenesis by endogenous neural progenitors in the injured adult spinal cord. J. Neurosci. **26,** 11948, 2006.
159. Romero, M. I., Rangappa, N., Garry, M. G., and Smith, G. M. Functional regeneration of chronically injured sensory afferents into adult spinal cord after neurotrophin gene therapy. J Neurosci **21,** 8408, 2001.
160. Haastert, K. and Grothe, C. Gene therapy in peripheral nerve reconstruction approaches. Curr Gene Ther **7,** 221, 2007.
161. Lu, P., Jones, L. L., Snyder, E. Y., and Tuszynski, M. H. Neural stem cells constitutively secrete neurotrophic factors and promote extensive host axonal growth after spinal cord injury. Exp Neurol **181,** 115, 2003.
162. Teng, Y. D., Lavik, E. B., Qu, X., Park, K. I., Ourednik, J., Zurakowski, D., Langer, R., and Snyder, E. Y. Functional recovery following traumatic spinal cord injury mediated by a unique polymer scaffold seeded with neural stem cells. Proc Natl Acad Sci **99,** 3024, 2002.

Address reprint requests to:
Diane Hoffman-Kim, Ph.D.
Box G-B387
Brown University
Providence, RI 02912

E-mail: dhk@brown.edu

Appendix B

Effects of RhoGTPases on Neurite Outgrowth on Multimolecular Gradients

The glial scar of hypertrophic astrocytes that form after an injury in the central nervous system is well documented to be inhibitory, with several classes of growth inhibitory molecules that are upregulated, including the family of extracellular matrix molecules known as chondroitin sulfate proteoglycans (CSPG) (Fitch and Silver, 1997; Jones et al., 2003; Morgenstern et al., 2002). Using microfluidic techniques, proteins can be adsorbed on glass substrates in a manner that mimics the gradient of CSPG found *in vivo* after spinal cord injury.

CSPG are organized in a crude gradient with the lowest concentrations in the lesion penumbra and the highest in the epicenter (Davies et al., 1999; Fitch and Silver, 1997), and surprisingly, a permissive molecule, laminin (LN) is also present in the microenvironment after an injury in a graded fashion. To study how gradients of guidance cues are detected and transduced as neurites navigate complex inhibitory microenvironments, the glial scar was modeled as two parallel gradients containing LN and CPSG, where higher concentrations of both cues are present at one edge and decrease towards the opposite edge of a microchannel.

Previous studies have used models of the glial scar that range from "scar-in-a-dish" coculture models where injured neurons and glia are excised and cultured on membranes to acellular models using gradients of LN and a common CSPG, aggrecan. Co-culture models incorporate the complexity of heterotypic cell cultures that exist after an injury, but are difficult to control with precise parameters and reproduce. Molecular gradients have been shown to elicit similar injury morphology, such as dystrophic endbulbs and are much more easily controllable and reproducible than scar-in-a-dish type experiments. Parallel gradients of LN and CSPG are therefore good models of the glial scar that have highly tunable features for the study of neuronal response to the glial scar (Tom et al., 2004).

To further study the effects of cytoskeletal reorganization on neurite outgrowth in these microenvironments, dorsal root ganglia neurons were cultured on parallel gradients with a pharmacological inhibitor against Rho kinase (ROCK; Y27632). The Rho family of GTPases have been shown to play a role in transducing the extracellular CSPG signal to intracellular cytoskeletal changes and growth cone turning away from the source of CSPG (Jain et al., 2004; Sandvig et al., 2004).

B.1 Materials and Methods

Microfabrication techniques of photolithography, soft lithography and microfluidic pump-driven flow were used to generate the adsorbed protein gradients using a gradient mixer described in previous chapters (Figure B.1). Briefly, gradient mixer patterns were designed on AutoCAD and transferred to silicon masters using photolithography. Polydimethyl siloxane (PDMS) molds bearing the pattern of the gradient mixer were cast using soft lithography. PDMS molds were then adhered to glass slides after plasma activation, and coated with 1mg/mL, MW 30-70kDa poly-L-lysine (pLL). Protein solutions were then delivered to the inlet ports using pump driven flow and allowed to adsorb onto the pLL coated glass surface. In this study, LN concentrations were varied from 10ug/mL to 50ug/mL and CSPG concentrations were varied from 1 ug/mL to 5ug/mL. This corresponds with LN slopes

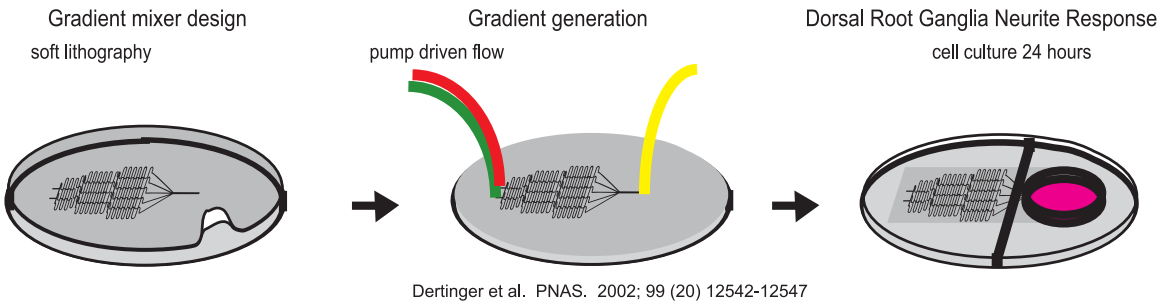

Figure B.1: Schematic of gradient fabrication methods.

ranging between -0.04ug/mL/um to -0.2ug/mL/um, and CSPG slopes ranging between -0.004ug/mL/um and -0.02ug/mL/um.

PDMS mold over the gradient channel was cut off to expose the channel for cell seeding. Dissociated dorsal root ganglia neurons (DRG) from postnatal day 0-4 rat pups were used in these experiments. DRG were cultured at 25,000 cells/well over these substrates for 24 hours, then fixed with 2% paraformaldehyde. Cell adhesion in each 50um region across the channel, neurite length and direction of neurite outgrowth were measured. All samples were run in duplicate, and data analysis was performed using ANOVA.

For pharmacological treatment against RhoGTPases to study the effects of Rho kinase in modulating the response to CSPG in parallel double cue gradients, 10uM Y27632 was applied after 1 hour to DRGs cultured on parallel gradients of LN30CS5/BSA. Image and data analysis was carried out after 24 hours in culture as described above.

Timelapse microscopy was performed on DRG cultures in LN30CSPG5/BSA substrates with and without the addition of Y27632. Gradient fabrication was performed as described above, and cell density was seeded at 100,000 cells/well. Phase-contrast images were taken at 10x. OpenLab software allowed selection of 5 fields of view along the channel for automated timelapse imaging at 10 minute intervals over 24 hours.

Data analysis of timelapse images was performed by manually tracking cell bodies and growth cones ("tips" of the neurites as determined by phase contrast). These coordinates were then used to determine the distance between cell body and growth cone, as well as the angle of this vector with respect to the channel. The angle of the vector was determined for

each time point, and each tracked cell and neurite was divided into four categories based on their outgrowth angles over time: consistently growing toward higher concentrations of LN and CSPG (180-359°), consistently growing away from higher concentrations of LN and CSPG (0-179°), turning toward LN and CSPG, or tuning away from LN and CSPG. The percentages of cells falling into each category were calculated, and the corresponding distance data for each of the angle groups was then grouped, averaged and the standard deviation was taken.

B.2 Results

B.2.1 Varying the slope of LN and CSPG parallel gradients changes the cellular adhesion patterns over the gradient channel

Cellular adhesion across the channel was evaluated by counting the number of cells in each 50um wide region as described above. Higher inlet concentrations of LN elicited relatively higher cellular adhesion in regions 1 and 2, corresponding to higher levels of higher LN and CSPG concentrations. Further, substrates with the highest inlet concentrations of LN tested (LN50+CS1/BSA and LN50+CS5/BSA), showed a graded adhesion pattern across the channel width. Lower concentrations of LN (10, 30ug/mL) applied elicited relatively higher cellular adhesion in regions 2 and 3, corresponding to moderate LN and CSPG concentrations (Figure B.2a).

Lengths of the longest neurites were compared for cultures presenting parallel double cue gradients of different slopes. Varying inlet concentrations of both LN and CSPG was found to affect neurite length, as tested using oneway ANOVA. Post-hoc tests using Bonferroni's test showed interesting comparisons between the groups tested. When the CSPG inlet concentration was held constant at 1ug/mL while LN inlet concentrations were varied between 10 and 50ug/mL, neurite lengths were significantly increased. When the CSPG inlet concentration was held constant at 5ug/mL while LN inlet concentrations were varied between 10, 30 and 50ug/mL, neurite lengths were significantly different between the samples.

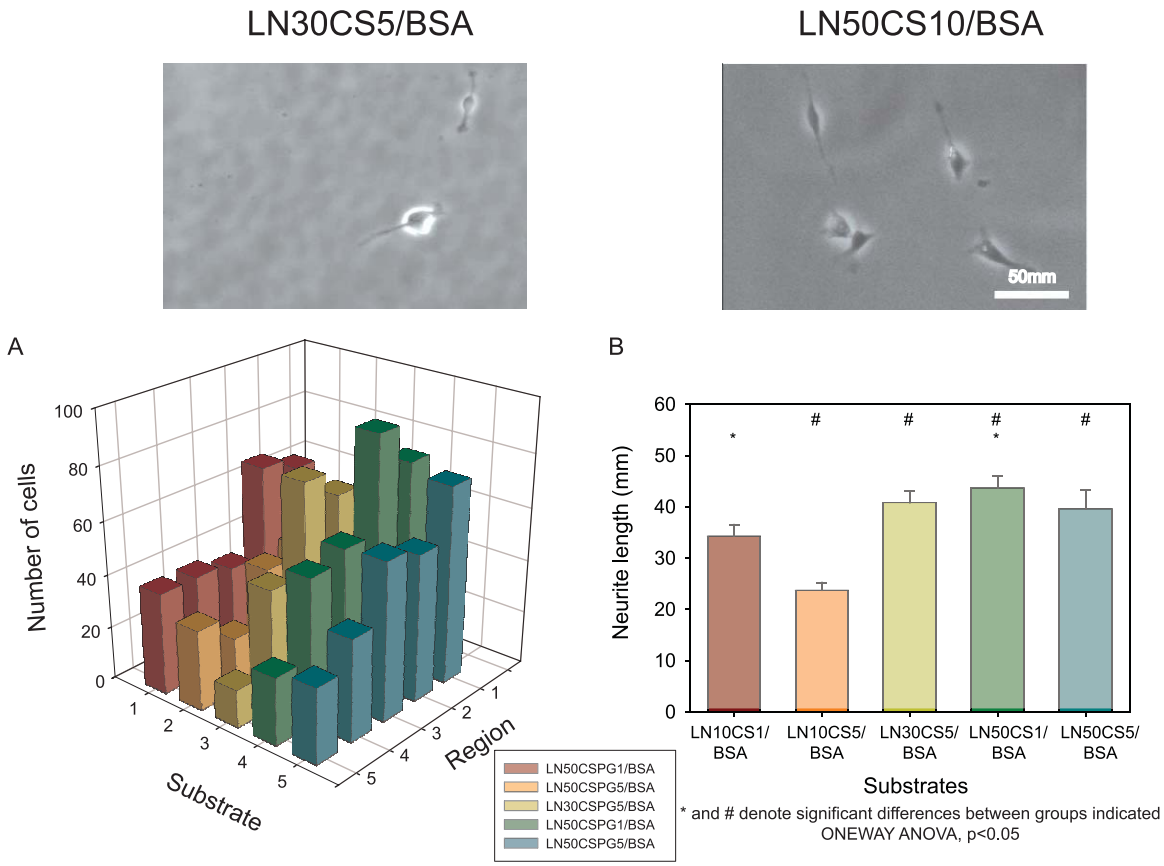

Figure B.2: Cellular adhesion (A) and neurite length (B) on parallel gradients with varying inlet concentrations and slopes of LN and CSPG.

	Cellular adhesion		Neurite length	
	% Contribution	p-value	% Contribution	p-value
LN	12.90	0.098	32.35	0.003
CSPG	62.11	0.009	58.62	0.008
Interaction	13.=6	0.090	not selected	N/A

Table B.1: Effect of LN and CSPG slopes on cell adhesion and neurite length.

B.2.2 CSPG slopes presented have a larger effect than LN slopes on cellular adhesion and neurite length on parallel gradient substrates

Using a 2 level factorial ANOVA design, the relationship between cellular responses (adhesion, mean neurite length) and inlet concentration was modeled. Equation 1 describes the relationship between LN and CSPG concentration and cell adhesion. Equation 2 describes the relationship between LN and CSPG concentration and neurite length. The statistical model showed that CSPG significantly affects cell adhesion and both LN and CSPG significantly affect neurite length. The contributions of each input parameter (inlet concentration of LN and CSPG) to the statistical model were calculated and tested for significance (Table B.1).

B.2.3 ROCK inhibition alters cell adhesion patterns on parallel LN/CSPG gradients

Parallel gradients presenting inlet LN concentration of 30ug/mL and inlet CSPG concentration of 5ug/mL show a preference for cells to adhere towards the middle of the channel, in Region 3, a region that corresponds to an intermediate concentration of both LN and CSPG. The addition of Y27632 allows more cells to adhere onto the leftmost area of the channel, Region 1, a region that corresponds with higher concentration of both LN and CSPG. This suggests that the addition of Y27632 to a culture with moderate levels of both LN and CSPG will allow cells to attach to LN rich areas that were inhibitory prior to the addition of the drug (Figure B.3).

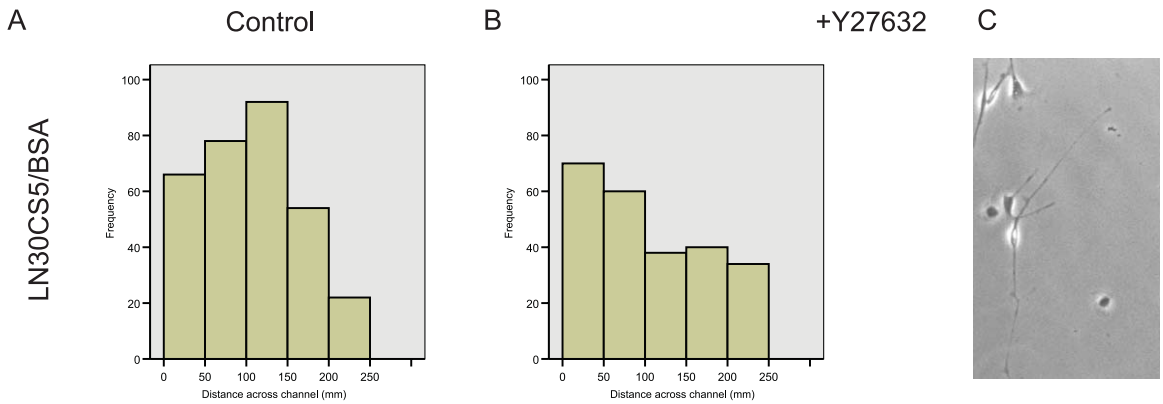

Figure B.3: ROCK inhibition alters cell adhesion patterns on parallel LN/CSPG gradients.

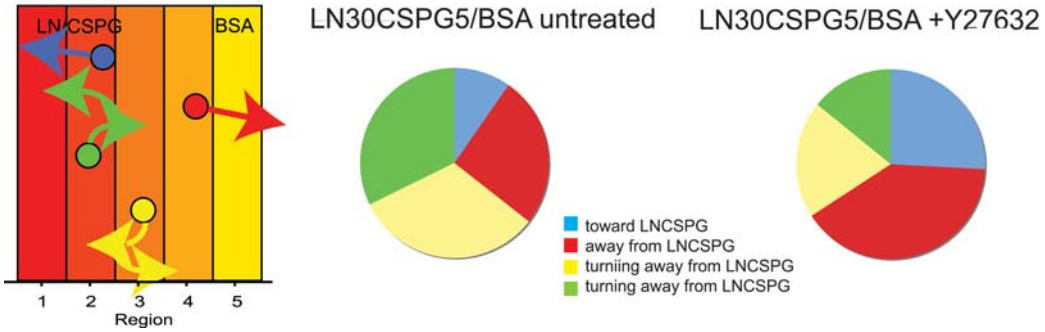

Figure B.4: ROCK inhibition increases neurite turning on parallel LN/CSPG gradients over 24 hours.

B.2.4 ROCK inhibition increases neurite turning on parallel LN/CSPG gradients over 24 hours

Timelapse anaylsis of neurite growth on LN30CS5/BSA substrates with the addition of Y27632 showed a decrease in neurite turning, in either direction (towards and away from regions of higher LN and CSPG concentrations) compared to the untreated controls (Figure B.4). On LN30CSPG5/BSA substrates with no Y27632 treatment, 67% of neurites changed directions over the 24 hour culture period, as compared to 34% on Y27632 treated cultures.

B.3 Discussion

Parallel LN and CSPG gradients of different slope were found to affect both cellular adhesion and neurite length. The complex environment of the glial scar contains both molecules, and

their interaction particularly when combined with spatial pattening of the molecule shows complex cellular responses. Studies in which antibodies to various antigens of laminin were used on substrates coated with both laminin and CSPG showed that CSPG did not interfere with the permissive effects of laminin by "masking" laminin (Qiu et al 2000). The mechanism by which these conflicting cues do interact or interefere with each other as the cell attempts to interpret them is still unclear. By varying the inlet concentration and slopes of each of the LN and CSPG gradients in a parallel gradient environment, we can start to investigate how the molecules may guide cellular adhesion or neurite outgrowth. Cellular adhesion and neurite outgrowth in this study are both more affected by CSPG inlet concentration than LN, the most marked result being that at lower concentrations of CSPG applied, LN gradients elicit selective cellular adhesion to the regions 1 and 2, corresponding to the higher LN and CSPG concentrations.

ROCK is a down stream effector of Rho, a member of the Rho family of GTPases, which has been shown to mediate neurite growth inhibition. Specifically, activation of Rho induces growth cone collapse and neurite retraction. Further, in the glial scar environment, an increase in Rho activity has been observed after injury. In this study, it was shown that ROCK inhibition was able to alter cellular adhesion patterns and increase the percentage of cells adhering to regions presenting higher molecular concentrations of CSPG. This agrees with results from previous studies which have shown that the inactivation of Rho is sufficient to stimulate axon regeneration in inhibitory encivironments (Dergham et al., 2002; Madura et al., 2004).

Dynamic stress fiber polymerization has been observed at the leading edge of growth cones (Suter and Forscher, 2000), and F-actin turnover is thought to occur rapidly at this leading edge, on the order of minutes: 3-5 minutes in neuroblastoma cells NG108-15 as visualized by photoactivation experiments (Mallavarapu and Mitchison, 1999) and up to 10 minutes in DRG growth cones (Gallo et al., 2002). Inhibiting actin turnover has been observed to cause growth cone contraction and neurite retraction (due to endogenous actomyosin contractility), and it has been hypothesized that some inhibitory cues may inhibit neurite extension by inhibiting actin turnover (Gallo et al., 2002). Hence, the mechanism by which ROCK

inhibition (thereby Rho) could promote neurite growth was investigated in this study using timelapse analysis of neurite growth dynamics. As RhoA is an important signaling molecule that governs the polymerization and depolymerization of these stress fibers in neurites; which influences neuronal motility and neurite extension, the dynamics of neurons over a 24 hour time period in culture, observed at 10 minute intervals, reflected the intracellular cytoskeletal organization. In this study, ROCK inhibition changed neurite extension/retraction dynamics and neurite turning was increased.

In conclusion, we have developed an *in vitro* model of the glial scar incorporating LN and CSPG with tunable gradient slope. LN appears to have a larger effect on cellular adhesion and neurite extension than CSPG. ROCK appears to play a large role in inhibiting neurite extension, as the inhibition of ROCK on these substrates resulted in longer neurites. ROCK appears to elicit these changes through altering neurite extension, retraction and turning, suggesting that regeneration across the scar may be successful if we can learn how to properly apply ROCK inhibitors in a directed manner. We now have a better understanding of how neurites navigate across the post injury environment of a glial scar, as modeled by two key proteins present in gradient form *in vivo*. Importantly, our data suggest that LN can play a large role in promoting cellular adhesion and neurite growth, even in the presence of the highly upregulated inhibitory molecules in the CSPG family.

B.4 References

Davies SJA, Goucher DR, Doller C, Silver J. Robust Regeneration of Adult Sensory Axons in Degenerating White Matter of the Adult Rat Spinal Cord. J. Neurosci., 1999; 19: 5810-22.

Dergham P, Ellezam B, Essagian C, Avedissian H, Lubell WD, McKerracher L. Rho signaling pathway targeted to promote spinal cord repair. J Neurosci, 2002; 22: 6570-7.

Fitch MT, Silver J. Glial cell extracellular matrix: boundaries for axon growth in development and regeneration. Cell Tissue Res, 1997; 290: 379-84.

Gallo G, Yee HF, Jr., Letourneau PC. Actin turnover is required to prevent axon retraction driven by endogenous actomyosin contractility. J. Cell Biol., 2002; 158: 1219-28.

Jain A, Brady-Kalnay SM, Bellamkonda RV. Modulation of Rho GTPase activity alleviates chondroitin sulfate proteoglycan-dependent inhibition of neurite extension. J Neurosci Res, 2004; 77: 299-307.

Jones LL, Margolis RU, Tuszynski MH. The chondroitin sulfate proteoglycans neurocan, brevican, phosphacan, and versican are differentially regulated following spinal cord injury. Exp Neurol, 2003; 182: 399-411.

Madura T, Yamashita T, Kubo T, Fujitani M, Hosokawa K, Tohyama M. Activation of Rho in the injured axons following spinal cord injury. EMBO Rep, 2004; 5: 412-7.

Mallavarapu, A., and Mitchison, T. Regulated actin cytoskeleton assembly at filopodium tips controls their extension and retraction. J. Cell Biol, 1999; 146:1097–1106.

Morgenstern DA, Asher RA, Fawcett JW. Chondroitin sulphate proteoglycans in the CNS injury response. Prog Brain Res, 2002; 137: 313-32.

Sandvig A, Berry M, Barrett LB, Butt A, Logan A. Myelin-, reactive glia-, and scar-derived CNS axon growth inhibitors: expression, receptor signaling, and correlation with axon regeneration. Glia, 2004; 46: 225-51.

Suter DM, Forscher P. Substrate-cytoskeletal coupling as a mechanism for the regulation of growth cone motility and guidance. J Neurobiol, 2000; 44: 97-113.

Tom VJ, Steinmetz MP, Miller JH, Doller CM, Silver J. Studies on the Development and Behavior of the Dystrophic Growth Cone, the Hallmark of Regeneration Failure, in an *In Vitro* Model of the Glial Scar and after Spinal Cord Injury. J. Neurosci., 2004; 24: 6531-9.

Appendix C

Bridging and motility on micropatterned grooves

C.1 Introduction

Neurons and glia respond to physical cues in their microenvironment. Surface topography has been shown to be important for tissue engineering, as a way in which biomaterials can influence cell behavior. Topographical features can direct a wide range of cellular functions such as activation, orientation, and migration (reviewed in (Curtis and Wilkinson, 1997)). One specific way in which topography can induce changes in cell response is through contact guidance, where anisotropic topographical features direct cells to align their orientation and morphology along the long axis of topographical features (Manwaring et al., 2004; Rajnicek and McCaig, 1997). The contact guidance phenomenon has been described in particular in regard to the response of cells to repeating grooved topography over a wide range of microscale features (Song and Uhrich, 2007). Many cell types have been shown to exihibit contact guidance when cultured on grooved substrates presenting nano- to micro-scaled features, including fibroblasts, astrocytes and neurons. Schwann cells (SC) in particular, have been shown to increase alignment to microgrooved substrates, as compared to flat substrates presenting no topographical cue (Hsu et al., 2005; Miller et al., 2002).

Anisotropic topographical features may also direct cell responses in a different manner from contact guidance. Grooved topographical features can also direct cells to extend across grooves and plateaus, with no apparent underlying support. This morphology, termed "cellular bridging" has been observed in primary neurons: dorsal root ganglia (DRG), hippocampal, neuroblastoma (B104) cells, SC, and fibroblasts (Goldner et al., 2006). Cells exhibit complex interactions with grooved substrates, where complex mechanisms of cell adhesion, process extension and tension are required for pulling a cell 50µm above its initial adhesion point.

Molecular cues also provide guidance information for neurons and glia. In the context of topography, non-uniformity in protein deposition on the edges of topographical features has been proposed to play a role in contact guidance (Lopez et al., 1993). Experiments studying the morphology of focal adhesion formations on fibroblasts on microtextured surfaces have shown that these surfaces can influence the orientation of intracellular and extracellular proteins (den Braber et al., 1998). Hence the presentation of both molecular and topographical cues may have synergistic effects on neurite outgrowth.

In this study, we evaluated the formation and dynamics of DRG and SC bridges on microgrooved substrates presenting different patterns of molecular cues using different methods of protein deposition (adsorbed and covalent binding of proteins to surfaces). Here we show that there are differences in DRG and SC adhesion preferences and bridging morphology, and that the cells undergoing the bridging formation process are highly motile and dynamic.

C.2 Materials and Methods

All reagents were obtained from Invitrogen unless otherwise specified.

C.2.1 Substrate preparation

Microgrooved substrates were fabricated using photolithography and soft lithography as described in Goldner et al. (Goldner et al., 2006). Briefly, masks containing the substrate

patterns were designed using AutoCAD, as a series of repeating lines 50µm wide, spaced 70µm apart, over a 1cm x 1cm area. Patterns were transferred onto silicon wafers using photolithography. Substrates for cell culture were then made by fabricating poly(dimethylsiloxane) (PDMS) impression replicas with 1-2mm thickness, of the pattern from the silicon wafer masters.

C.2.2 Protein coating

Several micropatterns were fabricated using both passive adsorption techniques and covalent attachment techniques. Several surfaces were selectively coated, all surfaces (total), plateau surfaces (plateau) and groove and wall surfaces (groove). Schematic of each are shown in Figure C.1.

C.2.2.1 Adsorption

Substrates were coated via adsorption with either 3% fluorescein isothiocyanate conjugated bovine serum albumin (FITC-BSA) or 50µg/mL LN. For coating on all surfaces (total coating), substrates were plasma activated at 10.5W for 60 s with a plasma cleaner/sterilizer (PDC – 32 G, Med RF level, Harrick), sterilized by immersion in 70% ethanol, and rinsed with sterile dH2O. Substrates were incubated with protein solutions for one hour, and rinsed with dH2O before plating.

For selective coating on surfaces of groove floors and walls (groove coating), the edges of the grooved substrates including the ends of the grooves were removed, creating channels. PDMS substrates were plasma activated as described above and reversibly adhered to a glass coverslip. FITC-BSA or LN solutions were applied to the open ends of the channel, allowing capillary action to passively draw the protein solution into the channels. Excess protein solution was applied at each end of the channel to prevent drying, and incubated at room temperature for 1 hour. Excess protein was then removed using an air stream and the PDMS substrate was then removed from the coverslip.

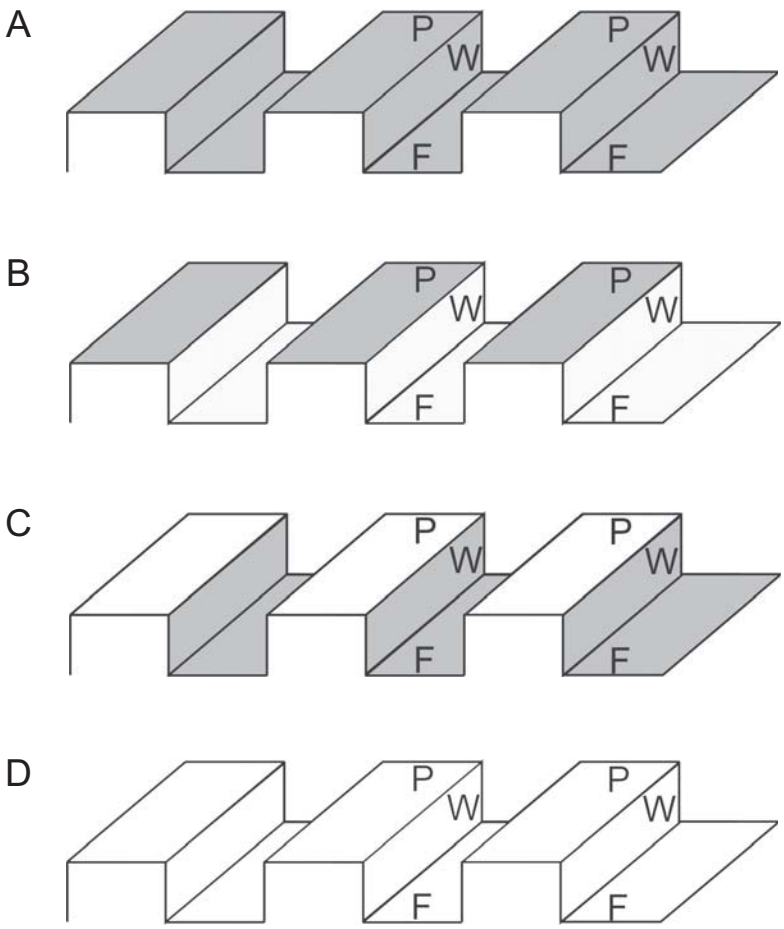

Figure C.1: Selective micropatterns of microgrooved substrates.
(A) total coated and (B) plateau coated substrates were fabricated via adsorption and covalent attachment methods, (C) groove coated substrates were fabricated via adsorption only, and (D) shows substrates with no surface modification. P, plateau, W, wall and F, floor.

For selective coating on plateau surfaces (plateau coating), a modified method of microcontact printing was used. Glass coverslips were submerged in 10% sodium docecyl sulfate (SDS; Sigma-Aldrich) and sonicated, rinsed in dH2O and dried. Coverslips were coated with 50µg/mL LN for one hour, and excess protein solution was removed using an airstream. PDMS substrates were plasma activated as described above and reversibly adhered to the coated glass coverslip for 1 hour at room temperature before being removed from the coverslip.

C.2.2.2 Covalent protein attachment

Substrates were coated covalently with ,either 3% FITC-BSA or 50µg/mL LN. Substrates were cleaned by immersion in 10% SDS solution and sonicated for 5 minutes. Substrates were rinsed with distilled H2O, then methanol, and baked at 45°C for 5 minutes. Substrates were then incubated with 5% 3-Aminopropyl Trimethoxysilane (APTS, Aldrich) in 100% ethanol at 30rpm for 10 minutes. Substrates were then rinsed with ethanol, dried, then baked at 80°C for 2 hours. The substrates were then coated with a 5mg/ml solution of the crosslinker Bis[sulfosuccinimidyl] suberate (BS3, Pierce) in Phosphate Buffered Saline (PBS) for 20 minutes at room temperature. Substrates were rinsed with PBS to remove excess BS3. For control samples, substrates were then dried with pressurized air in preparation for cell seeding. Protein solutions were then applied depending on the micropattern desired. For uniformly coated samples, substrates were then coated with protein solution for 1 hour at room temperature. For plateau coated samples, substrates were microstamped with a coverslip coated with protein solution (as described above). For orthogonally coated samples, substrates were microstamped with an adsorbed protein coated grooved substrate (as described above), applied orthogonally to underlying grooved substrates.

C.2.3 Cell culture

Dissociated DRG neurons from postnatal day 0-4 rat pups were used in these experiments. DRG were seeded at 110,000 cells/mL for bridging experiments. DRG were cultured in

Dulbecco's Modified Eagle Medium (DMEM), 10% fetal bovine serum (FBS), penicillin (100U/mL), streptomycin (100µg/mL) and 50ng/mL nerve growth factor, on microgrooved substrates described above for 24 hours.

SC from adult rat sciatic nerve (SC, P4 through P10, a gift from the Bunge lab) were used in these studies. SC were cultured in DMEM supplemented with 10%FBS, 1% L-glutamine, 2µM forskolin, 10µg/mL bovine pituitary extract, 226µM heregulin (gift from Genentech), and penicillin (100U/mL), streptomycin (100µg/mL) (SC media) on poly(L-lysine) coated surfaces 0.01% (PLL; Sigma). SC were seeded at 50,000 cells/mL for adhesion and endpoint bridging studies and 25,000cells/mL for timelapse studies.

Two methods of cell seeding were used in these studies: drop seeding, where the cell suspension with the final seeding density in 200 μL was dropped onto the surface of the microgrooved substrates. After the initial incubation at 37° for 3 hours with 200μL media where the cells adhered to the substrated, 3mL of media was added to the cultures. In solution seeding, a cell suspension with the final seding density in 5mL of media was added to the culture dish with the microgrooved substrate. Culture dishes were gently agitated (30rpm, 10min) for more even seeding across the entire substrate surface. Drop seeding was used for all DRG cultures, both drop seeding and solution seeding were used for SC cultures and specified in the relevant sections. Solution seeding was used for all SC timelape studies.

C.2.4 Image analysis

Epifluorescence microscopy with a Nikon Eclipse TE2000-S was used to visualize LN coated surfaces after immuohistochemistry. Phase contrast microscopy using a Nikon Eclipse TE2000-S was used to visualize cellular bridges. All analysis was performed on unfixed samples. A bridge was defined as a cell extension or cell body that spanned from one plateau or wall to the adjacent plateau or wall without underlying support. Distinction between bridge types was determined by varying the depth (z) plane of focus and determining the depth at which bridges formed. This was easily distinguishable as the bridge came into focus at specific focal planes that corresponded to the depth at which the bridge formed. Most

analyses done in this study was on "plateau-level bridges," defined as bridges that formed in z-planes within -10µm of the plateau. Some analysis was done on "wall bridges," defined as bridges that formed in z-planes between -10µm and -40µm from the plateau. For total coated and plateau coated samples, cells and bridges on 10 grooves were evaluated on n=2 or n=3 samples. For groove coated samples, cells and bridges on 20 grooves were evaluated on n=3 samples, as substrate preparation of groove coated samples required cutting half of the available grooved area.

C.2.5 Scanning electron microscopy

To visualize cellular morphologies and cellular bridges under scanning electron microscopy (SEM), samples were fixed using Karnovsky's fixative for 3 hours, rinsed in 0.1M sodium cacodylate buffer, and postfixed in 1% osmium tetroxide (OsO4) in 0.1M cacodylate buffer for 1hour. Samples were incubated in 1% thiocarbohydrazide (TCH) for 30 minutes, 0.5% OsO4 for 30 minutes and dehydrated using graded ethanols to 100% ethanol. Following air-drying and gold-palladium sputter coating, samples were imaged using a Hitachi S-270 SEM with 15kV acceleration voltage.

C.2.6 Timelapse analysis

Phase contrast images of four fields of view (two in the center of the grooves and two at groove edges) were captured every 10 minutes over 24 hours. Images at each field of view were captured as z-stacks of 70µm, with seven z-planes with 10µm intervals. Z-stacks were oriented so that an image was taken at 10µm above the level of the plateau and 10µm below the level of the groove. After 24 hours, image sequences were organized for analysis with Volocity software and exported as Quicktime movies.

Soma of individual SC were tracked over 24 hours using ImageJ Manual Tracker. Z-positions of soma over time were recorded and from those data, distance and velocity were calculated. Velocity was calculated both over the each 10 minute interval, and over the climbing period of bridge formation.

C.2.7 Modeling of force generation during bridging process

Tension forces required to pull a soma upwards on the groove were modeled as a system of two cables in static equilibrium. Figure C.2 shows a free body diagram with forces acting on the soma at particular geometries during bridge formation. Assumptions include no translational and rotational motion by the soma, equal contribution of each process, and frictionless and massless processes. Equations listed in Figure C.2 show the force calculations and parameters for the model. Figure C.2 shows the input parameters used in the force calculations, F_{zT} = forces in z direction, F_T =tension force, F_b =buoyancy force, F_d =drag force, F_g =force due to gravity, m=mass, a =acceleration, R =radius of cell, ρ =density. Values for cell density from (Schnaar and Schaffner, 1981).

C.3 Results

C.3.1 Preferential adhesion on micropatterned grooves

DRG and SC adhesion at 3 hours and 24 hours were evaluated on micropatterned substrates with selective LN coating. The majority of DRGs on all substrates tested were in the grooves at both 3 hours and 24 hours (Figure C.3). For SC on substrates with plateau or groove LN coating, the majority of cells initially adhered on surfaces in grooves at 3 hours, and moved onto the plateau surfaces by 24 hours in culture. For SC on substrates with total LN coating, cells were more evenly dispersed between groove and plateau surfaces at 3 hours, and more cells adhered on the plateau surfaces at 24 hours (Figure C.3).

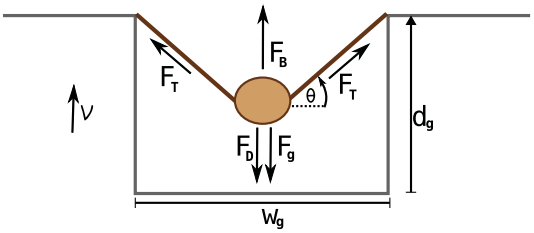

$$F_g = mg$$

$$F_b = -mv\rho g$$

$$F_d = -6\pi\eta r V$$

$$\sum F_{z=} ma = 0 = 2F_T \sin\theta + F_B - F_g - F_d$$

Parameters	SC	DRG
Cell density (g/cm^2)	1.049	1.004
Media density (g/cm^2)	1.00	1.00
Viscosity, η	1.69E-3	1.69E-3
Volume (μm^3)	8540	53400
Mass (g)	8.57E-9	5.36E-8

Figure C.2: Free body diagram showing forces acting on a cell soma during bridge formation under static equilibrium and input parameters used in the model.
Where F_g =gravitational force, F_b =buoyancy force, F_d =drag force, m= mass, g= acceleration due to gravity, v = specific vlume, ρ =density, η =viscosity, r= radius, V = velocity

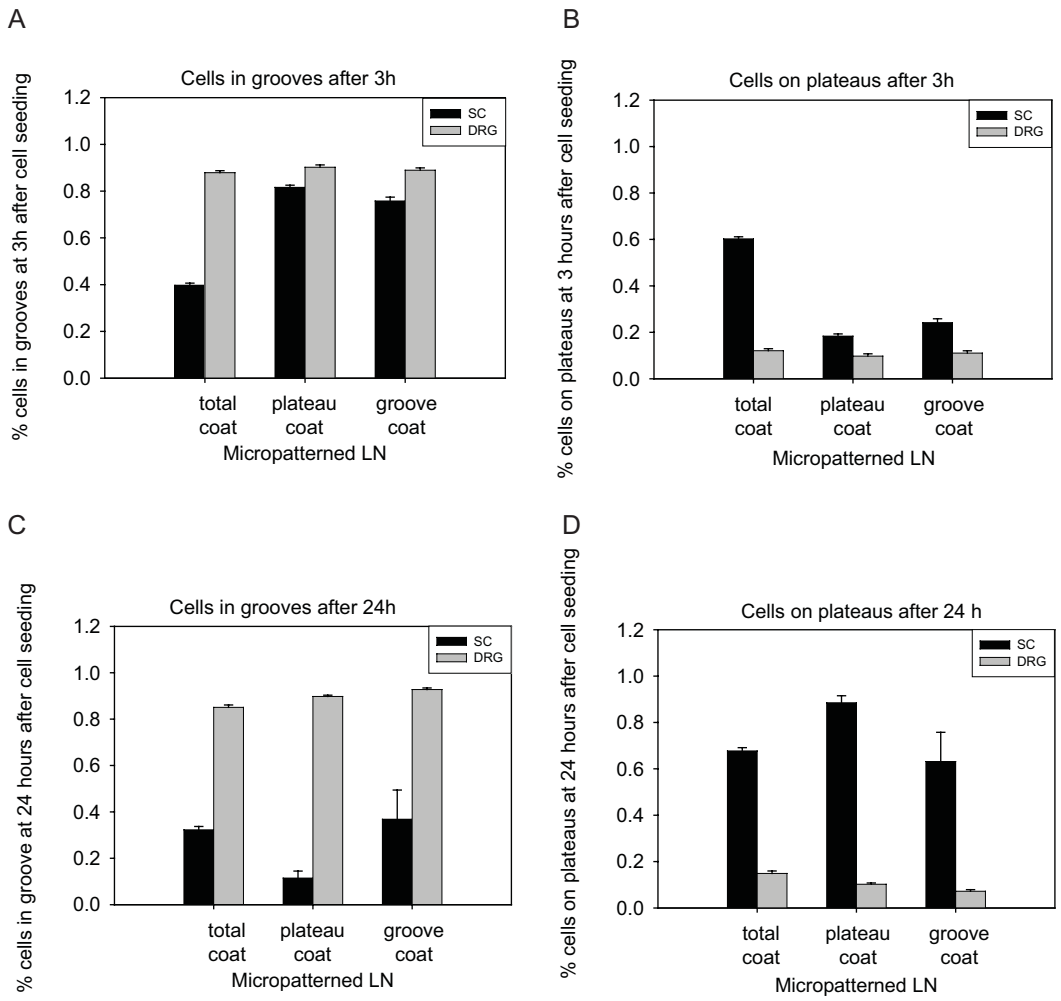

Figure C.3: Preferential cellular adhesion on micropatterned substrates.
(A) At 3 hours, DRG preferentially adhered to grooves on all micropatterned LN substrates tested. SC preferentially adhered to grooves, on plateau and groove coated substrates, and adhered to plateaus on total coated substrates. (B) At 24 hours, DRG preferentially adhered to grooves on all micropatterned LN substrates. SC preferentially adhered to plateaus on all micropatterned LN substrates.

C.3.2 Bridges across micropatterned grooves exhibit several stereotypic morphologies

DRG and Schwann cell processes formed bridges with diverse morphologies. Bridges were classified as "plateau" bridges and "wall" bridges, based on the depth at which the bridges were formed, as described in section C.2.4 (Figure C.4a, b). Plateau bridges were further classified as (1) "typical" bridges, described in Goldner et al. (Goldner et al., 2006), processes across two adjacent plateaus with no underlying support at the center of the groove (Figure C.4a), (2) "soma" bridges where a cell body along with processes spanned across two adjacent plateaus and (3) "end" bridges where processes across two adjacent plateaus at the groove edge (Figure C.4c). Bridges have been observed to be composed of a single neurite or multiple neurites, and qualitatively DRG bridges appear to be more complex, with more cell-cell interactions than Schwann cell bridges.

C.3.3 SC exhibit much higher incidence of bridging on selectively coated grooved substrates

The number of bridges formed over 24 hours on micropatterned susbtrates with selective LN coating was evaluated for DRG and Schwann cell culture. Only plateau bridges were evaluated in this comparison. SCs formed more bridges than DRGs on all substrates tested (Figure C.5). It is interesting to note that both SCs and DRGs were able to form bridges on selectively coated (plateau and groove coated) substrates using the drop seeding method.

C.3.4 Method of protein attachment on microgrooved substrates affects SC bridging

Protein coating was performed both by passive adsorption of LN solutions onto plasma activated PDMS surfaces, as well as covalent attachment of LN using bifunctional linkers APTS and BS3. Attachment of FITC-BSA showed that even coating was achieved using

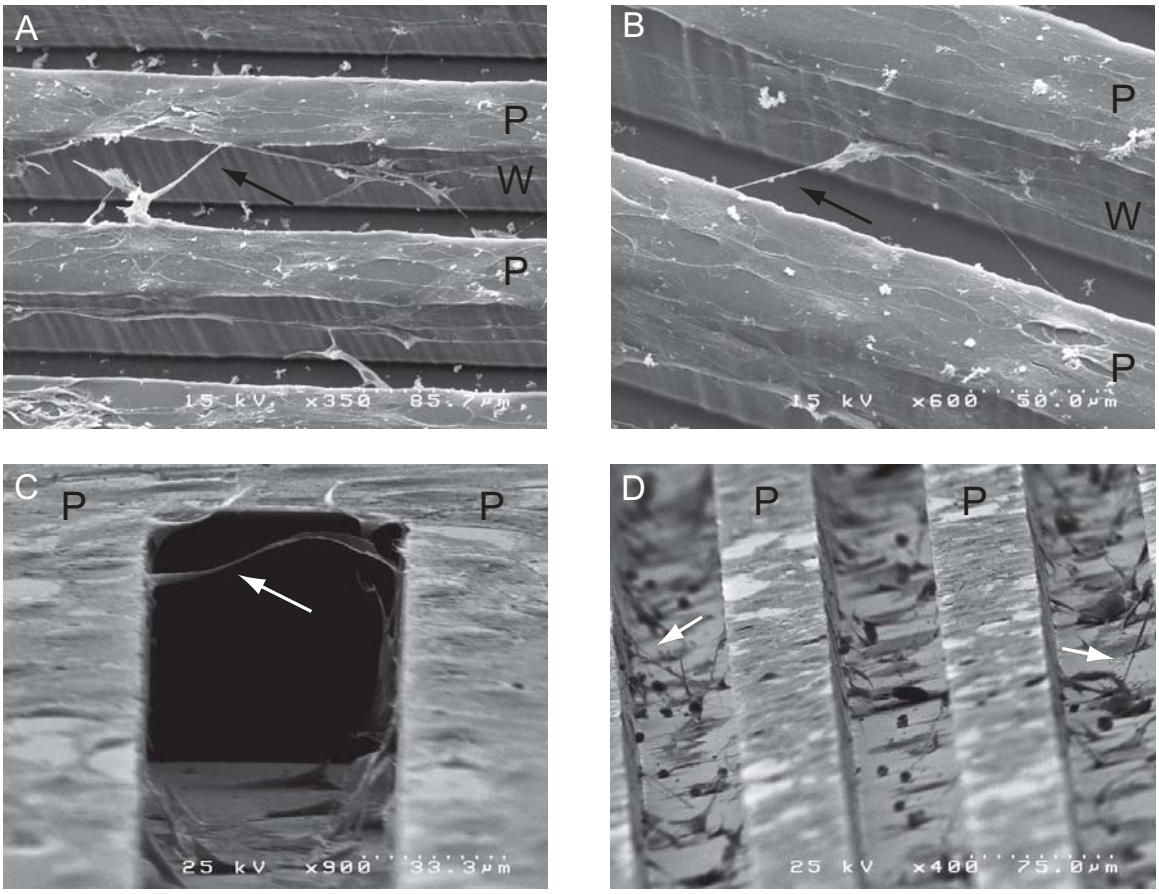

Figure C.4: Scanning electron micrographs of SC bridges of various morphologies. (A) plateau bridges with extensions at the z-plane of the plateau, (B) wall bridges, (C) end bridges that occur on the edge of the groove, and (D) floor-to-wall bridges. Only plateau bridges were evaluated for studies using DRGs, SCs on covalently attached LN substrates and timelapse studies. Plateau and wall bridges were evaluated in studies with SCs on adsorbed LN substrates. P, plateau, W, wall and arrow indicate bridges.

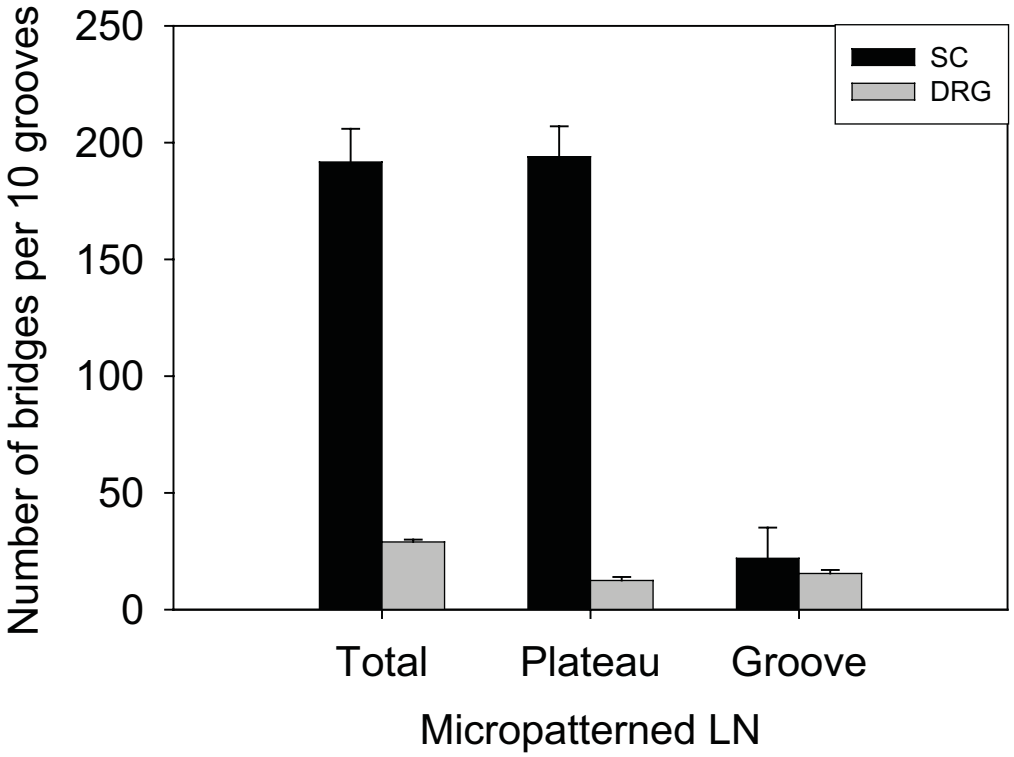

Figure C.5: Differences in bridge formation between SC and DRG on micropatterned grooves.
SC formed significantly more bridges than DRG on total and plateau coated substrates. These studies were performed using the drop seeding method during cell seeding on microgrooved substrates.

Bridge type	SC	DRG
fast (time to bridge in min)	<300	<1200
slow(time to bridge in min)	>300	>1200
variant	change in z direction	

Table C.1: Criteria for bridge types used in timelapse analysis

both of these methods, and selective coating of specific surfaces was feasible using micro-contact printing techniques. SC were seeded using the solution seeding method, and SC bridges on total and plateau coated substrates were directly compared (Figure C.6). SC plateau bridges formed on total LN coated substrates by either method, but significantly more bridges formed on covalent than on adsorbed LN substrates (t-test $p<0.05$). SC bridges were unable to form on adsorbed plateau LN coated substrates, but were observed on covalent LN coated substrates (Figure C.7). SC bridging on grooved substrates coated with intermediary chemicals used in the covalent linking process was also evaluated as a control (Figure C.7b).

C.3.5 Bridge formation dynamics

Soma of DRG and SC were tracked in the z-direction over time as bridges were forming over grooved substrates. This data was plotted in several ways to visualize cell trajectories over time: (1) all z heights measured for a particular cell type was averaged over each timepoint to obtain an "average" trajectory for the cell type (Figure 7a, b), (2) bridges were sorted by their dynamics into "fast", "slow" and "variant" (criteria listed in Table C.1 for each cell type), grouped and averaged over each timepoint for the average trajectory for each bridge type (Figure 7c, d), (3) only the climbing phase of the soma were evaluated such that t0 was taken to be when the soma was observed to make its first movement in the z-direction to determine the stereotypic trajectory each cell type (Figure 7e,f).

Average trajectories of SC (Figure 7a) and DRG (Figure 7b) show differences between SC and DRG bridging dynamics. DRG appear to make constant upward progress in the groove, whereas SC appear to have a climbing phase (0-400min), a suspension phase (400-800min) and then a climbing phase (800-1200min). This could be an effect of more variable SC

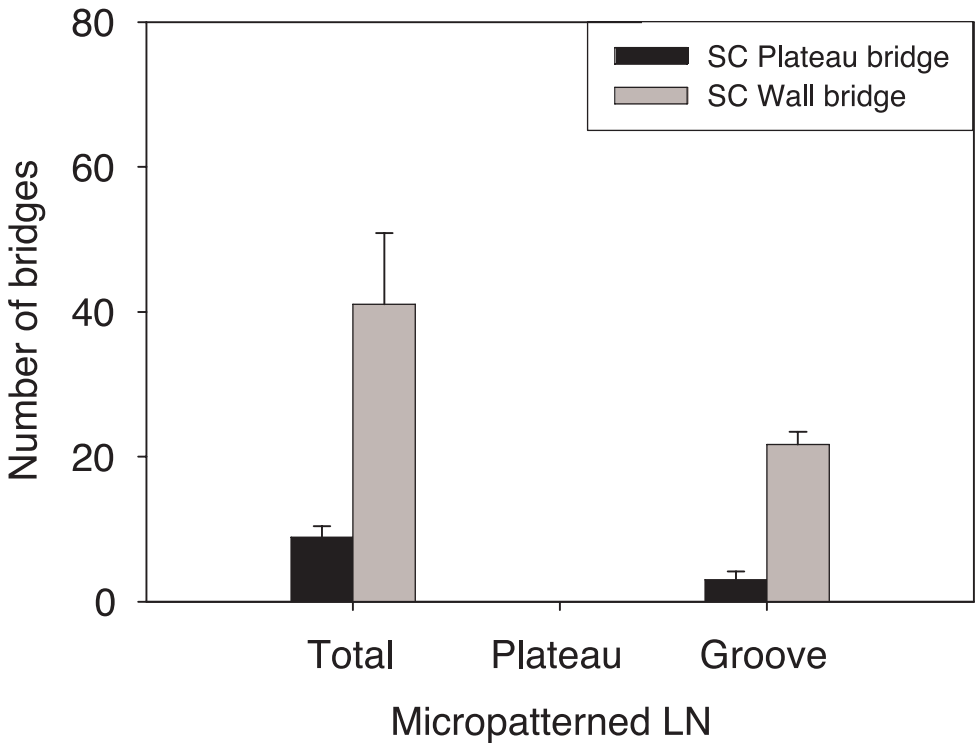

Figure C.6: Differences in SC bridge types between substrates with different micropatterned coatings.
SC preferentially form wall bridges on total and groove coated substrates. SC did not form bridges on plateau coated substrates. These studies were performed using the solution seeding method during cell seeding on microgrooved substrates.

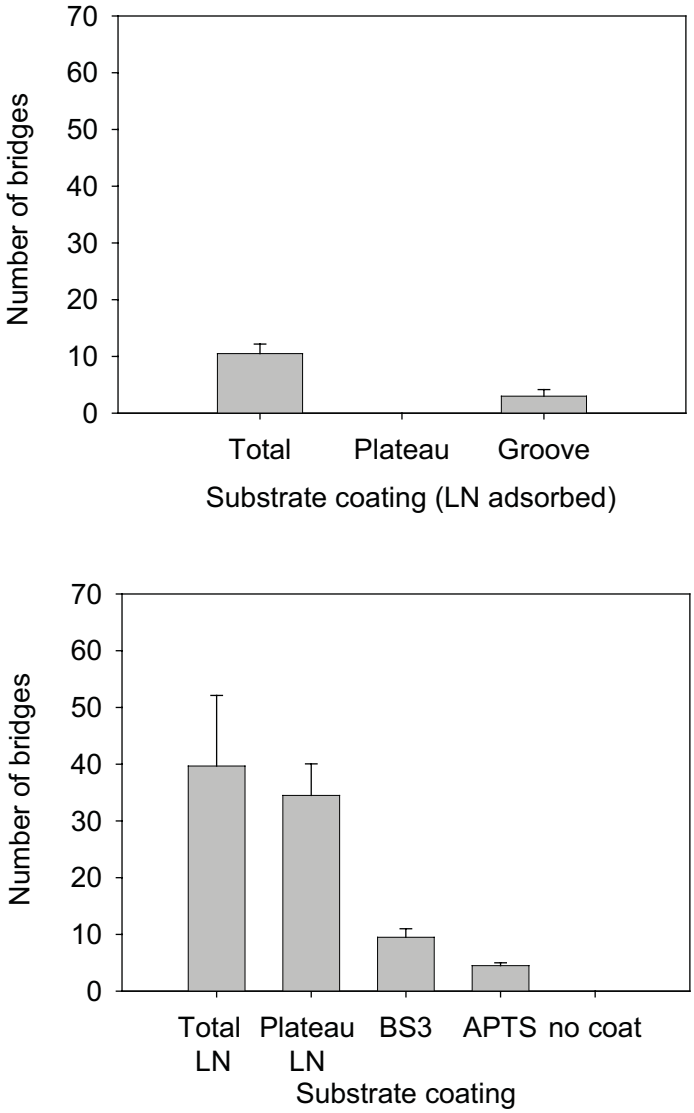

Figure C.7: SC formed more bridges on (B) covalently coated substrates than (A) adsorption coated substrates.
SC were able to form bridges on covalent plateau coated substrates. SC were also able to form bridges on coatings of intermediate chemicals used in the covalent attachment process (B).

	SC	DRG
F_g (N)	-8.79E-11	-5.25E-10
F_b (N)	8.37E-11	5.23E-10
F_d(N)	1.38E-15	5.36E-16
F_{zT}(N)	-1.72E-10	-1.05E-9

Table C.2: Gravitational, Buoyancy, Drag and Tension forces generated by SC and DRG during bridging as calculated by static equilibrium model.

bridging dynamics. The variability can be seen in Figure 7c, where the three types of SC bridges, fast, slow and variant were graphed and shown to be very different from each other. DRGs were more consistent in their trajectories as seen in Figure 7d. To determine if there were stereotypic climbing paths of SC and DRG, we reorganized the data so time 0 was taken to be the time at which climbing started. Figures 7e, f show that for SC, the initial climbing phases (<100min) between all bridges were very similar in trajectory and speeds, whereas the intermediate climbing phases (200-600min) for DRG bridging was much more consistent than the initial and ending phases of bridging.

C.3.6 Forces generated during cellular bridging

Table C.2 shows the estimated forces associated with the static equilibrium system, and the minimum amount of force generation in the z direction required by the cells to form bridges using two processes. DRG bridges appear to require a larger force than SC bridges, based on differences in soma size, and upward velocity of the cells. Figure C.9 shows the calculated tension forces (F_T) each process is required to generate as the soma moves up the groove. In these calculations, a cell is assumed to have only two processes, and forces required are then based on the geometry of static loading. This correlates to experimental observations of bridge morphology, where DRG neurite bridges are more likely than SC to involve networks of neurites, and more neurites appear to be involved in bridging. This could be due to the larger forces needed to form DRG bridges.

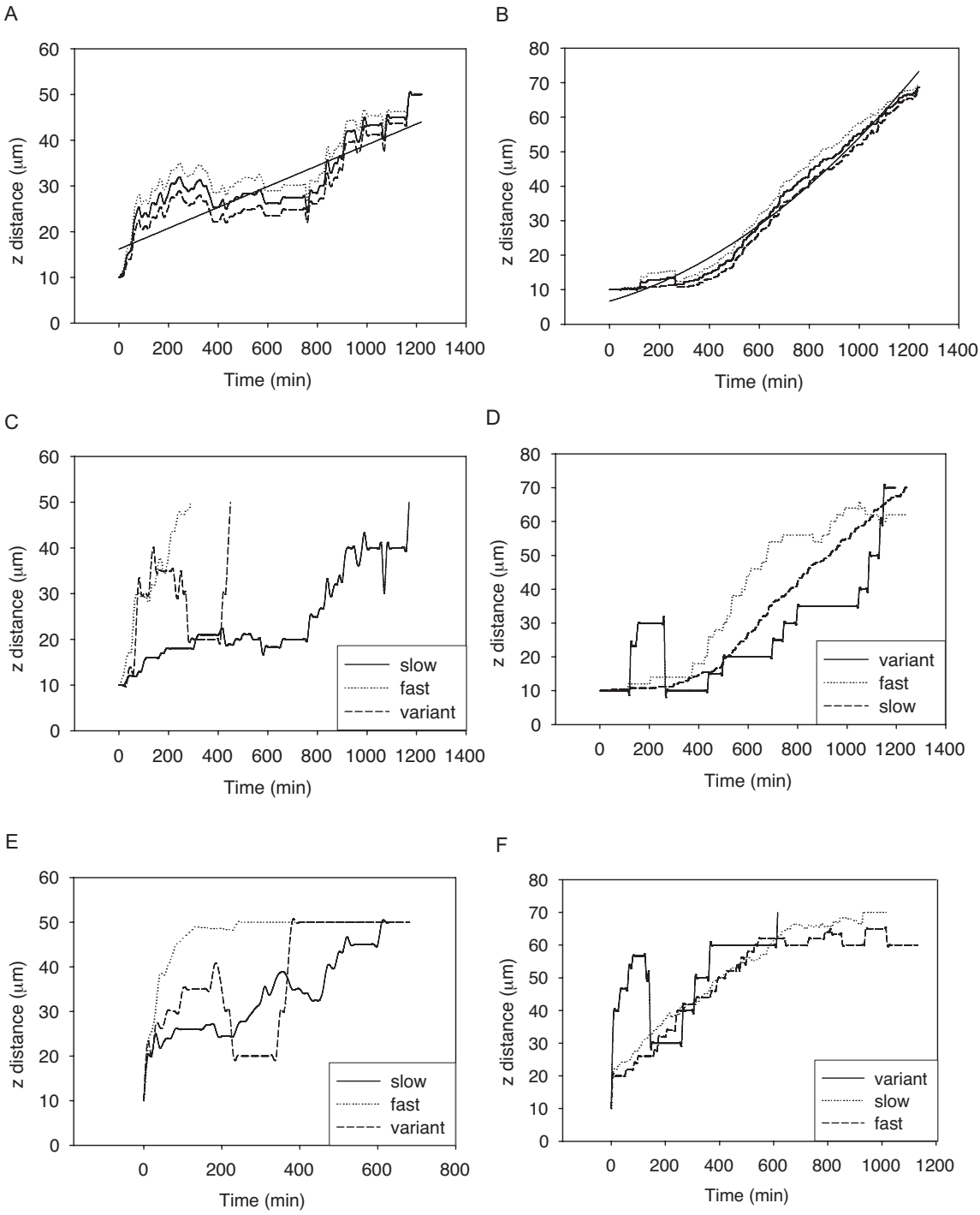

	SC	DRG
Velocity (μm/min)	0.521	0.101
Climbingvelocity (μm/min)	0.454	0.126
Time to reach plateau (min)	33.29	1015.5

Figure C.8: Timelapse trajectories of SC and DRG bridging and associated velocities. Trajectory data show data ± SEM of average z-distance of all SC bridges (A) and all DRG bridges (B) over time. Regression lines are fitted to each set of trajectory data, shown on graph. Trajectory data was then separated into "fast," "slow" and "variant" bridge types and plotted for SC (C) and DRG (D) bridges. Trajectory data was then normalized at the start of climbing, to normalize change in z direction. Average of climbing trajectories for (E) SC and (F) DRG were plotted.

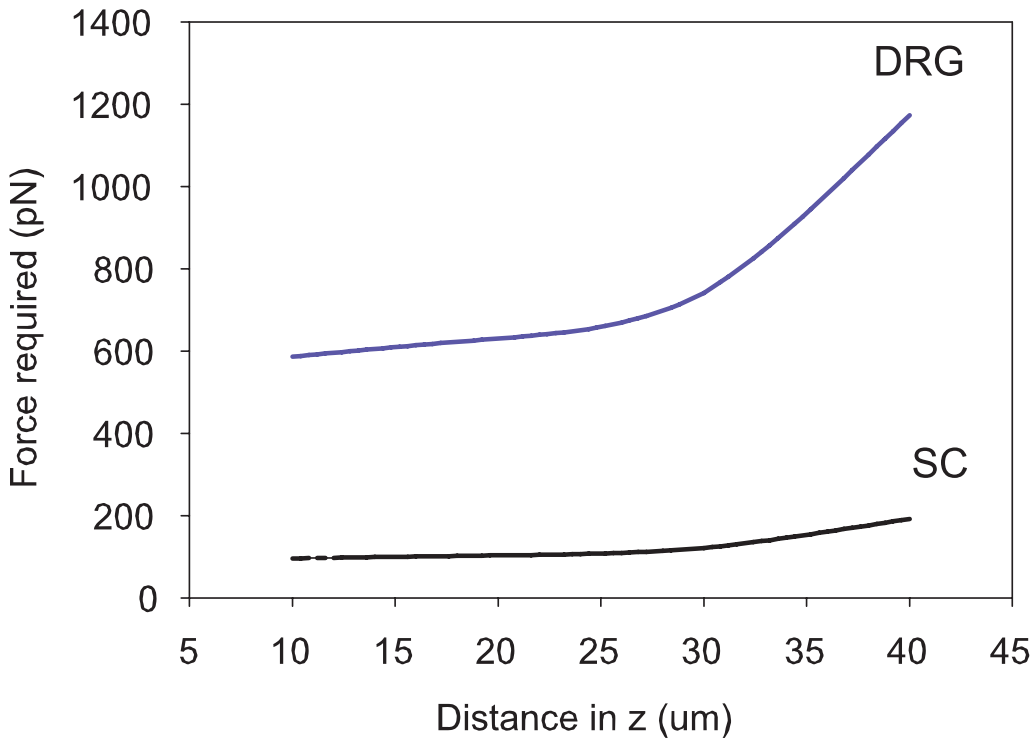

Figure C.9: Forces required during bridging process at soma moves up a groove.

C.4 Discussion

Extensive studies have shown that micropatterned coatings with permissive molecules and microgrooved topographies are able to direct neurons and glia in culture. Cellular bridging has been described as a phenomenon where cells pull their soma vertically upwards within a groove. Hence, how this bridging process occurs is of interest and in this study we studied several factors such as cellular adhesion, selective micropatterns of LN, and varied coating methods of LN to clarify their influence on the bridge formation process.

LN is an important extracellular matrix molecule for both cellular adhesion and the formation of protrusions for DRG and SC. DRG (Li et al., 2008) and SC (McCarthy et al., 1983) have shown haptotactic migration up gradients of LN in traditional two dimensional cell culture. Selective coating with LN on 3D substrates allows us to observe preferential seeding and migration on distinct areas of LN coating or no coating, depending on the micropattern applied. Differences between DRG and SC adhesion patterns on microgrooved substrates were observed, where initial cell seeding (after 3 hours) did not appear to achieve uniformity in cellular adhesion, where the majority of all cells adhered to the surfaces of the grooves. However at 24 hours, the majority of DRG remained in the grooves whereas the majority of SC were observed on the surfaces of the plateaus. This may indicate a higher motility of SC as compared to DRG.

Comparison of bridging at 24 hours also showed that SC formed significantly more bridges than DRG, under similar cell seeding conditions. Initial cell seeding conditions were varied slightly between SC and DRG as SC replicate while DRG neurons do not divide. SC were seeded at 50,000 cells/ substrate and DRG were seeded at 110,000 cells/substrate, and SC formed more bridges after 24 hours. Cell-cell interactions are involved in the bridging phenomenon as shown in Goldner et al. (Goldner et al., 2006), where an optimal cell seeding density of 125,000 cells/substrate was reported. In the subsequent parts of this study, cell seeding density was adjusted for optimal bridging density at 24 hours in order to make comparisons across different micropatterns on microgrooved substrates.

Coating method was found to significantly affect bridge formation on both types of mi-

cropatterned LN substrates tested (total and plateau coated substrates). Covalent binding of proteins is hypothesized to be a more controlled way of protein deposition and hence more effective in allowing cells to adhere to these surfaces. Studies with L1 and fibronectin have shown that adsorption with poly-D-lysine and covalent binding show similar amounts of protein on the substrate. However, depending on cell type, covalently attached L1 and fibronectin may or may not have an effect on cellular adhesion and neurite length (Webb et al., 2001). Covalent attachment of Tyr-Ile-Gly-Ser-Arg (YIGSR), a peptide found on the B1 chain of LN was found to allow for higher strengths of NG108-15 adhesion than compare to adsorbed LN (Cargill et al., 1999). Hence adhesion and process outgrowth on these substrates may be different. Our studies agree with these observations, where increased SC bridging was observed on covalently attached LN surfaces.

Timelapse studies show highly dynamic SC and DRG cultures and allowed the study of bridges that formed before the 24 hour period in endpoint studies. Cell motility appears to play a role in the bridging process, and within each cell type there are different trajectories and motilities exhibited by the cell. Metabolic and cytoskeletal functions could affect bridging dynamics and morphologies and would be a future direction of the research.

Topography is capable of eliciting various morphologies from neurons and glia, and understanding the underlying mechanisms by which bridges form and stabilize are important for understanding the roles of the microenvironment on the neurite growth phenomenon.

C.5 References

Cargill RS, Dee KC, Malcolm S. An assessment of the strength of NG108-15 cell adhesion to chemically modified surfaces. Biomaterials, 1999; 20: 2417-25.

Curtis A, Wilkinson C. Topographical control of cells. Biomaterials, 1997; 18: 1573-83.

den Braber ET, de Ruijter JE, Ginsel LA, von Recum AF, Jansen JA. Orientation of ECM protein deposition, fibroblast cytoskeleton, and attachment complex components on silicone microgrooved surfaces. J Biomed Mater Res, 1998; 40: 291-300.

Goldner JS, Bruder JM, Li G, Gazzola D, Hoffman-Kim D. Neurite bridging across micropatterned grooves. Biomaterials, 2006; 27: 460-72.

Hsu S, Chen C, Lu PS, Lai C, Chen CJ. Oriented Schwann cell growth on microgrooved surfaces. Biotechnology and Bioengineering, 2005; 579-88.

Li G, Liu J, Hoffman-Kim D. Multi-Molecular Gradients of Permissive and Inhibitory Cues Direct Neurite Outgrowth. Annals of Biomedical Engineering, 2008.

Lopez G, Biebuyck HA, Harteer R, Kumar A, Whitesides G. Fabrication and imaging of two-dimensional patterns of proteins adsorbed on self-assembled monolayers by scanning electron microscopy. Journal of the American Chemical Society, 1993; 115:10774-10782.

Manwaring ME, Walsh JF, Tresco PA. Contact guidance induced organization of extracellular matrix. Biomaterials, 2004; 25: 3631-8.

McCarthy JB, Palm SL, Furcht LT. Migration by haptotaxis of a Schwann cell tumor line to the basement membrane glycoprotein laminin. J. Cell Biol., 1983; 97: 772-7.

Miller C, Jeftinija S, Mallapragada S. Synergistic effects of physical and chemical guidance cues on neurite alignment and outgrowth on biodegradable polymer substrates. Tissue Eng, 2002; 8: 367-78.

Rajnicek A, McCaig C. Guidance of CNS growth cones by substratum grooves and ridges: effects of inhibitors of the cytoskeleton, calcium channels and signal transduction pathways. J Cell Sci, 1997; 110: 2915-24.

Schnaar RI, Schaffner AE. Separation of cell types from embryonic chicken and rat spinal cord: characterization of motoneuron-enriched fractions. J. Neurosci., 1981; 1: 204-17.

Song M, Uhrich KE. Optimal Micropattern Dimensions Enhance Neurite Outgrowth Rates, Lengths, and Orientations. Annals of Biomedical Engineering, 2007; 35: 1812.

Webb K, Budko E, Neuberger TJ, Chen S, Schachner M, Tresco PA. Substrate-bound human recombinant L1 selectively promotes neuronal attachment and outgrowth in the presence of astrocytes and fibroblasts. Biomaterials, 2001; 22: 1017-28.